The Role of Certain Phospho-Proteins in Regulating the Mode of Synaptic Vesicle Exocytosis

by

Stephen Gilbody (BSc)

A thesis submitted in partial fulfilment for the requirements for the degree of Doctor of Philosophy at the University of Central Lancashire

July 2021

DECLARATION

Type of Award **Doctor of Philosophy**

School **Pharmacy and Biomedical Sciences**

Concurrent registration for two or more academic awards

I declare that while registered as a candidate for the research degree, I have not been a registered candidate or enrolled student for another award of the University or other academic or professional institution

Material submitted for another award

I declare that no material contained in the thesis has been used in any other submission for an academic award and is solely my own work

Use of a Proof-reader

No proof-reading service was used in the compilation of this thesis.

Signature of Candidate:

STEPHEN GILBODY (BSc)

ABSTRACT

The presynaptic release of neurotransmitter requires the exocytosis of synaptic vesicles (SVs). There are three pools of such vesicles: the readily releasable pool (RRP), the reserve pool (RP) and the resting pool (RtP). Rat brain cerebral cortical synaptosomes were utilised in the presence of 5 mM extracellular Ca^{2+}, and various chemical stimuli have been established to release the RRP (1 mM 4-aminopyridine, 4AP5C) or the RRP and the RP (raised potassium [30 mM, HK5C] or ionomycin [5 µM, ION5C]) of glutamate (Glu) containing SVs.

Exocytosis of SVs involves the formation of a fusion pore between the vesicular membrane and the plasma membrane (PM) at the active zone (AZ), and once this is formed Glu can immediately exit the lumen of the vesicle and enter the extracellular space. The vesicle itself undergoes one of two processes: (i) full fusion (FF) whereby the fusion pore expands, and the vesicular membrane fully inserts into the PM with the vesicle being subsequently recycled by clathrin dependent endocytosis at the peri-active zone; (ii) kiss-and-run (KR) whereby the fusion pore closes < 0.5 s after opening. The contribution of each of these distinct pathways in normal transmission is still a matter of debate and in particular not much is known about the biochemical mechanisms underlying KR mode.

Reported herein, the role of cyclic adenosine monophosphate (cAMP) and protein kinase A (PKA) in regulating the exocytosis of the SV pools and their mode was investigated. The kinase PKA was studied using a specific inhibitor, KT5720 and a specific activator, Sp-5,6-DCl-cBIMPS (cBIMPS). It was observed that PKA inhibition did not interfere with the exocytosis of the RRP or RP but switched the RRP SVs to an FF mode for the dynamin dependent KR mechanism but not for the NMII dependent mechanism. Conversely, PKA activation had no effect on the Glu release from the SV pools but switched some of the RP SVs to a KR mechanism. Pre-treatment with the drug MiTMAB – which prevents dynamin binding to lipid membranes – did not perturb the dynamin dependent KR mode suggesting that the dynamin is already associated with the membrane(s) prior to the application of the stimulus or the drug. This may indicate that only a proportion of the total terminal dynamin contributes to the KR mechanism, which is associated with the PM.

The role of cAMP itself was studied by activating adenylate cyclase (AC) with forskolin or inhibiting this enzyme with 9-cyclopentyl-adenine monomethanesulfonate (9-cp-ade). The inhibitor 9-cp-ade had no effect on any stimulated release of the pools of SVs nor did it affect the mode of exocytosis. Activation of AC had two distinct effects: (i) the release of the RP of SVs was inhibited; (ii) the 4AP5C evoked RRP SVs which underwent FF mode were switched to KR mode. Forskolin increased change in intracellular Ca^{2+} with 4AP5C stimulation, which may have caused the RRP to switch to KR mode with 4AP5C; however, change in intracellular Ca^{2+} decreased with HK5C stimulation, which may have caused the loss of RP release. The forskolin induced inhibition of RP SV release was due to AC activation since this was prevented when synaptosomes were pre-treated with 9-cp-ade, but the cAMP was not acting on PKA as direct PKA activation did not inhibit the RP SV release. The cAMP produced was working on exchange proteins directly activated by cAMP (EPAC), evidenced as specific inhibitor of EPACs ESI-09 prevented the action of forskolin such that the RP of SVs could be released by HK5C.

The role of actin cytoskeleton in the release of the pools of SVs and the mode of exocytosis was studied. Intriguingly, stabilising microfilaments with jasplakinolide did not perturb the release of the RRP or RP with any of the stimuli and neither did it affect the mode of exocytosis.. Clearly, the first round of SV exocytosis does not need active reformation of actin microfilaments as microfilament stabilisation of does not affect SV release dynamics. However, disassembly of microfilaments with latrunculin A did have major effects: (i) it inhibited the release of the RP of SVs induced by either ION5C or HK5C; (ii) it switched the mode of exocytosis of the RRP to FF mode. Both the dynamin dependent and the NMII dependent KR mode of the RRP have been shown to require an intact actin cytoskeleton.

These results again emphasise that SVs can undergo both KR and FF mode and that these processes are regulated by PKA, EPAC and the cytoskeleton. Future experiments will aim to find relationships between these enzymes and other enzymes such as PKC and see if they are related to the microfilaments. Such knowledge may also help to ascertain whether there are specific phosphorylation sites on dynamin and NMII that control KR mode. Results with

MiTMAB appear to highlight that for dynamin the phosphorylation change may only occur on a very minor population of the total dynamin.

TABLE OF CONTENTS

DECLARATION i
ABSTRACT ii
TABLE OF CONTENTS v
ACKNOWLEDGEMENTS x
LIST OF FIGURES xi
LIST OF TABLES xvi
LIST OF ABBREVIATIONS xviii
CHAPTER 1: Introduction 1
1.1 Summary of Synaptic Vesicle Release 2
1.2 Synaptic Vesicle Functionality and Synaptic Vesicle Pools 5
1.3 Synaptic Vesicle Fusion and Exocytosis 10
1.4 Synaptic Vesicle Endocytosis and Recycling 14
1.5 Kiss-and-Run Mode 20
1.6 Non-Muscle Myosin II in Synaptic Vesicle Release Dynamics 21
1.6.1 Non-Muscle Myosin II Structure and Properties 21
1.6.2 The Role of Non-Muscle Myosin II and Actin in Regulating the Fusion Pore 24
1.6.3 Non-Muscle Myosin II in Vesicle Mobilisation 31
1.6.4 Non-Muscle Myosin II Phosphorylation and Activation State 32
1.7 Dynamin in Synaptic Vesicle Release Dynamics 36
1.7.1 Dynamin Structure and Properties 36
1.7.2 Dynamin Role in Regulating the Fusion Pore 38
1.7.3 Dynamin-1 Phosphorylation and Activation State 41
1.8 Research Aims 42
1.9 Hypothesis 43
CHAPTER 2: Materials and Methods 44
2.1 Methodological Approach 45
2.2 Rationale 46
2.2.1 Glutamate and FM 2-10 Assays of Drug Effects on Distinct Fusion Mechanisms 46
2.2.2 Fura-2 Assay of Drug Effects on Endogenous Ca^{2+} Release 47
2.2.3 Extracellular Flux Analysis of Drug Effects on Synaptosome Samples 48
2.3 Materials 50
2.3.1 Materials Lists 50
Formulated Materials 52

2.3.2 52
2.4 Method Brief 54
2.4.1 Preparation of Synaptosomes 54
2.4.2 Glutamate Release Assay 55
2.4.3 The FM 2-10 Styryl Dye Release Assay 57
2.4.4 The Fura-2 Intracellular Free Ca^{2+} Concentration Assay 58
2.4.5 Statistical Processing of Biochemical Assays 60
2.4.6 Bioenergetic Measurement of Extracellular O_2 Consumption Rate 61
CHAPTER 3: PKA and Dynamin Modulation Upon Synaptic Vesicle Release 63
3.1 Role of PKA Regulation in Synaptic Vesicle Release 64
3.2 Inhibition of PKA Using KT5720 Upon Synaptic Vesicle Release Dynamics 65
3.2.1 Treatment of KT5720 Upon Evoked Glutamate Release 65
3.2.2 Treatment of KT5720 Upon FM 2-10 Dye Release 67
3.2.3 Treatment of KT5720 Upon Changes in Intracellular Ca^{2+} Levels 70
3.2.4 Treatment of KT5720 Upon Synaptosome Bioenergetics 72
3.3 Activation of PKA Using cBIMPS Upon Synaptic Vesicle Release Dynamics 75
3.3.1 Treatment of cBIMPS Upon Evoked Glutamate Release 75
3.3.2 Treatment of cBIMPS Upon FM 2-10 Dye Release 77
3.3.3 Treatment of cBIMPS Upon Changes in Intracellular Ca^{2+} Levels 79
3.3.4 Treatment of cBIMPS Upon Synaptosome Bioenergetics 81
3.4 Specificity of KT5720 and cBIMPS for PKA Using Evoked FM 2-10 Dye Release 83
3.5 Dynamin Translocation on Synaptic Vesicle Release 85
3.6 Dynamin Translocation Inhibition Using MiTMAB Upon Synaptic Vesicle Release Dynamics 86
3.6.1 Treatment of MiTMAB Upon Evoked Glu Release 86
3.6.2 Treatment of MiTMAB Upon FM 2-10 Dye Release 88
3.6.3 Treatment of MiTMAB Upon Changes in Intracellular Ca^{2+} Levels 90
3.6.4 Treatment of MiTMAB Upon Synaptosome Bioenergetics 91
3.7 Prolonged MiTMAB Treatment on HK5C Evoked Synaptic Vesicle Release 93
3.8 Discussion 96
3.9 Conclusion 105
CHAPTER 4: Adenylate Cyclase Modulation Upon Synaptic Vesicle Release via PKA and EPAC Pathways 106
4.1 Adenylate Cyclase Regulation of Synaptic Vesicles 107
4.2 Adenylate Cyclase Inhibition Using 9-cp-ade on Synaptic Vesicle Release Dynamics 109
4.2.1 Treatment of 9-cp-ade Upon Evoked Glutamate Release 109
4.2.2 Treatment of 9-cp-ade on FM 2-10 Dye Release 111
4.2.3 Treatment of 9-cp-ade Upon Changes in Intracellular Ca^{2+} Levels 113

4.2.4 Treatment of 9-cp-ade Upon Synaptosome Bioenergetics 114
4.3 Adenylate Cyclase Activation Using Forskolin on Synaptic Vesicle Release Dynamics 116
4.3.1 Treatment of Forskolin Upon Evoked Glutamate Release 116
4.3.2 Treatment of Forskolin Upon FM 2-10 Dye Release 121
4.3.3 Treatment of Forskolin Upon Changes in Intracellular Ca^{2+} levels 126
4.3.4 Treatment of Forskolin Upon Synaptosome Bioenergetics 128
4.4 The Protein EPAC As a Potential Synaptic Vesicle Release Modulator 130
4.5 Inhibition of EPAC Using ESI-09 Upon Synaptic Vesicle Release Dynamics 131
4.5.1 Treatment of ESI-09 Upon Evoked Glutamate Release 131
4.5.2 Treatment of ESI-09 Upon Changes in Intracellular Calcium Levels 132
4.5.3 Treatment of ESI-09 Upon Synaptosome Bioenergetics 136
4.6 Discussion 139
4.6.1 Discussion of AC inhibition 140
4.6.2 Discussion of AC activation 141
4.6.3 Discussion of EPACs inhibition 144
4.7 Conclusion 146
CHAPTER 5: 147
Actin Modulation Upon SV exocytosis 147
5.1 Actin Regulation of Synaptic Vesicles 148
5.1.1 Properties of Actin 148
5.1.2 Role of Actin in Nerve Terminals 152
5.1.3 Role of Actin in Endocytosis 153
5.2 F-actin Depolymerisation Using Latrunculin A on Synaptic Vesicle Release Dynamics 156
5.2.1 Latrunculin A Treatment on Evoked Glutamate Release 156
5.2.2 Treatment of Latrunculin A Upon FM 2-10 Dye Release 158
5.2.3 Dual Treatment of Latrunculin A and Okadaic Acid Upon Evoked Glu and FM 2-10 Dye Release 160
5.2.4 Treatment of Latrunculin A Upon Changes in Intracellular Ca^{2+} Levels 165
5.3 Stabilisation of F-actin Using Jasplakinolide Upon Synaptic Vesicle Release Dynamics 166
5.3.1 Treatment of Jasplakinolide Upon Evoked Glutamate Release 166
5.3.2 Dual Treatment of Jasplakinolide and Latrunculin A Dual Upon Evoked Glutamate Release 168
5.3.3 Treatment of Jasplakinolide Upon FM 2-10 Dye Release 169
5.3.4 Treatment of Jasplakinolide and Latrunculin A Upon FM 2-10 Dye Release 171
5.3.5 Triple Treatment of Jasplakinolide, Latrunculin A and Okadaic Acid Upon FM 2-10 Dye Release and Evoked Glu Release 173

5.3.6 Treatment of Jasplakinolide Upon Changes in Intracellular Ca^{2+} Levels 177

5.3.7 Dual Treatment of Jasplakinolide and Latrunculin A Upon Changes in HK5C Evoked Intracellular Ca^{2+} Levels 179

5.4 Stimulation of ION5C Acts on the NMII regulated Kiss-and-Run Mode of RRP Following Activation of Certain PKCs 181

5.4.1 Treatment of 40 nM PMA Upon ION5C Evoked Glu Release in Latrunculin A and Okadaic Acid Combinations....181

5.4.2 Treatment of 40 nM PMA Upon ION5C Evoked FM 2-10 Dye Release in Latrunculin A and Okadaic Acid Combinations....184

5.4.3 Treatment of 40 nM PMA Upon ION5C Evoked Changes in Intracellular Ca^{2+} Levels in Latrunculin A and Okadaic Acid Combinations....186

5.4.4 Treatment of 40 nM PMA Upon ION5C Evoked Glutamate Release in Jasplakinolide, Latrunculin A and Okadaic Acid Combinations....188

5.4.5 Treatment of 40 nM PMA Upon ION5C Evoked FM 2-10 Dye Release in Jasplakinolide, Latrunculin A and Okadaic Acid Combinations....190

5.4.6 Treatment of 40 nM PMA Upon ION5C Evoked Changes in Intracellular Ca^{2+} Levels in Jasplakinolide, Latrunculin A and Okadaic Acid Combinations....192

5.4.7 Treatment of 40 nM PMA Upon ION5C Evoked Glu Release in Jasplakinolide, Latrunculin A and Blebbistatin Combinations 194

5.4.8 Treatment of 40 nM PMA Upon ION5C Evoked FM 2-10 Dye Release in Jasplakinolide, Latrunculin A and Blebbistatin Combinations 196

5.5 Discussion 199

5.5.1 The Effect of F-Actin Depolymerisation on Evoked Glutamate Release199

5.5.2 The Effect of F-actin Depolymerisation on FM 2-10 Dye Release Reflecting Effects on the Mode of Exocytosis....201

5.5.3 The Effect of F-Actin Stabilisation on Evoked Glutamate Release, FM 2-10 Dye Release and Change in Intracellular Ca^{2+} 202

5.5.4 Specificity of Latrunculin A and Jasplakinolide on Actin Microfilaments202

5.5.5 Actin Microfilament Requirement for Dynamin Dependent and NMII Dependent Kiss-and-Run of the RRP Synaptic Vesicles....203

5.6 Conclusion....205

CHAPTER 6: 206

General Discussion....206

6.1 Release Properties of the RRP and RP of Synaptic Vesicles....208

6.2 Regulating the Mode of Exocytosis of the RRP and RP Synaptic Vesicles..212

6.3 Concluding Statement....214

LIST OF REFERENCES....216

APPENDIX A: Review of Previous Results....1

A Review of Previous Research....2

A.1 Maximal Glutamate Release....2

A.2 Expression of Glutamate release....5

A.3 A Single Round of Exocytosis....6

A.4 Maximal Labelling of Synaptic Vesicles with FM 2-10 Dye 12
A.5 The Mode of Exocytosis is Stimulation Dependent 13
A.6 Presynaptic Proteins Regulating Exocytosis 17
A.7 Switching of HK5C Evoked Synaptic Vesicle Exocytosis From NMII Dependent KR to Dynamin Dependent KR 23
A.8 Switching of ION5C Evoked Synaptic Vesicle Exocytosis From Dynamin Dependent KR to NMII Dependent KR 25
APPENDIX B: Beeswarm Superplots of Results in This Thesis 28
B Beeswarm Superplots to Show Validity of Results 29
B.1 Beeswarm Introduction 29
B.2 Beeswarm Superplots for Chapter 3 31
B.3 Tabulated Statistical Differences Between Conditions Calculated From the Superplot Data for Chapter 3 44
B.4 Beeswarm Superplots for Chapter 4 49
B.5 Tabulated Statistical Differences Between Conditions Calculated from the Superplot Data for Chapter 4 59
B.6 Beeswarm Superplots for Chapter 5 63
B.7 Tabulated Statistical Differences Between Conditions Calculated From the Superplot Data for Chapter 5 78

ACKNOWLEDGEMENTS

I express my sincere thanks to many people who have made this thesis possible: To my supervisor Dr Anthony Ashton, a rigorous and diligent scientist whose guidance and support has helped to drive me on. To my colleague and friend Dr Adam Rostron who has supported me in and out of work since college days. To colleagues and friends Dr Deeba Singh and Dr Tae Guen Kuan, who have been helpful and whose presence made university work much more fun. And to the present and previous staff and students of UCLan who have sustained my aspirations and pursuits throughout this PhD course.

I give serious appreciation to my family and friends who have such faith and esteem in me, with special thanks to my Dad who has given to me immeasurably and my Brother who has helped me to actually have a social life.

I am grateful to one and all who have assisted in this venture, and with confident strides I pursue to make all these people, and myself, proud.

LIST OF FIGURES

Figure 1.1: Diagram of the synaptic vesicle cycle……4
Figure 1.2: Diagram of a representative section through the synaptic bouton/terminal, including 60 identified proteins……....6
Figure 1.3: Diagram of known vesicle pool classifications and relationships……...8
Figure 1.4: Diagram of the active zone proteins and interactions……12
Figure 1.5: Diagram of the SNARE/SM complex mediating synaptic vesicle fusion, and the role of synaptotagmin and complexin upon Ca^{2+} stimulus for fusion……13
Figure 1.6: Diagram of current understanding of endocytic mechanism dynamics at pre-synapses……18
Figure 1.7: Diagram of currently considered modes of synaptic vesicle endocytosis..19
Figure 1.8: Diagram of non-muscle myosin II activation and assembly with F-actin…23
Figure 1.9: Diagram of non-muscle myosin II, F-actin and dynamin control granule content release through neurosecretory fusion pore……...30
Figure 1.10: Diagram showing the various phosphorylation sites on NMII RLC and HC in its three different isoforms A, B and C……...34
Figure 1.11: Diagram of the structure of dynamin……..37
Figure 2.1: Graph of the Mito-Stress test time course to measure oxygen consumption rate……..49
Figure 3.1: The effect of 2 µM KT5720 vs control upon evoked Glu release……66
Figure 3.2: The effect of 2 µM KT5720 vs control upon evoked FM 2-10 dye release……...68
Figure 3.3: The effect of 2 µM KT5720 vs control upon evoked $[Ca^{2+}]_i$ levels……...71
Figure 3.4: The effect of 2 µM KT5720 vs control upon synaptosome bioenergetics...73
Figure 3.5: The effect of 2 µM KT5720 vs control upon mitochondrial function……74
Figure 3.6: The effect of 50 µM cBIMPS vs control upon evoked Glu release……..76
Figure 3.7: The effect of 50 µM cBIMPS vs control upon evoked FM 2-10 dye release……78
Figure 3.8: The effect of 50 µM cBIMPS vs control upon evoked $[Ca^{2+}]_i$ levels……80
Figure 3.9: The effect of 50 µM cBIMPS vs control upon synaptosome bioenergetics……..81
Figure 3.10: The effect of 50 µM cBIMPS vs control upon mitochondrial function……82
Figure 3.11: The effect of 2 µM KT5720 then 50 µM cBIMPS treatment vs control upon evoked FM 2-10 dye release……...84
Figure 3.12: The effect of 30 µM MiTMAB vs control upon evoked Glu release……...87
Figure 3.13: The effect of 30 µM MiTMAB vs control upon evoked FM 2-10 dye release……88

Figure 3.14: The effect of 30 µM MiTMAB vs control upon evoked $[Ca^{2+}]_i$ levels……..90
Figure 3.15: The effect of 30 µM MiTMAB vs control upon synaptosome bioenergetics……..91
Figure 3.16: The effect of 30 µM MiTMAB vs control upon mitochondrial function…...92
Figure 3.17: The effect of 20 min at 37ºC 30 µM MiTMAB vs control upon evoked Glu release……93
Figure 3.18: The effect of 20 min at 37ºC 30 µM MiTMAB vs control upon evoked FM 2-10 dye release……...94
Figure 3.19: The effect of 20 min at 37ºC using 30 µM MiTMAB or solvent (control), pre-stimulated with HK5C and subsequently stimulated with 4AP5C or ION5C upon evoked Glu release……...……95
Figure 4.1: The effect of 100 µM 9-cp-ade vs control upon evoked Glu release…….110
Figure 4.2: The effect of 100 µM 9-cp-ade vs control upon evoked FM 2-10 dye release……..112
Figure 4.3: The effect of 100 µM 9-cp-ade vs control upon evoked $[Ca^{2+}]_i$ levels…...113
Figure 4.4: The effect of 100 µM 9-cp-ade vs control upon synaptosome bioenergetics……114
Figure 4.5: The effect of 100 µM 9-cp-ade vs control upon mitochondrial function…115
Figure 4.6: The effect of 100 µM forskolin vs control upon evoked Glu release…..…118
Figure 4.7: The effect of 100 µM 1,9-dideoxyforskolin vs control upon evoked Glu release……..119
Figure 4.8: The effect of 100 µM 9-cp-ade plus 100 µM forskolin vs control upon evoked Glu release……120
Figure 4.9: The effect of 100 µM forskolin or 100 µM 9-cp-ade plus 100 µM forskolin on evoked FM 2-10 dye release……...123
Figure 4.10: The effect of 2 µM KT5720 plus 100 µM forskolin upon evoked FM 2-10 dye release……....……124
Figure 4.11: The effect of 0.8 µM OA or 0.8 µM OA plus 100 µM forskolin upon 4AP5C evoked FM 2-10 dye release……125
Figure 4.12: The effect of 100 µM forskolin vs control upon evoked $[Ca^{2+}]_i$ levels…..127
Figure 4.13: The effect of 100 µM forskolin vs control upon synaptosome bioenergetics……128
Figure 4.14: The effect of 100 µM forskolin vs control upon mitochondrial function...129
Figure 4.15: The effect of 100 µM ESI-09 upon HK5C evoked Glu release……....131
Figure 4.16: The effect of 100 µM ESI-09 plus 100 µM forskolin upon HK5C evoked Glu release……...132
Figure 4.17: The effect of 100 µM ESI-09 upon evoked $[Ca^{2+}]_i$ levels……...…134

Figure 4.18: The effect of 100 µM ESI-09 plus 100 µM forskolin upon evoked $[Ca^{2+}]_i$ levels……135
Figure 4.19: The effect of 100 µM ESI-09 vs control upon synaptosome bioenergetics……...137
Figure 4.20: The effect of 100 µM ESI-09 vs control upon mitochondrial function.....138
Figure 5.1: The effect of 15 µM latrunculin A vs control upon evoked Glu release….157
Figure 5.2: The effect of 15 µM latrunculin A vs control upon evoked FM 2-10 dye release……..159
Figure 5.3: The effect of 15 µM latrunculin A treatment upon total FM 2-10 dye content relative to non-drug treated control…….....160
Figure 5.4: The effect upon HK5C or ION5C evoked FM 2-10 dye release of 0.8 µM OA alone or in combination with of 15 µM latrunculin…….....162
Figure 5.5: The effect of latrunculin plus OA treatment on total FM 2-10 content relative to non-drug treated control……..163
Figure 5.6: The effect of latrunculin A plus OA upon HK5C and ION5C evoked Glu release compared to non-drug treated control……...……164
Figure 5.7: The effect of 15 µM latrunculin A vs control upon evoked $[Ca^{2+}]_i$ levels...165
Figure 5.8: The effect of 2.5 µM jasplakinolide upon evoked Glu release……167
Figure 5.9: The effect of 2.5 µM jasplakinolide plus 15 µM latrunculin A upon evoked Glu release……...…169
Figure 5.10: The effect of 2.5 µM jasplakinolide upon evoked FM 2-10 dye release.....170
Figure 5.11: The effect of 2.5 µM jasplakinolide plus 15 µM latrunculin A upon evoked FM 2-10 dye release……..172
Figure 5.12: The effect of 2.5 µM jasplakinolide plus 15 µM latrunculin A plus 0.8 µM OA upon evoked FM 2-10 dye release……174
Figure 5.13: The effect of various drug treatments on total FM2-10 content relative to non-drug treated control……175
Figure 5.14: The effect of jasplakinolide plus latrunculin A plus OA upon HK5C and ION5C evoked Glu release compared to non-drug treated control……176
Figure 5.15: The effect of 2.5 µM jasplakinolide upon evoked $[Ca^{2+}]_i$ levels……178
Figure 5.16: The effect of 2.5 µM jasplakinolide plus 15 µM latrunculin A upon evoked $[Ca^{2+}]_i$ levels……180
Figure 5.17: The effect of 40 nM PMA, 40 nM PMA plus 15 µM latrunculin A or 40 nM PMA plus 15 µM latrunculin A plus 0.8 µM OA vs control upon ION5C evoked Glu release……..183

Figure 5.18: The effect of 40 nM PMA, 40 nM PMA plus 15 µM latrunculin A or 40 nM PMA plus 15 µM latrunculin A plus 0.8 µM OA vs control upon ION5C evoked FM2-10 dye release……..185
Figure 5.19: The effect of PMA plus latrunculin A or PMA plus latrunculin A plus OA upon ION5C evoked $[Ca^{2+}]_i$ levels compared to control……187
Figure 5.20: The effect of PMA plus jasplakinolide, PMA plus jasplakinolide plus latrunculin A or PMA plus jasplakinolide plus latrunculin A plus OA upon ION5C evoked Glu release compared to non-drug treated control……...189
Figure 5.21: The effect of PMA plus jasplakinolide, PMA plus jasplakinolide plus latrunculin A or PMA plus jasplakinolide plus latrunculin A plus OA upon ION5C evoked FM 2-10 dye release compared to non-drug treated control……...191
Figure 5.22: The effect of PMA plus jasplakinolide, PMA plus jasplakinolide plus latrunculin A or PMA plus jasplakinolide plus latrunculin A plus OA upon ION5C evoked $[Ca^{2+}]_i$ levels compared to non-drug treated control……..……193
Figure 5.23: The effect of PMA plus latrunculin A plus blebbistatin or PMA plus jasplakinolide plus latrunculin A plus blebbistatin upon ION5C evoked Glu release compared to non-drug treated control……....195
Figure 5.24: The effect of PMA plus latrunculin A plus blebbistatin or PMA plus jasplakinolide plus latrunculin A plus blebbistatin upon ION5C evoked FM 2-10 dye release compared to non-drug treated control……...197
Figure 5.25: The effect of various drug treatments on total FM dye content relative to control non-drug treated samples……198

Figure A1: Effect of a range of $[Ca^{2+}]_e$ upon evoked Glu release…….App. 3
Figure A2: Effect of stimuli upon cytosolic free calcium $[Ca^{2+}]_i$…….App. 4
Figure A3: Different expressions of Glu release data…….App. 6
Figure A4: Effect of 1 µM bafilomycin A1 upon evoked Glu release……App. 8
Figure A5: Effect of 15 µM Pitstop® 2 vs control upon ION5C evoked Glu release……App. 9
Figure A6: Effect of 15 µM Pitstop® 2 vs control upon ION5C evoked FM 2-10 dye release……..App. 10
Figure A7: Effect of 15 µM Pitstop® 2 pre-treatment vs control upon ION5C evoked Glu release……App. 11
Figure A8: Effect of 15 µM Pitstop® 2 pre-treatment vs control upon 4AP5C evoked Glu release…….App.11
Figure A9: Difference between SVs loaded with 1 mM or 100 µM FM 2-10 dye……..App. 13
Figure A10: Mode of RRP release during control and 0.8 µM OA treatment……App. 15

Figure A11: Mode of RRP and RP release during control and 0.8 µM OA treatment….....App. 16
Figure A12: Effect of 160 µM dynasore vs control upon evoked Glu and FM 2-10 dye release…….....App. 17
Figure A13: Effect of 50 µM blebbistatin upon evoked Glu release……...App. 19
Figure A14: Effect of 50 µM blebbistatin upon evoked FM 2-10 dye release…...App. 20
Figure A15: Effect of 1 µM Cys A upon evoked Glu and FM 2-10 dye release…App. 22
Figure A16: Effect of 1 µM Go 6983 plus 50 µM blebbistatin or 160 µM dynasore upon evoked Glu release…….....App. 23
Figure A17: Effect of 1 µM Go 6983 plus 50 µM blebbistatin or 160 µM dynasore upon evoked FM 2-10 dye release…….....App. 24
Figure A18: Effect of 40 nM PMA plus 50 µM blebbistatin or 160 µM dynasore upon evoked Glu release…….....App. 26
Figure A19: Effect of 40 nM PMA plus 50 µM blebbistatin or 160 µM dynasore upon evoked Glu release…….....App. 27
Beeswarm Superplots for Chapter 3……..App. 31-43
Beeswarm Superplots for Chapter 4…….....App. 49-58
Beeswarm Superplots for Chapter 5…….....App. 63-77

LIST OF TABLES

Table 2.1: Materials list…….....51
Table 2.2: Machinery and software list…….....51

Table B3.1: 4AP5C Glu release control vs drug treatments statistics using superplot data……App. 44
Table B3.2: HK5C Glu release control vs drug treatments statistics using superplot data……...App. 45
Table B3.3: ION5C Glu release control vs drug treatments statistics using superplot data……...App. 45
Table B3.4: 4AP5C FM 2-10 release control vs drug treatments statistics using superplot data……...App. 45
Table B3.5: HK5C FM 2-10 release control vs drug treatments statistics using superplot data……...App. 46
Table B3.6: ION5C FM 2-10 release control vs drug treatments statistics using superplot data…….....App. 46
Table B3.7: Evoked Glu release control vs 5 min MiTMAB treatment statistics using superplot data…….....App. 47
Table B3.8: Evoked FM 2-10 release control vs 5 min MiTMAB treatment statistics using superplot data……App. 47
Table B3.9: HK5C Glu release control vs 20 min MiTMAB treatment statistics using superplot data……...App. 47
Table B3.10: HK5C evoked FM 2-10 release control vs 20 min MiTMAB treatment statistics using superplot data……...App. 48
Table B3.11: Evoked Glu release control vs MiTMAB pre-treatment statistics using superplot data…….....App. 48
Table B4.1: 4AP5C Glu release control vs drug treatments statistics using superplot data……...App. 60
Table B4.2: HK5C Glu release control vs drug treatments statistics using superplot data……App. 60
Table B4.3: ION5C Glu release control vs drug treatments statistics using superplot data……...App. 61
Table B4.4: 4AP5C FM 2-10 release control vs drug treatments statistics using superplot data……...App. 61
Table B4.5: HK5C FM 2-10 release control vs drug treatments statistics using superplot data…….....App. 62

Table B4.6: ION5C FM 2-10 release control vs drug treatments statistics using superplot data……...App. 62
Table B5.1: HK5C Glu release control vs drug treatments statistics using superplot data……...App. 79
Table B5.2: ION5C Glu release control vs drug treatments statistics using superplot data……...App. 80
Table B5.3: HK5C FM 2-10 release control vs drug treatments statistics from superplot data……...App. 81
Table B5.4: ION5C FM 2-10 dye release control vs drug treatments statistics using superplot data……...App. 82
Table B5.5: ION5C Glu release control vs PMA plus other drug treatments statistics using superplot data……...App. 83
Table B5.6: ION5C FM 2-10 dye release control vs PMA plus other drug treatments statistics using superplot data……...App. 84

LIST OF ABBREVIATIONS

$[Ca^{2+}]_e$ – extracellular calcium (Ca^{2+})

$[Ca^{2+}]_i$ – intracellular calcium (Ca^{2+})

4AP – 4-aminopyridine (1 mM)

5C – added extracellular calcium (Ca^{2+}; 5 mM)

9-cp-ade – 9-cyclopentyl-adenine monomethanesulfonate

AC – adenylate cyclase / adenylyl cyclase

ADBE – activity-dependent bulk endocytosis

ADP – adenosine diphosphate

AM – acetoxymethyl group (of Fura-2)

AP – action potential

Arp2/3 complex – actin related protein 2/3 complex

ATP – adenosine triphosphate

ATPase – adenosine triphosphate hydrolase

AZ – active zone

BAR domain – Bin/amphiphysin/Rrs domain

cAMP – cyclic adenosine monophosphate

cBIMPS – Sp-5,6-DCl-cBIMPS

C_c – critical concentration

Cdc42 – cell division control protein 42

CK2 – casein kinase 2

CME – clathrin-mediated endocytosis

CNS – central nervous system

Cys A – cyclosporine A

DMSO – dimethyl sulfoxide

EGTA –ethylene glycol-bis(β-aminoethyl ether)-N,N,N′,N′-tetraacetic acid

ELC – essential light chain

EPAC – exchange proteins directly activated by cAMP

F-actin – fibrous actin (polymeric)

F-BAR – FCH domain BAR

FCCP - carbonyl cyanide-p-trifluoromethoxyphenylhydrazone

FF – full fusion

Fig – Figure

FM 2-10 - (N-(3-triethylammoniumpropyl)-4-(4-(diethylamino)styryl)pyridinium dibromide)

G-actin – glomerular actin (monomeric)

GDH – glutamate dehydrogenase type II

GED – GTPase effector domain

Glu – glutamate

GTP – guanosine triphosphate

GTPase – guanosine triphosphate hydrolase

GTPγS – guanosine 5'-O-[gamma-thio] triphosphate

HC – heavy chain

HK – potassium (K^+; 30 mM)

HK0 – high potassium (K^+) buffer

HsC70 – heat shock cognate 70

ION – ionomycin (5 µM)

K_d – dissociation constant

KR – kiss-and-run

L0 – physiological basal buffer

MLCK – myosin light chain kinase

MRCK – myotonic dystrophy kinase-related Cdc42-binding kinase

$NADP^+$ - nicotinamide adenine dinucleotide phosphate

NADPH - nicotinamide adenine dinucleotide phosphate reduced form

NMII – non-muscle myosin II

NS – not significant / no significant difference

NSF – N-ethylmaleimide sensitive fusion protein

N-WASP – neutral Wiskott-Aldrich syndrome protein

OA – okadaic acid

OCR – oxygen (O_2) consumption rate

PBS – phosphate buffered saline

PDGF – platelet-derived growth factor

PH – pleckstrin homology

P_i – inorganic phosphate

PIP_2 – phosphatidylinositol 4,5-bisphosphate

PKA – protein kinase A

PKC – protein kinase C

PM – plasma membrane

PMA – phorbol 12-myristate 13-acetate / phorbol ester

PP2A – protein phosphatase 2A

PP2B – protein phosphatase 2B

PP2B – protein phosphatase 2B / calcineurin

PRD – proline rich domain

pre-mRNA – pre-messenger ribonucleic acid

R – 340/380 nm wavelength ratio

RIM – Rab3 interacting molecules

RIM-BP – RIM binding protein

RLC – regulatory light chain

R_{max} – 340/380 nm wavelength ratio during $[Ca^{2+}]_i$ saturation

R_{min} – 340/380 nm wavelength ratio during Ca^{2+}-free conditions

ROCK – rho-associated, coiled-coil containing kinase

RP – reserve pool

RRP – readily releasable pool

RtP – resting pool

SD – standard deviation

SEM – standard error of the mean

SM – Sec1/Munc18-like protein family

SNAP – soluble NSF attachment proteins

SNARE – SNAP receptor

SNX9 – sorting nexin 9

SV – synaptic vesicle

SV2 – synaptic vesicle protein 2

TRPM7 – transient receptor potential cation channel M7

t-SNARE – trans SNARE

UE – ultrafast endocytosis

V-ATPase – vacuolar H^+ ATPase

v-SNARE – vesicular SNARE

ZIPK – leucine zipper interacting kinase

β – ratio of average fluorescence of Fura-2 at 380 nm under Ca^{2+}-free and Ca^{2+}-bound conditions

CHAPTER 1: Introduction

1.1 Summary of Synaptic Vesicle Release

Synaptic transmission of chemical neurotransmitters at the neuronal synapse allows specific intercellular communication in the nervous system. Distinct neurotransmitters are released by complex mechanisms into the synaptic cleft by exocytosis and they subsequently bind to compatible post-synaptic receptors. Activation of such receptors causes excitation or inhibition of signal transduction, depending upon the type of receptor, which then regulates post-synaptic action potentials (AP). Specific neurotransmitter molecules are stored in synaptic vesicles (SVs). However, despite ongoing discoveries in this field, there is an insufficient understanding of the precise protein mechanisms of SV priming, exocytosis and consequent endocytosis and recycling, as well as SV membrane dynamics during these processes.

Dysfunction of neurotransmission is implicated in a wide range of nervous system disorders such as neurodegenerative diseases and psychiatric ailments. Therefore, it is of great importance - scientifically and medically - to understand the molecular biology of SV dynamics and neurotransmitter release in order to elucidate certain neuronal diseased states and devise therapeutic treatments for these.

Herein the aim is to help elucidate how SV release is controlled. This investigation involves the effects of intracellular signalling pathways on SV exocytosis, especially in relation to dynamin, non-muscle myosin II (NMII) and actin.

The chemical synapse is a structure composed of the presynaptic terminal, the synaptic cleft and the postsynaptic terminal. An AP arriving at the presynaptic terminal causes the opening of voltage-gated Ca^{2+} channels, subsequently causing an influx of Ca^{2+} into the terminal, and this leads to the release of SV contents into the synaptic cleft through distinct Ca^{2+} dependent mechanisms (Südhof and Rizo, 2011). The amount of neurotransmitter released is directly proportional to frequency of APs arriving at the terminal, until saturating or exhaustive conditions. It typically takes only 0.1 ms from the arrival of an AP at the terminal until Ca^{2+} induced SV exocytosis (Rizo and Rosenmund, 2008).

The approximate distance between the pre- and postsynaptic membrane is 20 nm i.e. the width of the synaptic cleft (Ahmari and Smith, 2002).

There are complex mechanisms involved in positioning, priming and releasing the SV contents although much of the core fusion machinery and its role in exocytosis have been described. Docked synaptotagmin-containing SVs are positioned at the active zone (AZ) of the presynaptic plasma membrane (PM). These SVs can contain SNARE (SNAP receptor) complexes that involve PM SNAREs interacting with the vesicular SNAREs. These may interact with Rab3 interacting molecules (RIM) protein complex, which simultaneously recruits voltage-gated Ca^{2+} channels to these release sites. An AP allows direct flow of Ca^{2+} through the voltage-gated Ca^{2+} channels, whereupon such ions bind to synaptotagmin, and this Ca^{2+} bound protein changes the conformation of the SNARE complexes, triggering SV fusion within a millisecond (Südhof, 2013).

The initial SV and PM fusion event involves the formation of a fusion pore, and thereafter the SV neurotransmitter content can enter the synaptic cleft via this pore. The emptied SV is then recovered from the PM into the terminal by endocytosis so that it can be recycled, refilled with neurotransmitter and become another competent releasable functional SV (Südhof, 2004; Saheki and De Camilli, 2012).

Neurons need to recycle SVs quickly and efficiently to maintain neurotransmission to correctly convey signal timing and intensity (Figure 1.1). Imbalance in SV recycling causes the PM surface area to fluctuate, deforming the presynapse (Schikorski and Stevens, 1997; Rizzoli, 2014). To adjust to different stimulation intensities, multiple modes of SV recycling are regarded to exist which appropriate SV release with demand – there is still much debate and limitation in understanding SV mechanics and its natural modulation.

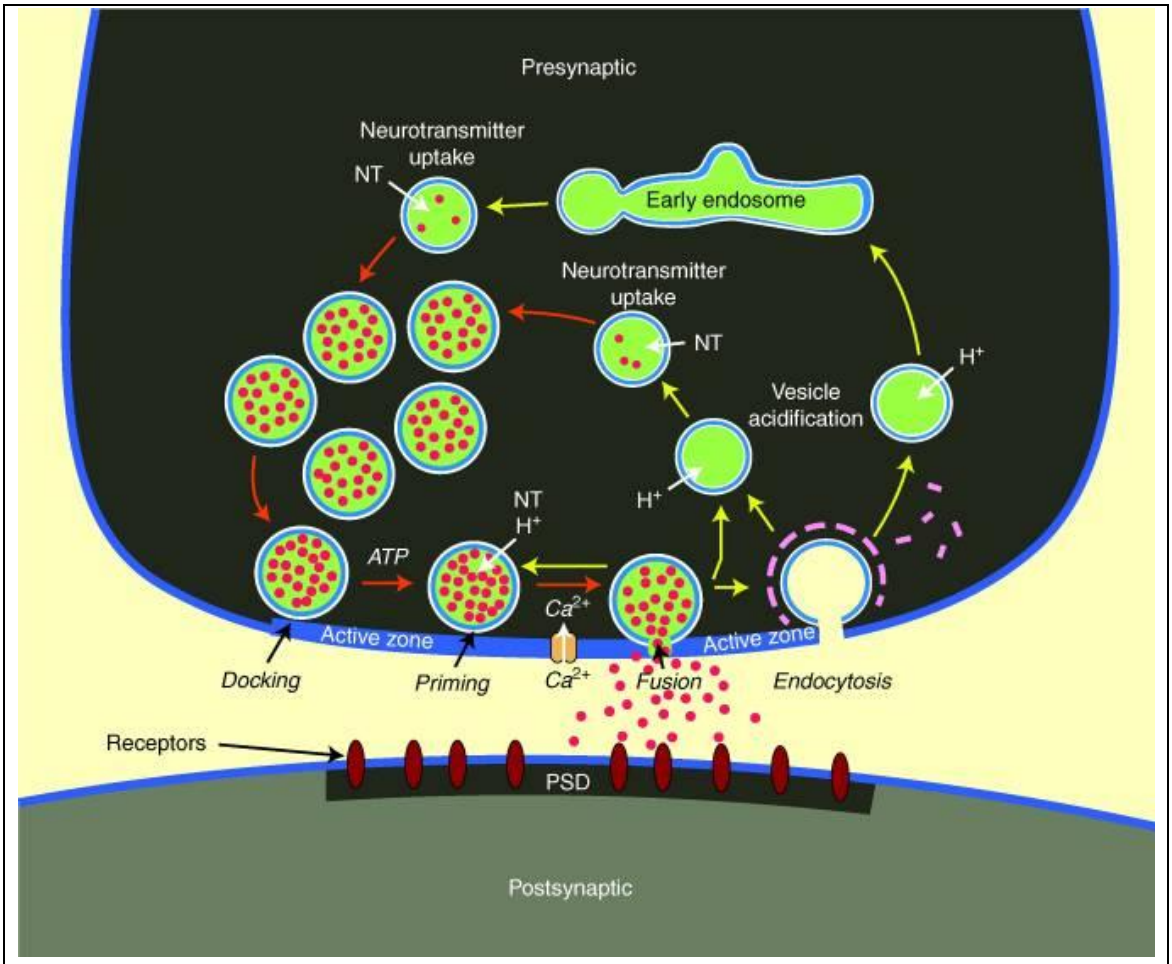

Figure 1.1: Diagram of the synaptic vesicle cycle. A presynaptic nerve terminal is depicted releasing neurotransmitter to a postsynaptic neuron. The cycle consists of exocytosis (red arrows) followed by endocytosis and recycling (yellow arrows). SVs (green circles) are filled with neurotransmitter (red dots). The SVs use an electrochemical gradient made by an ATP-dependent proton pump that acidifies the vesicle interior (green background). The SV is then filled with neurotransmitter by a neurotransmitter dependent proton antiport. In preparation for exocytosis, SVs are docked to protein machinery at the AZ and primed by an ATP-dependent process that renders the vesicles responsive to Ca^{2+} signal. When an AP depolarises the presynaptic terminal, Ca^{2+} channels open, causing local increase in intracellular Ca^{2+} at the AZ that triggers SV fusion using the protein machinery. Released neurotransmitter binds to receptors associated with the postsynaptic density. After fusion pore opening, SVs recycle either by refilling with neurotransmitter without undocking (kiss-and-stay), local recycling with undocking (kiss-and-run) or by full recycling which may include integration into an endosomal intermediate (diagram from Südhof and Rizo, 2011).

Differences in AP frequency can cause use dependent changes in the postsynaptic neuron, changing long and short-term plasticity. Impairment of

recycling has massive impact on the ability of neurons to communicate correctly and can lead to acute and chronic health problems related to the nervous system. Inefficacies and pathologies may develop in short and long-term memory and learning, and such changes are implicated in dementias. Thus, it is important to understand the molecular mechanisms of SV exocytosis and endocytosis in healthy models and to compare these mechanisms in pathological states (Waites and Garner 2011; Esposito *et al.*, 2012).

1.2 Synaptic Vesicle Functionality and Synaptic Vesicle Pools

It was discovered that acetylcholine release from the frog neuromuscular junction occurs in uniformly discrete packets, leading to a quantal hypothesis of neurotransmitter release – distinct uniform packets of neurotransmitter 'quanta' are released from the presynapse. At the time of this discovery, it was not clear if the neurotransmitter was released from the cytoplasm or from discrete organelles (Fatt and Katz, 1952; Del Castillo and Katz, 1954). However early electron microscope studies into what caused neurotransmitter release noted granular components present in presynaptic terminals. These components were40-60 nm in diameter, had uniform appearance and particular spatial organisation, and were named SVs (Palade and Palay, 1954; De Robertis and Bennett, 1955; Palay 1956). Their discovery suggested that quanta of neurotransmitter could be released by an SV fusing with the PM.

Synaptosomes are an experimental model that represents resealed nerve terminals which are prepared by subcellular fractionation by differential density centrifugation. These were first prepared by Whittaker, and the electron microscopy studies on such preparations gave further evidence of SVs being the neurotransmitter containing organelle (Whittaker, 1959; Gray and Whittaker, 1962). Synaptosomes contain no nuclei or microsomes but contain the highest proportion of neurotransmitter. It was concluded that this fraction is made up of nerve terminals, also known as presynaptic boutons, which have been pinched off from whole cell axons but retained structural integrity, as they must have resealed during the homogenisation procedure used to prepare them. Synaptosomes also are prepared with post-synaptic densities still attached.

These isolated terminals were first described as synaptosomes by Whittaker *et al*. (1964) and have since been used as a vital model for studying various synapse specific events.

Wilhelm *et al.* (2014) used electron microscopy and fluorescence microscopy to detect localisation of organelles and proteins in a presynapse along with quantitative immunoblotting and mass spectrometry to determine quantities of different proteins using rat brain cortex and cerebellum (Figure 1.2). This also represents the typical synaptosome without the attached post-synaptic density.

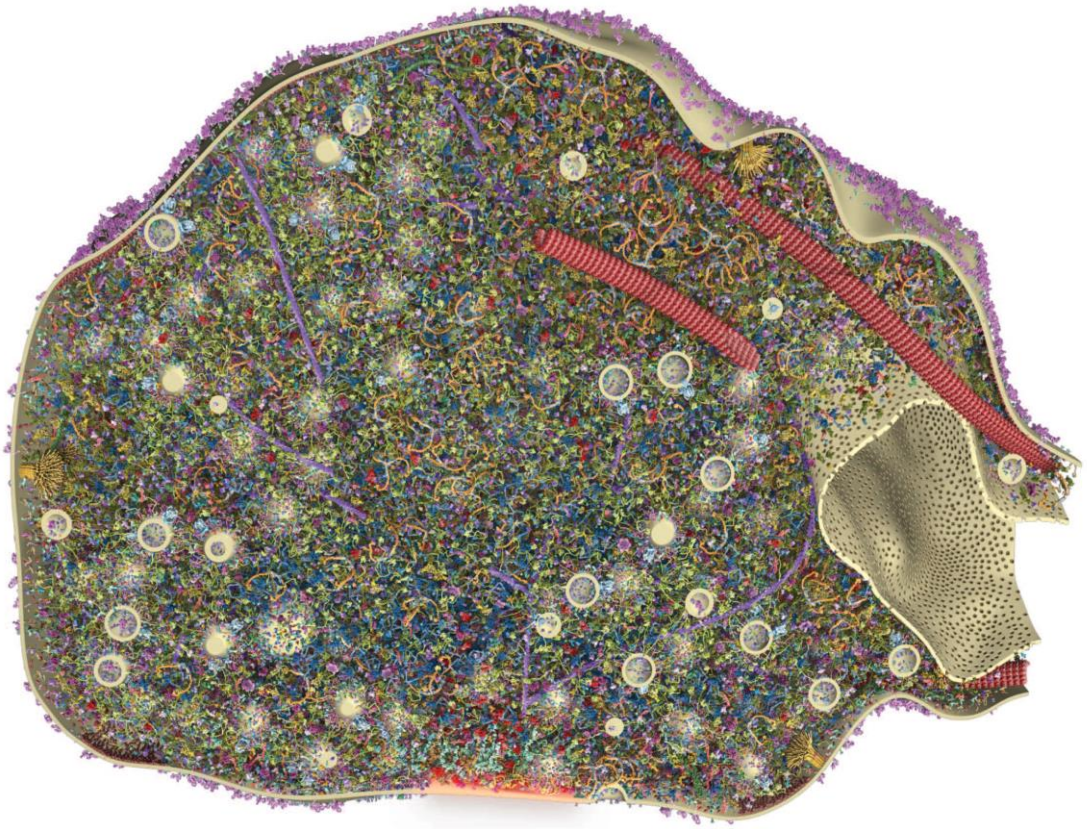

Figure 1.2: Diagram of a representative section through the synaptic bouton/terminal, including 60 identified proteins. The 3D model of an average presynapse is shown. Structure determined according to imaging data. The terminal includes the SVs, and the AZ is labelled in red (diagram from Wilhelm *et al.*, 2014).

Heuser *et al*., 1979 correlated quantal release of neurotransmitter with SV exocytosis. By quick-freezing frog neuromuscular junctions milliseconds after stimulation, a correlation was found between quantal release of neurotransmitter and SVs undergoing exocytosis. They also observed that each

SV released a similar volume of neurotransmitter (a quantum), similarly to Katz (Del Castillo and Katz, 1954).

Neurotransmitters are stored within SVs in the presynaptic terminal in neurons. SVs have an average diameter of 40-60 nm, made of a phospholipid membrane which contains regulatory protein components (Südhof 2004). Takamori *et al.* (2006) found over 400 types of proteins in isolated SVs, with more than 80 being integral proteins and the others being interaction partners. They also found that on average SVs are biochemically homogenous in that all SVs significantly contain the same protein constituents. However, Crawford and Kavalali (2015) have suggested that SVs are not homogenous organelles and contain molecular differences; they argue that vesicular membrane proteins such as v-SNAREs and calcium sensors give each vesicle a molecular identity. Soluble factors such as Munc13-1 or doc2 and PM proteins such as t-SNAREs guide vesicles through segregated, though likely partially overlapping, fusion pathways.

It has been estimated that the average number of active SVs in a hippocampal nerve terminal are ~100-200 (note that hippocampal cultured cells or slices are a major model employed in studying SV exocytosis and endocytosis). However synaptic transmission may require release of neurotransmitter that represents the contents of thousands of SVs (Schikorski and Stevens 1997; Schweizer and Ryan 2006; Ikeda and Bekkers, 2009; Maeno-Hikichi *et al.*, 2011). Therefore, a rapid recycling of SVs is required to allow efficacious and stable neurotransmission.

There is a lack of clarity about how to classify SV groups in any particular presynapse, due to a lack of knowledge of distinct functional and protein interaction differences between different groups of SVs. Groups of SVs are known to differ in terms of spatial organisation as well as stimulation-release paradigms. For example, electron microscope studies demonstrate that a small proportion of SVs are attached to the PM at the AZ, and these are already docked and maybe primed for SV release, whereas the majority are in the terminal lumen. There is little molecular evidence to suggest that SVs are organised based upon differences in protein isoform or phospholipid composition, and no markers for differential recycling have been found (Rizzoli

and Betz, 2003; Alabi and Tsien, 2012) apart from some work by Kavalali *et al.* (see above).

Groups of SVs are currently classified into pools according to physiological response to stimulation. The three pools currently described are the readily releasable pool (RRP), the reserve pool (RP, also known as recycling pool), and the resting pool (RtP, also known as the reluctant pool and somewhat confusingly some people call this the reserve pool) (Figure 1.3). It is not established yet if these pools can be defined further in terms of activation state, coined sub-pools (Doussau *et al.*, 2017).

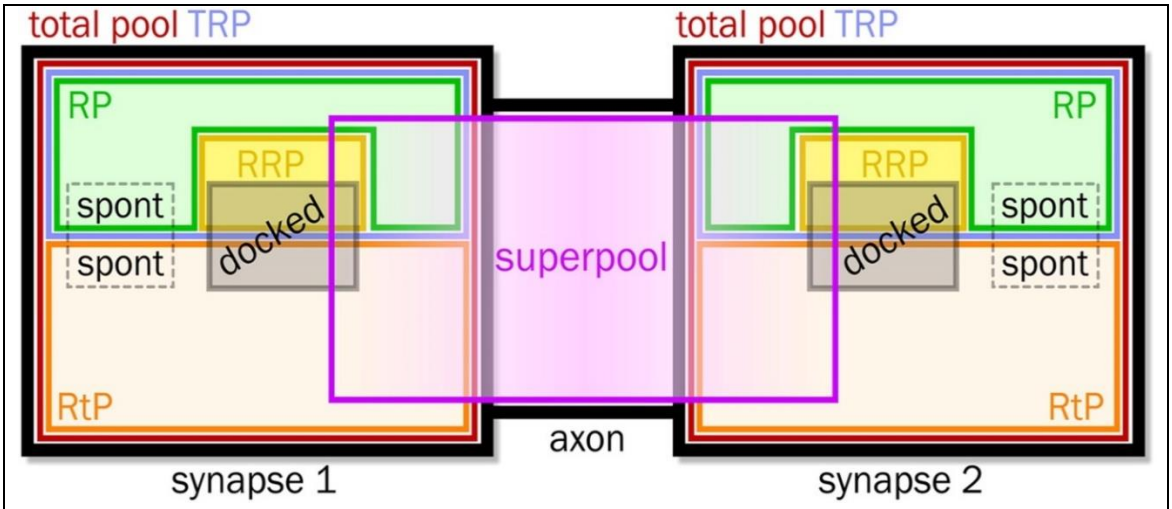

Figure 1.3: Diagram of known vesicle pool classifications and relationships. The pools shown are the total pool, total recycling pool (TRP), reserve pool (RP), resting pool (RtP), readily releasable pool (RRP), docked pool and superpool. The spontaneous pool is indicated by dashed rectangles reflecting uncertainty in defining its place within existing pool structures. The two synapses reflect a supposed neuron with two terminals. Approximate relative magnitudes of pools by vesicle number are indicated by relative box sizes. Note that these sizes are for hippocampal synapses and that the TRP represents the RP and RRP that releases and not the SP. Also note that in the model employed in this thesis there is no superpool of SVs as isolated nerve terminals cannot exchange SVs with others; the superpool only exists within en passant boutons along an axon and will not exist at true nerve terminals including those at neuromuscular junctions(diagram from Fowler and Staras, 2015).

All SV exocytosis occurs exclusively at AZs, and SVs are modulated to be targeted to this area for neurotransmitter release (Michel *et al.*, 2015). The AZs recruit certain proteins including RIM, Munc13, RIM binding protein (RIM-BP),

α-liprin and ELKS proteins, which dock and prime SVs at the AZs for release, coupled to voltage-gated Ca^{2+} channels (Südhof, 2013). The t-SNAREs, soluble N-ethylmaleimide sensitive fusion protein (NSF) attachment protein 25 (SNAP-25) and syntaxin, interact with the v-SNARE synaptobrevin at this location, and these are intimately involved in SV fusion (Rizo and Rosenmund 2008; Shi *et al.*, 2012; Zhou *et al.*, 2015). The first opening when SV and PM fuse is the fusion pore which is a direct channel between the SV lumen and the extracellular space. In neurons fusion pores are ≤ 20 nm in diameter and in ≤ 100 µs release neurotransmitter from the SVs (Lindau and Alvarez de Toledo, 2003; Jackson, and Chapman, 2006).

Normally the RtP is not able to be released under any observed physiological condition but can be released under intense non-physiological stimulation, or by pharmacological means (Fernandez-Alfonso and Ryan, 2008). Perhaps contrary to assumptions of efficiently utilising SVs, the RtP contains the largest proportion of SVs with approximately 80% (in hippocampal synapses), whilst the RRP contains less than 5% of SVs present (Rizzoli and Betz, 2005; Denker *et al.*, 2011; Fowler and Staras 2015). The reason for the large number of SVs in the RtP is still not understood although it is debated to be due to individual neuron plasticity or specific intracellular function, with the RtP size determined perhaps during cell maturation (Harata *et al.*, 2001; Rizzoli and Betz, 2005; Ikeda and Bekkers, 2009; Denker and Rizzoli, 2010). The RtP cannot be released during physiological stimulation and its *in vivo* function and natural conversion process into an active SV is unknown. The RP can be converted into the RRP, and the fused vesicles can be recycled back into the RP (Rizzoli and Betz, 2005).

1.3 Synaptic Vesicle Fusion and Exocytosis

Fusion of SVs is needed to release neurotransmitter cargo into the synaptic cleft. Much is currently unknown regarding SV activation and movement to the AZ. However, some protein mechanics have been described at the AZ for SV priming and fusion.

In vertebrates the AZs are disc-like structures with diameter 0.2-0.5 µm. The AZs are surrounded by peri-active zones, where much of the endocytosis of fully fused vesicles takes place. The AZs allow precise predictability of where neurotransmitter release takes place (Kittel and Heckmann, 2016).

After AP conduction to the terminal, a rapid increase in intracellular Ca^{2+} ($[Ca^{2+}]_i$) resulting from voltage-gated Ca^{2+} channels opening triggers exocytosis. The proteins that form part of the exocytotic machinery apart from the SNAREs are NSF and co-factor α-soluble NSF attachment protein (α-SNAP), Munc18/Sec1, Munc13, synaptotagmins and Rab3 with its effectors (Südhof, 2013).

In a resting neuron in physiological conditions, the RRP is already docked at the AZ awaiting to exocytose – Ca^{2+} concentration increases in physiological conditions due to terminal depolarisation from AP conduction to trigger the vesicle fusion. Fusion pores are rapidly formed due to coupling of the Ca^{2+} channel with RIM and its binding proteins RIM-BP, releasing the neurotransmitter content (Barclay *et al.*, 2005; Rizo and Rosenmund, 2008; Hosoi *et al.*, 2009). It is indicated that the RRP can be recycled independently of the RP during low intensity stimulation which keeps recycling efficiency with demand (Ashton and Ushkaryov, 2005; Rizzoli and Betz, 2004).

The RP begins to migrate toward the AZ and undergoes docking and fusion once the RRP is exhausted. This occurs when stimulation is more intense, or more frequent (Denker and Rizzoli, 2010). Such SVs are exposed to a lower $[Ca^{2+}]_i$ (as the initial high concentration at the AZ has dissipated) and so these may utilise distinct synaptotagmin isoforms or another Ca^{2+} sensor for their Ca^{2+} dependent release, although this process is not well understood (Volynski and Krishnakumar, 2018).Fasshauer *et al.* (1998) classified SNAREs into R-SNAREs and Q-SNAREs depending on conserved arginine or glutamine

sequence respectively in the SNARE motif. Synaptobrevin (also known as vesicle-associated membrane protein/VAMP-2) is an R-SNARE, syntaxin 1 and SNAP-25 are Q-SNAREs. These three proteins associate to form the SNARE complex, which will then form protein-protein interactions with Munc18/Sec1, Munc13, synaptotagmins and complexin. Initially the α-SNAP overlays the SNARE complex and allows NSF binding, which it was thought to mediate vesicle fusion action due to adenosine triphosphate (ATP) hydrolysis and allows binding. However, it is now generally considered that NSF is not involved to affect exocytosis. After exocytosis the SNARE complex disassembles (Barclay *et al.*, 2005; Seino and Shibasaki, 2005; Jahn and Fasshauer, 2012) and it is this process that requires NSF and α-SNAP.

The protein Munc18/Sec1 is a negative regulator of SNARE complex assembly by binding and constraining syntaxin 1 in a 'closed' inactive form(Barclay *et al.*, 2005; Seino and Shibasaki, 2005; Jahn and Fasshauer, 2012). The protein Munc13 is a positive regulator of the SNARE complex by physically preventing the binding of Munc18 to syntaxin 1, allowing activation of the SNARE complex. However, the role of Munc18 is complicated because it would appear that whilst part of this molecule binds to the syntaxin and this can be displaced by Munc13, another part can bind to the SNARE complex such that it may also be a positive regulator (Südhof and Rothman, 2009).

The RIM protein functions as the central organiser of the AZ. This protein tethers the Ca^{2+} channels to the AZs and also interacts with Rab3 once SVs have docked with guanosine triphosphate (GTP)-bound Rab3 (Barclay *et al.*, 2005; Seino and Shibasaki, 2005; Jahn and Fasshauer, 2012). In the presence of Ca^{2+}, synaptotagmin binds to Ca^{2+} using its C2 domains and interacts with the AZ phospholipid membrane. Binding of synaptotagmin to syntaxin SNARE protein also occurs using these C2 domains.

The process of SV exocytosis is summarised in Figure 1.4 and Figure 1.5, without distinction between full fusion (FF) and kiss-and-run (KR) modes.

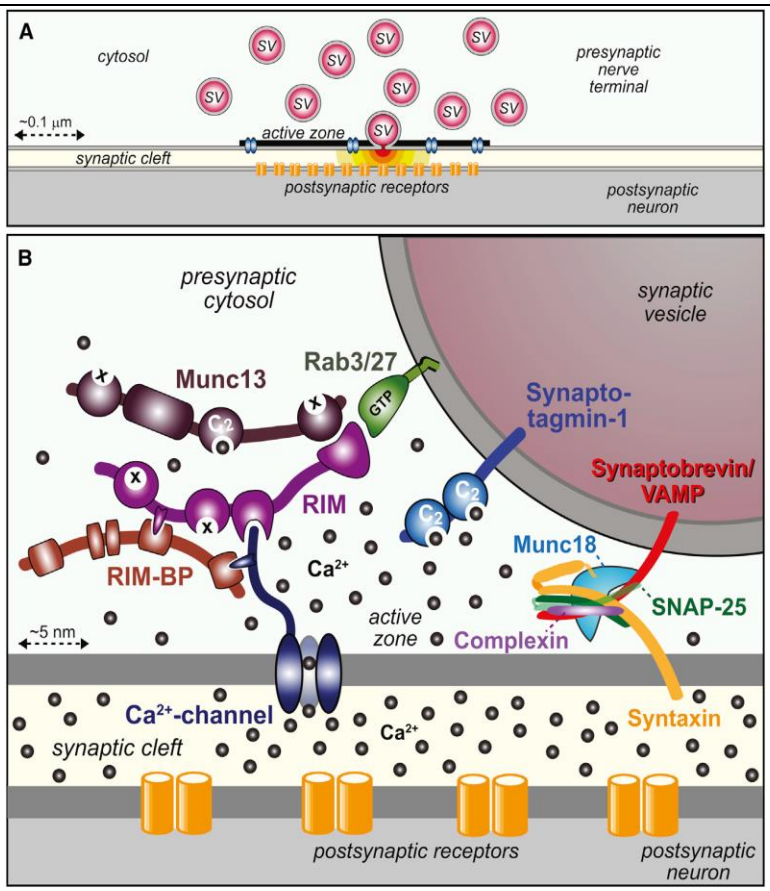

Figure 1.4: Diagram of the active zone proteins and interactions. (A) Synapse with SVs (red), an AZ containing Ca^{2+} channels (blue), and a postsynaptic cluster of receptors (orange). One vesicle in the AZ is depicted in the process of PM fusion at the AZ, with neurotransmitter released into the synaptic cleft. (B) Molecular machinery mediating SV fusion using Ca^{2+}. This depicts part of a docked SV on the top right and the AZ in the middle. Three functional elements of the neurotransmitter release machinery are depicted from right to left. On the right, the core fusion machine composed of the SNARE/SM protein complex is shown, comprising of SNARE proteins synaptobrevin/VAMP, syntaxin-1, SNAP-25 and SM (Sec1/Munc18-like protein family) protein Munc18-1. Ca^{2+} sensor synaptotagmin-1 is depicted in the middle, which binds Ca^{2+} to its cytoplasmic C2 domains, and functions using complexin (bound to SNARE complex) as an assistant. On the left is the AZ protein complex containing RIM, Munc13 and RIM-BP, with a Ca^{2+} channel in the presynaptic PM. In this protein complex RIM binding to specific target proteins coordinates all three functions of the AZ: RIM binding to vesicular Rab3 and Rab27 isoforms mediates vesicle docking; RIM binding to the Ca^{2+} channel, both directly and indirectly via RIM-BP, recruits Ca^{2+} channels within 100 nm of the docked vesicle for fast excitation-secretion coupling. The machinery here enables fast and efficient triggering of release in response to an AP by combining fusion machinery with Ca^{2+} trigger and AZ protein complex that is all positioned in efficient proximity (from Südhof, 2013).

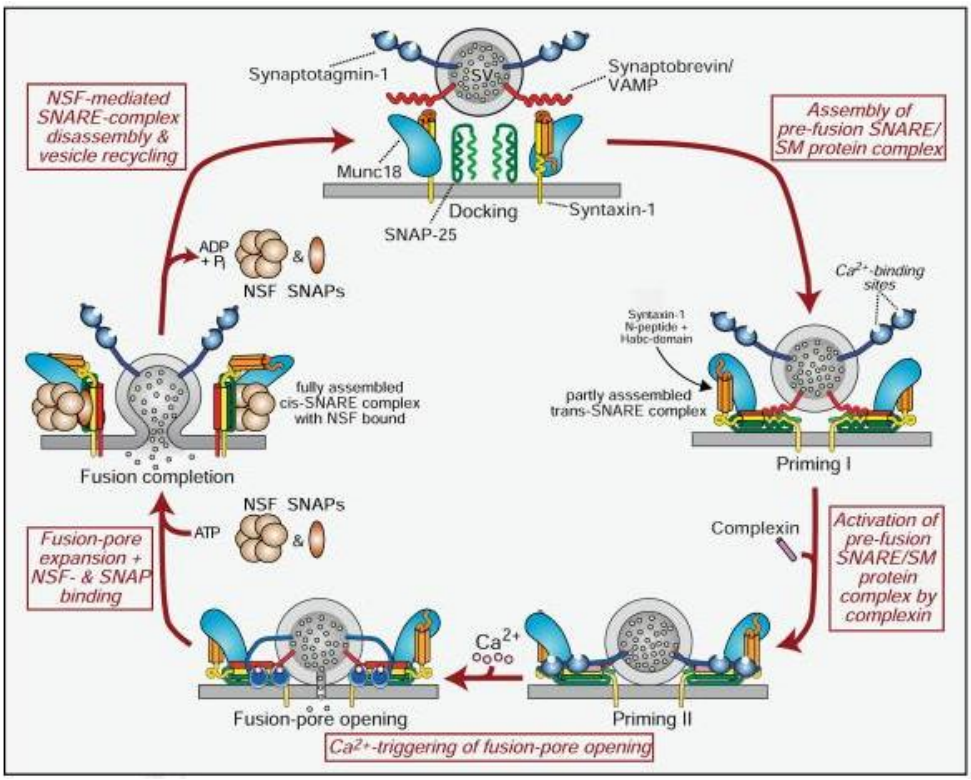

Figure 1.5: Diagram of the SNARE/SM complex mediating synaptic vesicle fusion, and the role of synaptotagmin and complexin upon Ca^{2+} stimulus for fusion. SNARE protein syntaxin-1 in closed conformation has its Habc-domain bound to its functional SNARE motif. Syntaxin-1 has to open for SNARE-complex assembly to start. Munc18-1 is associated with monomeric closed conformation syntaxin-1 – as syntaxin-1 opens during complex assembly, Munc18-1 alters the mode of its binding to syntaxin-1 by binding to assembling trans-SNARE complexes via interaction with syntaxin-1 N-peptide. The vesicular SNARE protein, synaptobrevin, assembles during priming into a trans-SNARE complex with the SNAREs on the PM, syntaxin-1 and SNAP-25. Once SNARE complexes are partially assembled, complexin binds to further increase priming. The 'superprimed' SNARE/SM protein complexes are ready for Ca^{2+} -triggered fusion pore opening by Ca^{2+} binding to synaptotagmin, which causes synaptotagmin to activate SNAREs and phospholipids. After fusion-pore opening and neurotransmitter release, the resulting cis-SNARE complexes are disassembled by NSF/SNAP ATPases and the SVs are then recycled (from Südhof, 2013).

A typical small nerve terminal in the CNS contains approximately 200 SVs in total (mainly based on work on hippocampal cultured cells) yet individual SV exocytosis occurs with high frequency for prolonged lengths of time, which would cause depletion of the releasable pools. Clearly, in normal physiological conditions the SVs are rapidly recycled so that the SV numbers are kept from

exhausting (Rizzoli, 2014). This will occur until short-term synaptic depression, caused by depletion of releasable SVs at the pre-synapse, until these SVs have recycled and neuron resting potential is reached (Fioravante and Regehr, 2011). Full fusion (FF) exocytosis was initially described by Heuser and Reece (1973) in experiments with frog neuromuscular junctions, describing a near instantaneous neurotransmitter release at the AZ. In FF mode the fusion pore expands and the SV, unable to retain shape, fully collapses into the PM (Rizzoli and Jahn, 2007; Rizo and Rosenmund, 2008). Upon collapse the SV protein complex and lipid arrangement keeps SV identity intact, a phenomenon still not fully understood, which then migrates from the AZ to the peri-active zone in the immediate vicinity, where these components allow for SV reconstitution by a clathrin-dependent endocytic process, described in Section 1.5.

The SV fully collapses into the PM in the FF process, whereas alternatively it may undergo kiss-and-run (KR) instead. Data obtained by Ashton and group support the hypothesis that KR mode exists (Ashton *et al.*, unpublished work; Bhuva, 2015; Singh, 2017). This data suggests that stimulation of synaptosomes with extracellular K^+ raised to 30 mM (HK) or 5 µM ionomycin (ION) with 5 mM Ca^{2+} causes the RRP to undergo the KR mode of exocytosis and the RP to undergo FF mode of exocytosis. The difference in exocytosis protein mechanics with KR is discussed in the following sections.

1.4 Synaptic Vesicle Endocytosis and Recycling

Each type of physiological endocytosis to retrieve SVs from the PM is used for different reasons by the neuron; most likely this represents a compromise between speed and energy efficiency. However, it is debated which modes of SV endocytosis physiologically exist and under what specific situations. The mode of endocytosis is maybe dependent upon factors such as stimulation intensity and duration, and short- and long-term plasticity (Granseth *et al*., 2006; Harata *et al*., 2006; Wu and Wu, 2007; Mellander *et al.*, 2012; Marland *et al.*, 2015; Nicholson-Fish *et al*., 2015). There are four main modes pertaining to SV recycling: clathrin-mediated endocytosis (CME), activity dependent bulk endocytosis (ADBE), kiss-and-run (KR) and ultrafast endocytosis (UE).

Of the considered modes of endocytosis, CME, ADBE and UE all act following FF exocytosis. Endocytosis can occur via clathrin and dynamin dependent means as this CME can directly recycle individual SVs without an endosomal intermediate. This occurs only at low frequency stimulation. Following high frequency stimulation, a large portion of the PM, containing many SVs, is retrieved to form an endosome, from which SVs are later generated, as with ADBE (Sone *et al.*, 2000; Cano and Tabares, 2016). Following one SV fusion event, UE retrieves sections of the PM approximately equal in surface area to four SVs which then proceeds to join into a large endosome in the terminal lumen from which SVs are later generated by a clathrin-dependent pathway. For an SV to completely recycle and be re-available for release it takes 5-10 s for UE, whereas it takes 1-2 s for recycling after KR. (Watanabe and Boucrot, 2017).

The process of CME is ubiquitous and vital in all eukaryotic cells to internalise extracellular or membrane material. In respect to nerve terminals clathrin coated vesicles are endocytosed from the peri-active zone. In CME, SVs are recovered at this region by clathrin and dynamin-dependent mechanisms (Figures 1.6a and 1.7). For 1-2 s clathrin coated pits are attached to the PM by a remaining narrow neck of phospholipid membrane. In order for the clathrin coated pit to detach and become a recycled SV, the neck must be severed to make an intact spherical vesicle. Dynamin is the active protein in this membrane scission, a guanosine triphosphate hydrolase (GTPase) motor protein which oligomerises and spirals around these necks to cause the membrane to destabilise and undergo fission to make a clathrin coated vesicle. The clathrin coat comes off and the recycled SV fills with neurotransmitter to be primed again (Stowell *et al.*, 1999; Hinshaw, 2000; Yamashita *et al.*, 2005; Heymann and Hinshaw, 2009; Ferguson and De Camilli, 2012; Cocucci *et al.*, 2014).

The clathrin coat consists of an inner layer of adaptors and the outer clathrin lattice. The inner layer is made of various proteins that bind to phospholipid heads of phosphatidylinositol 4,5-bisphosphate (PIP_2) and endocytic factors. The outer clathrin layer is a triskelion scaffold shaped protein complex that increases curvature of the membrane during formation, until an invaginated coated pit is formed, also utilising Bin/amphiphysin/Rrs domain (BAR domain) proteins and actin dynamics. Scission to separate the membranes is performed

by the dynamin complex. The clathrin coat is removed by heat shock cognate 70 (Hsc70) adenosine triphosphate hydrolase (ATPase) and auxilin. The vesicle generated is made available for use in another round of exocytosis. Since the protein composition of an SV membrane is vital to proper SV functioning, there must be checkpoints to ensure that all the essential proteins are included during recycling via this pathway, although these mechanisms are not fully understood. (Takei and Haucke, 2001; Shupliakov *et al.*, 2002; Saheki and de Camilli, 2012; Kononenko and Haucke 2014).

The ADBE pathway is activated during intense stimulation conditions, wherein a large amount of fully fused SVs require fast internalisation to keep the PM size and shape stable. In this pathway there is a large invagination of the PM, this infolding then undergoes fission (some suggest that this is via dynamin whilst others disagree) to form a large endosome upon which budding occurs in order to reconstitute recycled vesicles. These precursory endosomes disappear as new SVs are formed (Saheki and de Camilli, 2012). It has been suggested that ADBE replenishes the RP of vesicles (Cheung and Cousin, 2013). The speed of this process is debatable; in comparison to CME this could possibly be slower, although some claim that is quite fast, (as fast as normal CME) and ADBE may only be utilised to quickly retain PM size (Clayton *et al.*, 2008).

The ADBE process is mainly involved during strong stimulations wherein a quick membrane intake is needed due to a relatively large amount of SV fusion (Figures 1.6c and 1.7)**.** This process is observed to be dependent upon activation of the calcium/calmodulin dependent protein phosphatase calcineurin (also known as protein phosphatase 2B, PP2B). During intense stimulation PP2B dephosphorylates dynamin-1 (triggered by increasing $[Ca^{2+}]_i$) which results in interaction with the FCH domain BAR (F-BAR) protein syndapin, an interaction required to generate SVs from ADBE endosome intermediates (Cheung and Cousin, 2013; Cheung and Cousin, 2019).

In KR mode a transient fusion pore is made, then neurotransmitter is released without fusion of the SV into the PM. The fusion pore is instead closed, and the SV is translocated to be recycled without a clathrin dependence (Figures 1.6b and 1.7). This is the fastest of the hypothesised modes of endocytosis in

respect to forming recycled SVs ready for further release. There is further detail of KR mode in Chapter 1.5.

Ultrafast endocytosis (UE) is a relatively new discovery made by Watanabe *et al*. using *C. elegans* and mouse hippocampal models. In this process the SVs undergo FF and are then retrieved directly from endocytic invaginations that appear 50-100 ms after SV fusion (Watanabe *et al.*, 2013). The UE process retrieves sections of the PM approximately equal in surface area to four SVs which then proceeds to join into a large endosome in the terminal lumen from which SVs are later generated by a clathrin-dependent pathway (Figures 1.6d and 1.7). Note that UE does not at physiological temperature (37°C) require clathrin for the initial endocytosis. Through interactions with adaptor proteins, clathrin forms a spherical structure which invaginates the membrane into clathrin coated pits on the endosome (Von Kleist *et al.*, 2011; Rizzoli, 2014). It takes 1 s after stimulation to make an endosome. It then takes 3 s for clathrin coated vesicles to form and detach from the endosome. These coated vesicles transition into SVs 5-6 s after initial stimulation. The endosomal process occurs at the interstitial zone, which is adjacent to the AZ and surrounded by the peri-active zone. The endocytic invaginations formed are approximately 80 nm in diameter (Watanabe *et al*., 2013).

UE has been observed in mild stimulatory conditions – such as with 1 AP. The time taken for the whole recycling process is approximately 5 s whereas KR takes 1 s. Therefore, KR may still be a faster recycling process than UE which may only occur under low stimulation conditions (Saheki and de Camilli, 2012; Watanabe *et al.*, 2013; Kononeko and Haucke 2014; Watanabe *et al*., 2014; Zhou *et al*., 2015). This is particularly important as the PM would shrink drastically if lots of SVs' exocytosis led to UE.

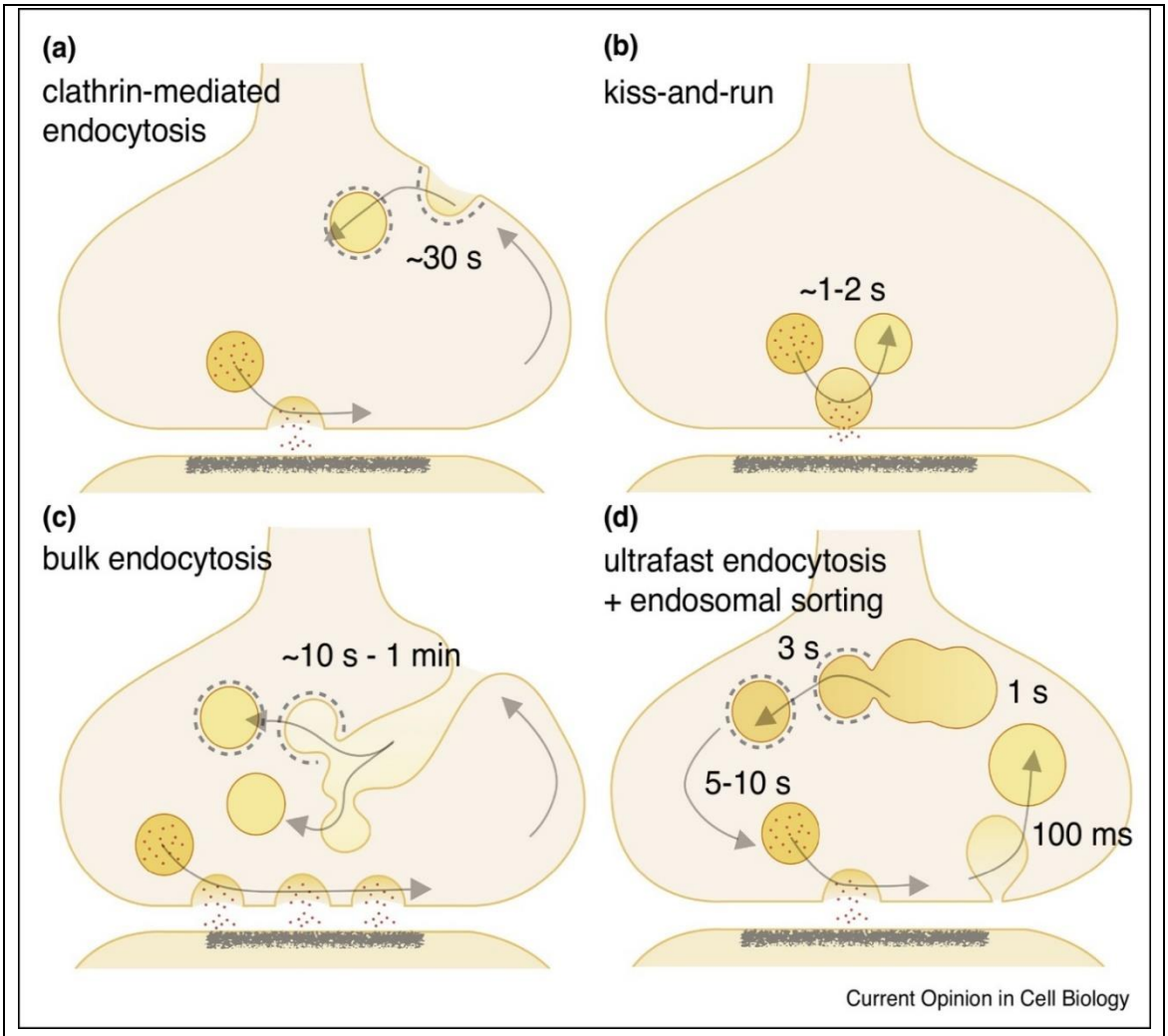

Figure 1.6: Diagram of current understanding of endocytic mechanism dynamics at pre-synapses. (a) Clathrin-mediated endocytosis (CME) from distal sites after FF of SVs. (b) KR of SVs comprising of the SV fusion pore opening and closing without full integration into AZ. (c) Activity-dependent bulk endocytosis (ADBE) from distal sites after intense stimulation-mediated FF. SVs may be reformed from internalised cisternae although it is possible that other types of this endocytosis may require clathrin. (d) Ultrafast endocytosis (UE) following FF, with clathrin-dependent reformation of SVs from endosomes (diagram from Watanabe and Boucrot, 2017).

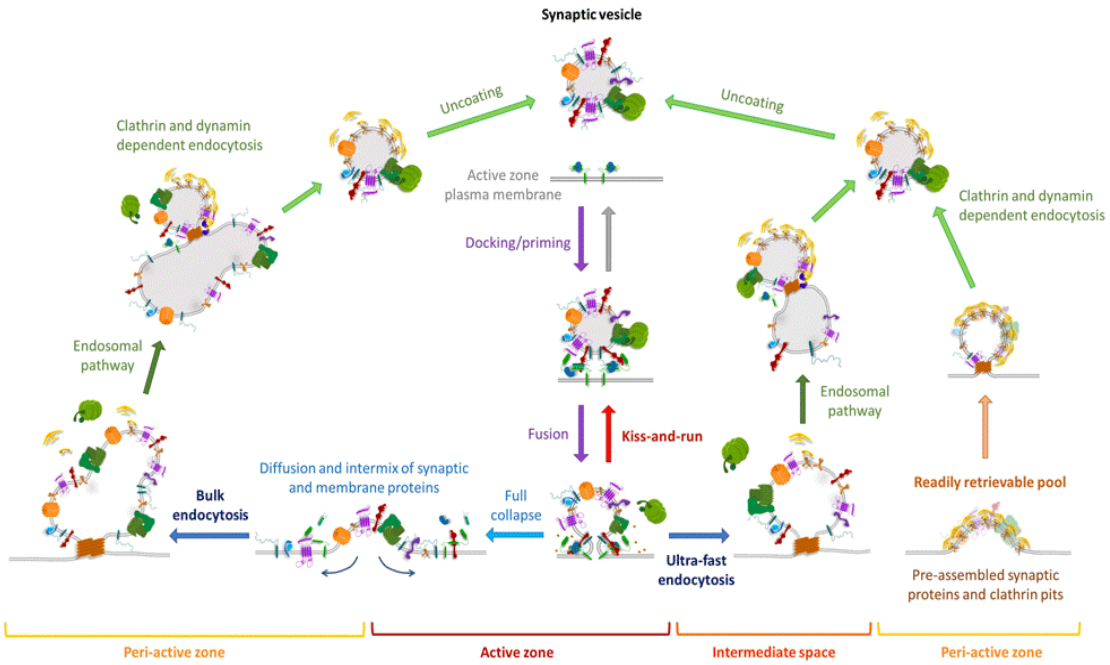

Figure 1.7: Diagram of currently considered modes of synaptic vesicle endocytosis. After docking and priming, SVs are ready to fuse with the AZ membrane (purple arrows). After fusion, SVs can be retrieved by the fastest way without morphological change, keeping SV identity, by closing the fusion pore (KR, red arrow). Alternatively they could fully collapse, intermixing components with the PM (FF exocytosis, light blue arrow). SV proteins can be specifically retrieved from the PM via ultrafast endocytosis (UE) (blue arrow, bottom right), or slowest via activity-dependent bulk endocytosis (ADBE) from sustained stimulation (blue arrow, bottom left), forming endosomal intermediates which are not confirmed to be morphologically or molecularly similar to each other. SVs may be regenerated from the endosomes by clathrin-dependent means (green arrows) although the well characterised ADBE may not have a clathrin requirement. SV proteins can also be rapidly retrieved from pre-assembled clusters containing adaptor protein and clathrin, which is endocytosed synchronously upon stimulation for neurotransmitter release, known as clathrin mediated endocytosis (CME, orange arrow) (from Chanaday and Kavalali, 2017).

1.5 Kiss-and-Run Mode

In the KR mode, neurotransmitter is released through a transiently open fusion pore that does not fully expand. It instead undergoes closure so that the SV can be recycled without having to be reconstituted, and this process bypasses both CME and sorting of SV proteins for recycling, making the SV recycling much faster (Kononenko *et al*., 2013). CME would put tremendous pressure on total recycling pool vesicles to maintain timely and efficient exocytosis, due to amount of time and energy invested in transporting, reconstituting and priming the endocytosed vesicles for more release. It is proposed that KR helps to conserve resources during periods of high frequency stimulation, ensuring that terminals do not lose neurotransmitter release capacity . Factors that cause KR activation rather than FF are not fully deciphered, but it is thought that relatively high frequency of stimulation and high $[Ca^{2+}]_i$ - which strong stimulation would cause - correlates with the switch of exocytotic mode to KR (Harata *et al.*, 2006). The rate of exocytosis in high stimulation circumstances can surpass the quantity of SVs present but the KR process, by substituting FF, speeds SV recycling to enable release to keep up with demand. KR was first studied by Ceccarelli *et al.* (1973) in frog neuromuscular junctions. The average time for CME is 15-20 s whilst for KR the fusion pore closes in 0.5 s or less. KR is hypothesised to be used as a means to bypass the time requirement of CME and to utilise less energy.

The contribution that KR makes to neurotransmitter release in nerve terminals is still a highly debated issue. However, results suggesting that KR is prevalent in nerve terminals include Harata *et al.* (2006) who have shown the prevalence of KR in hippocampal neurons using bromophenol blue to quench incompletely released FM dye. Bromophenol blue is a water-soluble reagent that quenches green emission of fluorophores and does not pass through membrane. Upon stimulation, any fusion pore formation – during KR exocytosis – will allow bromophenol blue to enter into the luminal domain of the SV and this will quench FM 2-10 dye bound to the vesicular membrane. This will reduce the fluorescence in a similar manner to when FM 2-10 dye de-partitions from the vesicular membrane during FF exocytosis. Thus, it caused little or no difference in fluorescence in FF mode of SVs, as FM dye would quench anyway, but quenched SVs undergoing KR, as FM dye would stay bound to the SV

membrane. Capacitance measurements by He *et al*. (2006), at giant synapses demonstrate presence of KR mode whilst Zhang *et al.* (2009) have used measurement of recycling of quantum dots in SVs to show KR mode. Some KR mechanisms have been shown to produce sub-quantal release of transmitter e.g., catecholamine release from adrenal chromaffin cells (Mellander et al., 2012). However, it has been argued that when all Glu from an SV is released by KR and that there is no sub-quantal release of this transmitter when this mode of exocytosis occurs (Alabi and Tsien, 2012). Ashton *et al.* (unpublished data; see Appendix A) have shown that a switch in the mode of exocytosis can be achieved by modulating $[Ca^{2+}]_i$ which regulates protein phosphorylation in such cases, in synaptosomes. Strong stimulations of nerve terminals cause the RRP to undergo KR mode whilst the RP fuses by FF mode.

This thesis presents research into the contribution of dynamin and NMII to the mode of SV exocytosis and the next section provides some information about NMII.

1.6 Non-Muscle Myosin II in Synaptic Vesicle Release Dynamics

1.6.1 Non-Muscle Myosin II Structure and Properties

NMII molecules are ubiquitous actin-based motors that generate force from chemical energy. They are well characterised and have a vital plethora of roles in cell dynamics, working not unlike their muscle counterparts in various mechanical reactions within the cell. These include cytokinesis, cell adhesion, cell migration and tissue morphogenesis. NMII also acts within specific actin structures such as stress fibres and contractile rings (Gormal *et al.*, 2015; Shutova and Svitkina, 2018).

NMII is an actin binding protein that has contractile properties mediated by phosphorylation of its heavy chains (HC) and light chains. NMII molecules either ‘walk along’, propel the sliding of or produce tension on fibrous actin (F-actin) using chemical energy from ATP hydrolysis induced by the catalytic sites on the N-terminal of NMII. The C-terminal of some myosins bind to and moves cargo

intracellularly whereas the C-terminal in other myosins self-associate into filaments which provide tension when tethered to F-actin (Beach *et al.*, 2011).

NMII is comprised of two 230 kDa HCs, two 20 kDa regulatory light chains (RLCs) that regulate NMII activity and two 17 kDa essential light chains (ELCs) that stabilise the HC structure. The two globular head domains of NMII contain a binding site for the enzymatic ATPase motor domains and the actin binding site. The ELC and RLC associate with the HCs via interaction with IQ motifs found near the globular head, known as the neck domain. This domain acts as a lever to amplify head rotation while the ATP is hydrolysed for chemical energy. The RLC is bound to the HC non-covalently. After the neck there is an α-helical coiled-coil rod/tail domain which mediates NMII HC homodimerisation and filament assembly. The molecule terminates with a non-helical tailpiece (Sandquist and Means 2008). More details of NMII protein mechanics can be found in Figure 1.8.

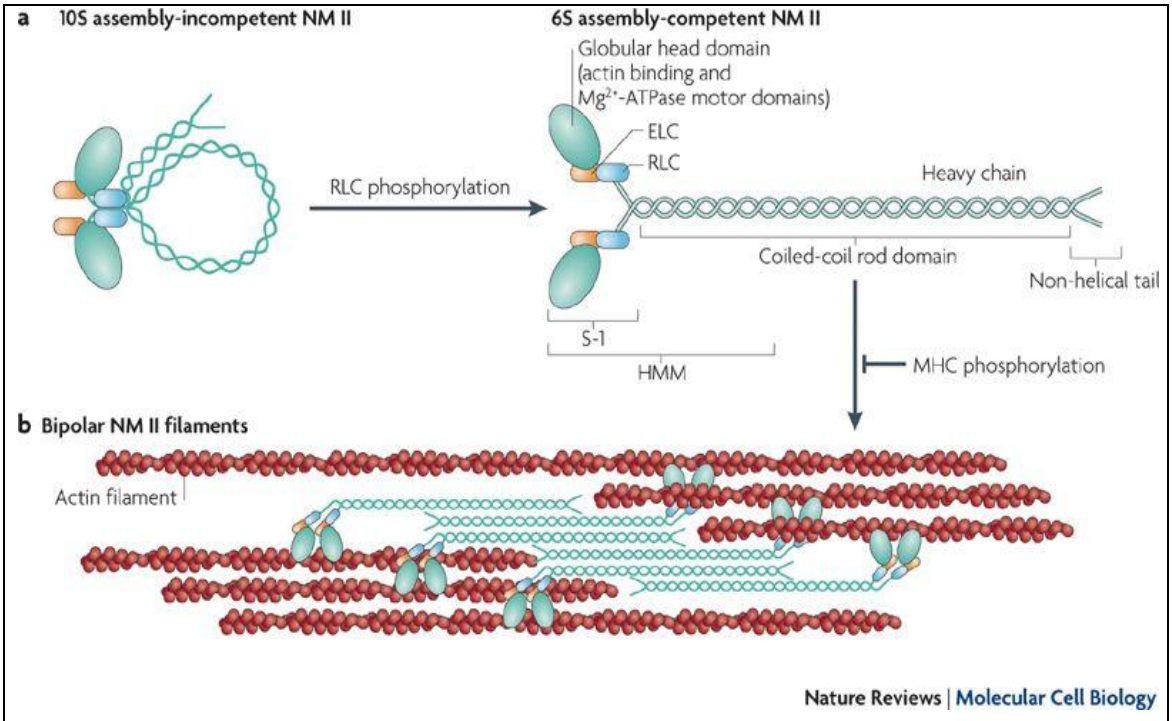

Figure 1.8: Diagram of non-muscle myosin II activation and assembly with F-actin. a) The subunit and domain structure of NMII, which dimerises through interaction of the α-helical coiled-coil domains. The globular head domain consists of the actin-binding regions and the Mg^{2+}-ATPase motor domains. The essential light chains (ELC) and the regulatory light chains (RLC) bind to the heavy chains (HC) at the lever arms that link the head and rod domains. When the RLC is unphosphorylated, NMII forms a compact assembly-incompetent 10S form through head-tail interaction, which is unable to associate with other NMII dimers. On RLC phosphorylation, the 10S structure unfolds to become a 6S assembly-competent form. b) NMII assembles into bipolar filaments by their rod domain interactions. These filaments bind to actin through their head domains and the ATPase activity of the heads enables a conformational change that moves actin filaments in an anti-parallel manner. Bipolar myosin filaments link actin filaments together into bundles which form a range of cellular structures, such as acto-NMII rings in granule endosome formation (from Vicente-Manzanares, 2009).

Three genes in mammalian cells encode NMII HC proteins: MYH9, MYH10 and MYH14. These genes determine the NMII isoform (distinguished by HC type), named NMHC-IIA, NMHC-IIB or NMHC-IIC respectively. For NMII motors to retain active conformations the LCs must be bound to the HCs. The mammalian HC pre-messenger ribonucleic acids (pre-mRNAs) that are transcribed as shown in humans and mice undergo alternative splicing, predominantly in neuronal tissue, which increases the total number of expressed NMHC-II proteins to nine (Li *et al.*, 2008, Jana *et al.*, 2009).

The LCs are encoded by a different set of genes, which can also undergo alternative splicing, and there is currently no known specificity of LCs for particular NMHC-IIs. Despite having a high degree of homology, particularly in their actin-binding globular heads, the NMII isoforms are spatially segregated in some areas of cells, but clearly overlap in others. Some cellular fractionations are isoform-specific whereas others are redundant (Vicente-Manzanares *et al.*, 2007). NMIIB is particularly well suited to exert tension on actin filaments for longer periods of time and with less expenditure of energy than NMIIA. Whereas the different enzymatic and motor activities of NMII reside in the N-terminal, the C-terminal rod and non-helical tail determine the assembly of NMII filaments and the intracellular localisation of the NMII isoforms (Kovács *et al.*, 2007).

The three NMII isoforms expressed in mammals co-assemble to form mixed bipolar filaments implicating possible diversity in function of the NMII congregates. Studies in cell lines and mice have demonstrated specific and redundant roles for all three isoforms (Wang *et al.*, 2011). Isoform role in SV release dynamics is not established. All three isoforms are able to assemble into bipolar filaments and contract F-actin in an ATP-dependent manner (Sandquist and Means, 2008).

1.6.2 The Role of Non-Muscle Myosin II and Actin in Regulating the Fusion Pore

Although the transient fusion pore is kept open < 0.5 s in KR exocytosis in neurons (Harata *et al*., 2006), the precise mechanisms that control fusion pore maintenance and closure are not well understood. Several research groups have shown in non-neuronal cells that NMII plays important roles in shifting the exocytotic mode from KR exocytosis to FF exocytosis and speeds up the release of catecholamine in FF exocytosis (Doreian *et al.*, 2008; Berberian *et al.*, 2009; Chan *et al.*, 2010 b).

Although very little is known about NMII mechanics in the the SV release cycle, NMII in SV exocytosis might have analogous roles to those in granule exocytosis in other cell types. Therefore, it is important to try to understand NMII

and actin mechanics in nerve terminals, as such results obtained pertaining to NMII mechanics with SV exocytosis will be novel.

NMII is activated by phosphorylation of the RLC by activation of myosin light chain kinase (MLCK). In chromaffin cells, NMII regulates the final steps of granule recruitment to the PM at the cell periphery (Aoki *et al.*, 2010). Furthermore, NMII phosphorylation increased the rate of fusion pore dilation whereas inhibition of NMII activity led to stabilisation of the secretory fusion pore in chromaffin cells. Indeed, NMII is selectively phospho-activated under elevated firing conditions where it drives collapse of the KR fusion event to full granule collapse and content release (Chan *et al.*, 2010 b). The control of the FF exocytotic process requires that NMII is active at the site of granule fusion, either directly pulling on the granule membrane or through dynamic rearrangement of F-actin surrounding the granules; an issue still not clarified. This action could compress the vesicle or exert a force driving full vesicle collapse.

These models are very intriguing because in glutamatergic nerve terminals, Ashton and colleagues have found the opposite result with NMII (see Figures A9-A10 Appendix A and results in thesis). In its active state, when phosphorylated by conventional protein kinase C (PKC), it would appear to drive KR mode and when it is inhibited, FF mode can occur. This may simply represent a subtle difference between non-neuronal and neuronal cells. This could also be due to the way NMII interacts with the actin cytoskeleton; indeed, if the actin forms a ring around the fusion pore and this is contracted by NMII, with actin as a lasso, then this could lead to pinching off (fusion pore closing) of the SV. Fusion pore closure in KR may depend upon different macromolecular complexes forming because in the chromaffin cell it has been suggested that dephosphorylated active dynamin-1 can produce a pore expansion complex that would also include recruitment of active NMII to actively dilate the fusion pore during elevated sympathetic firing for full granule collapse (Chan *et al*., 2010 b). Fusion pore closing in KR of SVs may be comparable to granule endocytosis in that they both include an acto-NMII framework, indicating some similar protein types involved. One hypothesis of the actin ring formation and bulk endosome formation by Gormal *et al.* (2015) includes an acto-NMII ring

and dynamin pinching. NMII constricts the ring to aid separation of the nascent endosome from the PM.

It would appear that constricting acto-NMII rings appearing following stimulation are critical for the fission of bulk endosomes from the PM in neurosecretory cells. In this context, PIP_2, actin, NMII, and dynamin provide a molecular framework on which to build a more comprehensive picture of the mechanism underpinning bulk endocytosis. Revealing bulk endocytosis in neurosecretory cells may lead to further understanding of the molecular mechanism driving ADBE in other cellular systems. This shows the possibilities of NMII constricting the fusion pore, but it is important to emphasise that in nerve terminals Ashton has found that when NMII is activated to contribute to the KR mode of the RRP of SVs, the dynamin-1 molecule is inactivated by phosphorylation at the same time. This again suggests a difference in the role of NMII between nerve terminals and other non-neuronal secretory cells. Furthermore, some of the effects characterised for actin and NMII on chromaffin cell secretion would appear to involve accelerating dissociation of catecholamines from the intergranular matrix possibly through generation of mechanical forces, perhaps compressing this matrix when activated (Berberian *et al.*, 2009). Such a matrix does not exist for glutamate present inside SVs; thus, the cytoskeleton and NMII may exert different effects on different vesicle types.

Analysis showed that SV dynamics are highly dependent on the expression level of NMII at *Drosophila* neuromuscular junctions wherein NMII is present in the presynapse and is important for SV mobility. NMII contributes to the spontaneous release of vesicles differentially from evoked release, suggesting differential contribution to these two release mechanisms (Seabrooke *et al.*, 2010)

It was found that NMII is important for normal synaptic transmission under high-frequency stimulation (Seabrooke and Stewart, 2011). This result is complementary to Ashton and colleagues' findings wherein NMII only participates in regulating the mode of exocytosis under strong stimulation conditions. Inactivation of presynaptic NMII decreases the probability of synaptic retrieval but did not impede synaptic release. These results indicate that NMII driven tension or actin dynamics regulate the major pathway for SV

retrieval and that strength of synaptic transmission in cultured hippocampal neurons strongly depends upon NMII activity (Chandrasekar *et al.*, 2013). In the studies carried out by Ashton and colleagues, a role of NMII during recycling has not been investigated as the data obtained is exclusive to exocytosis of SVs and not their subsequent endocytosis. However, one can regard fusion pore closure during KR as a form of endocytosis.

The actin filaments also serve as a molecular scaffold for the recruitment of actin priming molecules, which form functional nanoclusters at exocytic sites, which have activity in actin remodelling and subsequent steps of exocytosis. This has been shown in Weibel-Palade granule exocytosis in endothelial cells, where the focal adhesion protein zyxin is enriched in the actin framework which then recruits α-actinin and NMIIA which are needed for actin filament cross-linking and contractility of the actin complex structure around the granules (Nightingale *et al*., 2011; Han *et al.*, 2017).

Secretagogue stimulation in chromaffin cells remodels the actomyosin network to not only translocate and dock granules but also contributes toward fusion pore kinetics (Meunier and Gutierrez, 2016). The movement of cortical structures and secretory vesicles appear to be linked, and NMII inhibitor blebbistatin and F-actin stabiliser jasplakinolide treatment increases distance of secretory vesicles to the PM fusion sites. Thus, there was slower single vesicle fusion kinetics in these drug treated cells, linked to the retraction of the F-actin cytoskeleton from the PM (Villaneuva *et al.*, 2012). Also, inhibition of NMII by blebbistatin decreases the number of granule release events. Expression of non-phosphorylatable NMII prevents fusion pore expansion (Berberian *et al*., 2009). Inhibition of actin polymerisation by cytochalasin D decreases expansion rate of fusion pore and increases opening duration (Neco *et al.*, 2008). Further, cortical actin filaments form actin coats, also known as actin rings, at the surface of large granular vesicles (Merrifield *et al.*, 2016).

Actin polymerisation and nucleation, mediated by nucleation factors are critical for actin ring formation, triggered at the boundary between PM and the vesicle membrane, as shown in *Xenopus* ovum granules. The main function of these actin rings is to constrict the granules, in order to expel the cargo as compensatory exocytosis. NMII is recruited to exocytosing cortical granules late

in coat compression; NMII inhibition slows coat compression without affecting actin assembly. Inhibition of actin assembly negates cortical granule exocytosis completely. Thus, actin dynamics are needed for cortical granule exocytosis, and NMII is used for efficient completion. Myosin 1e is recruited to cortical granules immediately after egg activation, and its inhibition results in only partial actin coat assembly and induces cortical granule collapse into the PM. Therefore, myosin 1e and NMII are part of machinery that coordinates coat compression at exocytosing cortical granules (Yu and Bement, 2006).

Evidence suggests that actin-coating is completed by these steps: actin monomers (G-actin) are recruited to make linear actin fibres (F-actin) mediated by elongation factors (Miklavc *et al*., 2015), then actin related protein 2/3 complex (Arp2/3 complex) binds to linear actin and catalyses formation of actin branches (Merrifield, 2016). NMII is recruited to the actin coat structure where it functions as the molecular motor that drives contractility of the coat. Inhibition of NMII leads to prolonged lag time between fusion and complete cargo release, indicating less efficient exocytosis (Nightingale *et al*., 2011).

Changes in the acto-NMII network tension could contribute to granule exocytosis with NMII exerting its action via actin network contraction (Miklavc *et al*., 2015). Src kinases that regulate actin polymerisation also regulate fusion pore expansion. Two processes appear to regulate different stages of exocytosis: formation of new actin filaments and disruption of the cortical actin network are induced by Ca^{2+} concentrations that trigger exocytosis.

Inhibition of actin polymerisation with neutral Wiskott-Aldrich syndrome protein (N-WASP) inhibitor wiskostatin restricts fusion pore expansion, limiting the release of transmitter (in cells where transmitter needs to de-complex before leaving the granule interior). The disruption of cortical actin with cytochalasin D increases amount of transmitter released per event. Further, Src kinase inhibitor protein phosphatase 2 and c-Src also suppress Ca^{2+} dependent actin polymerisation, and slow down fusion pore expansion without disturbing cortical F-actin structure. Finally, the isolated Src homology 3 domain of c-Src prevents both the disruption of the actin network and increase in quantal release induced by cytochalasin D. These results support a model where a rise in the cytosolic Ca^{2+} triggers actin polymerisation through a Src kinase involvement. The newly

formed actin filaments would speed up expansion of the initial fusion pore, whereas pre-existing actin network might control a different part of the exocytotic process. The Src kinases that may regulate actin polymerisation also regulate expansion of the fusion pore. Chromaffin cell secretory vesicles release through KR mode with low-frequency electrical stimulation (0.5 Hz) whereas elevated electrical stimulation (15 Hz) evokes FF mode of release, which causes additional release of the neuropeptide-containing proteinaceous granule core (Olivares *et al*., 2014).

Also, the Src kinase substrates cortactin and N-WASP similarly promote actin polymerisation and regulate fusion pore expansion (González-Jamett *et al*., 2017). Actin polymerisation regulator, cell division control protein 42 (Cdc42) also regulates expansion of the vesicle fusion pore by regulating membrane tension (Bretou *et al*., 2014).

At low-frequency stimulation in chromaffin cells, the actin cortex has a key role in stabilising the KR fusion event. Increases in stimulation disrupts the actin cortex and causes FF mode. These same results are replicated *in vivo* where basal sympathetic firing causes transient KR mode of exocytosis and low catecholamine release, whereas elevated frequency under the sympathetic stress response results in FF mode of exocytosis which releases catecholamines and peptide transmitters into blood circulation. Thus, an intact actin cortex favours KR mode whereas actin cortex disruption favours FF mode (Doreian *et al.*, 2009).

The identification of nanoscale functions of the actin network demonstrates that cortical actin can regulate exocytosis behaviour both on the larger scale of the cortical actin network and nanoscale around secretory vesicles and between the plasma and vesicle membranes. However, these remodelling processes share some effectors, such as NMIIA, which could provide the basis for coupling and synchronicity to conduct exocytosis events (Papadopulos *et al*., 2015; Nightingale *et al*., 2011).

Microscale cortical actin remodelling is required to recruit various regulatory proteins. Similarly, the cortical actin filaments are reorganised to form nanoscale clusters that contain proteins and lipids that contribute to crosslinking

between actin and the vesicular and PMs, as shown in chromaffin cells (Gabel and Chasserot-Golaz, 2016). The molecules in these nanoclusters, including several signalling transduction proteins, are recruited to the fusion site of the PM by the exocytotic SNARE complex (Gabel *et al*., 2015). Both cyclic adenosine monophosphate (cAMP) and Ca^{2+}-mediated pathways use mutual effectors such as NMIIA, although effector function may vary (Miklavc *et al*., 2012). NMII is involved in the microscale function of the cortical actin network by mediating relaxation for vesicle translocation to the PM (Papadopulos *et al*., 2015; Meunier and Gutierrez, 2016). The formation of the actin framework and contractility of the actin coat after granule fusion pore opening also requires the presence and activity of NMIIA (Nightingale *et al*., 2011; Miklavc *et al*., 2012).

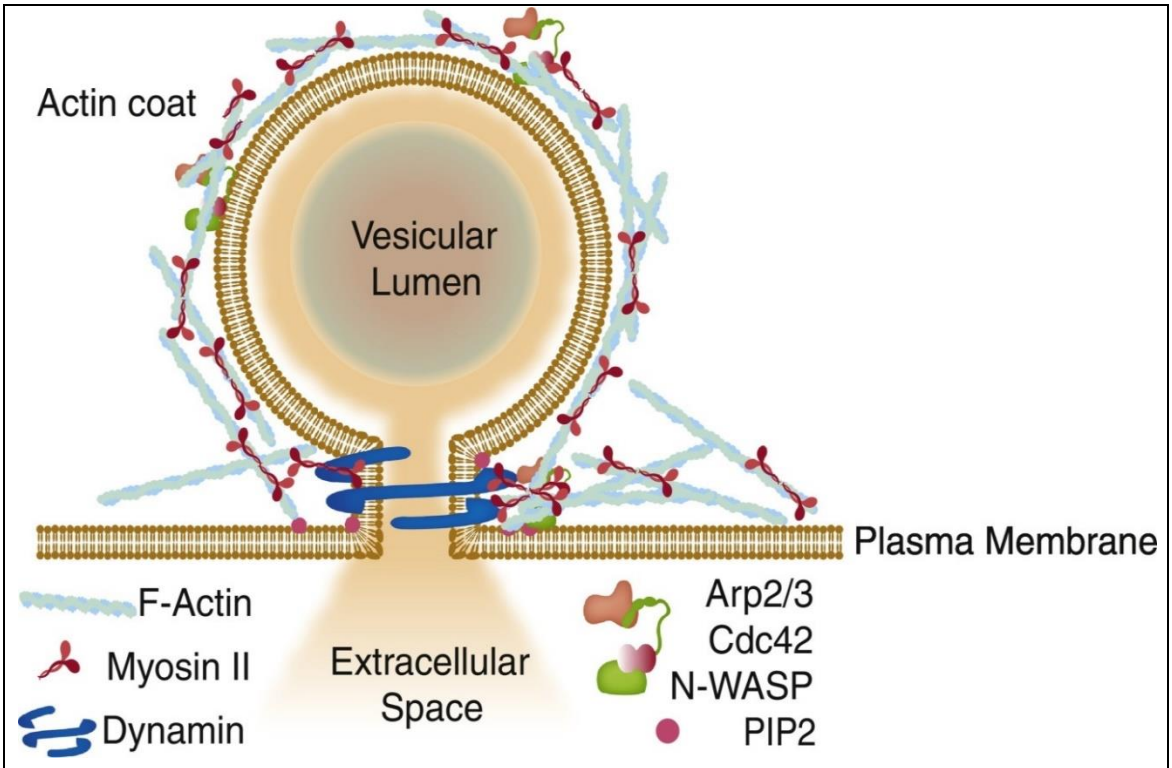

Figure 1.9: Diagram of non-muscle myosin II, F-actin and dynamin control granule content release through neurosecretory fusion pore. Upon formation of a fusion pore, both dynamin and NMII control width and duration of the fusion pore and thus the mode of exocytosis and the amount of neurotransmitter released in these non-neuronal cells. Nucleation and binding is mediated by interaction with PIP_2 and Arp2/3 complex including Cdc42 and N-WASP. In some secretory systems F-actin and NMII were found to form coats around fused granules to help release neurotransmitter by compression of the membrane-fused vesicle (from Papadopulos, 2017).

1.6.3 Non-Muscle Myosin II in Vesicle Mobilisation

In neurosecretory vesicle exocytosis, once the vesicles are tethered to the actin network, they are translocated to the PM activity-dependently. Green fluorescent protein-bound F-actin can demonstrate that secretory vesicles and the actin network simultaneously translocate toward the PM upon secretagogue stimulation, and shows that this is dependent on NMII function, including relaxation of the actomyosin network (as in Figure 1.9) (Papadopulos *et al*., 2015). In some studies, NMII has also been implicated in the involvement of mobilisation of RP SVs to near the synaptic membrane as inhibition of NMII phosphorylation appeared to perturb this process (Ryan, 1999).

In neurosecretory cells there is a dense mesh of cortical actin network, so how the secretory granules reach the PM is unclear. Granules embedded in the cortical actin network undergo a synchronised movement towards the PM and Munc18-1-dependent docking in response to secretagogue presence, coinciding with translocation of the cortical actin network, with Munc18-1 priming synataxin 1A for SNARE complex assembly (Kasula *et al.*, 2016). Both effects are abolished with NMII inhibition or knockdown, suggesting changes in acto-NMII generated forces are involved in this process. There is also reduction in cortical actin network tension upon secretagogue stimulation which is reversed by NMII inhibition. It is thought that the cortical actin network acts as a casting net that undergoes activity-dependent relaxation, allowing granules toward the PM for docking (Papadopulos *at al*., 2015).

A study of Ω-shaped profiles of SVs, which corresponds to the shape of SVs undergoing fusion, identified a novel tentative role of actin polymerisation in generating the tension needed to pull SVs back into the terminal during KR endocytosis. Inhibition of actin polymerisation in lamprey synapses led to accumulation of Ω-shaped membrane profiles at AZs. Actin polymerisation inhibitor cytochalasin D and actin de-polymerisation drug latrunculin A induce Ω-profile accumulation in lamprey synaptic AZs (Wen *et al*., 2016). This concept is supported by demonstrating SV fusion upon an increase in membrane tension (Staykova *et al.*, 2011). In adrenal chromaffin cells, where the relevance and prevalence of KR in neurosecretory granules is accepted, the Ω-shaped profiles are also made when actin is stabilised by drug treatment when KR is

induced; the actin acts as a scaffold that transiently supports and stabilises the Ω-shaped profile (Doreian *et al.*, 2008).

The actin network in other cell types also aids fusion pore formation and maintenance with the generation of actomyosin surrounding the secretory vesicles to help extrude the neurosecretory contents following release trigger (Miklavc *et al*., 2012). This granule profile is prevalent upon low frequency stimulation or low Ca^{2+} concentration, whereas high frequency stimulation or high Ca^{2+} concentration effectively disrupts the actin network, leading to FF of granules. It is possible that the SVs have analogous dynamics with KR as compared to the neurosecretory granules (Meunier and Gutierrez, 2016). The dynamic actin structures and nanoscale remodelling optimises the AZ environment for SV/granule release for fusion and promoting full release of cargo.

1.6.4 Non-Muscle Myosin II Phosphorylation and Activation State

More than a dozen kinases have been reported to phosphorylate the RLCs of NMII including MLCK, rho-associated, coiled coil-containing kinase (ROCK), citron kinase, leucine zipper interacting kinase (ZIPK) and myotonic dystrophy kinase-related CDC42-binding kinase (MRCK) (Somlyo and Somlyo, 2003). These kinases phosphorylate RLCs on Ser19, Thr18 or both, to make the NMII complex assembly competent.

The regulation of NMII depends upon reversible phosphorylation of the RLC on Ser19. This phosphorylation event greatly increases ATPase activity of NMII in the presence of actin by controlling myosin head conformation, and as stated before this allows the myosin HC to become assembly competent. However, phosphorylation has little to no effect on NMII affinity for actin. The additional phosphorylation of Thr18 in the presence of phosphorylated Ser19 further increases total actin-activated ATPase activity at sub-saturating actin concentrations (Wendt *et al.*, 2001).

The RLC can also be phosphorylated at Ser1/Ser2/Thr9 by PKC, although Beach *et al.*, (2011) investigated the role of Ser1/Ser2/Thr9 phosphorylation in

live cells but found that manipulation of these sites did not significantly alter NMII function in a number of assays. It may be possible though that PKCs have a role with NMII in other cellular processes or types of cells *in vivo*. This is particularly relevant in view of the role of NMII that A. Ashton's group have ascertained (see Appendix A). It is that NMII is activated by PKC, which of course may be working on Ser1/Ser2/Thr9 site. This suggests that A. Ashton's group is studying a distinct process for NMII than has been previously described.

There are several phosphorylation sites near the C-termini of NMHCs, in both the coiled-coil domain and the non-helical tail, including sites that are phosphorylated by PKC and casein kinase 2 (CK2) (Dulyaninova *et al.*, 2005). A number of laboratories have reported that Ser1917 in rat NMHC-IIA is phosphorylated by PKC, and phosphorylation of this site by PKCβ correlates with exocytosis in mast cells (Ludowyke *et al.*, 2006). It is clear that considerable regulation of NMII occurs through phosphorylation of the HCs, particularly in the tail region (phosphorylation details are described in Figure 1.10). The continued characterisation of the roles of these different phosphorylation events on NMII function and isoform-specific regulation should produce important new insights of phosphorylation effect on NMII activation state.

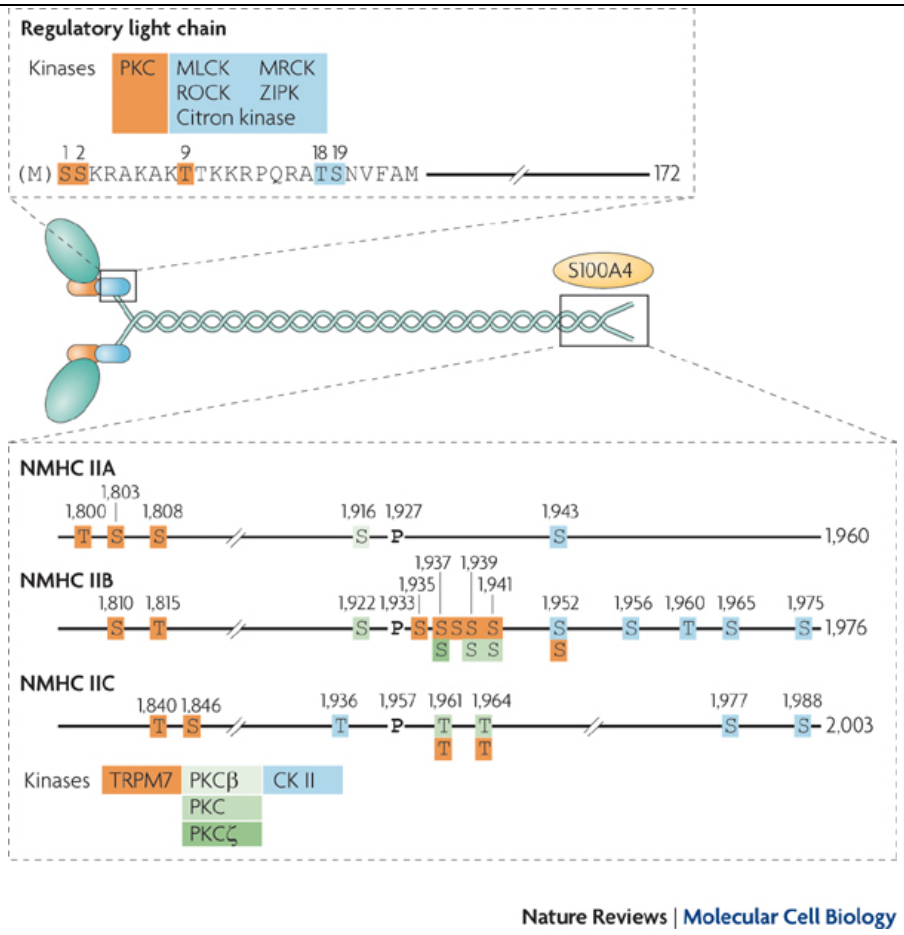

Figure 1.10: Diagram showing the various phosphorylation sites on NMII RLC and HC in its three different isoforms A, B and C. Multiple kinases, including myosin light chain kinase (MLCK), Rho-associated, coiled coil-containing kinase (ROCK), citron kinase, myotonic dystrophy kinase-related CDC42-binding kinase (MRCK) and leucine zipper interacting kinase (ZIPK) can phosphorylate the regulatory light chain (RLC) on Ser19 or on both Thr18 and Ser19 and activate it. Protein kinase C (PKC) can phosphorylate the RLC on Ser1, Ser2 and Thr9 to inhibit it. NMII filament assembly is regulated by phosphorylation of the NMII HC coiled-coil and tail domains. The HC phosphorylation sites are phosphorylated by the corresponding kinases, including transient receptor potential melastatin (TRMP7), PKC proteins and casein kinase 2 (CK2) for all human NMII HC isoforms. PKC mediated phosphorylation of the HC on Ser1916 and Ser1937 and CK2 on Ser1943 prevent assembly of NMII into filaments. Phosphorylation of NMII HC by CKII blocks the binding of S100A4 to the HC tail to prevent S100A4 inhibiting NMII filament assembly. How these modifications are integrated to induce whole protein activation states to induce physiological responses has yet to be elucidated (from Vicente-Manzanares *et al.*, 2009).

Several kinases phosphorylate NMHC-II isoforms directly. Transient receptor potential cation channel M7 (TRPM7) phosphorylates Thr1800, Ser1803 and

Ser1808 which reduces NMHC-IIA integration with the actin cytoskeleton. PKC phosphorylates NMHC-IIA on Ser1916 and -IIB on multiple tailpiece serines leading to inhibition of filament assembly. CK2 phosphorylates NMHC-IIA on Ser1943 and increases disassembly of 2A filaments (Breckenridge *et al*., 2009). Phosphorylation of RLC at Thr18 and Ser19 is well-established to activate NMII motor activity and increases NMII filament stability and is the basis for its contractile motion. By contrast other phosphorylation sites on RLC may inhibit NMII activity. PKC phosphorylates Ser1/Ser2 and Thr9 and this phosphorylation decreases activated NMII interaction with actin, as well as inhibiting RLC interaction with the activation site kinase, MLCK (Tan *et al.*, 1992).

Although as stated before, *in vivo* such phosphorylations have not been shown to be important in some cells, the Ser1/Ser2 site is proposed as a major inhibitory site since Ser1 is phosphorylated during platelet-derived growth factor (PDGF)-induced stress fibre disassembly and expression of unphosphorylatable Ser1/Ser2 suppresses disassembly (Komatsu and Ikebe, 2007). When activated by general PKC activator phorbol ester/phorbol 12-myristate 13-acetate (PMA), PKC can phosphorylate Ser1 and Ser2 residues of RLC *in vivo* and it can also phosphorylate Thr9 *in vitro*. This PKC phosphorylation not only inhibits the rate of MLCK enacted phosphorylation of the RLCs, but also inhibits the ATPase activity of NMII once it is phosphorylated by MLCK. In case of NMIIA HCs, Ser1916 and Ser1943 are phosphorylated by PKC and CKII respectively. Ser1939 and Ser1941 of NMIIB HCs are phosphorylated by PKC (Bresnick 1999).

In endothelial cells, NMIIA is phosphorylated at different serine sites, Ser1916 and Ser1943 during exocytosis. A high level of phosphorylated Ser1943 is associated with positioning and translocation of vesicles, whereas after exocytotic stimulation Ser1916 is phosphorylated and mediates remodelling of the actin structures. This precise temporal regulation of NMIIA activity is controlled by the recruitment of CK2 by zyxin, which is responsible for Ser1943 phosphorylation (Li *et al.*, 2018). The microscale functions of the cortical actin network such as oscillation and relaxation of the cortex and nanoscale functions such as actin bundling and contractility are closely orchestrated for sequential exocytosis steps. This coupling on a higher order scale is highly dependent on PM protein nanoclusters.

It should be noted that PKC phosphorylations of all of these sites may be involved in activation of NMII. Thus, it will clearly depend upon what amino acid sites are phosphorylated as to what specific roles NMII may participate in – one should be aware that different site phosphorylation state combinations on the HCs may alter the activation state of the protein in differing ways, making the implications of single site phosphorylation on specific NMII roles difficult to understand due to many different phosphorylation site combinations. There is no current evidence to distinguish these individual protein states.

1.7 Dynamin in Synaptic Vesicle Release Dynamics

1.7.1 Dynamin Structure and Properties

Dynamin is a prototypical member of an atypical, multidomain family of GTPases involved in membrane fission and fusion implicated in vital endo- and exocytotic mechanisms of membrane fission and remodelling multiple organelles. In dynamin catalysed fission, it is proposed that dynamin's mechanochemical activities induce localised curvature stress which allows the catalytic lipid interacting pleckstrin homology (PH) domain to guide lipid remodelling through hemifission intermediate (Schmid and Frolov, 2011).

Dynamin family members share a highly homologous N-terminal GTPase domain as well as an α-helical middle domain and GTPase effector domain. Classical dynamins also encode a lipid-binding PH domain between the middle domain and GTPase effector domain and a C-terminal proline-arginine domain that mediates protein interactions with Src homology 3 domain–containing binding partners. Dynamin exists as a tetramer in solution. The GTPase effector domain and middle domain interact to form a stalk-connecting the lipid-binding PH domains to the guanosine binding domains. Mutations in the stalk disrupt both tetramerization and higher-order assembly (Schmid and Frolov, 2011). Figure 1.11 pictures the structure of monomeric and tetrameric dynamin.

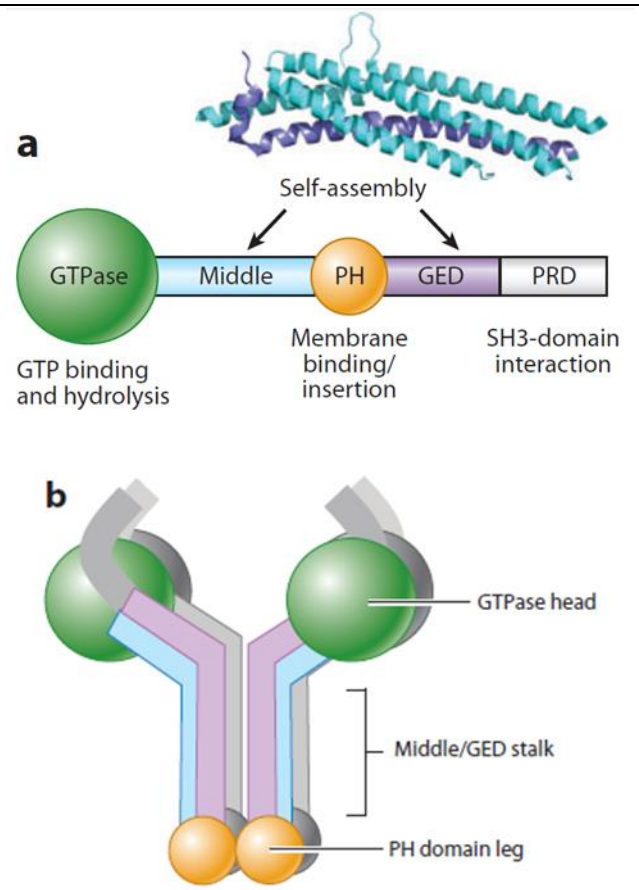

Figure 1.11: Diagram of the structure of dynamin. (a) Monomeric form of dynamin showing pleckstrin homology (PH) domain, GTPase effector domain (GED), and proline rich domain (PRD). (b) Tetrameric form of dynamin. Taken from Schmid and Frolov (2011).

Dynamin interacts, either directly or indirectly, with several proteins that are known to be important in exocytosis, including actin (Gu *et al.*, 2010), the SNAREs (Galas *et al.*, 2000), and synaptotagmin (Robinson and Bonifacino, 2001).

1.7.2 Dynamin Role in Regulating the Fusion Pore

The hypothesis for dynamin having a role in membrane fission came from structural analysis of Drosophila that express a temperature-sensitive dynamin homologue *shibire*, wherein the flies are paralyzed upon shifting to the non-permissive temperature due to synaptic dysfunction (Grigliatti *et al.*, 1973). Electron micrographs revealed that presynaptic nerve terminals are depleted of SVs and instead accumulate Ω-shaped endocytic profiles, many of which are encircled at their necks by single or double electron-dense bands, or collars (Koenig & Ikeda, 1989).

In subsequent studies, long membrane invaginations, coated with clathrin at their base and encircled by multiple electron-dense bands, were shown to accumulate in permeabilised rat synaptosomes treated with the non-hydrolysable analogue guanosine 5'-O-[gamma-thio] triphosphate (GTPγS) (Takei *et al.*, 1995). The accumulation of these structures suggested a role for GTP hydrolysis in disassembling dynamin collars and/or severing these necks.

Total internal reflection fluorescence microscopy in living non-neuronal cells has revealed that green fluorescent protein-labelled dynamin is detected at low levels associated with nascent clathrin-coated pits, but also transiently accumulates at clathrin-coated pits just prior to clathrin-coated vesicle release (Merrifield *et al.*, 2002). These studies have established that the vesicle neck is a narrow, short-lived structure that is severed abruptly. Narrow necks have been detected by electron microscopy, although collars are seen, and the transient nature of these intermediates makes it difficult to analyse their geometry.

Interactions between Src homology 3 domain–containing proteins such as endophilin, sorting nexin 9 (SNX9), amphiphysin, intersectin and dynamin's proline-arginine domain occur early in the process and only later assembles at the neck in a PH domain-dependent manner (Bethoney *et al.*, 2009). Dynamin also regulates the turnover of early abortive intermediates in clathrin-coated vesicle formation (Loerke *et al.*, 2009) and when overexpressed in non-neuronal cells, most dynamin mutants block early stages of clathrin-coated vesicle formation (Damke *et al.*, 2001). Overexpression of some hypomorphic dynamin

mutants has been shown to accelerate the early, rate-limiting steps in CME (Song *et al.*, 2004). Acute inhibition of dynamin by the inhibitor dynasore blocks early as well as late stages of CME (Macia *et al.*, 2006).

The mechanism for dilation of adrenal chromaffin cell fusion pores using of peptide transfection, electrophysiology, electrochemistry and quantitative imaging techniques shows that disruption of dynamin-1 alters fusion mode of FF and KR. Under low stimulation, interference with dynasore does not affect granule fusion but blocks its re-internalisation. In FF mode, disruption of dynamin-1 limits fusion pore dilation, but does not block membrane re-internalization. These data suggest that dynamin-1 is involved in both modes of exocytosis by regulating contraction or dilation of the fusion pore and thus contributes to activity-dependent differential transmitter release from the adrenal medulla (Fulop *et al.*, 2008). It should be noted that just as with the role of NMII being investigated in the KR mode in nerve terminals, some of the results from other models would appear to suggest different requirements for dynamin between these and synaptosomes. This may be because the conditions employed are distinct or that different pathways are being activated.

Unexpectedly, mice lacking dynamin-1 were able to form functional synapses, even though their postnatal viability was limited. However, during spontaneous network activity, branched, tubular PM invaginations accumulated, capped by clathrin-coated pits, in synapses of dynamin-1 knockout mice. SV endocytosis was severely impaired during strong exogenous stimulation but resumed efficiently when the stimulus was terminated. Thus, dynamin-1 independent mechanisms can support limited SV endocytosis, but dynamin-1 is needed during high levels of neuronal activity. This contrasts with the collared but uncoated pits of the *Drosophila shibire* mutant synapses after stimulation at the nonpermissive temperature. This suggests that dynamin-1 is specifically dedicated to control plastic adaptation of the SV recycling machinery to high levels of activity (Ferguson *et al.*, 2007).

Dynamin-1 and dynamin-2 are neuronal and ubiquitously expressed isoforms, respectively, of the multidomain GTPase required for CME. Although they are 79% identical, dynamin-1 and dynamin-2 are not fully functionally redundant. Through direct measurements of basal and assembly-stimulated GTPase

activities, membrane binding, self-assembly, and membrane fission on planar and curved templates, it is shown that dynamin-1 is an efficient curvature generator, whereas dynamin-2 is primarily a curvature sensor (Liu *et al.*, 2011).

Dynamin-1/dynamin-2 chimeras identified the PH domain as being responsible for the different *in vivo* properties of these two isoforms. Remarkably, *in vitro* activities are reversed by a single amino acid change in the membrane-binding variable loop 3. Reconstitution of KO mouse embryo fibroblasts showed that both the PHand the Pro/Arg-rich domains determine the differential abilities of these two isoforms to support CME. These domains are specific to classical dynamins and are involved in regulating their activity. Such findings reveal opportunities for fundamental differences in the regulation of dynamin-1, which mediates rapid endocytosis at the synapse, contrary to dynamin-2, which regulates early and late events in CME in non-neuronal cells (Liu *et al.*, 2011).

The post-fusion fate of the granule membrane is regulated by dynamin GTPase activity. When dynamin GTPase activity is reduced (by inhibitor or expression of a dynamin mutant), expansion of the fusion pore is slowed with concomitant long-lasting membrane deformations. When dynamin GTPase activity is elevated by mutation, fusion pore expansion is accelerated, with more rapid curvature transitions. The findings expand the membrane-sculpting repertoire of dynamin to include the regulation of immediate post-fusion events in exocytosis and provide a direct biochemical and mechanistic link between secretion and endocytosis (Anantharam *et al.*, 2012).

Dynamin plays an important role in accelerating the fission event, preferentially in endocytotic vesicles of regular size, by increasing the rates of pore closure. Results suggest that fusion pores are dynamic structures that form thin and long membrane necks regulated by $[Ca^{2+}]_i$. (Cabeza *et al.*, 2010).

Dynamin is dephosphorylated in a calcium dependent manner by the phosphatase PP2B and recruited to sites of endocytosis. Dynamin forms a helical collar around the neck of a nascent vesicle. At the neck, dynamin can physically constrict membranes or undergo a lengthwise extension that drives the vesicle away from the membrane, causing lipid fission (Cabeza *et al.*, 2010).

1.7.3 Dynamin-1 Phosphorylation and Activation State

Dynamin is dephosphorylated on nerve terminal stimulation by PP2B and then re-phosphorylated by cyclin-dependent kinase 5 on termination of the stimulus. Dynamin-1 is present in both the cytosol and membrane of nerve terminals, however phosphorylated dynamin-1 is restricted to the cytosol although the resolution to detect low amounts of phosphorylated dynamin is problematical. Thus, the phosphorylation status of dynamin-1 would appear to regulate its localisation within the nerve terminal. It is assumed that the dephosphorylation of dynamin-1 facilitates its translocation to the PM for CME and its rephosphorylation directs its return to the nerve terminal cytosol (Smillie and Cousin, 2005).

Endocytosis kinetics at hippocampal and cortical nerve terminals show a bi-phasic dependence on electrical activity. Endocytosis accelerates for the first 15-25 APs during bursts of AP firing, after which it slows with increasing burst length creating an optimum stimulus for this kinetic parameter. Armbruster *et al.* (2013) showed that activity-dependent acceleration is only prominent at physiological temperature and that the mechanism of this modulation is based on the dephosphorylation of dynamin-1. Using versions of dynamin that were either permanently phosphorylated or never phosphorylated, a decrease in dynamin phosphorylation was required for the initial acceleration of endocytosis. This type of regulation seems to optimize the recycling of vesicles to enable neurons to respond effectively to brief bursts of stimulation. Given that dynamin phosphorylation is conserved in evolution, it is likely that regulation of synaptic endocytosis is a key mechanism for ensuring the efficient functioning of the nervous system.

It was investigated whether the isoforms of dynamin-1, at the whole brain and subcellular level, had differential phosphorylation. It is established that the dynamin-1 isoforms xa, xb, and xd were expressed in nerve terminals. Dynamin-1 xa was constitutively phosphorylated to a higher extent than the other isoforms despite identical sequences in the phosphorylated subdomains. Dynamin-1 xa had a 10-fold higher stoichiometry of diphosphorylation at Ser774 and Ser778 than dynamin-1 xb and xd combined. Diphosphorylation was 2-fold enriched in nerve terminals relative to whole brain and was preferentially

targeted for stimulus-dependent dephosphorylation. There are large differential phosphorylation of dynamin-1 phospho-sites in different variants and in different neuronal compartments that would be completely imperceptible to a large-scale phosphoproteomics approach (Chan *et al.*, 2010 a). This indicates that a low level of phosphorylation of dynamin in a subcellular fraction may not be detected by most conventional methods.

1.8 Research Aims

Ashton and colleagues have determined that under certain stimulation conditions, the RRP SVs undergo KR exocytosis, whereas the RP SVs undergo FF mode. Under strong stimulation conditions it has been found that NMII is activated by PKC and that this protein induces KR exocytosis of the RRP. Inhibition of NMII with the drug blebbistatin prevents closure of the fusion pore and now the fusion pore undergoes expansion producing FF mode. However, the use of ION5C – under conditions where specific PKCs are not activated – means that NMII does not regulate the KR mode of the RRP and instead dynamin-1 does.

In this project the role of cAMP, and protein kinase A (PKA) in regulating the KR mode of the RRP and the FF mode of the RP will be investigated. Exchange proteins directly activated by cAMP (EPAC) comes in two forms, EPAC1 and EPAC2, which function as nucleotide exchange factors for the Rap subfamily of Ras-like small GTPases. They are attributed to function in a number of cellular processes and they have demonstrated several roles for cAMP which are not mediated by the activation of its traditional effector cAMP - PKA (Schmidt *et al*., 2013). However, EPAC has not been tested for its role in SV exocytosis as of yet. Thus, as part of this study of the regulation of the KR mode by changes in cAMP, the roles of EPAC will be studied as well as PKA.

As NMII normally associates with F-actin microfilaments as a motor protein and dynamin can interact with this cytoskeletal component, the role of actin in the release of the SVs and the mode of exocytosis of the SVs will be investigated by employing various drugs which perturb the actin cytoskeleton. This is done by inhibiting or hyper-stabilising actin microfilaments using latrunculin A and

jasplakinolide. It is envisaged that perturbation of the actin may perturb the release of the RP of SVs but if this is determined then one can still study the RRP of SVs by using 4-aminopyridine (4AP) as a stimulus as this has been shown by A. Ashton to exclusively release just the RRP vesicles.

1.9 Hypothesis

The results obtained will provide further evidence that KR, as well as FF exocytosis, contributes to SV exocytosis.

Working hypothesis:

1. cAMP regulated processes including activation of PKA and EPAC will play some role in the release of the RRP and RP of SVs and may also regulate the actual mode of exocytosis of such SVs. These chemical reactions may distinguish between the dynamin dependent and NMII dependent KR modes of the RRP SVs.
2. The actin cytoskeleton may play a role in the release of the pools of SVs and may also play roles in either one or both of the dynamin and NMII dependent KR mode for the RRP.

CHAPTER 2: Materials and Methods

2.1 Methodological Approach

All the studies performed will utilise a preparation of nerve terminals (synaptosomes) prepared from the cerebral cortex of adult Wistar rat brain tissue.

To deduce the mode of exocytosis of SVs from synaptosomes with different drug treatments, the synaptosomes are preloaded with FM 2-10 dye and subsequently this dye is released by various stimuli. FM dye will be released from the SV providing that the SV exocytose by either an FF mode or by extended KR mode whereby the fusion pore opens for more than 0.5 s as after this time period FM dye will escape from the fusion pore but it will not be released by KR. Equivalently treated terminals will be stimulated, and endogenous Glu release will be measured using an enzyme coupled mechanism. Glu is released from all SVs that undergo fusion in glutamatergic terminals independent of the fusion mode. Such measurements will reveal which SV pools are exocytosed following various drug treatments. Both these assays are routinely used in lab, and it is these that have determined that KR and FF do exist, and that SVs can switch between these modes.

The effect on synaptosome bioenergetics after drug treatment will be determined to ensure the specificity of a drug's effect on evoked release. An extracellular flux analyser will be used to measure any perturbation of mitochondrial respiration after drug addition.

2.2 Rationale

2.2.1 Glutamate and FM 2-10 Assays of Drug Effects on Distinct Fusion Mechanisms

The glutamate and FM 2-10 release assays can be employed to investigate the mode of SV exocytosis by comparing any differences between the release of the neurotransmitter and the dye. Data on glutamate released directly correlates to the number of SVs that undergo exocytosis, and the FM data shows what proportion of the vesicles undergo full fusion and thus leads to a release of dye and a decrease in fluorescence. These two data groups can be compared to check what distinct pools are induced to undergo exocytosis and what type of fusion is induced.

These assays were used to investigate exocytosis upon protein kinase A (PKA) activation (using cBIMPS) or inhibition (using KT5720), adenylate cyclase (AC) activation (using forskolin) or inhibition (using 9-cp-ade). ESI-09 is an EPAC inhibitor that works directly downstream of AC by cAMP activation, so this drug is used to check for changes in exocytosis and any implications of this protein in neurotransmitter mode of release. The role of dynamin attachment to membranes will be investigated with MiTMAB, whilst the role of the cytoskeleton can be investigated with latrunculin A, an actin depolymeriser and jasplakinolide, an actin stabiliser. Phorbol myristate acetate (PMA; 40 nM) can be used to activate certain PKCs whilst okadaic acid (OA) is used to switch the RRP SVs to an FF mode and blebbistatin is used to inhibit NMII activity.

HK5C and ION5C stimulation is focussed upon in particular because from previous data by A. Ashton it is established that there is NMII independence in 4AP5C and ION5C stimulation evoked release but there is NMII dependence for HK5C evoked release of the RRP (see Figure A12-A14 in Appendix A). This is hypothesised to occur because HK5C cause high Ca^{2+} concentration at the active zone, allowing the phosphorylation of the NMII LC by conventional PKC but also by some unspecified various kinases (possibly MLCK, MRCK, ROCK, ZIPK, citron kinase). The higher Ca^{2+} also allows more dynamin to be phosphorylated, inactivating its action in regulating the mode of exocytosis of the RRP SVs. 4AP5C results are included because it has been shown to

release only the RRP whilst ION5C releases both the RRP and the RP but by a dynamin dependent process (see Appendix A). This allows comparison of 4AP5C, ION5C and HK5C results.

The results have implications on the details of distinct protein modification mechanisms that function on activating and deactivating SV pool fusion and the type of exocytosis.

2.2.2 Fura-2 Assay of Drug Effects on Endogenous Ca^{2+} Release

Control of mode of exocytosis may be dependent on $[Ca^{2+}]_i$ levels. To ascertain whether the drugs utilised show trends between $[Ca^{2+}]_i$ levels and mode of exocytosis a Fura-2 assay can determine the evoked changes in $[Ca^{2+}]_i$ after drug treatment.

Fura-2 AM is a cell permeable and Ca^{2+} insensitive fluorophore which is hydrolysed in the synaptosomes by endogenous esterases that remove the acetoxymethyl (AM) groups, leaving the negatively charged Fura-2 molecules intracellularly confined as they are unable to pass the PM. This acid form is Ca^{2+} sensitive and produces maximum fluorescence when bound to Ca^{2+} and excited at 340 nm and produces minimum fluorescence when Ca^{2+} free at 380 nm; emission wavelengths in both cases is 512 nm.

Thus $[Ca^{2+}]_i$ is estimated by calculating ratio of fluorescence 340/380 nm, expressed by the Grynkiewicz equation (Grynkiewicz *et al*., 1985):

$$[Ca^{2+}]_i = \frac{K_d \times \beta \times (R - R_{min})}{(R_{max} - R)}$$

Wherein dissociation contant (K_d) for Ca^{2+}/Fura-2 binding is 224 nM, R is the 340/380 ratio, R_{max} is 340/380 ratio during $[Ca^{2+}]_i$ saturation, R_{min} is 340/380 ratio during Ca^{2+} free conditions and β is ratio of average fluorescence of Fura-2 at 380 nm under Ca^{2+}-free and Ca^{2+}-bound conditions.

This assay can be used to estimate changes in intracellular Ca^{2+} when stimulated by a stimulation buffer following drug treatment. This enables one to

determine what effect a specific drug will have on Ca^{2+} levels. This is useful in elucidating whether it is the effect of modulated Ca^{2+} levels that cause changes in mode of exocytosis, and what pathways the drug may be involved in to cause this change.

2.2.3 Extracellular Flux Analysis of Drug Effects on Synaptosome Samples

One can be more confident in the validity of the experiments in this project by ensuring that aerobic mitochondrial respiration is not perturbed after drug administration, since vesicle transport and fusion is an active ATP-dependent process. It is possible that if a drug acts on more than the desired target or the target modulation leads to downstream perturbation of respiration that short-term glycolysis, aerobic respiration and ATP generation is reduced. A compromised bioenergetic environment may cause fewer vesicles to fuse at the AZ or cause a change in fusion mode. Therefore, after drug addition it is important that the bioenergetics is similar to control samples.

The Seahorse Biosciences XFp Extracellular Flux Analyser™ can measure the competence of mitochondrial respiration by measuring oxygen consumption by the sample to give oxygen consumption rate (OCR) values: this is determined by changes in the fluorescence of specific sensors incorporated into the probe of the analyser that measures oxygen in the extracellular environment. This gives a running trace over approximately 120 min (Figure 2.1). Using the addition of specific mitochondrial electron transport chain inhibitors after certain time points this will give a more comprehensive check to find if there is a difference between drug-treated and control samples in terms of oxygen consumption and proton production.

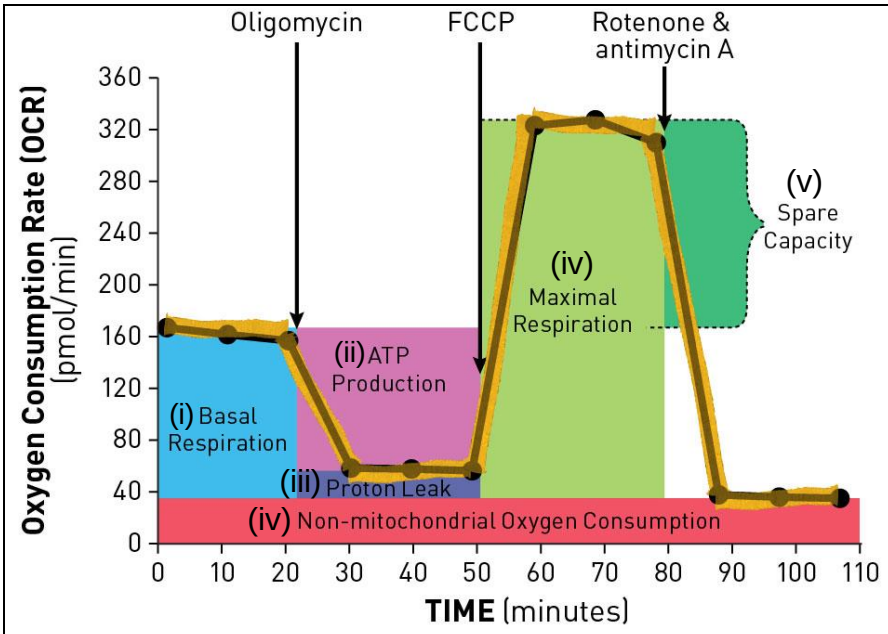

Figure 2.1: Graph of the Mito-Stress test time course to measure oxygen consumption rate. The Mito-Stress test detects six parameters of mitochondrial function to determine if ATP generation is compromised: (i) basal respiration – mitochondrial OCR at baseline conditions (ii) ATP production – ATP produced by the mitochondria at baseline conditions (iii) proton leakage – remaining basal respiration not caused by mitochondrial ATP production (may be due to mitochondrial damage or a factor that regulates ATP production (iv) maximal respiration – maximal OCR of the synaptosome sample, once the mitochondria are induced to function at maximum capacity (v) spare capacity – the difference between basal and maximal respiration, which indicates the range that the mitochondria can adjust to energetic demand (vi) non-mitochondrial respiration – shows any OCR which cannot be correlated to mitochondrial function. Oligomycin, an ATP synthase (complex V) inhibitor, when added should reduce the oxygen consumption so that one can get a measure of the ATP production. Carbonyl cyanide-p-trifluoromethoxyphenylhydrazone (FCCP) is an ionophore that disrupts ATP synthesis by transporting hydrogen ions through the inner mitochondrial membrane before they can be used to provide the energy for oxidative phosphorylation, causing the mitochondria to overcompensate oxygen consumption despite no further successful ATP production, allowing maximal respiration. The rotenone and antimycin A mixture is a complex I and complex III inhibitor respectively and this causes the mitochondria to become non-functional, meaning any further oxygen consumption is non-mitochondrial (graph from Agilent Technologies, 2019).

Specially designed 8 well utility plates (A-H) along with a sensor cartridge are used by the Xfp analyser. The sensor cartridge fits on a utility plate, placing drug ports (A-D) and a sensor probe into each of the 8 wells of the utility plate.

The design of the wells makes isolated micro-chambers while the sensor cartridge is fitted, which is analysed by the probes in each well. The drug ports contain the mitochondria-targeted drugs which are added at specific points during the assay to the wells to make the trace as described in Figure 2.1.

2.3 Materials

2.3.1 Materials Lists

Notable materials are listed in Table 2.1, Table 2.2. Note that adult Wistar rats (from 250-600g) were used, supplied by Charles River, USA.

RESOURCE	SOURCE
Drugs	
(±)-blebbistatin	Tocris
1-9-dideoxyforskolin	Tocris
4-aminopyridine	Sigma-Aldrich/Merck
9-cyclopentyl-adenine monomethanesulfonate	Sigma-Aldrich/Merck
antimycin A	Sigma-Aldrich/Merk
dynasore	Sigma-Aldrich/Merck
ESI-09	Sigma-Aldrich/Merck
Carbonyl cyanide-p-trifluoromethoxyphenylhydrazone (FCCP)	Sigma-Aldrich/Merck
forskolin	Tocris
ionomycin free acid	Tocris
jasplakinolide	Tocris
KT 5720	Tocris
latrunculin A	Tocris
MiTMAB	Tocris
okadaic acid	Tocris
oligomycin A	Sigma-

	Aldrich/Merck
phorbol 12-myristate 13-acetate	Tocris
rotenone	Sigma-Aldrich/Merck
Sp-5,6-DCl-cBiMPS	Santa Cruz Biotechnology
Reagents, Equipment and Solutions	
ADVASEP™-7	Sigma-Aldrich/Merck
Fura 2-AM	Thermo Fisher Scientific
Invitrogen™ FM™ 2-10 (N-(3-Triethylammoniumpropyl)-4-(4-(Diethylamino)styryl)Pyridinium Dibromide)	Thermo Fisher Scientific
L-glutamate dehydrogenase	Sigma-Aldrich/Merck
Seahorse Xfp Miniplate + Sensor Cartridge	Agilent
Triton™ X-100	Sigma-Aldrich/Merck
β-nicotinamide adenine dinucleotide phosphate ($NADP^+$)	Sigma-Aldrich/Merck

Table 2.1: Materials list. A list of specialised resources used in this thesis, noted with the source company.

MACHINERY AND SOFTWARE	SOURCE
Beckman-Coulter Avanti J-25 series centrifuge	Beckman
Eppendorf™ A-2-MTP Rotor	Thermo Fisher Scientific
JA-17 Rotor	Beckman
Seahorse XFp Analyzer and Wave Desktop Software	Agilent
Tecan GENIOS Pro infinite 200 plate reader and i-control™ software	Tecan
Teflon Potter Elvehjem tissue homogeniser	-

Table 2.2: Machinery and software list. A list of hardware and accompanying software used in this thesis with the source company.

2.3.2 Formulated Materials

Stimulus buffers:

Three 5mM Ca^{2+} based stimuli are used for differing synaptic vesicle pool release, established from previous work by A. Ashton; HK5C, ION5C and 4AP5C (containing 30mM K^{+}, 5µM ionomycin, 1mM 4-aminopyridine respectively). These stimuli have different modes of action to attain the individual effects, and 5mM Ca^{2+} gives maximal release for all these stimuli, with the RRP and RP released for HK5C and ION5C, and RRP only released for 4AP5C(see Figure A1 in Appendix A). They are used to compare similarities and differences in Ca^{2+} dependent exocytosis in each case (McMahon and Nicholls, 1991; Tibbs, *et al.*, 1989).Ca^{2+}-free solutions termed HK0 and 4AP0 are employed for basal conditions in Glu assays, as the lack of Ca^{2+} means that SV exocytosis does not occur. Due to the nature of ionomycin as a Ca^{2+} ionophore, which inserts into external and internal lipid membranes and releases Ca^{2+} stores, it is not possible to form a Ca^{2+}-free solution with synaptosomes, thus basal buffer (L0) is employed. By comparison within FM 2-10 dye assays it has been determined that L0 produces indistinguishable results compared to HK0 and 4AP0 treated synaptosomes, thus L0 is used in the basal condition as they have the same impact on SV mode of exocytosis.

Rather than a buffer for bioenergetics assays being a derivative of L0, the bioenergetics buffer devised by Nicholls (Choi *et al.*, 2009) and suggested by Agilent Technologies was used. This is because the drugs used in the assay (oligomycin A, FCCP, rotenone and antimycin A) may cause different observable effects using a derived L0 buffer system. By using the same buffer system previously established we can be confident that we can reproduce the same results as Nicholls.

Buffers:

- Physiological basal buffer (L0): 125mM NaCl, 5mM KCl, 1mM $MgCl_2$, 20mM Hepes and 10mM glucose; pH 7.4
- Homogenisation sucrose buffer: 320mM sucrose and 10mM Hepes; pH7.4
- Stock high potassium (HK0) buffer: 130mM KCl, 20mM Hepes, 1mM $MgCl_2$ and 10mM glucose; pH 7.4 (This is diluted 5-fold when employed as a stimulus)
- Bioenergetics buffer: 120mM $NaCl_2$, 15mM D-glucose, 3mM KCl, 2mM $MgSO_4$, 12mM $NaSO_4$, 1.3mM $CaCl_2$, 0.4mM KH_2PO_4, 10mM pyruvate, 60µM bovine serum albumin; pH7.4. Note that there is no actual pH buffer component due to the need to measure proton production. This was used instead of L0 to allow comparison of results with previous data using the Seahorse Xfp Analyser in which this particular solution was employed.

Drugs and final concentration employed (dissolved in dimethyl sulfoxide; DMSO):

- 1-9-dideoxyforskolin (100 µM)
- 9-cyclopentyladenine mesylate (9-cp-ade) (100 µM)
- blebbistatin (50 µM)
- ESI-09 (100 µM)
- forskolin (100 µM)
- jasplakinolide (2.5 µM)
- KT5720 (2 µM)
- latrunculin A (15 µM)
- MiTMAB (30 µM)
- okadaic acid (OA) (0.8 µM)
- phorbol 12-myristate 13-acetate (PMA) (40 nM)
- sp-5,6-dichloro-cBIMPS (cBIMPS) (50 µM)

For bioenergetics assays:

- antimycin A (5 or 50 µM) (0.5 or 5 µM final; dissolved in ethanol)
- FCCP (18µM) (2µM final)
- oligomycin A (32µM) (4µM final)
- rotenone (5 or 50µM) (0.5 or 5µM final)

2.4 Method Brief

2.4.1 Preparation of Synaptosomes

Synaptosomes prepared from the cerebral cortex of adult male Wistar rats (*Rattus norvegicus*, Charles River, USA) are used as the model system for all experiments. The rat is killed by cervical dislocation and the cerebral cortex immediately put into 320 mM sucrose plus 10 mM Hepes (pH 7.4) (homogenisation buffer) at 4˚C. The tissue is homogenised using a Teflon Potter-Elvehjem tissue homogenizer, especially designed to prepare synaptosomes, at 900 rpm and 150 µm clearance which ensures preparations of active intact synaptosomes (Sihra, 1997).

The homogenate is centrifuged at 1941 × g for 10 min to separate cell bodies (nuclear debris) from the nerve terminals. The supernatant is centrifuged at 21,075 × g for 20 min and the subsequent pellet is re-suspended in basal physiological buffer (L0) at 4˚C and re-centrifuged at the same conditions of 21,075 × g for 20 min. The resulting pellet is re-suspended in 8 ml L0 and gassed with oxygen throughout the experiment, at 4˚C.

Synaptosomes prepared by this method represent a functional semi *in vivo* model due to the presence of intact ion channels, receptors, and signallingpathways. All synaptosomes are used within 4 hr for live assays, after which viability decreases.

2.4.2 Glutamate Release Assay

An aliquot of 2 ml of the prepared synaptosomes are washed by pelleting and re-suspending in L0. These synaptosomes are then stimulated for 90 s with HK5C. This causes all the releasable vesicles to fuse with the AZ and release neurotransmitter. Following a wash by centrifugation, thus removing the stimulus, and then resuspension in L0 and a further round of pelleting and resuspensions, synaptosomes are then left for 10 min at room temperature for maximal recycling of SVs (this step is only used to keep the assay comparable to FM assay where this HK5C pre-stimulation step is needed).

The synaptosomes are incubated with the appropriate drug dissolved in dimethyl sulfoxide (DMSO) (DMSO only in control tests) at 37°C for between 5 and 20 min. For dual drug treatments, one drug may be added first, followed by the second drug. The samples are then, pelleted, washed, resuspended, pelleted and then re-suspended in 1.6 ml L0 with corresponding amount of drug or DMSO to compensate for any possible reversibility of drug action.

Aliquots of 121 µl from this sample are then added to 12 wells of a row of a black Greiner 96 well microtiter plate (black, flat transparent bottom) with each well already containing 20 µl L0. 10 µl of 20 mM $NADP^+$ and 9 µl of GDH is added to each well and this mixture is incubated for 10 minutes at room temperature (final well volume 160 µl, concentration 1 mM $NADP^+$, 36 mUnits GDH). At this stage non-evoked extracellular glutamate is converted to α-ketoglutarate by GDH in the presence of $NADP^+$ which is itself converted to reduced form NADPH. Although the oxidative deamination of glutamate by GDH is a reversible reaction, in these experiments the reaction always favours forward direction due to loss of ammonia (NH_3) from the open well plate. The reaction using GDH as catalyst is as follows:

$$GDH: L-glutamate \; + \; H_2O \; + \; NADP^+ \rightleftharpoons \; \alpha - ketoglutarate + NH_3 + NADPH \; + \; H^+$$

NADPH fluoresces and background fluorescence indicates free glutamate before stimulation. After the incubation, Ca^{2+} containing stimulus (HK5C, ION5C or 4AP5C) is added to wells 1-5, then wells 6-12 have a corresponding stimulus without Ca^{2+} (HK0, 4AP0, or L0 for ION5C) added. Increase in fluorescence

after Ca^{2+} containing stimulus is added is directly caused by evoked Glu release from SVs using the aforementioned reaction.

The fluorescence of the wells in the plate is immediately measured after stimulation by the Tecan GENIOS Pro infinite 200 plate reader (excitation wavelength: 340 nm, emission wavelength: 465 nm, gain: 100, read mode: bottom, no. of cycles: 21; in 5 min measurement).

There are 21 cycles, making ~ 5 min time course, to ensure that GDH has maximally reacted with the released Glu.

Following the measurement 10 µl L0 is added to wells 7-9 and the same volume of 1mM (10 nmol) glutamate is added to wells 10-12. Wells 7-12 are immediately measured for 15 cycles (~4 min) with the same settings as previously. This measurement step allows for an internal control and calibration for a particular drug condition and also allows for normalization of all the rows to account for sensitivity.

This method is repeated for every row needed.

Subtracting the Ca^{2+} free stimulus values from the Ca^{2+} stimulation values provide a representation of Ca^{2+} dependent glutamate release. The 10 nmol glutamate measurement allows conversion of arbitrary units of fluorescence into nmol of glutamate. If the amount of synaptosomes is known, then data can be converted to nmol of Glu per mg of protein. Significance is calculated using unpaired two-tailed Student's *t*-test, $\alpha = 0.05$, of the end-points of the time-course.

The glutamate release assay is a method developed by Nicholls *et al*. (1987) and adapted by Sim *et al.* (2006). A. Ashton's previous work has established these measurement parameters using the same model.

2.4.3 The FM 2-10 Styryl Dye Release Assay

Previous research by A. Ashton's group has established that FM 2-10 dye can be loaded into all functional SVs within synaptosomes. The dye binds to the luminal domain of the SV membranes and fluoresces. Upon subsequent stimulation FM dye can dissociate from the membrane by the resulting SV exocytosis, with the unbound dye losing fluorescence. However, loss of fluorescence occurs only when the SVs exocytose by FF, rather than KR mode. This is because the dye takes time to dissociate from the membrane, which will not occur if the fusion pore closes in less than 0.5 s (Klingauf *et al.*, 1998). Studying the amount of dye released following drug treatments can reveal the modes of release for the RRP and the RP.

Aliquots of 2 or 1 ml from the prepared synaptosomes (depending on the volume they were initially suspended in) were re-suspended in oxygenated L0. A concentration of 100 µM FM 2-10 dye is added and incubated for 60 s followed by the addition of HK5C for 90 s. This stimulus allows all the releasable SVs to undergo exocytosis and during the period of vesicle exposure to extracellular buffer, the FM 2-10 dye can bind to the vesicle membranes for fluorescent labelling. The synaptosomes are centrifuged at 9589 × g (12,800 rpm) for 45 s and then re-suspended in L0 with 100 µM FM 2-10 dye (this step is repeated to ensure that all the stimulus is removed whilst dye is maintained in the buffer) and incubated for 10 min at room temperature, to allow all the vesicles to internalise and recycle.

Synaptosomes were then treated with appropriate amount of drug dissolved in DMSO (DMSO only for control), and incubated for 37°C for 5-20 min. A concentration of 1 mM ADVASEP-7 (final concentration) is added at room temperature, and this removes FM dye from the synaptosomal PM, leaving the vesicle-bound FM dye intact due to the membrane impermeability of ADVASEP-7. The synaptosomes are washed twice with L0 and re-suspended in 1.5 ml L0 along with corresponding concentration of drug in DMSO in order to prevent drug reversibility.

Aliquots of 160 µl from this preparation are added to wells 1-8 of a black Greiner 96 well microtiter plate with opaque bottom. Wells 1-4 are stimulated with 40 µl

of relevant stimulus (HK5C, ION5C or 4AP5C) and an equivalent volume of L0 is added to wells 5-8 before reading. Note each well is measured separately. Fluorescence measurements are performed by the Tecan GENIOS Pro infinite 200 plate reader with ~2 min time course (excitation wavelength: 465 nm, emission wavelength: 565 nm, gain: 40, read mode: top, no. of cycles: 461). This method is repeated as many times as is needed for different rows of the microtiter plate.

Note that routinely the same condition is repeated with the same experimental conditions, but the second time basal stimuli is added to wells 1-4, and stimulus added to wells 5-8. The results for the two measurements (8 wells for each condition) are then combined and averaged. This is to take into account any changes due to the age of synaptosomes since being labelled.

Basal data is subtracted from the corresponding stimuli data to obtain data of Ca^{2+} dependent SV release expressed as decrease in fluorescence over time. All rows are normalised to a constant starting fluorescence. However, the initial starting basal fluorescence (before any normalisation) can be used to check that the drug treatments do not perturb the total dye labelled SV content prior to stimulation. Significance values are calculated with unpaired two-tailed Student's *t*-test, $\alpha = 0.05$, of the end-points of the time-course.

2.4.4 The Fura-2 Intracellular Free Ca^{2+} Concentration Assay

Prepared synaptosomes are incubated with 5 µM Fura-2 AM stock (dissolved in DMSO) at 37ºC for 30 min whilst the synaptosomes are continuously oxygenated. Fura-2 AM enters the synaptosomes where it is hydrolysed by esterases whereby the dye is trapped in the synaptosomes. Following incubation synaptosomes are washed twice with 1 ml L0 by microfuge to remove excess extracellular Fura-2 AM, then the re-suspension is kept at 4 ºC with oxygenation until required.

Aliquots of 2 × 0.8 ml are taken for each row of a microtitre plate to be used for a particular test condition. These aliquots are stimulated with 2 × 0.2 ml HK5C for 90 s following which the stimulus is removed by microfuge at 9589 × g for 45

s. The pellets formed are suspended in 2 × 0.5 ml L0 and combined before incubating at room temperature for 10 min. This initial stimulation is required to keep the assays of the investigation comparable.

Following 10 min incubation the synaptosomes are incubated for 5-20 min at 37ºC with the appropriate concentration of drug dissolved in DMSO (DMSO only for control), followed by washing and re-suspending (repeated a second time) and then resuspension in 1.6 ml oxygenated L0 containing the appropriate concentration of drug or DMSO (for control) to prevent reversal of drug action.

Aliquots of 120 µl from the suspension is added to a row of 12 wells of a black Greiner 96 well plate with 40 µl L0 in each well, making the total volume 160 µl in each well. Fluorescence of Fura-2 is measured using Tecan GENIOS Pro infinite 200 plate reader (excitation wavelength: 340 ± 35 nm or 390 ± 25 nm, emission wavelength: 535 nm, gain: 30, read mode: top, no. of cycles: 40 or 160).

To consider the measurements needed for ratiometric calculations the following steps are used to obtain values for excitation wavelength 340 nm and 535 nm after stimulation, as well as values for saturated free $[Ca^{2+}]_i$ and quenched free $[Ca^{2+}]_i$:

Each well is measured for fluorescence with the first measured at 40 cycles (~10 s) with excitation 340 nm and emission 535 nm, to provide an average baseline fluorescence value. Following this the well is injected with 40 µl of either the appropriate stimulus or L0 buffer for control and measured for 160 cycles (~40 s) with excitation 340 nm and emission 535 nm. Well number 2 follows a similar protocol except the excitation wavelength is 390 nm to calculate the 340/390 ratio for these two well (390 nm filter is the nearest filter to 380 nm available, although it has bandwidth including 380 nm). For each row, six wells are stimulated with 40 µl desired stimulus and the other six wells are stimulated with 40 µl L0 for control. In the case of ionomycin stimulus it cannot be injected, thus ionomycin is added to the appropriate well just before injection with L0 containing 25 mM Ca^{2+}, making final well concentration 5 mM Ca^{2+}.

The 340/390 ratios calculated from the L0 control wells are subtracted from the 340/390 ratios from the stimulated wells to calculate $\Delta[Ca^{2+}]_i$ due to external

stimulus employed. Each row of 12 wells produces three sets of 340/390 ratios for a particular drug and stimulus combination along with control conditions.

After measuring the 12 wells of a row aliquots with final concentrations 2.25 mM Ca^{2+} and 0.3% Triton X-100 detergent are added to every well previously stimulated with Ca^{2+} containing stimulant, making final well volume 240 µl per well. To the rest of the L0 treated wells aliquots with final concentration of 15 mM ethylene glycol-bis(β-aminoethyl ether)-N,N,N′,N′-tetraacetic acid (EGTA; Ca^{2+} chelator) and 0.3% Triton X-100 is added. These wells are measured simultaneously for 40 cycles at excitation 340 nm, then excitation 390 nm. The values obtained are used to calculate R_{max} using the extra Ca^{2+} wells and R_{min} using the EGTA wells. The Grynkiewicz equation is used to calculate the $[Ca^{2+}]_{i.}$ Significance values were calculatedusing unpaired two-tailed Student's *t*-test, α = 0.05.

This calculation enables one to determine the change in $[Ca^{2+}]_i$ with time for the stimulated samples (average of 3) and for the basal samples. The basal values are then subtracted from the stimulated values to get the Ca^{2+} dependent change in $[Ca^{2+}]_i$.

2.4.5 Statistical Processing of Biochemical Assays

All the graphs presented have selected time interval data points showing their SEM. For the FM dye experiments, the 461 data points with SEM bars makes the values blurred and so in some cases SEM is only shown every 10 s and the statistics are just done on these points. Unpaired two-tailed Student's *t*-test is used to determine the significance to compare between any two treatments. The sample size (n value) used to perform the statistical tests is the sum of all the independent sample treatments used for producing the average.

The time interval data obtained from individual experiments is averaged together to obtain mean fluorescence, glutamate concentration or calcium concentration at a range of time points with corresponding SEM bars (positive bars shown only). The two-tailed unpaired student *t*-test was used on two time-corresponding data points of different traces to obtain significance level at that

point. This is performed similarly on all data points at time intervals 10 s and if significance value was less than 0.05 for most of the time points it was considered a significant difference between the two traces. In graphs wherein more than two samples are shown the samples are analysed in pairs using the aforementioned *t*-test.

In order to show the validity of the data, beeswarm superplots are shown in Appendix B for all the Glu and FM dye experiments shown in chapters 2 to 5,to display data that highlight experimental robustness and experiment run-to-run variability. The details of these are discussed in Appendix B.

Note that we have routinely found over the last 20 years that the RRP and the RP of cerebrocortical synaptosomes have a similar FM 2-10 dye content and that they represent similar numbers of SVs as each of these pools releases similar amounts of Glu. Data from studying specific individual synapses may reveal differences in the size of the RRP and RP but it has been found that this will vary depending upon which synapse one is studying (e.g., hippocampal cultured cells or calyx of held giant synapse). As cerebrocortical synaptosomes are heterogeneous containing many different synapse types, it may be that the average of all these just comes out to produce similar size RRP and RP SV pools.

2.4.6 Bioenergetic Measurement of Extracellular O_2 Consumption Rate

A Seahorse Xfp Miniplate had been pre-treated with 1:1500 dilution of a 50% solution of polyethyleneimine: solution is left overnight, then removed and plate allowed to air dry. An aliquot of 0.02 to 0.04 ml from the final synaptosome suspension (4-8 ml) is re-suspended in 1.2 ml of the bioenergetics solution containing 4 mg/ml bovine serum albumin. Then 0.175 ml of this suspension is aliquoted into the treated Seahorse Xfp Miniplate (wells B-G). The synaptosomes are spun in an Eppendorf™ A-2 MTP swing-out rotor for 20 min at 4˚C at 2000 × g to allow the synaptosomes to adhere onto the well floors. The supernatant in the wells is removed from the immobilised synaptosomes and these are treated with 37˚C bioenergetics buffer containing the required concentration of selected drug dissolved in DMSO into wells A-D or buffer and

DMSO only into wells E-H for control. This is incubated for the appropriate time usually employed with the drug at 37˚C followed by two washes of bioenergetics buffer. Note that wells A and H had just buffer and DMSO added to them without synaptosomes, and these represent background controls used by the Seahorse Xfp analyzer.

A sensor cartridge is hydrated overnight at 37˚C in calibration phosphate buffered saline (PBS) buffer, and just before the experiment the relevant drug stock dissolved in DMSO (antimycin A is dissolved in ethanol) are added into all the injectors A-H (32 µM oligomycin A in port A, 18 µM FCCP in port B, 5 µM or 50 µM rotenone/antimycin A in port C). The sensor cartridge was introduced to the Xfp Extracellular Flux Analyser™ to calibrate and the loaded miniplate is added. The synaptosomes had to be fresh so only one experiment was run per synaptosome preparation. Note that 25 µl of each of these drugs is injected into the extracellular buffer above the synaptosomal monolayer and the final concentration of the drugs employed are 4 µM oligomycin, 2 µM FCCP in port B, 0.5 µM or 5 µM rotenone/antimycin A.

The program then measures 3 × 3 min measurements of basal oxygen consumption rate (OCR). Then there was automatic injection of oligomycin A into all the wells (final concentration 4 µM) and further 3 × 3 min measurements. This is followed by injection of FCCP (final concentration 2 µM) and 3 × 3 min measurements. Finally, there is an injection of rotenone/antimycin A (final concentration 0.5 µM or 5 µM) and 3 × 3 min measurements. This gives average OCR traces of the wells according to drug-treated (wells B-D) and control (wells E-F), minus the baseline (wells A, H).

The resulting data is averaged with repeat experiments, analysed with two-way Student’s t-test and plotted in a line graph. Note that earlier Mito-Stress tests are conducted at 37°C, however a hardware update allows the test to be conducted at room temperature, similarly to the plate reader assays.

CHAPTER 3: PKA and Dynamin Modulation Upon Synaptic Vesicle Release

3.1 Role of PKA Regulation in Synaptic Vesicle Release

The kinase PKA has many protein substrates and pathways in the presynapse, some of which can modulate SV exocytosis and recycling (Park *et al*., 2014). Activity of PKA can increase Ca^{2+} influx (Yoshihara *et al*., 2000) and has been implicated in long-term potentiation, affecting synaptic strength through phosphorylation and modulation of the secretory machinery (Leenders and Sheng, 2005). Increased PKA activity has been shown to enhance release probability of neurotransmitters by promoting Ca^{2+} influx through specific voltage-gated Ca^{2+} channels (Wang and Sieburth, 2013). Activation of α7 nicotinic acetylcholine receptors at presynaptic sites has a critical role in enhancing synaptic efficiency of hippocampal mossy fibre transmission via a PKA mechanism, by increasing AP dependent Ca^{2+} transient (Cheng and Yakel, 2014). This further describes how PKA is involved in an AP potentiation pathway within the presynapse to increase neurotransmitter release probability.

Normally, PKA is also involved in modulating SNARE priming. The SNARE regulatory protein tomosyn is directly phosphorylated by PKA which reduces interaction with syntaxin-1 and enhances formation of the SNARE complex, increasing fusion-competent RRP SVs, increasing neurotransmitter release. This mechanism is involved in facilitation of neurotransmitter release induced by pituitary AC-activating polypeptide in superior cervical ganglion neurons (Baba *et al.*, 2005).

Cousin and Evans (2011) demonstrated that PKA activates presynaptic silent synapses, which may be an important process for cerebellar motor learning; the PKA substrates to cause such activation are yet to be identified. Park *et al.* (2014) have suggested that presynaptic PKA is critical for synaptic plasticity and memory by regulating the RRP – PKA inhibition elicits a rapid decay in synaptic response and reduces levels of synaptic vesicle protein 2 (SV2) which is necessary for SV exocytosis.

This chapter describes the investigation into the role of PKA activation and inhibition upon regulating the mode of Glu release from the RRP and RP of SVs.

3.2 Inhibition of PKA Using KT5720 Upon Synaptic Vesicle Release Dynamics

3.2.1 Treatment of KT5720 Upon Evoked Glutamate Release

The PKA inhibitor KT5720, which blocks PKA action through competitive inhibition of the ATP binding site, has been utilised in this study (Kase *et al*., 1987).

The treatment of synaptosomes with 2 µM KT5720 caused no significant change in 4AP5C evoked Glu release from the RRP (note only this pool is stimulated by 4AP5C) (Figure 3.1a). There was also no significant change with KT5720 treatment during HK5C stimulation (Figure 3.1b) or ION5C stimulation (Figure 3.1c) compared to non-drug controls, indicating that neither the release of the RRP or the RP are perturbed by this inhibitor.

Previous research has established that 5 mM $[Ca^{2+}]_e$ evoked maximal release of Glu from the RRP when used with 4AP, and maximal release of Glu from both the RRP and RP when 5 mM $[Ca^{2+}]_e$ was used with HK and ION (Bhuva, 2015) (Figure A1 Appendix A). Thus Figure 3.1b and 3.1c demonstrates maximal Glu release from the RRP and RP even with KT5720 treatment.

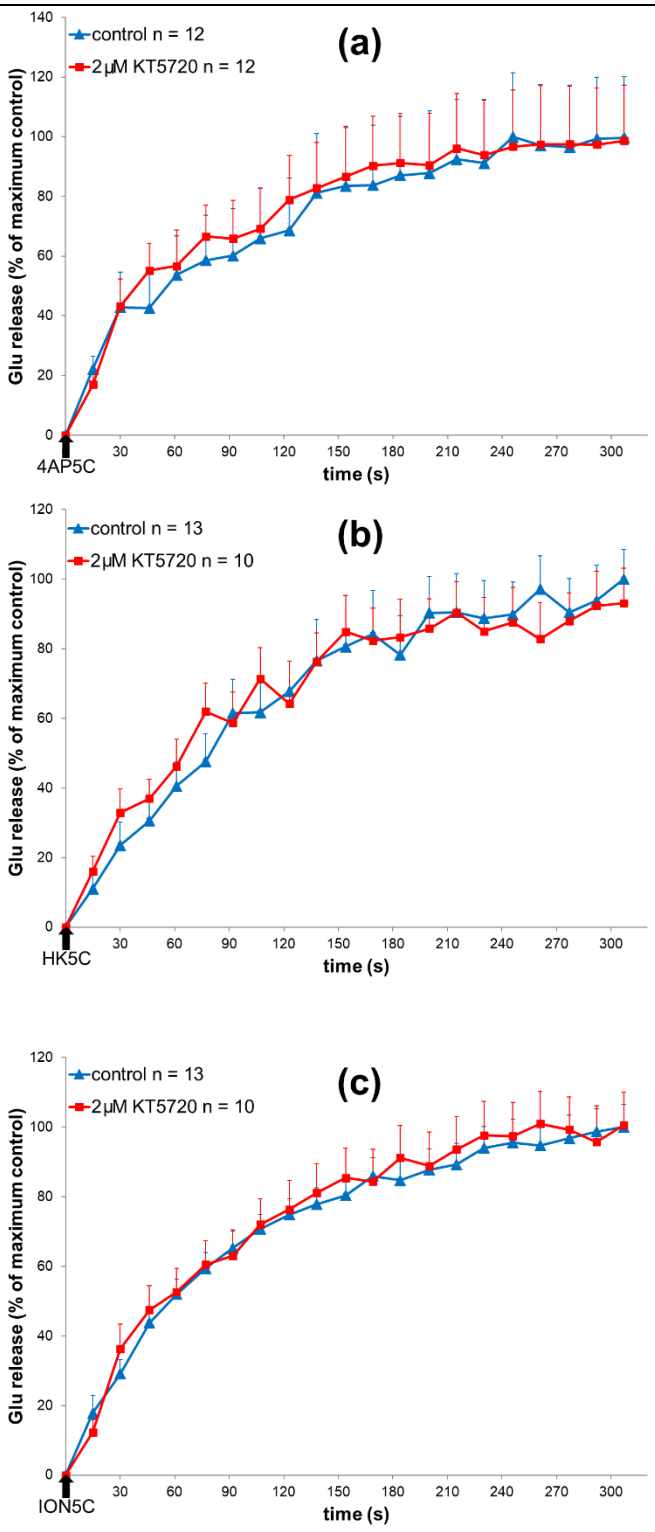

Figure 3.1: The effect of 2 μM KT5720 vs control upon evoked Glu release. PKA inhibition with 2 μM KT5720 had no effect upon (a) 4AP5C (p = 0.750 NS), (b) HK5C (p = 0.934 NS) or (c) ION5C (p = 0.840 NS) evoked Glu release, compared to non-drug controls. Values represented are the mean plus SEM from 3 independent experiments.

3.2.2 Treatment of KT5720 Upon FM 2-10 Dye Release

Pre-loaded FM 2-10 dye containing synaptosomes preparations, treated with 2 µM KT5720, released significantly more FM 2-10 dye compared to control conditions, when stimulated with 4AP5C (Figure 3.2a) or with ION5C (Figure 3.2c), whereas stimulation with HK5C produced no significant change in release (Figure 3.2b).

These results suggest that SVs from the RRP, which all undergo KR in control conditions with ION5C (Figure A10 Appendix A), switch to an FF mode of exocytosis during PKA inhibition when released with KT5720. With 4AP5C stimulus, only some RRP SVs underwent KR in control conditions (Figure A10 Appendix A), but exocytosis was switched to FF by KT5720 treatment. Stimulation with HK5C did not switch the mode of exocytosis of any SVs in KT5720 treated synaptosomes and RRP still underwent KR mode and the RP still underwent FF mode (Figure 3.2b) as observed in control conditions (Figure A11 in Appendix A).

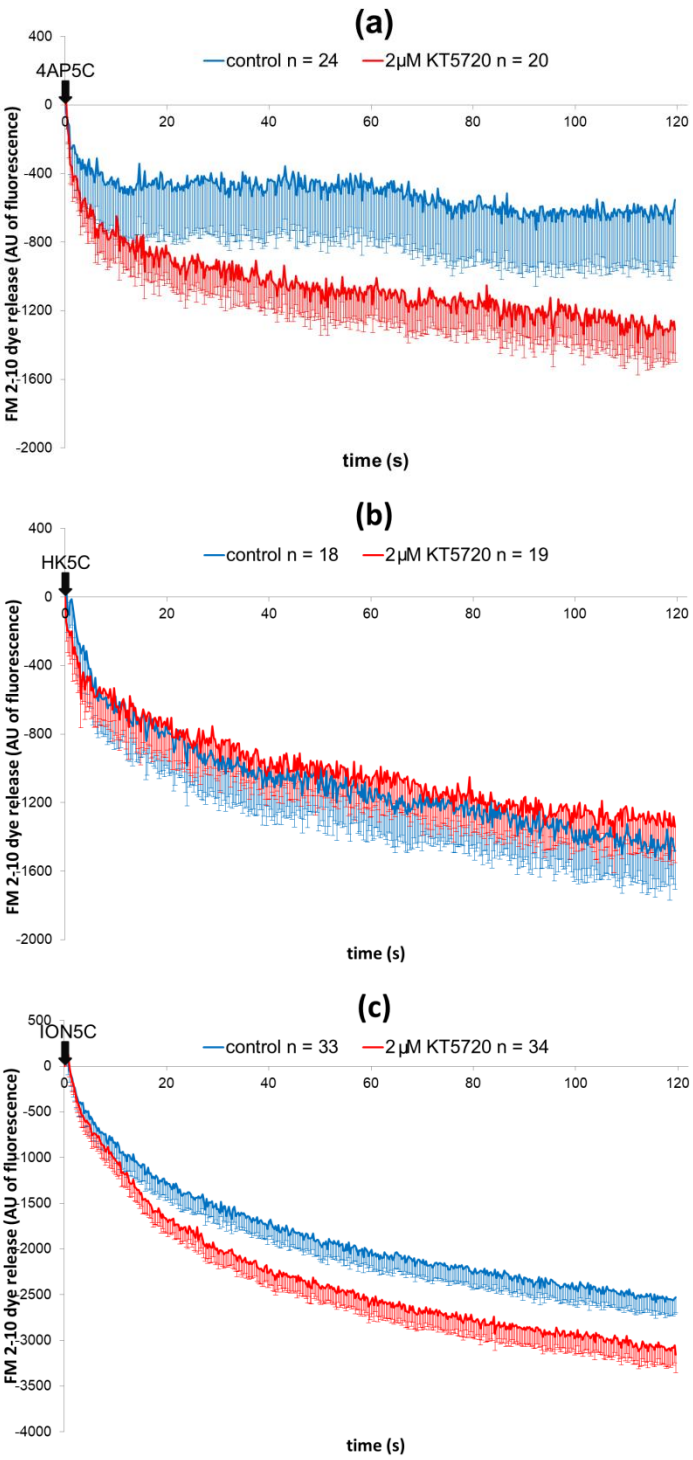

Figure 3.2: The effect of 2 μM KT5720 vs control upon evoked FM 2-10 dye release. PKA inhibition with 2 μM KT5720 significantly increased (a) 4AP5C ($p < 0.001$) and (c) ION5C ($p < 0.001$) evoked FM 2-10 dye release but had no effect upon (b) HK5C ($p = 0.753$) evoked FM 2-10 dye release, compared to non-drug controls. Values represented are the mean plus SEM from 4 (a and b) and 5 (c) independent experiments.

These data are remarkably similar to previous data collected when Glu and FM 2-10 dye release was studied with the dynamin-1 and dynamin-2 inhibitor dynasore (Bhuva, 2015), a reversible, non-competitive GTPase activity inhibitor of dynamins (Macia, *et al*., 2006). Synaptosomes treated with 160 µM dynasore maximally released Glu from the RP and RRP when stimulated with HK5C (Figure A12a in Appendix A) or ION5C (Figure A12b in Appendix A), and from the RRP when stimulated with 4AP5C (Figure A12c in Appendix A). This demonstrated that inhibition of dynamins does not perturb the vesicular release of Glu. Furthermore, there was no significant increase in FM 2-10 dye release observed with 160 µM dynasore treatment when stimulated with HK5C (Figure A12d in Appendix A). However, a substantial increase in FM 2-10 dye release was observed when dynasore treated synaptosomes were stimulated with ION5C (Figure A12e in Appendix A) and 4AP5C (Figure A12f in Appendix A).

From these observations of the action of dynasore upon FM 2-10 dye release, it was determined that the ION5C and 4AP5C stimuli had a dynamin-1 requirement for closing the fusion pore during exocytosis (Bhuva, 2015). These stimuli induced a lower Ca^{2+} concentration at the AZ, which activated local dynamin-1 creating a dynamin-dependent KR mode of exocytosis, while HK5C induced a higher Ca^{2+} change at the AZ, inhibiting local dynamin-1 creating a dynamin-independent mode of exocytosis. When the GTPase activity of dynamin-1 was blocked with dynasore a mode switch to FF was observed, and when PKA was blocked with 2 µM KT5720, the same mode switch to FF was seen with the same stimuli (4AP5C and ION5C). This could demonstrate that PKA activity played a role in regulating properties of dynamin-1, allowing it to induce a KR mode of exocytosis at the fusion pore and this could be through changes in the evoked $[Ca^{2+}]_i$ levels or changes in dynamin-1 via protein partners or phosphorylation. Indeed, there are four dynamin-1 phosphorylation sites at Ser512, Ser822, Ser851 and Ser347 found in dynamin *in vivo* in addition to the three well characterised sites (Ser774, Ser778, and Ser857) which may indicate that other protein kinases (possibly PKA) can phosphorylate dynamin and presumably regulate its properties. Some of these less characterised phosphorylation sites are in the PRD and this may regulate binding of other SH3 domain-containing proteins to play a role in KR mode (Graham et al, 2007).

3.2.3 Treatment of KT5720 Upon Changes in Intracellular Ca^{2+} Levels

It has been demonstrated by Ashton's group that an increase in $[Ca^{2+}]_i$ can switch a portion of RP SVs to KR (e.g., the action of cyclosporine A (Cys A) shown in Figure A15 in Appendix A; see Bhuva, 2015). It is therefore possible that changes in mode of exocytosis may be the result of drug induced changes in $[Ca^{2+}]_i$ levels which then may affect pools of SVs. Thus, it was possible that switching the mode of RRP SVs to FF with 4AP5C and ION5C in KT5720 treated terminals may be because inhibiting PKA lowered the level of stimulated $[Ca^{2+}]_i$. However, the treatment of synaptosomes with 2 µM KT5720 had no significant effect upon $[Ca^{2+}]_i$ levels evoked by 4AP5C (Figure 3.3a), HK5C (Figure 3.3b some increase but not significant) or ION5C (Figure 3.3c) compared to non-drug controls. This suggested that inhibition of PKA changed the mode of RRP SVs for 4AP5C and ION5C to FF mode, independently of drug induced changes in the level of $[Ca^{2+}]_i$.

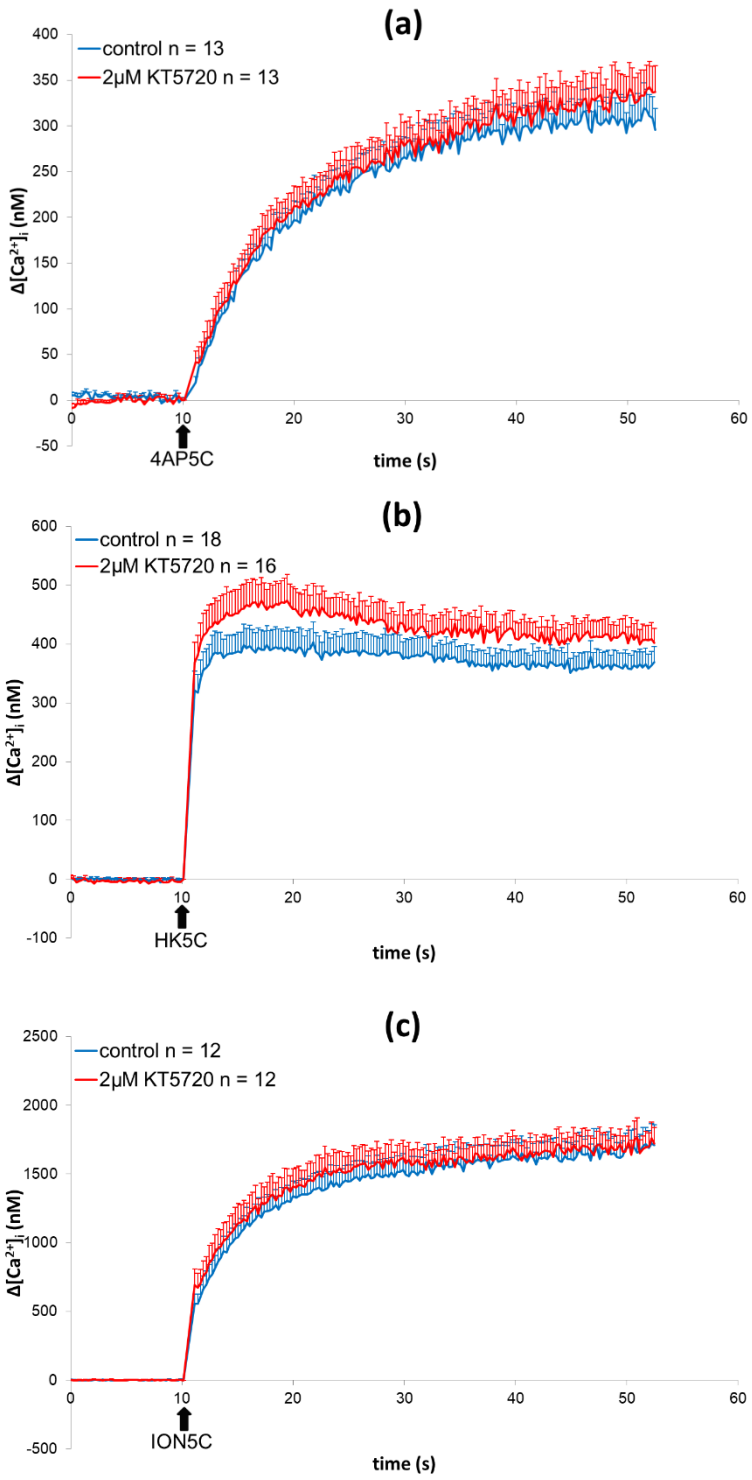

Figure 3.3: The effect of 2 μM KT5720 vs control upon evoked $[Ca^{2+}]_i$ levels. PKA inhibition with 2 μM KT5720 did not significantly affect intracellular Ca^{2+} levels when stimulated with (a) 4AP5C (p = 0.397), (b) HK5C (p = 0.425) or (c) ION5C (p = 0.455) compared with non-drug controls. Values represented are the mean plus SEM from 3 independent experiments.

3.2.4 Treatment of KT5720 Upon Synaptosome Bioenergetics

As discussed previously in Chapter 2, drug induced changes to the mode of release during FM 2-10 dye assays could have been the result of respiratory perturbation in the synaptosome samples or compromised mitochondrial function. Such a finding would mean that one could not specifically investigate a specific drug protein target that may affect Glu release or the mode of exocytosis. The Mito-Stress test by measuring OCR under various induced respiratory parameters can determine various bioenergetic factors.

There was no significant difference in OCR of synaptosomes when treated with 2 µM KT5720 compared to non-drug treated control synaptosomes (Figure 3.4). Figure 3.5 outlines the effect of 2 µM KT5720 upon mitochondrial function parameters that were measured during the Mito-Stress test. The bar graphs show the average values measured over three time points for each section of the Mito-Stress test, presenting respiration over time as OCR: basal (0-15 min), oligomycin A treatment (20-35 min), FCCP treatment (40-55 min) and rotenone plus antimycin A treatment (60-75 min). Mitochondrial function parameters (Figure 3.5) show that the effect of 2 µM KT5720 caused a small significant increase in basal mitochondrial respiration (Figure 3.5a), although there was no significant effect on the other parameters measured.

These data show that treatment with 2 µM KT5720 (Figure 3.4) does not perturb the mitochondrial respiration of the synaptosomes under conditions in which the terminals would have been exposed to the drug at 37°C for 90 min. Therefore, KT5720 treatments of 37°C for 5 min, as used in release assays, would not disrupt synaptosome respiration. This indicates that there is less probability of non-specific effects upon release measurements following KT5720 incubation, despite slight increase in basal respiration.

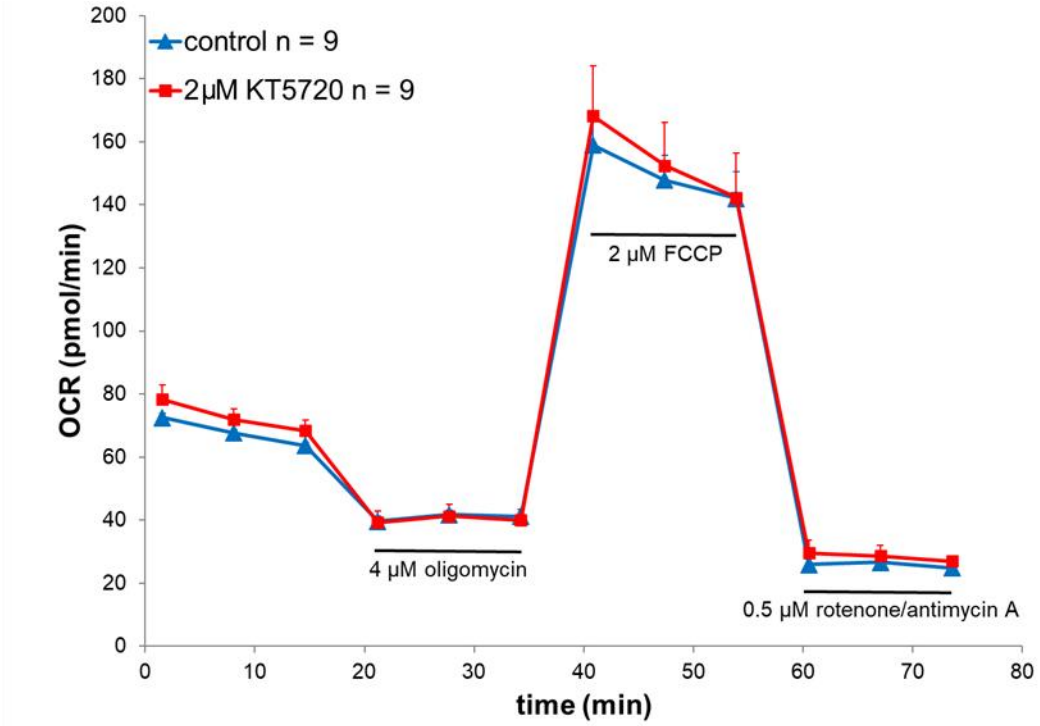

Figure 3.4: The effect of 2 µM KT5720 vs control upon synaptosome bioenergetics. Treatment of 2 µM of PKA inhibitor KT5720 did not significantly affect the bioenergetics of synaptosomes compared to control during a Mito-Stress test (p = 0.891). Values represented are the mean plus SEM from 3 independent experiments. The experiments were performed at 37˚C in the Seahorse Xfp flux analyser.

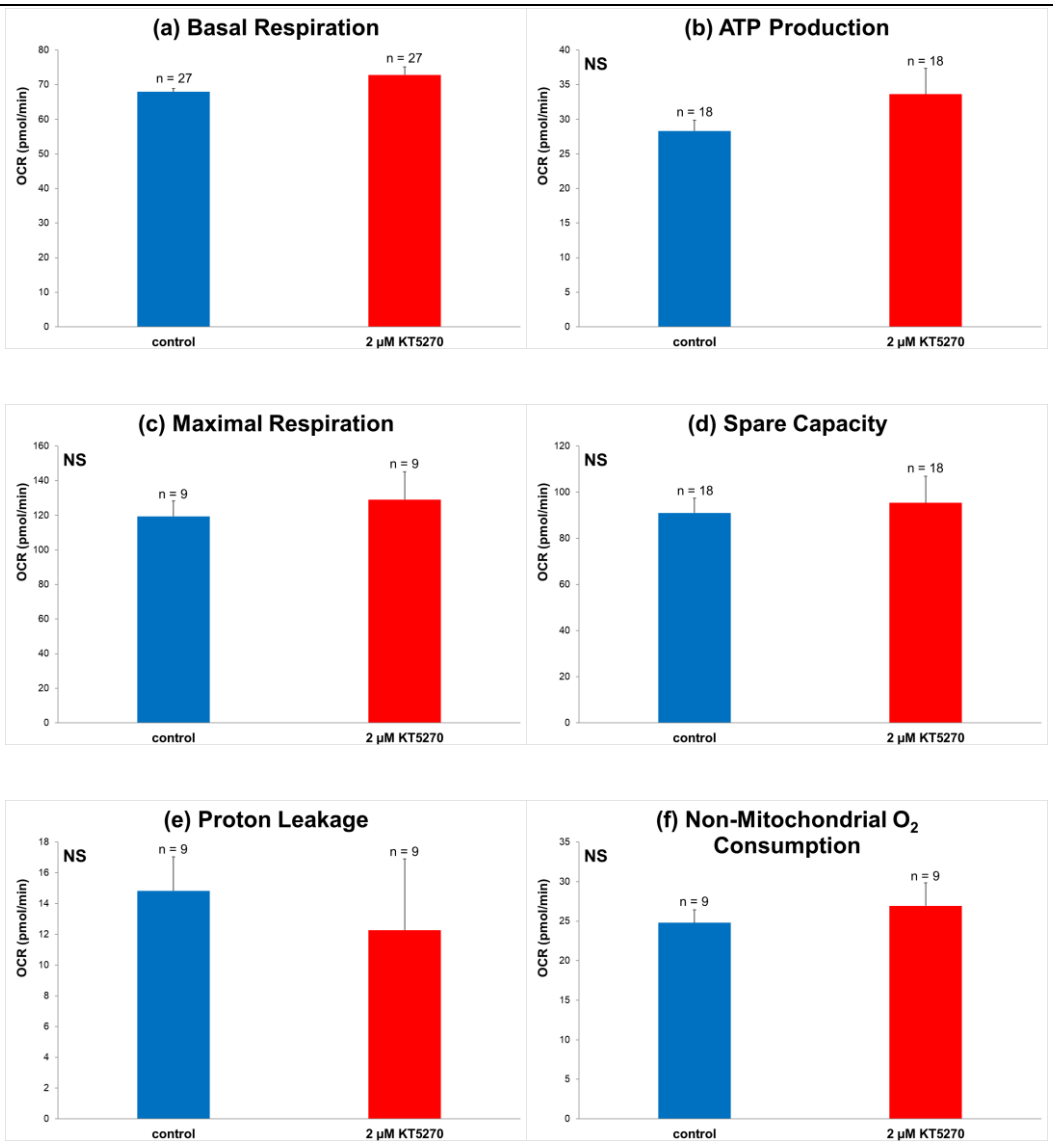

Figure 3.5: The effect of 2 µM KT5720 vs control upon mitochondrial function. (a) PKA inhibition with 2 µM KT5720 caused significant difference of p = 0.0483 to basal respiration compared to non-drug control synaptosomes. Treatment of 2 µM KT5720 showed no significant change in (b) ATP production, (c) maximum respiration), (d) spare capacity, (e) proton leakage or (f) non-mitochondrial oxygen consumption, compared to non-drug control synaptosomes (all parameters p > 0.05). Values represented are the mean plus SEM from 3 independent experiments.

3.3 Activation of PKA Using cBIMPS Upon Synaptic Vesicle Release Dynamics

3.3.1 Treatment of cBIMPS Upon Evoked Glutamate Release

Sp-5,6-DCl-cBIMPS (cBIMPS) is a cAMP analogue which is a potent and specific activator of PKA by binding to regulatory subunits, exposing the catalytic sites of PKA allowing phosphorylation of its substrates (Sandberg, *et al.*, 1991).

Treatment of synaptosomes with 50 µM cBIMPS had no significant effect upon release of Glu from the RRP evoked by 4AP5C (Figure 3.6a) or from the RRP plus RP evoked by HK5C (Figure 3.6b) or ION5C (Figure 3.6c) compared to non-drug controls. These figures demonstrate that drug activation of PKA does not perturb the maximal release of Glu from the RRP or RP. As there is no significant change in amount Glu release, any measurable difference in FM 2-10 dye release must be rather due to changes in mode of exocytosis.

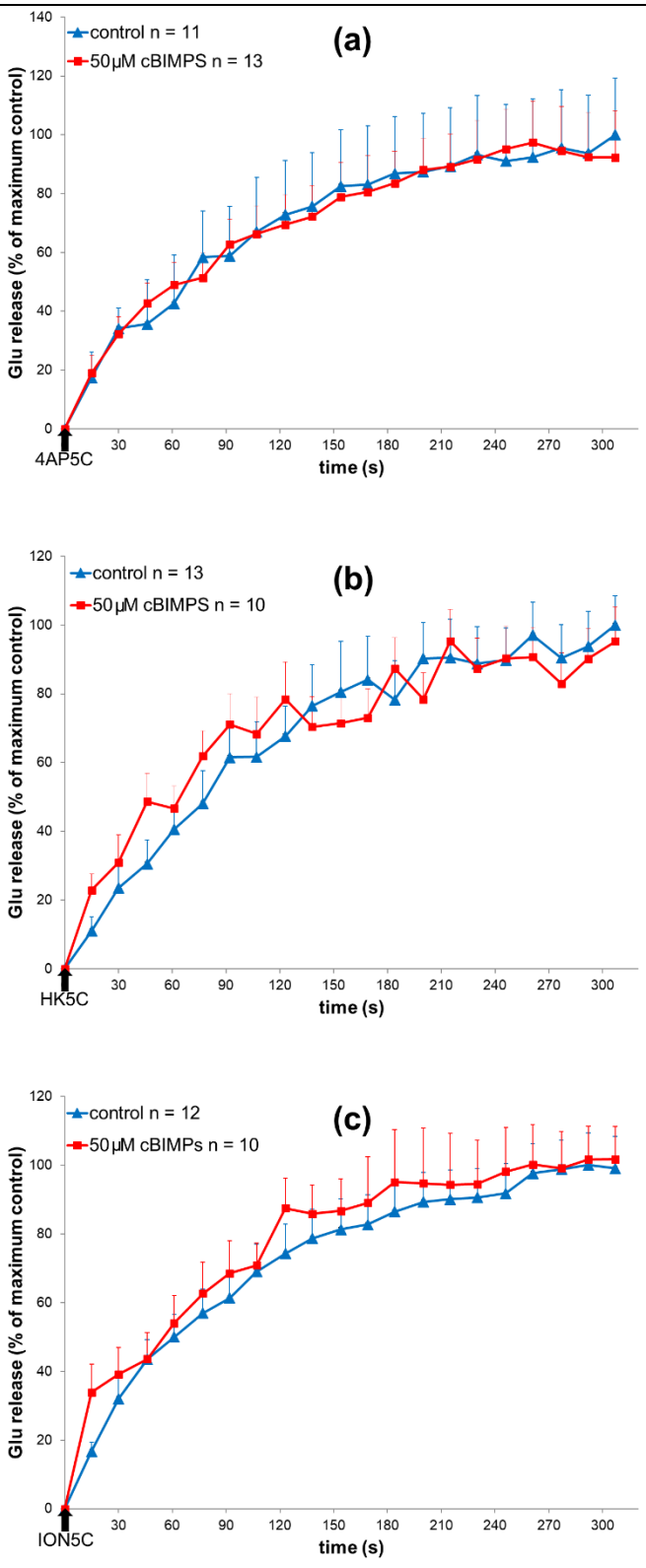

Figure 3.6: The effect of 50 µM cBIMPS vs control upon evoked Glu release. PKA activation with 50 µM cBIMPS had no effect upon (a) 4AP5C (p=0.960 NS), (b) HK5C (p=0.841 NS) or (c) ION5C (p=0.548 NS) evoked Glu release, compared to non-drug controls. Values represented are the mean plus SEM from 3 independent experiments.

3.3.2 Treatment of cBIMPS Upon FM 2-10 Dye Release

Activation of PKA with 50 µM cBIMPS made no significant change to the amount of FM 2-10 dye released compared to controls when synaptosomes were stimulated with 4AP5C (Figure 3.7a). However, there was a significant decrease in FM 2-10 dye release when synaptosomes were stimulated with HK5C (Figure 3.7b) or ION5C (Figure 3.7c), compared to non-drug controls. This indicates that some SVs in the RP, all of which usually undergo FF release, have switched to KR mode.

It can be interpreted that with 4AP5C stimulation, PKA activation did not regulate that mode of exocytosis of the RRP, because SVs had not changed mode from FF. These findings indicated that PKA activation had a specific role in regulating mode of the RP independently of the RRP, as PKA activation changed some of the RP to KR mode. This phenotype is similar to previous research results when synaptosomes were treated with PP2B inhibitor Cys A; treatment with 1 µM Cys A did not perturb Glu release with any stimulation (Figure A15a-c in Appendix A and Bhuva, 2015). This wasdifferent from some studies which showed that Cys A could increase Glu release (Gaydukov *et al*., 2013), although that study does not use maximal Glu release conditions such as the study herein. A significant decrease in FM 2-10 dye release was seen when synaptosomes treated with 1 µM Cys A were stimulated with HK5C and ION5C, whilst no significant difference was observed with 4AP5C stimulation (Figure A15d-f in Appendix A and Bhuva, 2015). This indicated an RP change tomore KR mode, similarly to PKA activation. This data may have indicated that the PKA substrate that regulated mode of the RP may also have been regulated by PP2B or that PKA may have phosphorylated PP2B and inhibited it or that PP2B inhibition increased the activity of PKA. It has been shown that phosphorylated PKA can be a substrate for PP2B (Blumenthal *et al.*, 1986). More interestingly, it is well known that both enzymes can be localized at specific membrane sites by AKAPs. The most common one, AKAP-79 anchors both proteins at the post-synaptic density (Nygren and Scott, 2016). However, there are pre-synaptic AKAPs that could possibly localize these enzymes to help regulate the fusion mode of exocytosing SVs. This would need to be investigated in more detail in the future.

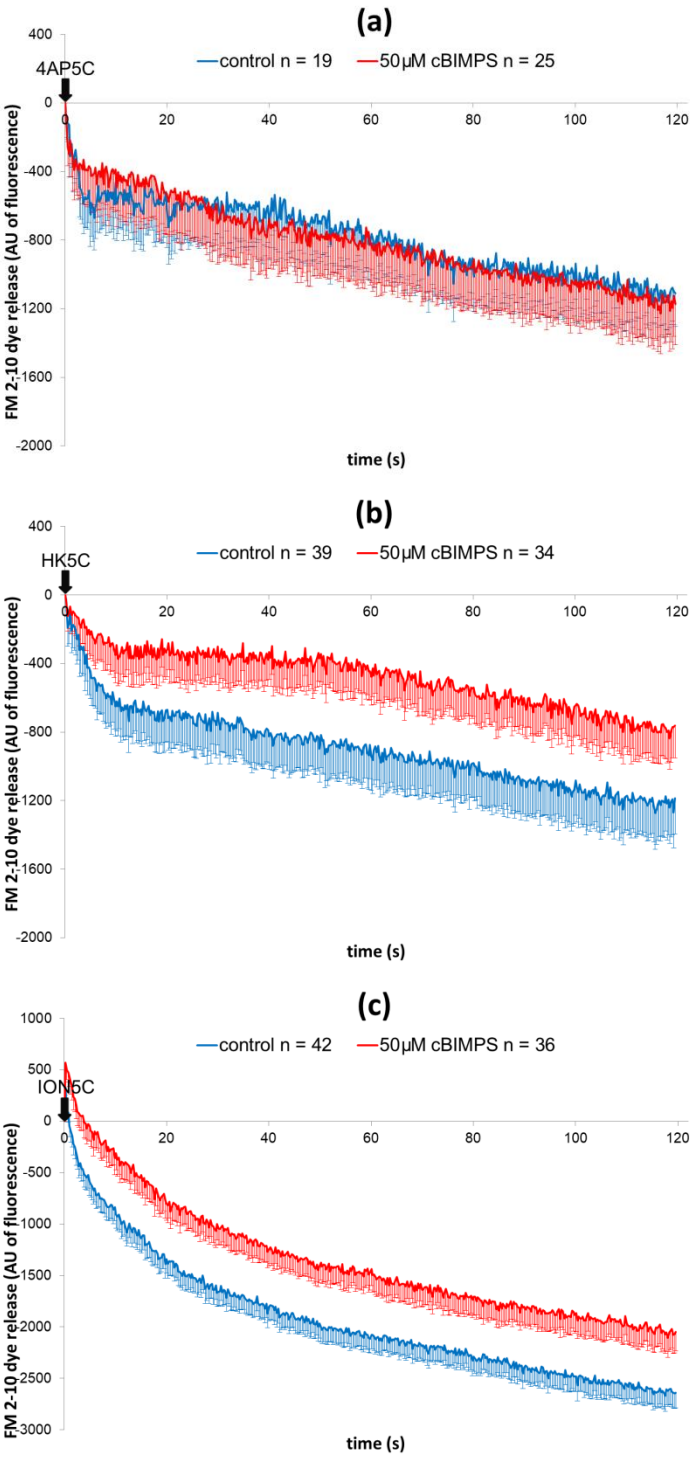

Figure 3.7: The effect of 50 µM cBIMPS vs control upon evoked FM 2-10 dye release. PKA activation with 50 µM cBIMPS had no effect upon (a) 4AP5C evoked FM 2-10 dye release ($p = 0.302$) but significantly decreased dye release with (b) HK5C ($p < 0.001$) and (c) ION5C ($p < 0.001$) stimulation, compared to non-drug controls. Values represented are the mean plus SEM from 3 (a and b) and 6 (c) independent experiments.

3.3.3 Treatment of cBIMPS Upon Changes in Intracellular Ca^{2+} Levels

Previous research with Cys A has suggested that an increase in $[Ca^{2+}]_i$ could switch RP SVs to a KR mode of release when stimulated with HK5C or ION5C (Figure A15 in Appendix A; Bhuva, 2015). Therefore, it was predicted that 50 µM cBIMPS treatment may also cause an increase in $[Ca^{2+}]_i$ level when synaptosomes are also stimulated with HK5C or ION5C. This may explain why cBIMPS induced more RP SVs to undergo KR mode of exocytosis. However treatment with 50 µM cBIMPS had no significant effect upon $[Ca^{2+}]_i$ levels evoked by HK5C (Figure 3.8a) or ION5C (Figure 3.8b) stimulation. Therefore PKA activation may have caused a switch of the RP from FF to KR mode without inducing changes in $[Ca^{2+}]_i$ levels. This was different to previous results wherein higher $[Ca^{2+}]_i$ levels correlate with a change of the RP to KR mode (Figure A15 in Appendix A; Bhuva, 2015) using Cys A.

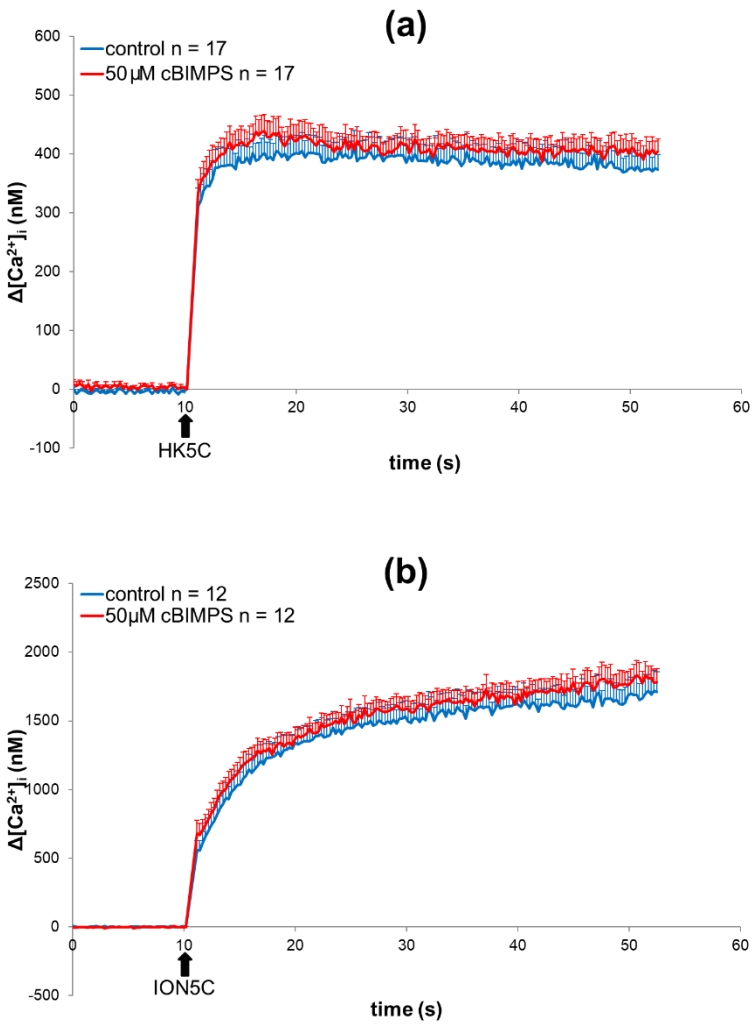

Figure 3.8: The effect of 50 µM cBIMPS vs control upon evoked $[Ca^{2+}]_i$ levels. PKA activation with 50 µM cBIMPS did not significantly affect intracellular Ca^{2+} levels when stimulated with (a) HK5C ($p = 0.223$) or (b) ION5C ($p = 0.301$) stimuli, compared to non-drug controls. Values represented are the mean plus SEM from 3 independent experiments.

3.3.4 Treatment of cBIMPS Upon Synaptosome Bioenergetics

Synaptosomes treated with 50 µM cBIMPS were subjected to the Mito-Stress test. No significant in OCR was seen compared to control (Figure 3.9). A significant increase in basal respiration was observed (Figure 3.10a) but this difference was small and other parameters had no significant difference compared to control.

These data show that treatment with 50 µM cBIMPS (Figure 3.9) did not perturb the mitochondrial respiration of the synaptosomes at conditions of 37°C for 90 min. Therefore, cBIMPS treatments of 5 min, as used in these plate reader assays, would not disrupt synaptosome respiration. This indicates that there was less probability of non-specific effects upon cBIMPS measurements, despite slight increase in basal respiration.

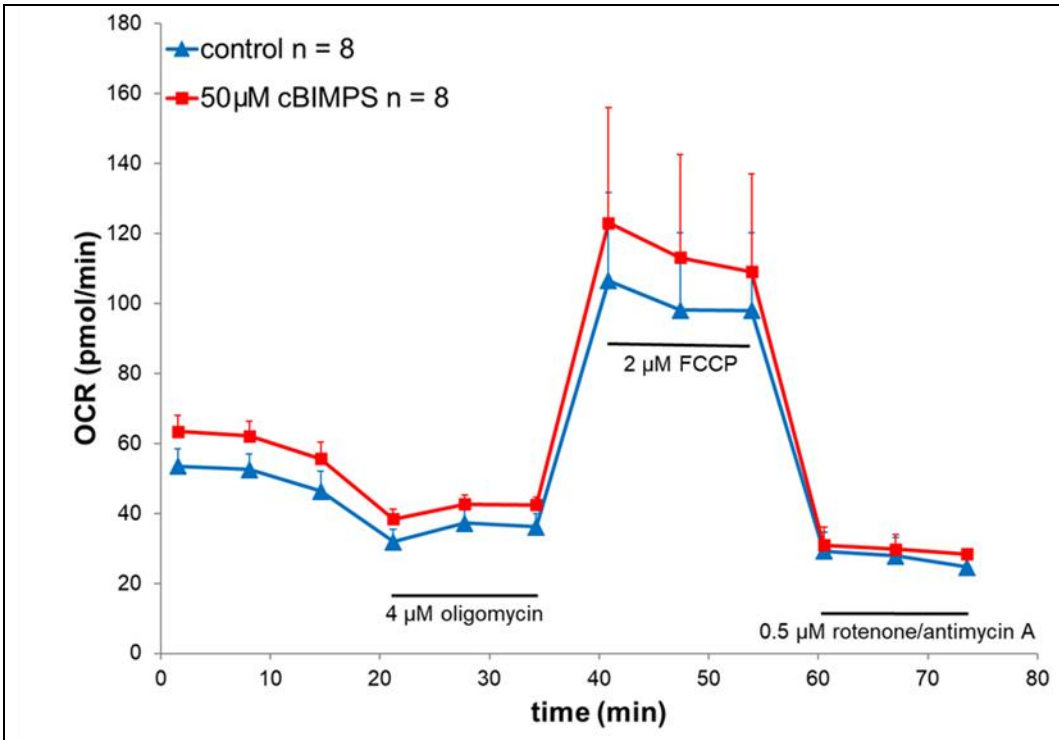

Figure 3.9: The effect of 50 µM cBIMPS vs control upon synaptosome bioenergetics. Treatment of 50 µM cBIMPS did not significantly affect the oxygen consumption rate of synaptosomes compared to control during a Mito-Stress test (p = 0.547). Values represented are the mean plus SEM from 3 independent experiments. The experiments were performed at 37˚C in the Seahorse Xfp flux analyser.

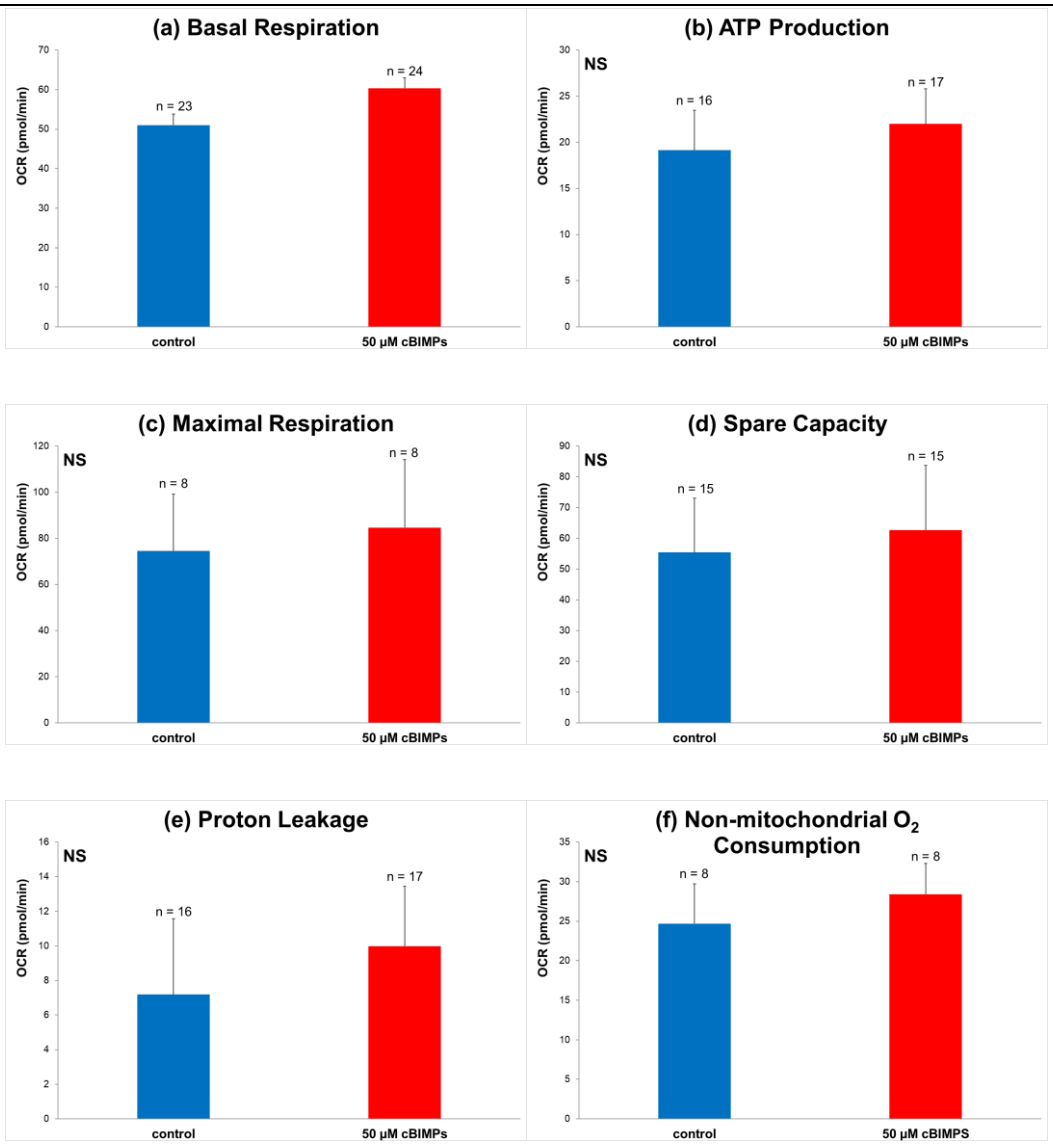

Figure 3.10: The effect of 50 µM cBIMPS vs control upon mitochondrial function. (a) PKA activation with 50 µM cBIMPS caused significant difference of p = 0.0184 to basal respiration compared to non-drug control synaptosomes. Treatment of 50 µM cBIMPS showed no significant change in b) ATP production, (c) maximum respiration), (d) spare capacity, (e) proton leakage or (f) non-mitochondrial oxygen consumption, compared to non-drug control synaptosomes (all parameters p > 0.05). Values represented are the mean plus SEM from 3 independent experiments.

3.4 Specificity of KT5720 and cBIMPS for PKA Using Evoked FM 2-10 Dye Release

To ensure that the effect of KT5720 and cBIMPS was specifically due to their action on PKA, synaptosomes were pre-treated with 2 µM KT5720 before treatment with 50 µM cBIMPS. Pre-treatment of KT5720 would block cBIMPS action if this action is specific to PKA; this would block or significantly reduce the proportion of SVs switching to KR mode of exocytosis.

Release of FM 2-10 dye from synaptosomes dual treated with KT5720 then cBIMPS showed results not significantly different to control synaptosomes during stimulation with HK5C (Figure 3.11a) or ION5C (Figure 3.11b). These results show that the actions of KT5720 and cBIMPS were specific for PKA and reveal pool dependent mode switching for distinct stimuli.

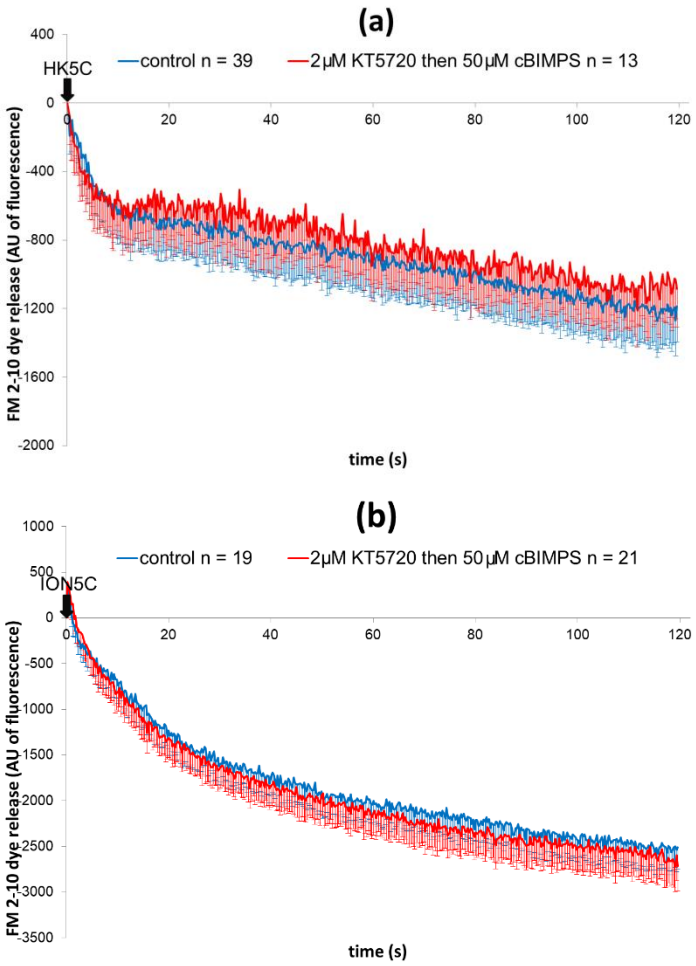

Figure 3.11: The effect of 2 μM KT5720 then 50 μM cBIMPS treatment vs control upon evoked FM 2-10 dye release. PKA inhibition with 2 μM KT5720 followed by treatment of 50 μM cBIMPS did not significantly affect FM 2-10 dye release with (a) HK5C ($p = 0.461$) or (b) ION5C ($p = 0.804$) stimulation, compared with non-drug controls. Values represented are the mean plus SEM from 6 (control a and control and drug treated b) and 3 (drug treatment in a) independent experiments.

3.5 Dynamin Translocation on Synaptic Vesicle Release

As highlighted herein, there appears to be a dynamin dependent KR mode for the RRP of SVs that is activated by specific stimuli (ION5C or 4AP5C). The criteria for the specificity towards dynamin-1 is that the KR mode is switched to FF mode if the GTPase activity of dynamin-1 is blocked using dynasore (see Appendix A). Such GTPase activity is required for dynamin to play a role in the pinching of the neck (fusion pore) to allow KR recycling. If this process is prevented, then the SV membrane can expand into the PM and FF will take place. In this case as one is measuring only one round of SV exocytosis, the subsequent fate of the vesicular membrane regarding recycling is not investigated. Surprisingly, the RRP SVs can also undergo a distinct dynasore insensitive KR mode of exocytosis following stimulation by a distinct stimulus (HK5C) and this mode is switched to FF if NMII ATPase activity is blocked by blebbistatin. This NMII dependent KR mode requires the activation of certain PKC isoforms.

The HK5C induced KR mode of the RRP has been described as dynamin independent, because inhibiting the dynamin GTPase activity did not prevent such KR. However, it is possible that dynamin may have interacted with NMII independently of this activity and therefore the location of dynamin may have been important for this KR as it may have participated in positioning the NMII in the correct location, perhaps at the fusion pore membrane. This has been tested as another drug, MiTMAB has been found to specifically prevent dynamin I and II from translocating from the cytosol to the membrane by binding to the PH domain of dynamin (Quan *et al.*, 2007; Linares-Clemente *et al.*, 2015). Thus, it was possible that MiTMAB pre-treatment may prevent dynamin interacting with the membrane and this may have perturbed KR exocytosis of the RRP SVs. Indeed, such treatment has been used to answer two questions:

(i) Does dynamin have to be translocated to the relevant membrane site to allow the dynasore sensitive dynamin dependent KR exocytosis?

(ii) Does dynamin have to be translocated to the relevant membrane site to allow for the dynasore insensitive NMII dependent KR exocytosis?

3.6 Dynamin Translocation Inhibition Using MiTMAB Upon Synaptic Vesicle Release Dynamics

3.6.1 Treatment of MiTMAB Upon Evoked Glu Release

Evoked Glu release by 4AP5C, HK5C and ION5C was measured in synaptosomes following their treatment with 30 µM MiTMAB for 5 min at 37ºC (Figure 3.12). Such drug treatment did not perturb the 4AP5C (Figure 3.12a), HK5C (Figure 3.12b) or ION5C (Figure 3.12c) evoked Glu release.

Clearly, the data from Figure 3.12 indicates that this MiTMAB treatment did not perturb either the release of Glu from the RRP (Figure 3.12a) or the release of Glu from both the RRP and the RP (Figure 3.12b, 3.12c). By measuring FM dye release evoked by HK5C or ION5C following MiTMAB treatment one can attempt to answer the questions set above (Figure 3.13).

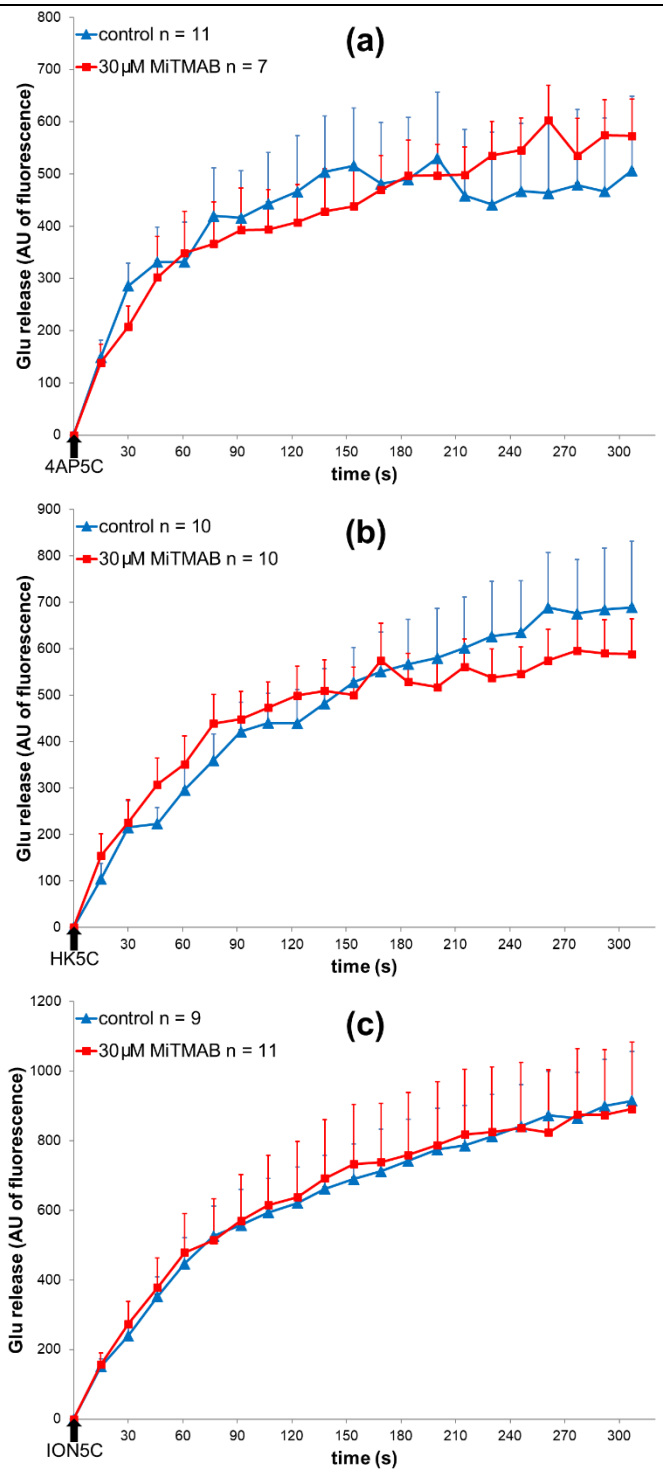

Figure 3.12: The effect of 30 µM MiTMAB vs control upon evoked Glu release. Treatment of 30 µM MiTMAB had no significant effect upon (a) 4AP5C, (b) HK5C or (c) ION5C evoked Glu release, compared to non-drug controls ($p > 0.05$). Values represented are the mean plus SEM from 3 independent experiments.

3.6.2 Treatment of MiTMAB Upon FM 2-10 Dye Release

In contrast to results with dynasore, 5 min MiTMAB treatment at 37ºC failed to change the amount of FM 2-10 dye release evoked by HK5C (Figure 3.13a) or ION5C (Figure 3.13b).

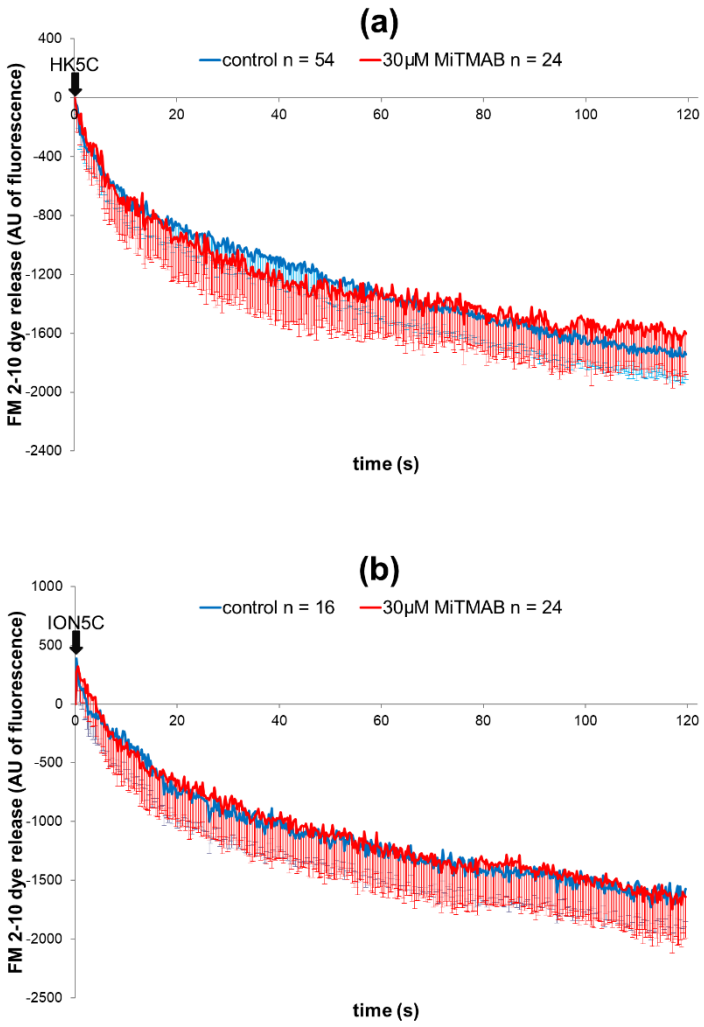

Figure 3.13: The effect of 30 µM MiTMAB vs control upon evoked FM 2-10 dye release. Treatment of 30 µM MiTMAB had no significant effect upon (a) HK5C or (b) ION5C evoked FM 2-10 dye release, compared to non-drug controls ($p > 0.05$). Values represented are the mean plus SEM from 4 (a and drug-treated b) and 8 (control b) independent experiments.

It would appear that the 5 min pre-treatment with 30 µM MiTMAB - which has been shown to perturb dynamin dependent processes previously (Quan *et al.*, 2007) - failed to affect the dynasore sensitive ION5C evoked KR release of the RRP. Clearly, as CME of the RP SVs dis not happen with MiTMAB treatment

and dynamin is required for CME then this means that MiTMAB did inhibit dynamin from binding to membranes. In this case dynamin binding to membranes was required to allow clathrin coated pits to pinch off from the PM.

This importantly indicates that the dynamin required to regulate the KR mode was already on the membrane prior to the treatment with MiTMAB. As such treatment also failed to perturb the HK5C dynasore insensitive KR release of the RRP SVs, this may indicate that any dynamin required to interact with NMII at the level of the membrane was already localised there. Note that for dynamin dependent clathrin dependent SV endocytosis, dephosphorylation by PP2B is normally required for the dynamin to interact with the membranes. Such dephosphorylation of dynamin-1 requirements for regulation of KR of the RRP has been previously investigated (Bhuva 2015; Singh, 2017) and it was suggested that only a minor population of the total dynamin-1 may be involved. This is complicated further if it is the population that is already dephosphorylated (prior to stimulation) and it is already present on the membrane. However, this dephosphorylated population can be phosphorylated by PKC and under such circumstances this dynamin can no longer play a role in regulating KR. There is recently appearing evidence that dynamin does indeed gather at the PM in a dephosphorylated state, explained later in this chapter in 3.8 Discussion (Imoto *et al.*, 2022).

3.6.3 Treatment of MiTMAB Upon Changes in Intracellular Ca^{2+} Levels

For completeness, the effect of 5 min pre-treatment with 30 µM MiTMAB on evoked changes in $[Ca^{2+}]_i$ and on bioenergetics was also measured. Such drug treatment failed to effect the evoked changes in intracellular Ca^{2+} induced by HK5C (Figure 3.14a) or ION5C (Figure 3.14b).

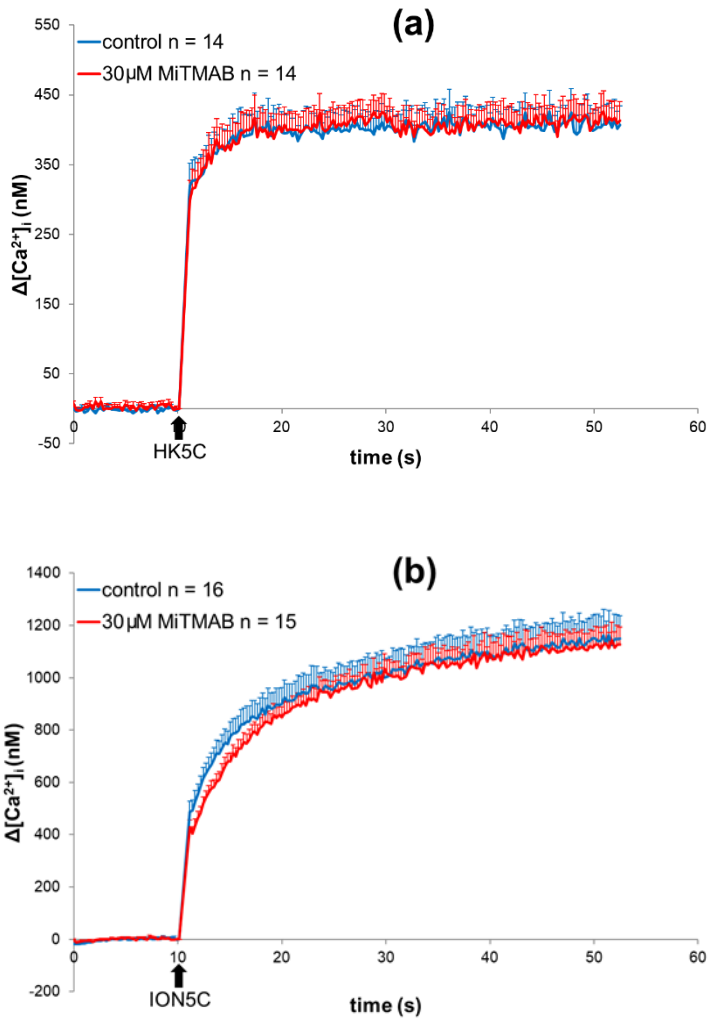

Figure 3.14: The effect of 30 µM MiTMAB vs control upon evoked $[Ca^{2+}]_i$ levels. Treatment of 30 µM MiTMAB did not significantly affect intracellular Ca^{2+} levels when stimulated with (a) HK5C or (b) ION5C stimuli, compared to non-drug controls ($p > 0.05$). Values represented are the mean plus SEM from 3 independent experiments.

3.6.4 Treatment of MiTMAB Upon Synaptosome Bioenergetics

Utilising the bioenergetics analyser and measuring mitochondrial function as reflected in oxygen consumption rate, it is clear that pre-treatment with 30 µM MiTMAB did not perturb the bioenergetics of the synaptosomes (Figure 3.15).

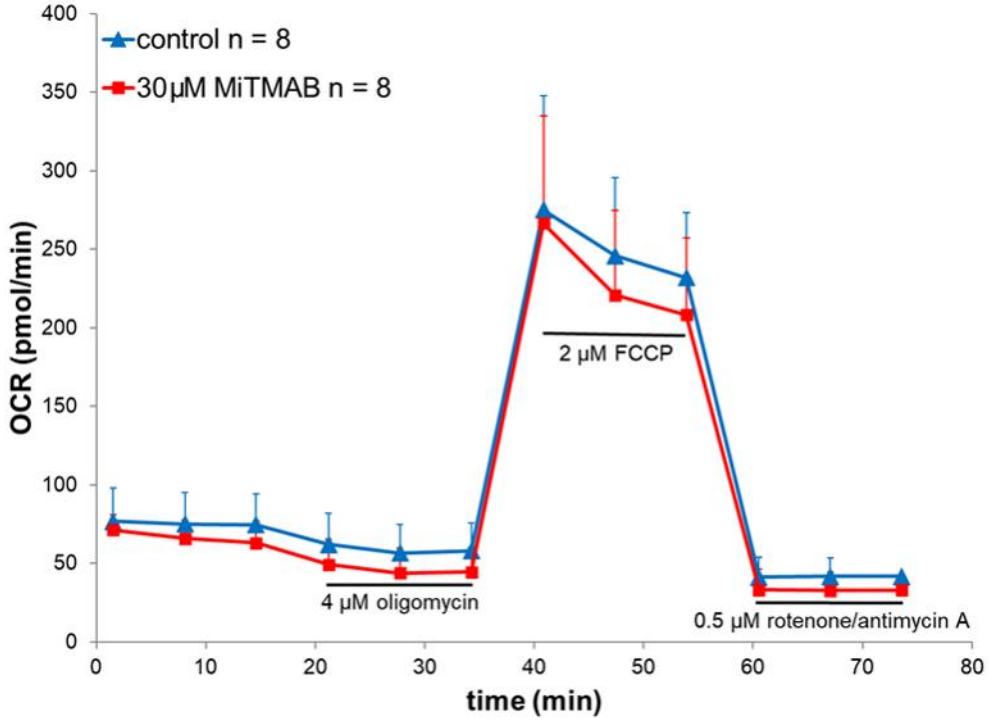

Figure 3.15: The effect of 30 µM MiTMAB vs control upon synaptosome bioenergetics. Treatment of 30 µM MiTMAB did not significantly affect the OCR of synaptosomes compared to control during a Mito-Stress test ($p > 0.05$). Values represented are the mean plus SEM from 3 independent experiments. The experiments were performed at 37˚C in the Seahorse Xfp flux analyser**.**

There was no significant difference between any of the parameters apart from the non-mitochondrial respiration where there is a small significant reduction (Figure 3.16). However, as this particular OCR parameter represents non-mitochondrial respiration, it is difficult to know what this means.

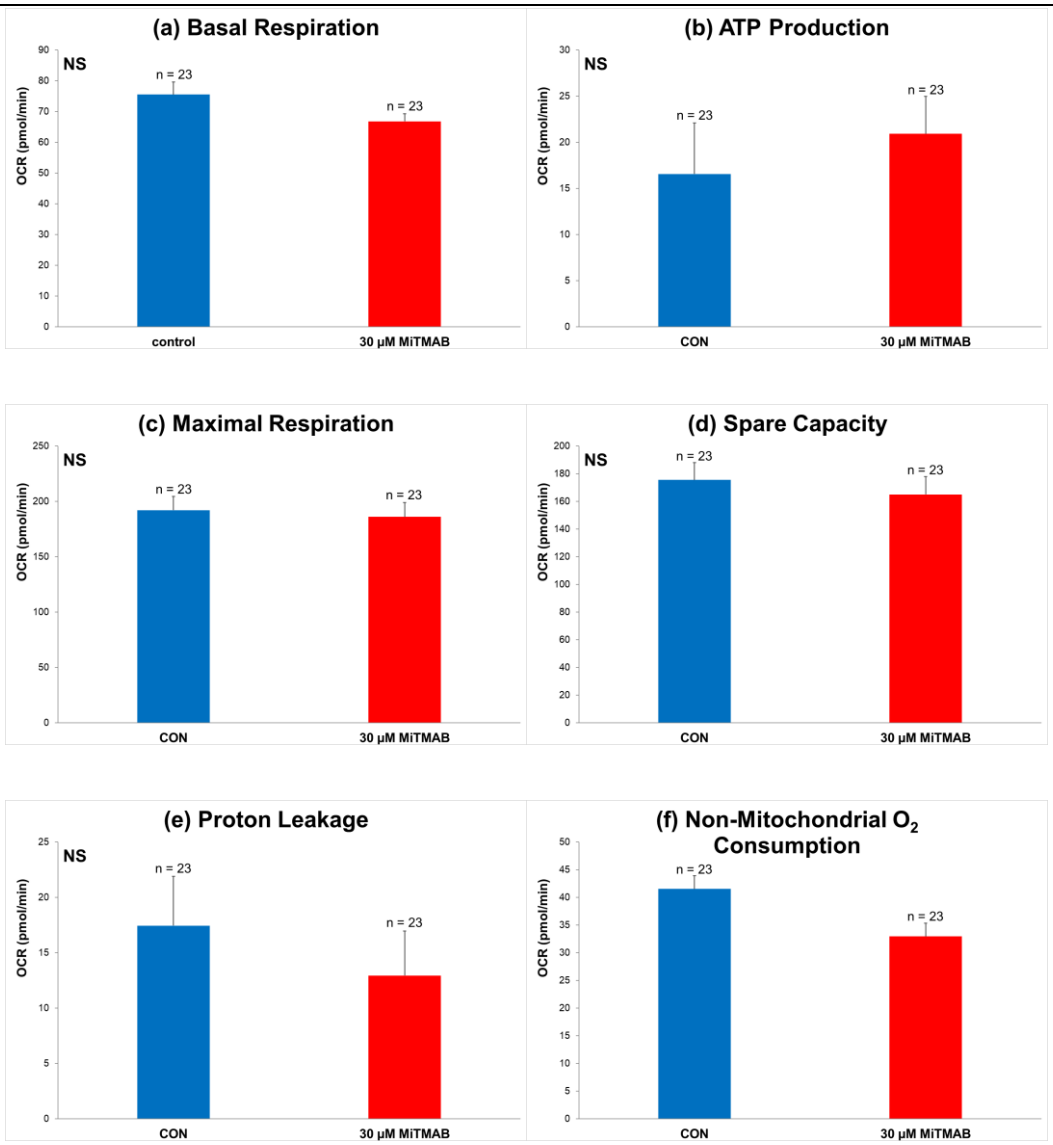

Figure 3.16: The effect of 30 µM MiTMAB vs control upon mitochondrial function. Treatment of 30 µM MiTMAB caused no significant difference in (a) basal respiration, (b) ATP production, (c) maximal respiration, (d) spare capacity or (e) proton leakage compared to non-drug control synaptosomes ($p > 0.05$). (f) Non-mitochondrial oxygen consumption had a significant difference of $p = 0.0154$ compared to non-drug control synaptosomes. Values represented are the mean plus SEM from 3 independent experiments.

3.7 Prolonged MiTMAB Treatment on HK5C Evoked Synaptic Vesicle Release

The dephosphorylation/phosphorylation cycle for dynamin-1 action on SV endocytosis is suggested to consist of a stimulus evoked dephosphorylation to allow dynamin to interact with the membrane, followed by a subsequent re-phosphorylation step which in a period of approximately 5 min then allows dynamin to detach from membranes (Robinson, 1991). Our interpretation of the results above is that there is some dynamin-1 already attached to membranes that can participate in regulating the KR mode of exocytosis of the RRP SVs. However, it was hypothesised that this dynamin would eventually dissociate from the membrane with time so that utilising a prolonged incubation with MiTMAB might then reveal that fresh dynamin has to re-associate with the membrane in order for dynamin dependent dynasore insensitive, but blebbistatin sensitive, KR exocytosis to occur following HK5C stimulation.

The time chosen for a prolonged incubation was a compromise since too long a pre-incubation at 37ºC may perturb the size of the Glu containing pools of SVs. Synaptosomes were pre-treated for 20 min at 37ºC with 30 µM MiTMAB and both HK5C Glu release (Figure 3.17) and HK5C FM2-10 dye release (Figure 3.18) were measured.

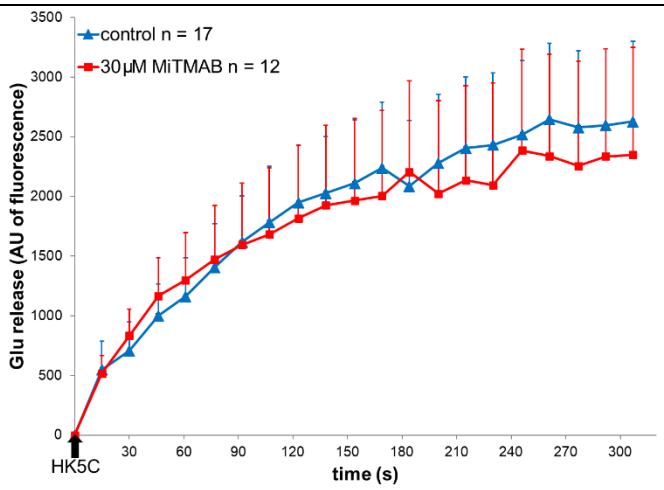

Figure 3.17: The effect of 20 min at 37ºC 30 µM MiTMAB vs control upon evoked Glu release. Treatment of 30 µM MiTMAB had no significant effect upon HK5C evoked Glu release, compared to non-drug controls ($p > 0.05$). Values represented are the mean plus SEM from 4 (control) or 3 (MiTMAB) independent experiments.

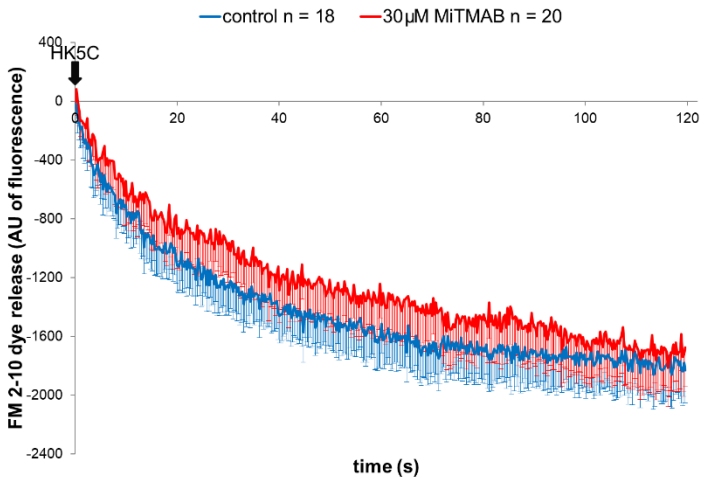

Figure 3.18: The effect of 20 min at 37ºC 30 µM MiTMAB vs control upon evoked FM 2-10 dye release. Treatment of 30 µM MiTMAB had no significant effect upon HK5C evoked FM 2-10 dye release compared to non-drug controls ($p > 0.05$). Values represented are the mean plus SEM from 3 independent experiments.

Clearly, under prolonged MiTMAB treatment, there was still no effect on HK5C evoked KR exocytosis of the RRP SVs suggesting that NMII does not require the protein dynamin to regulate the fusion pore.

To ensure that MiTMAB was perturbing dynamin binding to membranes, one can check its effect on recycling of SVs that involve the clathrin dependent dynamin requiring endocytosis. To do this, the synaptosomes were pre-treated for 20 min at 37ºC with 30 µM MiTMAB. Following this the synaptosomes were pre-stimulated with HK5C and then the SVs were allowed to recycle. Those SVs that required clathrin and dynamin (the RP SVs) should not recycle whilst the RRP SVs undergoing KR via NMII dependent KR should still recycle. This can then be measured by stimulating the synaptosomes to release Glu and observing whether there was less SVs exocytosing following MiTMAB pre-treatment. Figure 3.19a shows that there was no reduction in 4AP5C evoked Glu release following this protocol. This indicates that the RRP SVs have recycled independently of a dynamin requirement. However, Figure 3.19b demonstrates that there is less ION5C evoked Glu release following the protocol outlined – similar to that released by 4AP5C - and this shows that the MiTMAB was perturbing the dynamin association with the membrane so that the RP recycling following FF exocytosis is blocked.

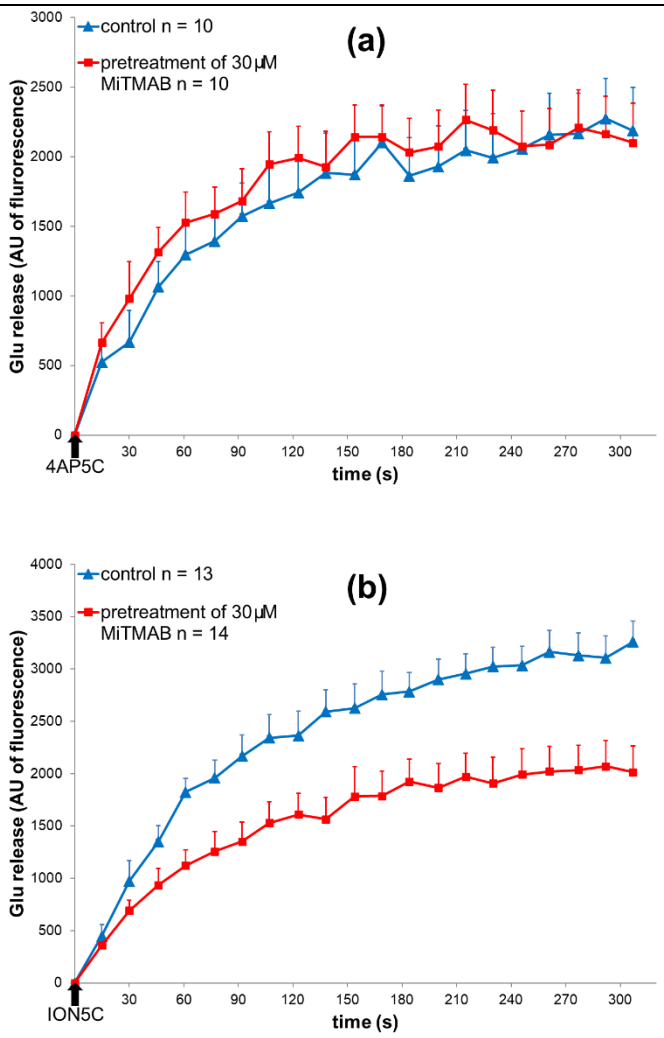

Figure 3.19: The effect of 20 min at 37ºC using 30 µM MiTMAB or solvent (control), pre-stimulated with HK5C and subsequently stimulated with 4AP5C or ION5C upon evoked Glu release. (a) There was no significant reduction in 4AP5C evoked release in synaptosomes treated with MiTMAB compared to control. Experiment performed 3 independent times ($p > 0.05$). (b) There was a significant reduction in ION5C evoked release in synaptosomes treated with MiTMAB compared to control ($p < 0.05$). Values represented are the mean plus SEM from 4 independent experiments.

3.8 Discussion

This chapter describes the roles that PKA may play in the regulation of amount and the mode of exocytosis of glutamatergic SVs in rat cerebral cortical synaptosomes. The effects of drug induced PKA inhibition and activation upon Glu release, FM 2-10 dye release, $[Ca^{2+}]_i$ levels and terminal bioenergetics were studied. It has been demonstrated, herein, that PKA modulation can switch the mode of Glu release in distinct SV pools during stimulation, without affecting the amount of Glu released or the $[Ca^{2+}]_i$ levels. Synaptosome bioenergetics were not perturbed.

Research has shown that PKA can enhance neurotransmitter release probability (Trudeau, *et al*., 1996), modify synaptic transmission by acting on neurotransmission machinery (Boczan, *et al*., 2004), and regulate synaptic plasticity and SV priming through phosphorylation of multiple downstream proteins (Nguyen and Woo, 2003; Leenders and Sheng, 2005; Wang and Sieburth, 2013).

The kinase PKA did not regulate evoked release of Glu from synaptosomes. Treatment with 2 µM KT5720 (Figure 3.1) and 50 µM cBIMPS (Figure 3.6), had no significant effect upon Glu release. As HK5C or ION5C can induce the maximum amount of Glu release from the RRP and RP SVs, ascertained by $[Ca^{2+}]_e$ dose response curves (Figure A1 in Appendix A; Bhuva 2015), these data indicate that neither inhibition nor activation of PKA affected the amount of SVs undergoing exocytosis with maximal stimuli. This finding concurs with research which finds no reduction in Glu release, or the availability of SVs to undergo release, when PKA activity was modulated (Trudeau *et al.*, 1996; Menegon *et al.*, 2006).

Any change in SV release by modifying PKA activity may be related to control SV release being sub-maximal in other studies (Chavez-Noriega and Stevens, 1994; Weisskopf, *et al*., 1994; Tzounopoulos, *et al*., 1998). In those conditions PKA may have been able to mobilise more SVs to exocytose, although it could not induce a greater release than with maximal stimulation, as such were the conditions of the experiments of this thesis.

Previous research by Ashton's group established that 4AP5C, HK5C and ION5C all evoked SVs to undergo one round of release (Bhuva, 2015). If SV recycling was occurring, the observed level of evoked Glu release would continue to rise over the duration of the assay and not plateau as seen in the Glu release figures shown within this chapter. Further, acute treatment of bafilomycin A1, which allows the first round of SV release but prevents further rounds, has no effect on the 4AP5C, ION5C or HK5C evoked Glu release (Figure A4 in Appendix A).

Similarly, as discussed earlier, it has been shown that 4AP5C maximally releases the RRP, whilst HK5C and ION5C both maximally release the RRP and the RP; therefore figures herein cannot reflect sub-maximal PKA activity for SV release or recycling of any vesicle pool. The drug Pitstop® 2 is a selective, membrane permeable clathrin inhibitor, which competitively inhibits the clathrin terminal domain of clathrin to selectively inhibit CME (Von Kleist *et al.*, 2011; Robertson *et al.*, 2016). Inhibition of clathrin dependent recycling with Pitstop®2 does did reduce SV release, which is further evidence that only one round of SV release occurs in this model (see Appendix Figures A5-A8).

Although PKA activity did not regulate the release of SV pools it did have a direct role in regulating the mode of SV exocytosis. Figure 3.2 shows that inhibition of PKA caused significantly more FM 2-10 dye release than controls, when stimulated with 4AP5C (Figure 3.2a) and ION5C (Figure 3.2c). Stimulation with 4AP5C released only the RRP of SVs, with approximately half releasing via KR mode and the rest via FF mode during controls; stimulation with HK5C and ION5C released the RRP exclusively by KR mode, and the RP exclusively by FF mode during controls (Figures A6 and A7 in Appendix A; Bhuva, 2015). Figure 3.2 indicates that inhibition of PKA with KT5720 caused SVs in the RRP to switch their mode of exocytosis from KR to FF mode, when stimulated with 4AP5C and ION5C. However, HK5C stimulation did not increase FM 2-10 dye release in a similar manner when PKA was inhibited (Figure 3.2b) showing that the RRP SVs were remaining in KR mode. A similar phenotype was also observed in previous research when dynamin-1 was inhibited with 160 µM dynasore (see Figure A12 in Appendix A) (Bhuva, 2015). It was concluded that dynamin-1 is required to close the fusion pore during KR exocytosis of the RRP when synaptosomes were stimulated with 4AP5C and

ION5C. Ashton's group previously demonstrated that 4AP5C and ION5C stimulation induced $[Ca^{2+}]_i$ changes through different kinetics at the AZ, whereas HK5C is known to have induced a higher and faster initial $[Ca^{2+}]_i$ level at the AZ (Figure A2 in Appendix A; Bhuva 2015). Even though dynamins appear to have been inactivated for SV exocytosis during HK5C stimulation, RRP SVs are hypothesised to still have been able to release via KR mode as the higher $[Ca^{2+}]_i$ activated NMII which could have closed the fusion pore, making a dynamin-independent KR mode (Figures A9a and A10a in Appendix A).

Dynamins appear to have been inactivated, thus did not take part in SV exocytosis during HK5C stimulation - this is a complex phenomenon. The NMII present did override any effect of dynamin so that the mode of exocytosis was regulated by NMII during HK5C stimulation. However, if dynamin was active along with NMII then when NMII was inhibited, any active dynamin should have still functioned and regulated the KR. Yet it did not, suggesting that the dynamin must have been inactivated/inhibited. The idea that this was due to active PKC inactivating dynamin but activating NMII holds up because when PKC was inhibited then NMII was no longer activated whilst dynamin became active and dynasore then blocked HK5C induced KR. Further, we could make ION5C function through the NMII pathway if we activated PKC with 40 nM PMA, which inactivated dynamin but activated NMII (see Appendix A).

The PKA protein has not been observed to directly phosphorylate dynamin-1 but it does have some phosphorylation targets in the pre-synaptic terminal such as syntaphilin, which regulates the availability of dynamin-1. Such regulation may inhibit dynamin-mediated endocytosis (Das *et al.*, 2003; Boczan *et al.*, 2004). Potentially the activity of PKA could regulate syntaphilin to affect the availability of dynamin-1, and such processes could then regulate the KR during 4AP5C and ION5C stimulation. As NMII is not being inhibited by syntaphilin, NMII is still free to mediate KR during HK5C stimulation, when dynamin-1 is inactive anyway, and this is worth investigating further by assessing the phosphorylated state of syntaphilin following PKA inhibition. Alternatively, PKA could phospho-regulate an unknown phosphatase to dephosphorylate dynamin-1, thus allowing it to mediate KR. Clearly, inhibition of PKA prevents such interactions, leading to FF at the AZ, since KR cannot occur.

Figure 3.7 shows that PKA activation can also specifically regulate mode of exocytosis of RP SVs. Activation of PKA with 50 µM cBIMPS caused significant decrease in FM 2-10 dye released from synaptosomes when stimulated with HK5C (Figure 3.7b) and ION5C (Figure 3.7c) but not 4AP5C (Figure 3.7a). As mentioned, both HK5C and ION5C released the RP via FF mode when in control conditions. PKA activation showed that SVs in the RP were switched from FF mode to KR mode, as less FM 2-10 dye was released. This effect was found to be specific to the RP as no mode switch was seen for the sub-pool of SVs in the RRP which undergo FF when stimulated with 4AP5C. Thus, increasing PKA phosphorylation activity leads to increase of RP SVs using KR mode in this model.

This phenotype resembles previous research in which PP2B inhibited with Cys A (Figure A15 in Appendix A; Bhuva, 2015). The phosphatase PP2B dephosphorylates dynamin-1 during terminal depolarisation (Liu *et al.*, 1994; Bauerfeind *et al.*, 1997; Marks and McMahon, 1998). It was inferred that dynamin-1 localised to the RP may have required PP2B mediated dephosphorylation in order to drive fusion pore expansion during FF mode exocytosis (Bhuva, 2015). Thus, inhibiting dynamin-1 dephosphorylation could prevent some RP SVs switching to FF mode of exocytosis.

However, inhibiting dynamin-1 with dynasore did not give the same result as Cys A treatment (see Figure A12 in Appendix A). Whereas dynasore treatment caused a switch of the RRP to KR mode with 4AP5C and ION5C, Cys A treatment caused a switch of the RP to KR with HK5C and ION5C. This demonstrated that although inhibition of PP2B led to an increase in SVs undergoing KR, it was not directly through regulating dynamin-1 activity. It has been demonstrated by Ashton's group that HK5C stimulated RRP release was mediated by NMII whereas dynamin-1 regulated RP release. With ION5C however both the RRP and RP were released via dynamin-1 involved mechanisms (Bhuva, 2015). Although the phenotype produced from Cys A was distinct from dynasore treatment and argued against PP2B dephosphorylation of dynamin-1, it would be useful to test the effect of the combined treatment of dynasore and Cys A; this might help elucidate the mechanisms occurring.

Similarly, FM 2-10 dye was still lost from the RP SVs when PKA was activated with cBIMPS (Figure 3.b and c), indicating that not all of the RP is being switched to KR mode by PKA activation. This result may suggest that there is a sub-pool of SVs within the RP which are available to switch to a KR mode of exocytosis under certain conditions, however further investigation is required. Some unpublished results from Ashton's group suggests that if all the RRP is undergoing KR mode, it is not possible for all the RP to also undergo KR mode. This indicates that the sites for KR exocytosis may become saturated in some stimulation conditions. If one converts the RRP to FF mode only, it appears that all RP SVs can undergo KR (Ashton *et al.*, unpublished). These data may indicate that PKA and PP2B share an unknown substrate which regulates the release dynamics of the RP, without regulating the RRP. Future experiments involving the release in isolation of just the RP may help us to understand the phenotypes described. As no RRP SVs would have undergone KR then treatment with cBIMPS or Cys A may switch all the RP SVs to a KR mode. However, one may still only see a partial switch to KR mode indicating that there may be two distinct populations of RP SVs, showing different sensitivities to these two drugs.

Some articles have scrutinised the specificity of KT5720 for PKA, stating that KT5720 may potentially inhibit other kinases and alter receptor-binding affinities through non-specific effects when used (Olsen, *et al*., 1998; Davies, *et al*., 2000; Lazareno, *et al*., 2000). Although KT720 may appear to be non-specific for PKA according to these articles, there are a few differences in methodology to be highlighted: in some models, *in vitro* cells were chronically incubated with KT5720 for longer than 10 min, in some cases hours (Davies, *et al*., 2000; Lazareno, *et al*., 2000). In the case of the experiments of this thesis, all drugs were incubated for only 10 min at 37°C and then added back at room temperature during the release assays or Fura-2 measurements. In some studies, cultured cells were kept at 30°C for the duration of the experiments (Davies, *et al*., 2000), whilst measurements of release in this thesis took place at room temperature. All models in those studies were either *in vitro*, using tissue cultures, bacterial cultures or cells with disrupted membranes (Olsen, *et al*., 1998; Lazareno, *et al.*, 2000), whilst synaptosomes used in this study herein

represent physiologically mature nerve terminals that exhibit Ca^{2+} dependent vesicular Glu release during the timescale of the experiments.

These differences can lead to fallacious assumptions about the specificity of drugs in these experiments and their long-term actions during chronic treatments. To highlight the specificity of both KT5720 and cBIMPS for PKA, a dual treatment was conducted for FM 2-10 dye release. Synaptosomes pre-treated with 2 µM K5720 followed by 50 µM cBIMPS treatment released an amount of FM 2-10 dye equal to controls when stimulated with HK5C and ION5C (Figure 3.11). If cBIMPS was not specific for PKA a decrease in evoked FM 2-10 dye would have been observed during ION5C stimulation with this dual treatment.

Changes to $[Ca^{2+}]_i$ levels have been linked to switching in the mode of exocytosis, where an increase may have led to a larger proportion of KR mode (Alés, *et al.*, 1999; Bhuva 2015; Singh 2017). When PKA was inhibited or activated, although distinct changes in the mode of exocytosis were observed for each stimuli, there was no significant change in $[Ca^{2+}]_i$ levels measured. This is convincing evidence that PKA activity regulates mode of exocytosis independently of $[Ca^{2+}]_i$, through phosphorylation of protein substrates.

Prevention of PKA from phosphorylating a target protein using KT5720 may inhibit the action of dynamin-1 during exocytosis, as this phenotype is similar to dynamin-1 inhibition with dynasore (Bhuva, 2015; Figure A12 in Appendix A), however further studies must be conducted to determine if there is a link between these proteins, and the extent of the signalling pathway. During control conditions it can be speculated that PKA could be phosphorylating - and thus activating - a phosphatase which dephosphorylates dynamin-1 allowing it to mediate KR mode; the inhibition of PKA may then prevent the activation of the phosphatase and of dynamin-1, leading to the same phenotype as direct dynamin-1 inhibition. Although this is speculative it provides new ideas to test in the future. The results of this thesis show that it appears possible that PKA may phosphorylate dynamin but there is not enough evidence for this. However, there are some functionally uncharacterised phosphorylation sites on dynamin 1 (Graham et al, 2007) that could be altered by the conditions highlighted here.

In previous studies, when PP2B inhibition was shown to give the same phenotype as PKA activation, it was assumed to be through activation changes to signalling pathways; however, Bhuva has demonstrated that inhibition of PP2B with Cys A significantly raised the $[Ca^{2+}]_i$ level, and also switched the RP to KR mode (Bhuva, 2015; see Figure A15 in Appendix A). However, PKA activation had no significant effect upon the $[Ca^{2+}]_i$ level, demonstrating that the activation of PKA could change the mode of RP exocytosis through signalling pathways rather than through changes to $[Ca^{2+}]_i$.

In order to ensure that distinct changes to mode of release were due to targeted drug action and not non-specific perturbation of synaptosome respiration by the drugs utilised in this study, drug treated synaptosomes were subjected to the Mito-Stress test. This test measures mitochondrial function by recording the OCR of synaptosomes under different induced respiratory parameters. If a drug treatment or condition negatively affected the energetic demands or the molecular integrity of the synaptosomes, the assay measurements would make this apparent. Drug induced inhibition and activation of PKA was not found to compromise synaptosome respiration during chronic or acute treatments of less than 5 min, as utilised with the Glu, FM 2-10 and Fura-2 assays. Thus we have confidence that KT5720 and cBIMPS treatment caused differences in mode of exocytosis without causing non-specific drug action or synaptosome perturbation, as there was no significant effect upon mitochondrial ATP production, maximal respiration, spare capacity, proton leakage or non-mitochondrial respiration (Figures 3.5b-f and 3.10b-f). Both drugs caused an increase in basal respiration (Figures 3.5a and 3.10a). Basal respiration is the OCR of the mitochondria of the sample to meet cellular ATP demands during resting conditions. Such an increase in basal respiration reflects the cells having an increased energy demand on the mitochondria (Agilent Technologies, 2019). Potentially, some activation or inhibition of PKA pathways may cause slight increase in basal respiration This effect would need to be studied in more detail to determine the functional significance.

Attempts have been made to correlate the phosphorylation state of dynamin-1 and the mode of exocytosis using phospho-specific antibodies to various sites on dynamin (see Bhuva 2015; Singh 2017). Although there is some preliminary data to suggest Ser 795 maybe important, studies have been quite elusive in

establishing the precise role. It was predicted that if only a small fraction of dynamin-1 is involved in the process of defining KR then this would mean that only small changes in phosphorylation of this fraction (and not the total dynamin) would be required, and western blotting may not be sensitive enough to show this.

The MiTMAB data indicates that only dynamin already attached to membranes (either the PM or SV membrane) must play a role in regulating the mode of exocytosis as prevention of evoked increase in membrane associated dynamin had no effect on the mode. As the cytosolic dynamin represents the major pool and this is the pool that is phosphorylated then clearly the resting membrane bound pool is only a small fraction of total dynamin and this is usually dephosphorylated. Future immunoprecipitation of the relevant phosphorylated dynamin-1 may help to elucidate the role of the small sub-population of dynamin regulating the mode of exocytosis. Also, future subcellular fractionation experiments (in the presence of kinase and phosphatase inhibitors) could isolate synaptic PMs, SVs and the cytosol, which could then be individually probed for the changes in specific phosphorylation sites on dynamin-1 including Ser774 and Ser778 and Ser795.

There is emerging evidence that dynamin may be pre-recruited to SV endocytic sites in molecular condensates to facilitate vesicle fission from the PM with required speed (Imoto *et al.*, 2022). When dynamin is recruited from the cytosol to endocytic sites, this requires seconds to tens of seconds (Cocucci *et al.*, 2014) however, UE in neurons internalises SVs as quickly as 50 ms from the PM during endocytosis (Watanabe *et al.*, 2013).

Dynamin-1 splice variant 1xA specifically interacts with syndapin 1 to form liquid-like concentrated molecular condensates on the inner surface of the PM in peri-active zones (in a punctum formation); disruption of dynamin-1xA and syndapin 1 interaction stops these condensate puncta from forming, slowing UE by 100-fold. Syndapin 1 acts as an adaptor by binding to dynamin-1xA and the PM, bypassing dynamin recruitment and allowing accelerated endocytosis at synapses (Imoto *et al.*, 2022).

That these liquid-like condensates were clearly visualised in a primary hippocampal mouse model and were required for membrane scission at speeds of under a second is compelling evidence that dynamin is usually pre-recruited at the PM to facilitate UE endocytosis in mammalian synapses. However, these studies did not inquire into any role of this dynamin pre-recruitment in dynamin-dependent KR endocytosis, which is a subject of interest for further study. Imoto *et al*. also suggested that these condensates may not have such a role in CME, as dynamin is not as concentrated, needing recruitment to the PM; that dynamin gradually accumulates near endocytic pits and is recruited to the endocytic neck by other proteins such as endophilin and amphiphysin (Cocucci *et al.*, 2014). Therefore, it is plausible that these dynamin subpopulations – in these condensate puncta – may not be affected by the PH domain inhibiting activity of MiTMAB and may be a major reason why MiTMAB treatment did not affect dynamin-dependent KR endocytosis after stimulation in synaptosomes (Figure 3.13).

The experiment wherein synaptosomes were pre-treated with MiTMAB prior to the pre-stimulation with HK5C was very revealing. First it showed that MiTMAB pre-treatment did work as it produced a reduction in Glu release showing that the clathrin pathway was being perturbed. More excitingly it revealed that the RRP SVs recycled via a clathrin-independent pathway following the stimulation of their exocytosis (fitting in with the idea that the RRP SVs were undergoing KR exocytosis/endocytosis when stimulated by HK5C). However, the RP SVs which underwent FF recycled by a clathrin dependent pathway such that MiTMAB pre-treatment prevented the subsequent release of the ION5C evoked RP SVs as these clearly were not available for release indicating that part of their recycling pathway following FF did require clathrin.

3.9 Conclusion

This chapter presents evidence that PKA inhibition potentially switches a proportion of SVs undergoing KR mode to FF mode of exocytosis. This is probably through blocking the action of dynamin-1. Conversely, PKA activation increases number of SVs undergoing KR mode, probably from the RP, possibly also throughdynamin-1. The PKA inhibitor KT5720 and the PKA activator cBIMPS have been shown to function acutely without perturbing Glu release, the viability of the synaptosomes, or affecting the $[Ca^{2+}]_i$ level within this synaptosome model.

The dynamin PH domain inhibitor MiTMAB did not perturb a first round of release of the RRP and RP SVs, but it did perturb a subsequent round of release of the RP SVs but not the RRP SVs. Thus, MiTMAB revealed that the dynamin involved in dynamin dependent KR is already on the membrane prior to the stimulation.

CHAPTER 4: Adenylate Cyclase Modulation Upon Synaptic Vesicle Release via PKA and EPAC Pathways

4.1 Adenylate Cyclase Regulation of Synaptic Vesicles

Chapter 3 of this thesis established that PKA inhibition could inhibit dynamin-1 dependent RRP KR mode (causing FF mode of the RRP), but that PKA activation could increase RP KR mode without causing observable change to the RRP. Furthermore, that chapter also demonstrated that membrane bound but not cytosolic dynamin-1 is required to regulate the RRP mode of exocytosis.

This chapter describes how modulation of the secondary messenger cAMP – by drug inhibition and activation of the cAMP synthesiser AC – affected the mode of exocytosis of the RRP and RP of SVs. Molecules of cAMP activate PKA, and this chapter describes whether cAMP modulation affects the mode of exocytosis exclusively via PKA activation or whether cAMP can work through other mediators.

The ribonucleotide cAMP is synthesised from ATP by the transmembrane enzyme AC. There are nine AC isoforms, and these are activated by the GTP-bound α subunit of stimulatory G protein (Sunahara *et al.*, 1996; Hanoune and Defer 2001; Sandana and Dessauer, 2009). The cAMP cascade is important in synaptic facilitation and potentiation and has a role in synaptic plasticity in memory and learning (Zhong and Wu, 1991; Grandoch *et al.*, 2010). Raised intracellular levels of cAMP can increase neurotransmitter release frequency (Chen and Regehr, 1997). As already stated, cAMP can activate PKA (Walsh *et al.*, 1968, Knighton *et al*., 1991) and it is this process which is believed to contribute to the pathways outlined above. However, there can be other pathways and in particular, cyclic nucleotide-regulated cation channels (Biel, 2008) may participate in some processes. The discovery of a family of cAMP activated proteins, exchange proteins directly activated by cAMP (EPACs) (de Rooij *et al.*, 1998; Kawasaki *et al.*, 1998), has led to the realisation that some PKA-independent effects of cAMP can be attributed to EPAC modulation by this cyclic nucleotide (Beaumont *et al.*, 2002; Ster *et al.*, 2007; Grandoch *et al.*, 2010).

Although NMII is implicated in SV fusion mechanisms, it is not known whether AC and PKA can modulate NMII action in this pathway. The research described

herein indicates novel ways in which AC activation can modulate SV dynamics and whether NMII participates in these mechanisms.

A relationship between cAMP and NMII has been established in various cells. It has been shown that adrenomedullin-induced relaxation of brain pericytes is related to reduced phosphorylation of MLC through a cAMP/PKA pathway (Takata *et al*., 2009). In the SH-EP neuroblastoma cell line, maintenance of focal adhesion complexes via NMII regulation underlies the ability of Cdc42 to protect against the effect of elevated cAMP on inducing stellate morphology (Dong *et al.*, 2002).

As cAMP – produced by activation of AC – can activate PKA, modulation of cAMP levels within the terminals may have been expected to cause similar mode switching conditions as to when PKA activity was directly modulated with KT5720 and cBIMPS treatments (see Chapter 3). However, cAMP activation of EPACs may also directly affect SV release dynamics (Almahariq *et al.*, 2013; Schmidt *et al.*, 2013).

Forskolin is used to activate AC (Seamon and Daly, 1981; Tang and Hurley, 1998) and such treatment naturally raises the amount of intracellular cAMP. Forskolin would appear to activate AC through a unique mechanism involving both direct activation of the enzyme and facilitation or potentiation of the modulation of enzyme activity by receptors or the guanyl nucleotide-binding subunit, or both. The drug 9-cp-ade is used to inhibit AC by inhibiting ACs non-competitively, via a domain referred to as the P-site because of its requirement for an intact purine moiety; 9-cp-ade acts as an analogue of the cAMP-pyrophosphate transition state to block ATP binding, which prevents AC action in generating cAMP molecules (Johnson *et al.* 1997). An inhibitor of EPACs, ESI-09 was also used to elucidate EPACs' relation to cAMP and SV release. ES1-09 is a cell-permeable compound that targets cAMP-binding domain of EPAC/cAMP-GEF and inhibits cAMP-dependent EPAC GEF activity (Almahariq *et al.*, 2013). These drugs were utilised to ascertain what effects activation and inhibition of AC, and the inhibition of EPACs, has upon Glu release, FM 2-10 dye release and the level of $[Ca^{2+}]_i$ induced by various stimuli.

4.2 Adenylate Cyclase Inhibition Using 9-cp-ade on Synaptic Vesicle Release Dynamics

4.2.1 Treatment of 9-cp-ade Upon Evoked Glutamate Release

The enzyme AC can be specifically inhibited by 9-cp-ade, a non-competitive inhibitor which targets the P-site of AC that prevents ATP binding, preventing cAMP synthesis (Johnson *et al*., 1997).

There was no significant change in Glu release from the RRP when synaptosomes were treated with 100 µM 9-cp-ade and 4AP5C stimulation (Figure 4.1a) nor from the RRP and RP when stimulated with HK5C (Figure 4.1b) or ION5C (Figure 4.1c).

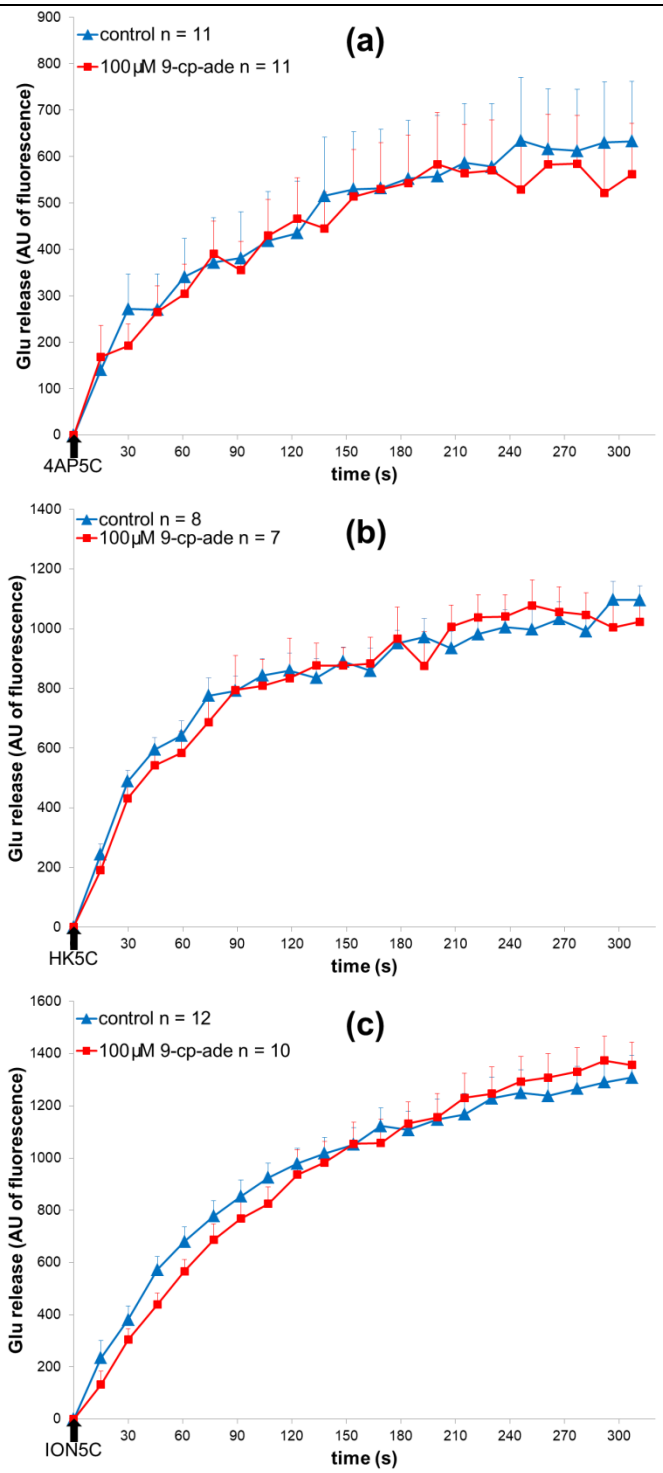

Figure 4.1: The effect of 100 µM 9-cp-ade vs control upon evoked Glu release. AC inhibition with 100 µM 9-cp-ade had no significant effect upon (a) 4AP5C (p = 0.655), (b) HK5C (p =0.700) or (c) ION5C (p = 0.872) evoked Glu release, compared to non-drug controls. Values represented are the mean plus SEM from 3 independent experiments.

4.2.2 Treatment of 9-cp-ade on FM 2-10 Dye Release

The release of FM 2-10 dye was investigated in synaptosomes treated with 100 µM 9-cp-ade. Inhibition of AC showed no significant effect upon dye released from RRP stimulation with 4AP5C (Figure 4.2a) nor RRP and RP stimulation with HK5C (Figure 4.2b) or ION5C (Figure 4.2c). Clearly, inhibition of AC did not regulate the mode of exocytosis from the RRP or RP under any of the stimulation conditions employed.

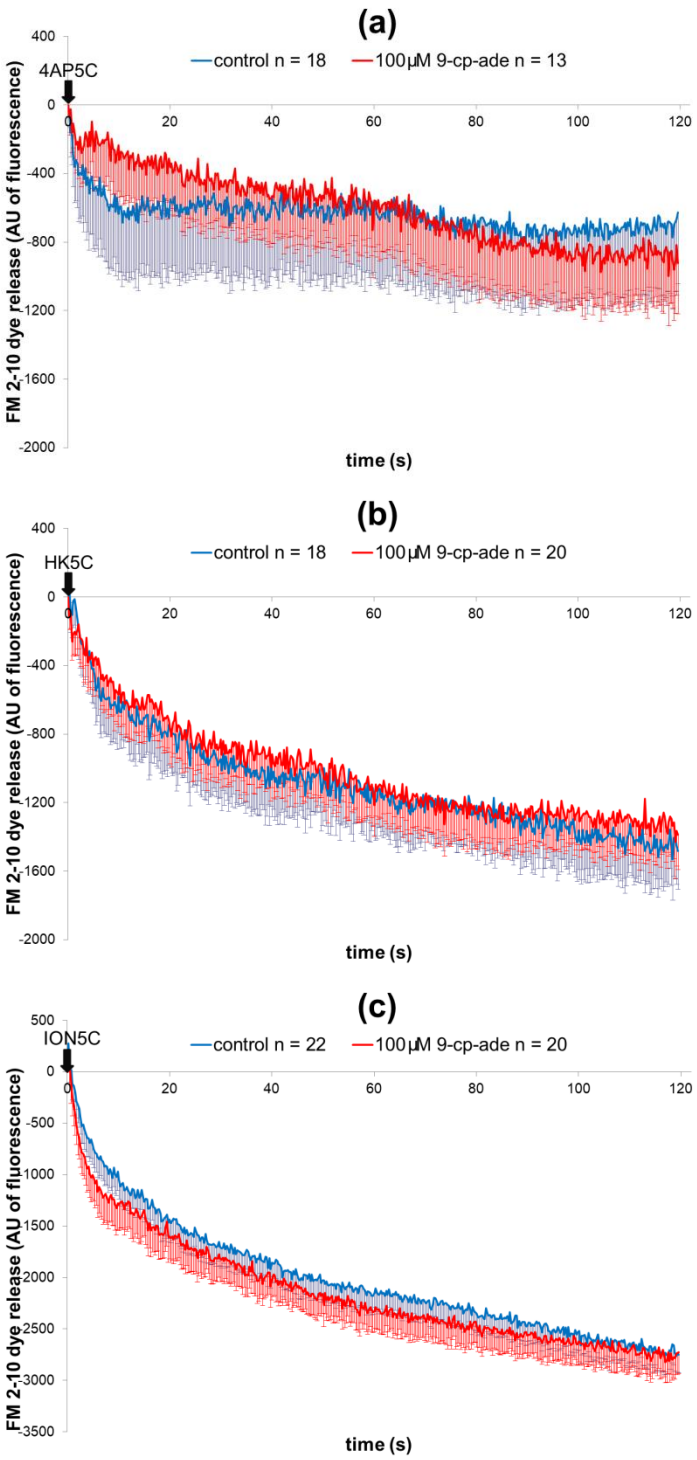

Figure 4.2: The effect of 100 µM 9-cp-ade vs control upon evoked FM 2-10 dye release. AC inhibition with 100 µM 9-cp-ade had no significant effect upon (a) 4AP5C ($p = 0.572$), (b) HK5C ($p = 0.8064$) or (c) ION5C ($p = 0.6343$) evoked FM 2-10 dye release, compared to non-drug controls. Values represented are the mean plus SEM from 3 independent experiments.

4.2.3 Treatment of 9-cp-ade Upon Changes in Intracellular Ca^{2+} Levels

Although using any of the stimuli there were no significant changes in maximal Glu release or mode of exocytosis with addition of 9-cp-ade compared to control, it was still possible that 9-cp-ade treatment may induce changes in evoked changes in $[Ca^{2+}]_i$ levels. Thus, evoked changes in $[Ca^{2+}]_i$ levels following 9-cp-ade treatment was measured using the Fura-2 assay. Synaptosomes treated with 100 µM 9-cp-ade showed no significant difference in their evoked $[Ca^{2+}]_i$ levels when stimulated with HK5C (Figure 4.3a) or ION5C (Figure 4.3b) compared to non-drug controls.

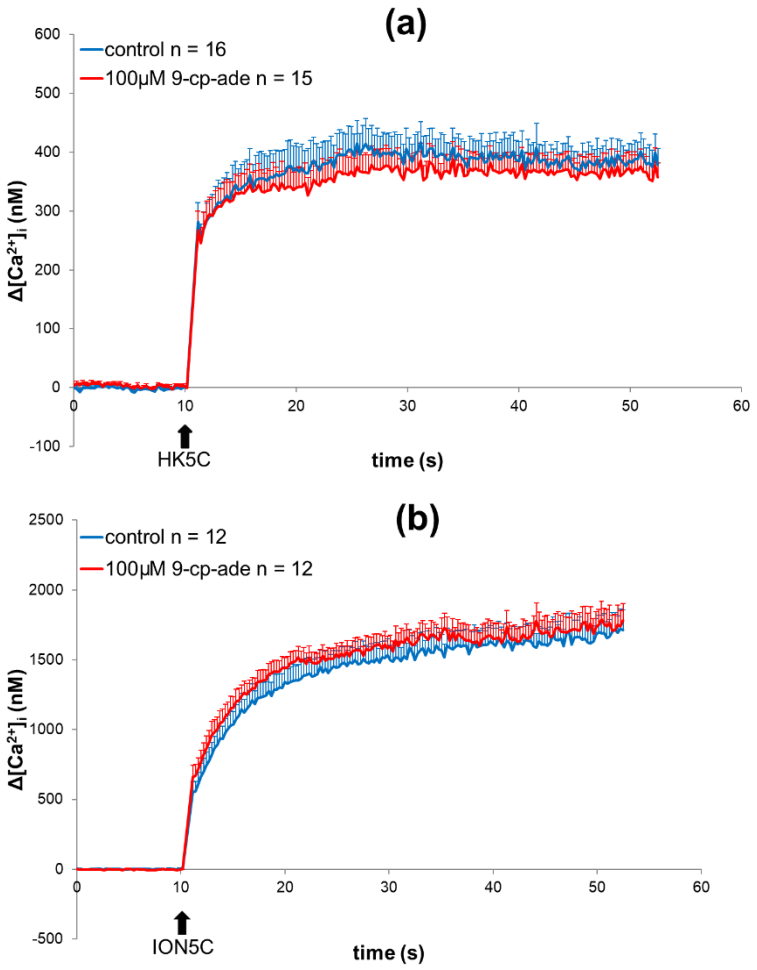

Figure 4.3: The effect of 100 µM 9-cp-ade vs control upon evoked $[Ca^{2+}]_i$ levels. AC inhibition with 100 µM 9-cp-ade did not significantly affect evoked $[Ca^{2+}]_i$ levels when stimulated with (a) HK5C ($p = 0.271$) or (b) ION5C ($p = 0.289$), compared to non-drug controls. Values represented are the mean plus SEM from 3 independent experiments.

4.2.4 Treatment of 9-cp-ade Upon Synaptosome Bioenergetics

In order to test for any respiratory perturbation after 9-cp-ade treatment, synaptosomes treated with 100 µM 9-cp-ade were subjected to the Mito-Stress test (these tests take over 90 min to complete and was performed at 37°C). No significant difference was observed compared to control (Figure 4.4) and there were no significant effects upon the mitochondrial function parameters (Figure 4.5 a-f).

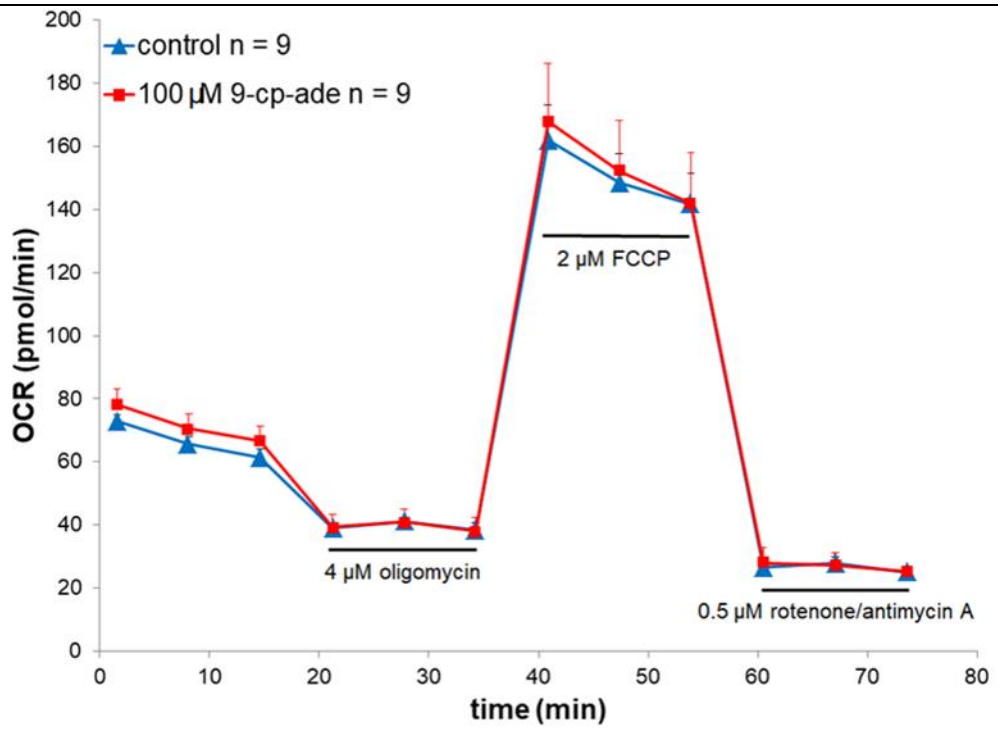

Figure 4.4: The effect of 100 µM 9-cp-ade vs control upon synaptosome bioenergetics. Treatment of 100 µM of AC inhibitor 9-cp-ade did not significantly affect the bioenergetics of synaptosomes compared to control during a Mito-Stress test (p = 0.920). Values represented are the mean plus SEM from 3 independent experiments. The experiments were performed at 37˚C in the Seahorse Xfp flux analyser.

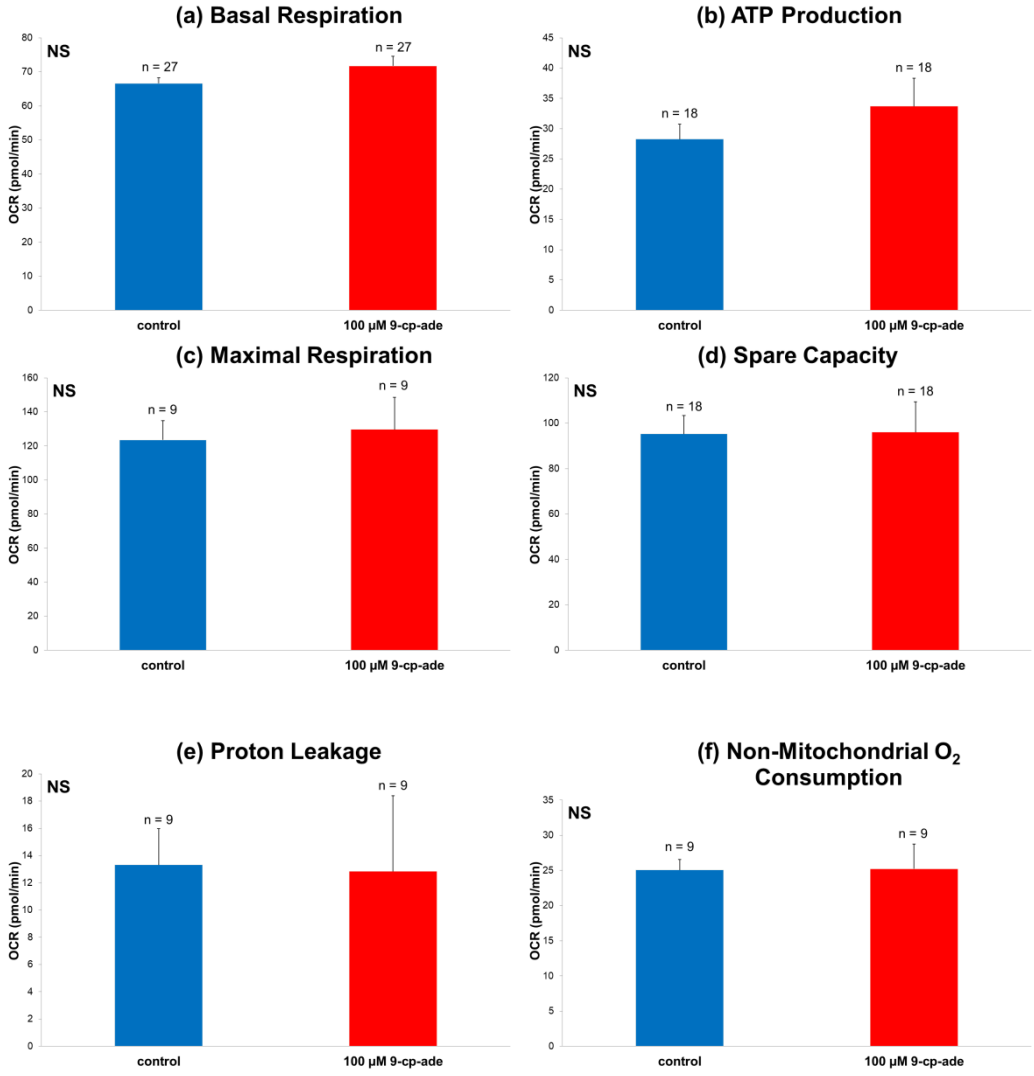

Figure 4.5: The effect of 100 µM 9-cp-ade vs control upon mitochondrial function. AC inhibition with 100 µM 9-cp-ade showed no significant change in (a) basal respiration, (b) ATP production, (c) maximum respiration, (d) spare capacity, (e) proton leakage or (f) non-mitochondrial oxygen consumption, compared to non-drug control synaptosomes (all parameters $p > 0.05$). Values represented are the mean plus SEM from 3 independent experiments. *NS*, not significant.

4.3 Adenylate Cyclase Activation Using Forskolin on Synaptic Vesicle Release Dynamics

4.3.1 Treatment of Forskolin Upon Evoked Glutamate Release

As inhibition of AC with 9-cp-ade did not affect evoked Glu release, the effect of the selective AC activator forskolin was investigated. Forskolin increases the binding affinity of cytoplasmic domains C1 and C2 of AC to each other and this produces a protein conformation that is more efficient for cAMP synthesis, and it is shown that the drug significantly increases intracellular cAMP levels (Seamon and Daly, 1981; Dessauer *et al*., 1997). Forskolin via increasing cAMP levels has also been shown to increase $[Ca^{2+}]_i$ levels (Herrero and Sánchez-Prieto, 1996) through activation of PKA and EPACs (Ferrero *et al.*, 2013).

Treatment of synaptosomes with 100 µM forskolin showed no significant change in Glu release from the RRP when stimulated with 4AP5C compared to non-drug controls (Figure 4.6a). However, evoked Glu release was significantly lower than non-drug controls in synaptosomes stimulated with HK5C (Figure 4.6b) and ION5C (Figure 4.6c). The interpretation of this is that forskolin reduced SV exocytosis exclusively from the RP rather than from the RRP, and indeed, comparing the release evoked by all three stimuli in the presence of forskolin indicates that they all released similar amounts of Glu (differences between the various stimuli were not significant in forskolin treated terminals), and therefore similar numbers of SVs were exocytosing, and this is from the RRP.

To confirm that the forskolin-induced decrease in RP exocytosis was due to a specific activation of AC, synaptosomes were treated with 100 µM of 1,9-dideoxyforskolin which is an inactive homologue of forskolin unable to activate AC and HK5C-evoked release of the RRP and RP was measured (Pinto *et al*., 2009). There was no significant change in HK5C evoked Glu release compared to non-drug treated control (Figure 4.7). This result indicates that the effect of forskolin on the release of the RP was due to the specificity of forskolin induced AC activation.

The specific effect of forskolin upon AC was further confirmed when synaptosomes were pre-treated with 100 µM 9-cp-ade to inhibit AC prior to their

subsequent treatment with 100 µM forskolin. As AC should have been inhibited forskolin should have no longer been able to stimulate its activity. Under such conditions HK5C was able to release both the RRP and the RP (Figure 4.8b). As expected, such dual treatment failed to affect the release evoked by 4AP5C compared to non-drug treated control since neither drug individually affected such release (Figure 4.8a). These results showed that forskolin specifically inhibited release of HK5C evoked release of the RP by activating AC. As a corollary they also further confirm that 9-cp-ade inhibited AC.

As forskolin raised cAMP levels one might expect this to have activated PKA and that therefore, the results with forskolin should have been similar to those when PKA was activated by cBIMPS. This was clearly not the case because in Chapter 3 cBIMPS treatment did not perturb HK5C (Figure 3.6 b) and ION5C (Figure 3.6 c) evoked Glu release, and there was no perturbation of the release of the RP. This indicated the possibility of a different cAMP substrate being modulated following forskolin treatment and it is the regulation of this substrate that caused the reduction in RP exocytosis. This was the reason that we investigated the role of EPACs by perturbing their action with ESI-09, described later in this chapter.

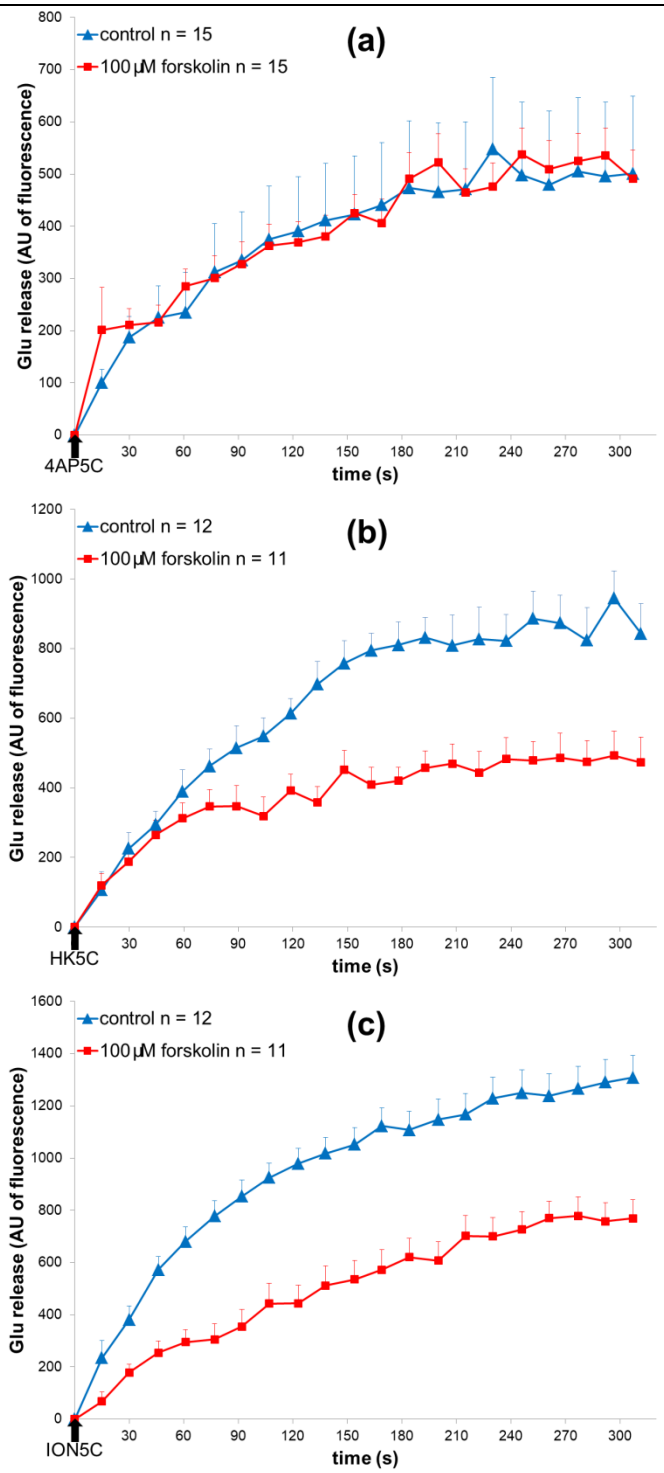

Figure 4.6: The effect of 100 µM forskolin vs control upon evoked Glu release. AC activation with 100 µM forskolin had no significant effect upon (a) 4AP5C ($p = 0.861$), but significantly decreased (b) HK5C ($p < 0.001$) and (c) ION5C ($p < 0.001$) evoked Glu release, compared to non-drug controls. Values represented are the mean plus SEM from 3 (a) and 5 (b and c) independent experiments.

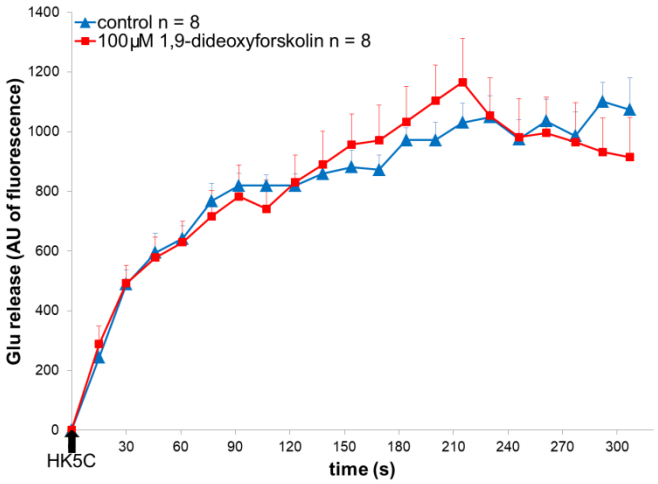

Figure 4.7: The effect of 100 µM 1,9-dideoxyforskolin vs control upon evoked Glu release. 100 µM 1,9-dideoxyforskolin had no significant effect upon HK5C evoked Glu release (p = 0.991), compared to non-drug controls. Values represented are the mean plus SEM from 3 independent experiments.

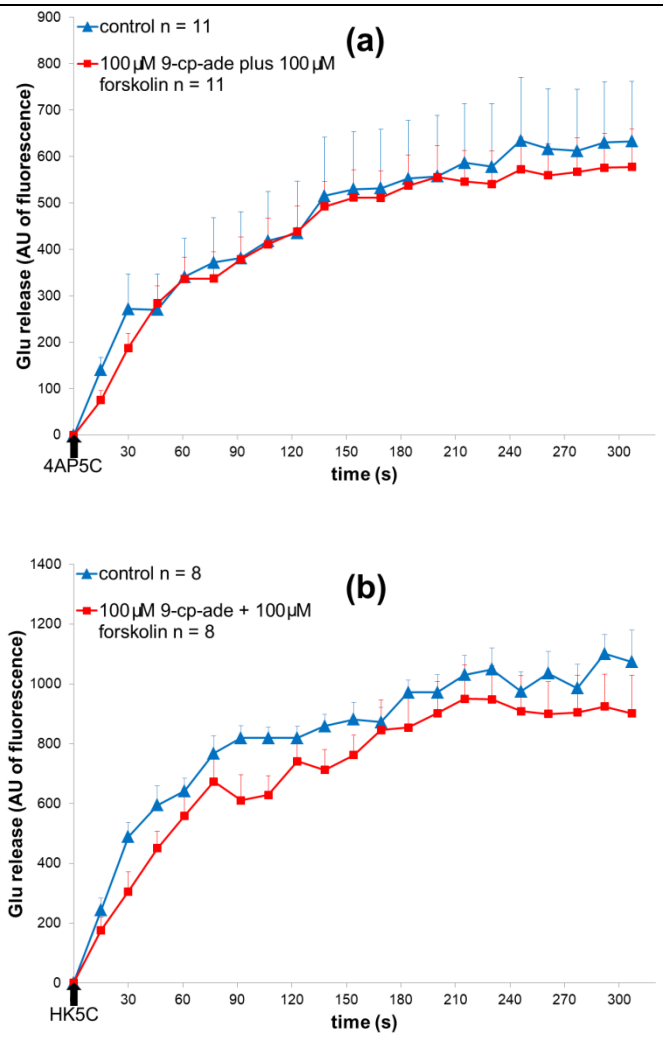

Figure 4.8: The effect of 100 µM 9-cp-ade plus 100 µM forskolin vs control upon evoked Glu release. AC inhibition with 100 µM 9-cp-ade then subsequent addition with 100 µM forskolin had no significant effect upon (a) 4AP5C ($p = 0.587$) or (b) HK5C ($p = 0.197$) evoked Glu release, compared to non-drug controls. Values represented are the mean plus SEM from 3 independent experiments.

4.3.2 Treatment of Forskolin Upon FM 2-10 Dye Release

As forskolin inhibited Glu release from the RP, only the RRP mode of exocytosis could be studied using the FM 2-10 dye assay. Synaptosomes treated with 100 µM forskolin released significantly less FM 2-10 dye from the RRP compared to non-drug controls with 4AP5C stimulation (Figure 4.9a). As approximately half of the SVs in the RRP undergo exocytosis via FF mode and half by KR mode following 4AP5C stimulation, this result indicated that those SVs which normally undergo FF mode had been switched to the KR mode of exocytosis.

To ensure that this forskolin effect on FM dye release was due to forskolin specifically working through AC, a pre-treatment with 100 µM 9-cp-ade before 100 µM forskolin was again employed and this showed that the amount of 4AP5C evoked FM 2-10 dye release was not significantly different to non-drug control levels (Figure 4.9b), indicating that AC activation specifically induced RRP SVs that usually undergo FF mode to switch to KR mode. Note that 9-cp-ade and subsequent forskolin treatment caused a non-significant reduction in FM dye release, although this slight decrease may have been due to the 5 min 9-cp-ade pre-treatment not completely inhibiting all AC before forskolin addition, meaning forskolin may have still affected remaining active AC molecules.

As shown in Chapter 3, inhibition of PKA with 2 µM KT5720 caused all 4AP5C evoked SVs to undergo FF mode (Figure 3.2a), without perturbing Glu release (Figure 3.1a), however no change in 4AP5C evoked FM 2-10 dye was observed when PKA was activated with cBIMPS (Figure 3.7a). Although when PKA was inhibited with KT5720 then forskolin was added, similar levels of FM 2-10 dye release was observed with 4AP5C stimulation compared to controls (Figure 4.10a), dissimilar to when KT5720 was used alone (all KR SVs switched to FF mode). This was a significant increase in release when compared to FM 2-10 dye release with forskolin only, which showed less release compared to controls (Figure 4.9a). However, the difference of KT5720 plus forskolin was not significant compared to controls. In fact, the interpretation of these results may be complicated; whilst the amount of FM 2-10 dye released may have been similar to non-drug controls when PKA was activated by cBIMPS (Figure 3.7a), this may have been due to switching of SVs undergoing KR to FF mode, and

those undergoing FF to KR mode, so that there was no significant difference in results when compared. This interpretation may indicate that the RRP has distinct sub-pools with exclusive mechanisms to modulate SV mode of release.

Pre-treatment of KT5720 and subsequent forskolin treatment (Figure 4.10) indicated that forskolin no longer switched RRP SVs which undergo FF to KR mode but the SVs which normally undergo KR had been switched to FF mode. This result was consistent with forskolin acting upon the RRP via activation of PKA, although in this case PKA was inhibited by KT5720. However, forskolin no longer produced an effect during KT5720 treatment (KT5720 produced the same phenotype as KT5720 plus forskolin) and it could be that the target for KT5720 is downstream of forskolin's target such that forskolin action may not involve PKA modulation.

The results with KT5720 plus forskolin, in which the RRP switched to a predominantly FF mode of exocytosis was similar to previous results in which FM 2-10 dye release assays were performed with protein phosphatase 2A (PP2A) and protein phosphatase 1 (PP1) inhibitor OA. The experiments have been repeated and presented herein: 0.8 µM OA significantly increased FM 2-10 dye release, switching mode of all RRP SVs to FF mode with 4AP5C stimulation (Figure 4.11a) compared to non-drug controls.

It was hypothesised that OA may have stopped the action of forskolin switching the RRP to a KR mode majority, similarly to KT5720 treatment. However, synaptosomes treated with 0.8 µM OA plus 100 µM forskolin released significantly less dye than controls and this was similar to the effects of forskolin alone (Figure 4.11b). This was clearly different to KT5720 action, which prevents forskolin action, and this suggests that OA might have acted on different substrates to any that forskolin acted upon, or that forskolin caused effects downstream of OA action.

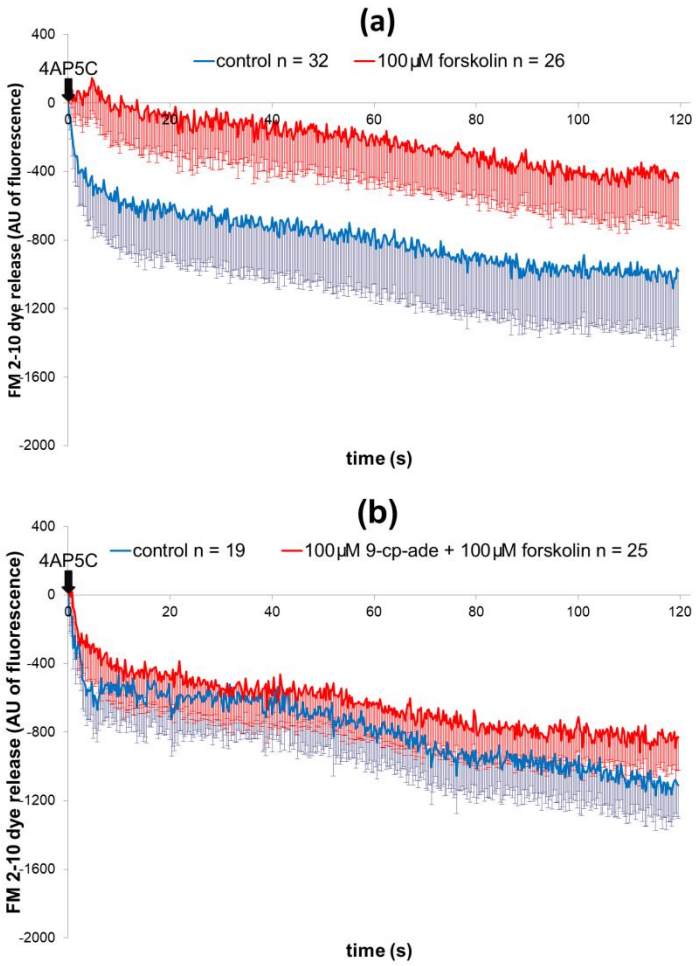

Figure 4.9: The effect of 100 µM forskolin or 100 µM 9-cp-ade plus 100 µM forskolin on evoked FM 2-10 dye release. (a) AC activation using 100 µM forskolin significantly reduced 4AP5C evoked FM 2-10 dye release, compared to non-drug controls ($p < 0.001$). (b) AC inhibition using 100 µM 9-cp-ade and subsequent addition of 100 µM forskolin has no significant effect on 4AP5C evoked FM 2-10 dye release, compared to non-drug controls ($p > 0.145$). Values represented are the mean plus SEM from 6 (a) and 4 (b) independent experiments.

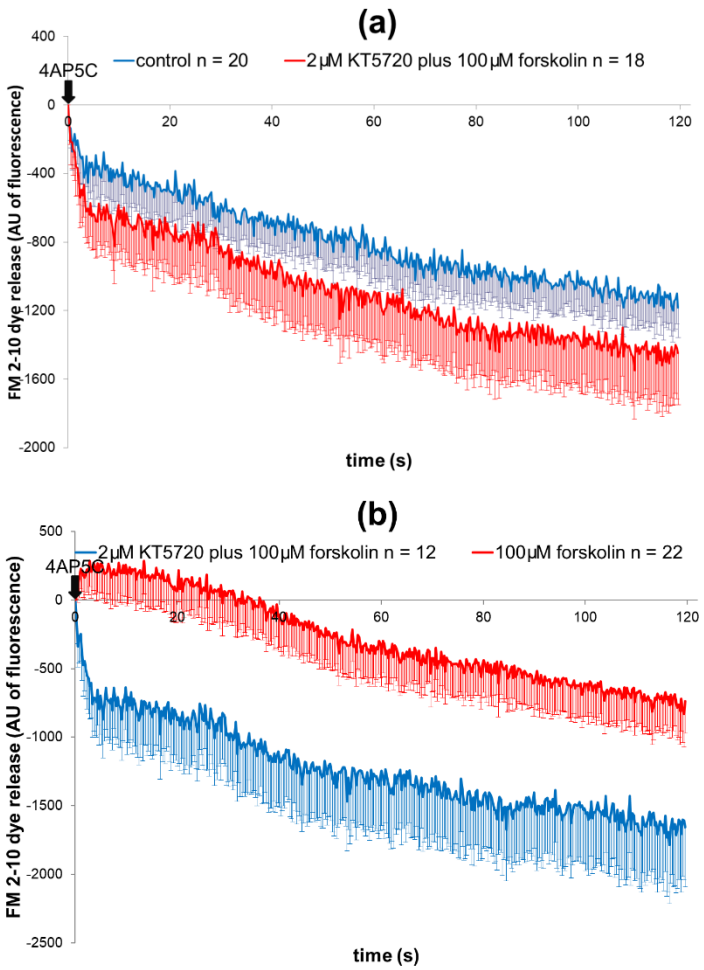

Figure 4.10: The effect of 2 µM KT5720 plus 100 µM forskolin upon evoked FM 2-10 dye release. (a) PKA inhibition using 2 µM KT5720 with subsequent addition of 100 µM forskolin followed by 4AP5C stimulation may appear to induce more FF of the RRP compared to non-drug treated control but this difference does not show a significant difference compared to non-drug controls ($p > 0.05$). (b) KT5720 + forskolin has a significant increase in FM 2-10 dye release compared to 100 µM forskolin only ($p < 0.001$). Values represented are the mean plus SEM from 4 independent experiments.

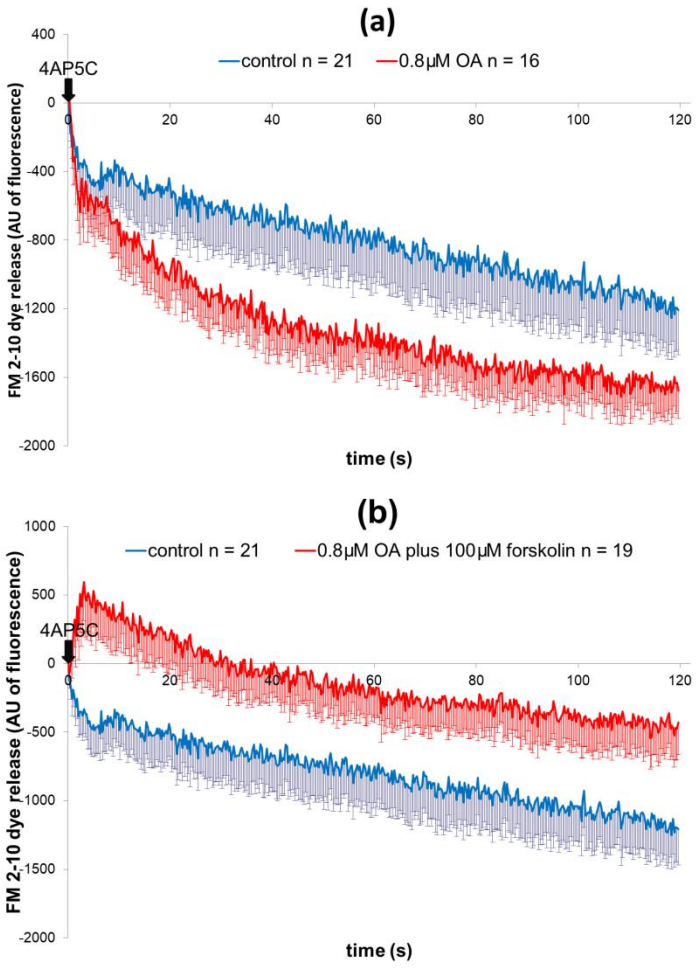

Figure 4.11: The effect of 0.8 µM OA or 0.8 µM OA plus 100 µM forskolin upon 4AP5C evoked FM 2-10 dye release. (a) PP1 and PP2A inhibition with 0.8 µM OA significantly increased 4AP5C evoked FM 2-10 dye release ($p < 0.001$) compared to non-drug controls. (b) PP1 and PP2A inhibition with OA followed by 100 µM forskolin treatment produced a significantly decreased 4AP5C evoked FM 2-10 dye release ($p < 0.001$) compared to non-drug controls. Values represented are the mean plus SEM from 3 independent experiments.

4.3.3 Treatment of Forskolin Upon Changes in Intracellular Ca^{2+} levels

Previous research by A. Ashton's group (Bhuva, 2015; Singh, 2017) and other groups (Alés *et al*., 1999) have demonstrated that increases in $[Ca^{2+}]_i$ during nerve terminal stimulation can switch SVs to KR mode of exocytosis (e.g., Figure A15 in Appendix A). As forskolin treatment switched the RRP to KR mode majority (Figure 4.9a), Fura-2 assays were performed to explore the effects of forskolin on changes in $[Ca^{2+}]_i$, which may have expected to raise $[Ca^{2+}]_i$ similarly to previous results.

Synaptosomes treated with 100 µM forskolin exhibited a significant increase in $[Ca^{2+}]_i$ levels when stimulated by 4AP5C compared to non-drug treated terminals (Figure 4.12a) whilst intriguingly $[Ca^{2+}]_i$ levels significantly decreased with HK5C stimulation (Figure 4.12b) compared to the control terminals. The 4AP5C results suggested that AC activation, thus cAMP level increase, led to an increase in $[Ca^{2+}]_i$ levels, causing the RRP to switch to KR mode. Previous research by A. Ashton's group has determined that RP release required a sufficient increase in $[Ca^{2+}]_i$ throughout the terminal, which explained why in control conditions 4AP5C stimulus failed to stimulate release of the RP – as 4AP5C did not produce as much $[Ca^{2+}]_i$ increase throughout the terminal as HK5C or ION5C stimulation (see Appendix A).

The increase in 4AP5C evoked $[Ca^{2+}]_i$ with forskolin treatment was still not sufficient to induce the RP to release, however forskolin inhibiting the release of the RP (Figures 4.6b and 4.6c) could be explained by the average amount of HK5C evoked $[Ca^{2+}]_i$ decreasing during forskolin treatment being insufficient to induce mobilisation and fusion of the RP vesicles (Figure 4.12b). This difference in effect may reflect that 4AP5C evoked release may not have worked via increase in voltage-gated Ca^{2+} channels like HK5C; rather 4AP perturbed K^+ channels and could have functioned via releasing Ca^{2+} from intracellular Ca^{2+} stores (Kasatkina, 2016). Further, it is clear that HK5C caused more Ca^{2+} entry than 4AP5C and that this was due to the opening of distinct voltage-gated Ca^{2+} channels whilst 4AP5C may not have activated some of these and so evoked lower Ca^{2+} entry.

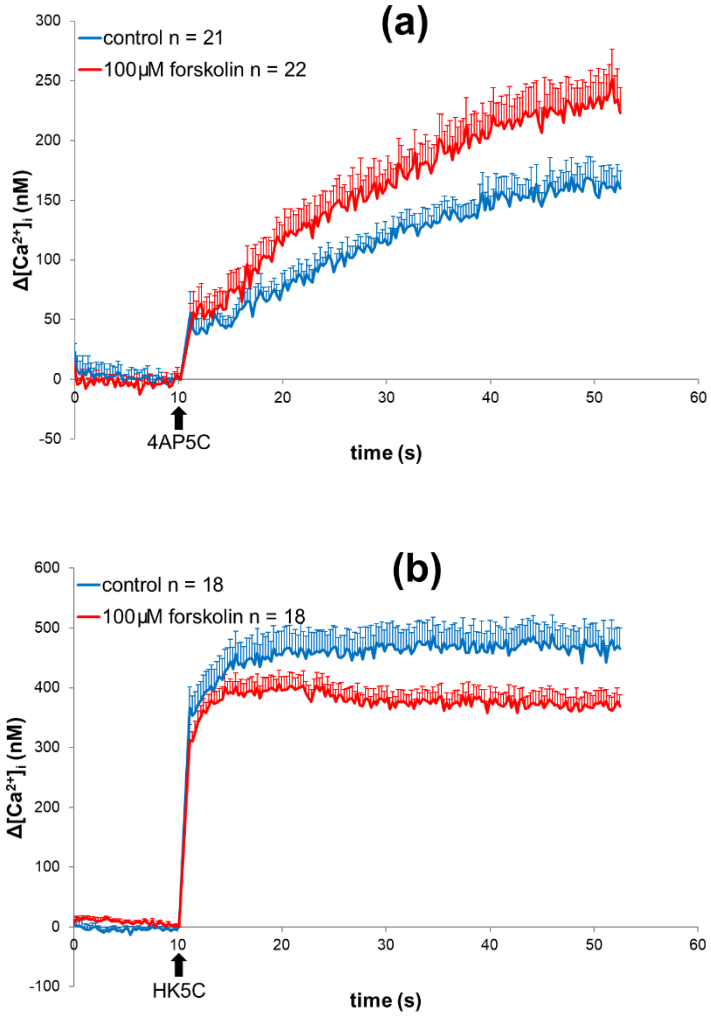

Figure 4.12: The effect of 100 µM forskolin vs control upon evoked $[Ca^{2+}]_i$ levels. AC activation with 100 µM forskolin (a) significantly increased evoked $[Ca^{2+}]_i$ levels after 4AP5C stimulation compared to non-drug controls ($p < 0.001$), but (b) forskolin significantly decreased evoked $[Ca^{2+}]_i$ levels after HK5C stimulation compared to non-drug controls ($p < 0.001$). Values represented are the mean plus SEM from 4 independent experiments.

4.3.4 Treatment of Forskolin Upon Synaptosome Bioenergetics

The Mito-Stress test was performed on synaptosomes treated with 100 µM forskolin. There was no significant difference in OCR compared to controls (Figure 4.13). Such treatment also did not show significant difference of the parameters of mitochondrial function (Figure 4.14).This showed that the synaptosome respiration was not affected by forskolin treatment for over 80 min at 37˚C, suggesting that synaptosome integrity would not be perturbed during forskolin acute treatments of ≤ 5 min in the other assays performed. Any changes to Glu release, FM 2-10 dye release or $[Ca^{2+}]_i$ are due to specific forskolin action on AC and not due to non-specific action.

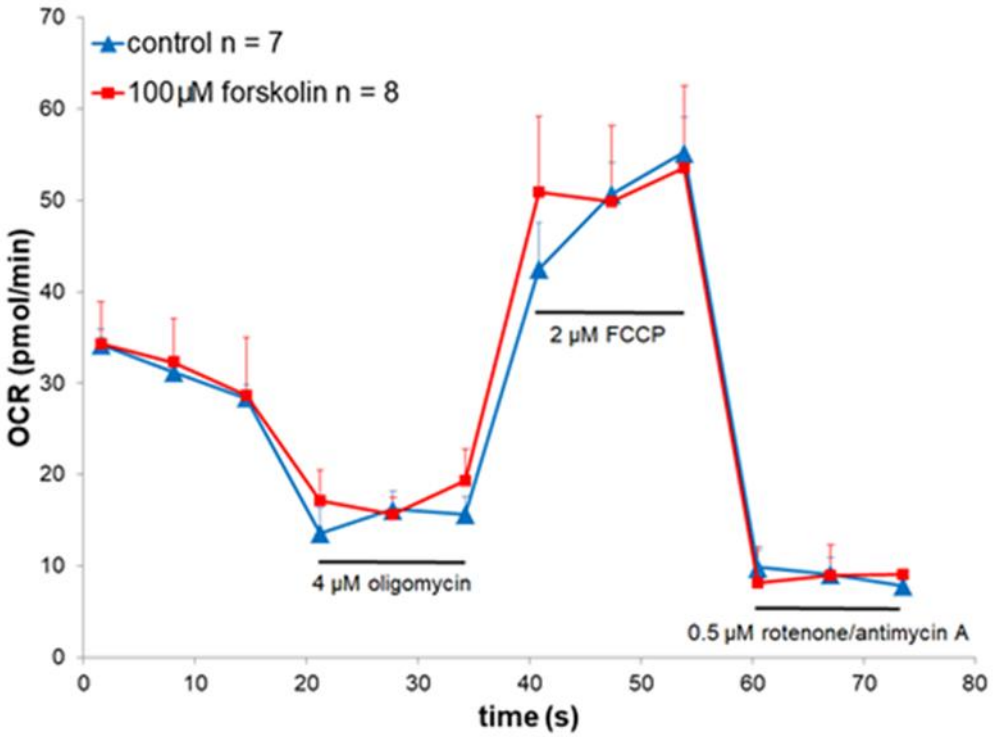

Figure 4.13: The effect of 100 µM forskolin vs control upon synaptosome bioenergetics. Treatment of 100 µM of AC activator forskolin did not significantly affect the bioenergetics of synaptosomes compared to control during a Mito-Stress test (p = 0.868). Values represented are the mean plus SEM from 3 independent experiments. The experiments were performed at 37˚C in the Seahorse Xfp flux analyser.

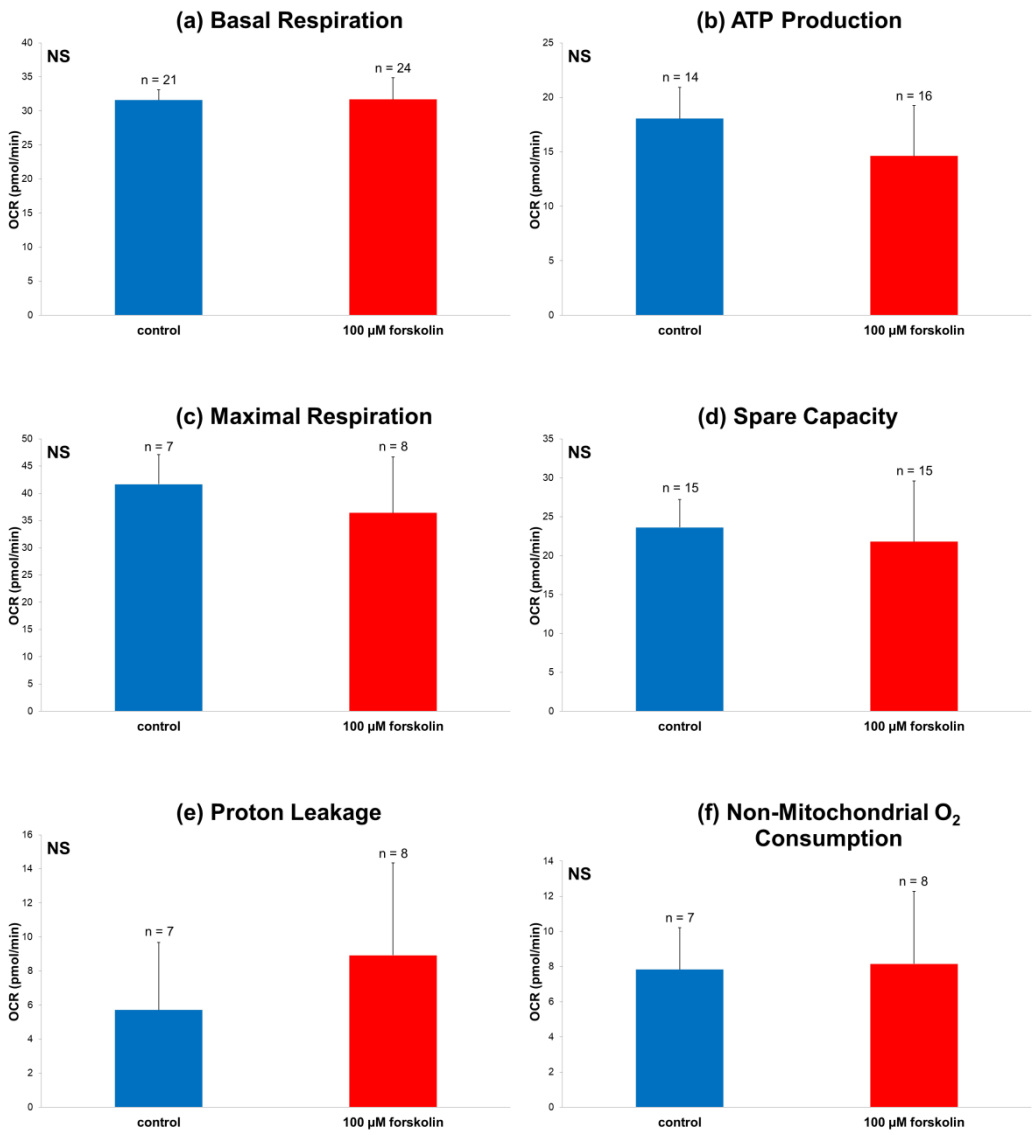

Figure 4.14: The effect of 100 µM forskolin vs control upon mitochondrial function. AC activation with 100 µM forskolin showed no significant change in (a) basal respiration, (b) ATP production, (c) maximum respiration), (d) spare capacity, (e) proton leakage or (f) non-mitochondrial oxygen consumption, compared to non-drug control synaptosomes (all parameters $p > 0.05$). Values represented are the mean plus SEM from 3 independent experiments. *NS*, not significant.

4.4 The Protein EPAC As a Potential Synaptic Vesicle Release Modulator

There are two major cellular targets of cAMP, PKA and EPACs. The proteins EPAC1 and EPAC2 have guanine-nucleotide exchange factor (GEF) activity which is used to switch GDP for GTP in the EPAC substrates Rap1 and Rap2, classified as small GTPases (de Rooij *et al*., 1998; Kawasaki *et al*., 1998).

The increase in cAMP production within synaptosomes increases number of activated PKA and EPACs (Dao *et al*., 2006). Activation of EPACs has been shown to enhance neurotransmitter release from glutamatergic terminals (Grandoch *et al*., 2010; Ferrero *et al*., 2013) and has a role in regulation of exocytosis (Fernandes *et al*., 2015).

As forskolin treatment blocked RP release by increasing cAMP levels, this could be through activation of EPACs, as PKA modulation did not affect SV pool release (see Chapter 3). Inhibition of EPACs with inhibitor ESI-09, and dual treatment with forskolin should reveal whether EPACs regulate RP release.

ESI-09 is a competitive inhibitor of the cAMP binding domain (CBD) B-site present on the regulatory domain of both EPAC1 and EPAC2 (Almahariq *et al*., 2013), which prevents EPACs' conformational change which exposes the binding site for Rap1 and Rap2 on their catalytic domain (de Rooij *et al*., 2000; Bos, 2006).

4.5 Inhibition of EPAC Using ESI-09 Upon Synaptic Vesicle Release Dynamics

4.5.1 Treatment of ESI-09 Upon Evoked Glutamate Release

Treatment with 100 µM ESI-09 had no significant effect upon evoked Glu release from synaptosomes stimulated with HK5C compared to non-drug treated controls (Figure 4.15). Pre-treatment of 100µM ESI-09 prior to treatment of 100 µM forskolin also had no significant effect upon evoked Glu release from synaptosomes stimulated with HK5C compared to non-drug controls (Figure 4.16). Clearly, the phenotype exhibited by forskolin is reversed by inhibiting EPACs prior to activating AC. This result indicated that reduction of Glu release from the RP during forskolin induced AC activation could rather be caused by downstream activation of EPACs due to increase in cAMP levels (Figure 4.6).

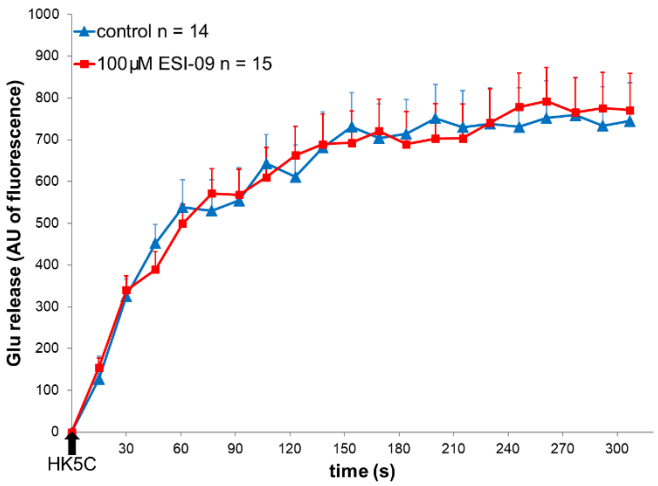

Figure 4.15: The effect of 100 µM ESI-09 upon HK5C evoked Glu release. EPACs inhibition using 100 µM ESI-09 had no significant effect upon HK5C evoked Glu release, compared to non-drug controls (p = 0.964). Values represented are the mean plus SEM from 3 independent experiments.

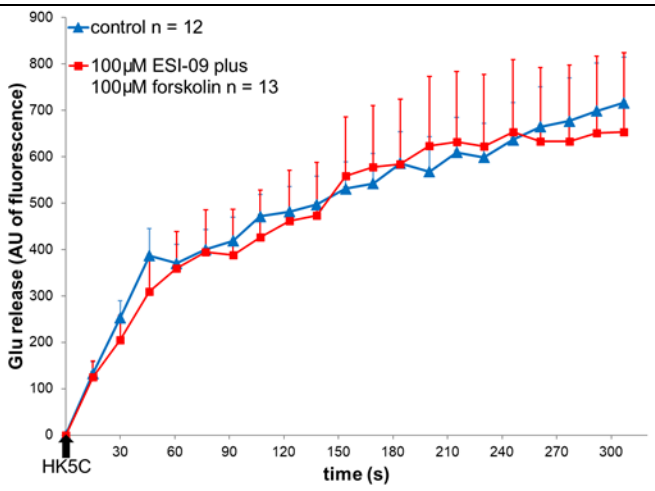

Figure 4.16: The effect of 100 µM ESI-09 plus 100 µM forskolin upon HK5C evoked Glu release. 100 µM ESI-09 plus subsequent 100 µM forskolin addition had no significant effect upon HK5C evoked Glu release, compared to non-drug controls ($p = 0.823$). Values represented are the mean plus SEM from 3 independent experiments.

4.5.2 Treatment of ESI-09 Upon Changes in Intracellular Calcium Levels

Activation of AC using forskolin decreased HK5C evoked $[Ca^{2+}]_i$ levels within synaptosomes (Figure 4.12) and blocked release of SVs from the RP (Figure 4.6).Inhibition of EPACs using ESI-09 and subsequent AC activation using forskolin enabled the RP to release with HK5C stimulation (Figure 4.16). The inhibition of EPACs may restore RP release by restoring or increasing the evoked $[Ca^{2+}]_i$ levels; thus the Fura-2 assay was performed to establish what effect inhibition of EPACs has upon evoked $[Ca^{2+}]_i$ levels.

Synaptosomes treated with 100 µM ESI-09 exhibited a significant increase in evoked $[Ca^{2+}]_i$ levels when stimulated with 4AP5C (Figure 4.17a) and HK5C (Figure 4.17b) compared to non-drug controls. As inhibition of EPACs significantly increased $[Ca^{2+}]_i$ level this may be the reason how ESI-09 pre-treatment followed by forskolin treatment was able to restore RP release. The effect of activation of EPAC may involve either voltage-gated Ca^{2+} channels or the regulation of release of Ca^{2+} from intracellular stores. As a consequence of inhibiting EPAC, there was increase in cytosolic Ca^{2+} which could then

contribute to the mode of SV exocytosis or the number of SVs exocytosing (Tan *et al.*, 2022). How EPAC affects $[Ca^{2+}]_i$ level is still undiscovered in neurons and would require further extensive study.

To determine whether forskolin was working to decrease HK5C evoked $[Ca^{2+}]_i$ levels through EPACs activation, synaptosomes were pre-treated with 100 µM ESI-09 to inhibit EPACs, then treated with 100 µM forskolin to activate AC. These synaptosomes exhibited significant increase in $[Ca^{2+}]_i$ evoked by 4AP5C stimulation (Figure 4.18a) and HK5C stimulation (Figure 4.18b). These results indicated that EPACs inhibition may reverse the action of forskolin to inhibit release of the RP by raising the evoked changes in $[Ca^{2+}]_i$ levels within the synaptosomes.

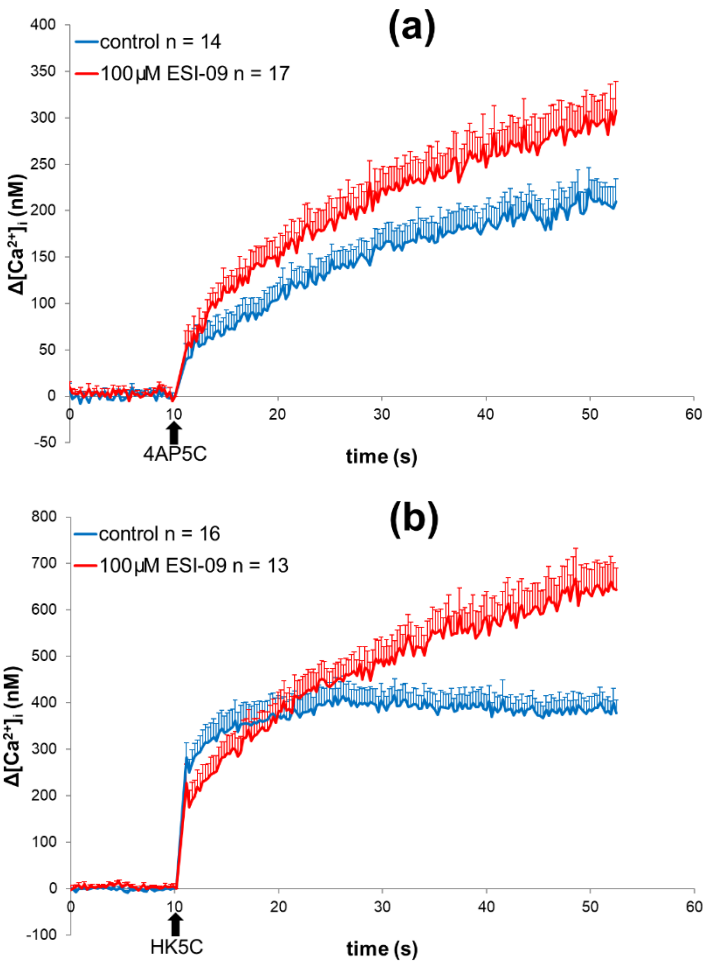

Figure 4.17: The effect of 100 µM ESI-09 upon evoked $[Ca^{2+}]_i$ levels. EPACs inhibition with 100 µM ESI-09 significantly increased evoked $[Ca^{2+}]_i$ levels when stimulated with (a) 4AP5C ($p < 0.001$) and (b) HK5C ($p < 0.001$), compared to non-drug controls. Values represented are the mean plus SEM from 3 independent experiments.

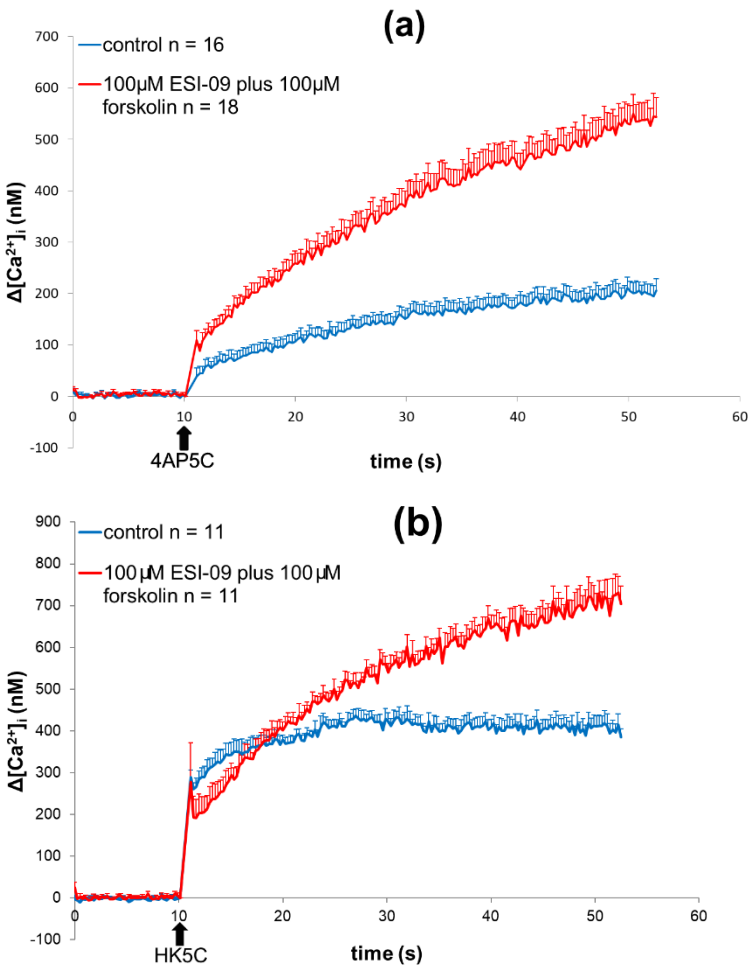

Figure 4.18: The effect of 100 μM ESI-09 plus 100 μM forskolin upon evoked $[Ca^{2+}]_i$ levels. EPACs inhibition with 100 μM ESI-09 then subsequent addition with 100 μM forskolin significantly increased evoked $[Ca^{2+}]_i$ levels when stimulated with (a) 4AP5C ($p < 0.001$) and (b) HK5C ($p < 0.001$), compared to non-drug controls. Values represented are the mean plus SEM from 3 independent experiments.

4.5.3 Treatment of ESI-09 Upon Synaptosome Bioenergetics

Inhibiting EPACs with ESI-09 did not perturb Glu release (Figure 4.15) but ESI-09 was able to prevent forskolin from blocking release of the RP by increasing $[Ca^{2+}]_i$ levels (Figure 4.18). To test whether ESI-09 treatment could raise $[Ca^{2+}]_i$ through perturbing synaptosome respiration, the Mito-Stress test was performed on synaptosomes. The Mito-Stress test (Figure 4.19) demonstrated that EPACs inhibition using 100 µM ESI-09 had no significant effect on synaptosomes at 37°C for 90 min apart from one parameter (see below), suggesting that acute drug treatment of ≤ 5 min such as used in the other assays of this thesis would not disrupt synaptosome respiratory integrity by producing non-specific drug effects upon the measurements taken. The parameters of mitochondrial function (Figure 4.20) calculated show that ESI-09 did not perturb the mitochondria except for proton leakage. The relevance of this is not understood, however part of this is apparently due to higher basal respiration (Figure 4.19), which although is statistically insignificant may have made the following injection of oligomycin A produce higher oxygen consumption in ESI-09 treated terminals, whilst following rotenone/antimycin A injection there was similar oxygen consumption to control levels – the difference between these parameters which measure proton leakage can explain this significant difference to control levels.

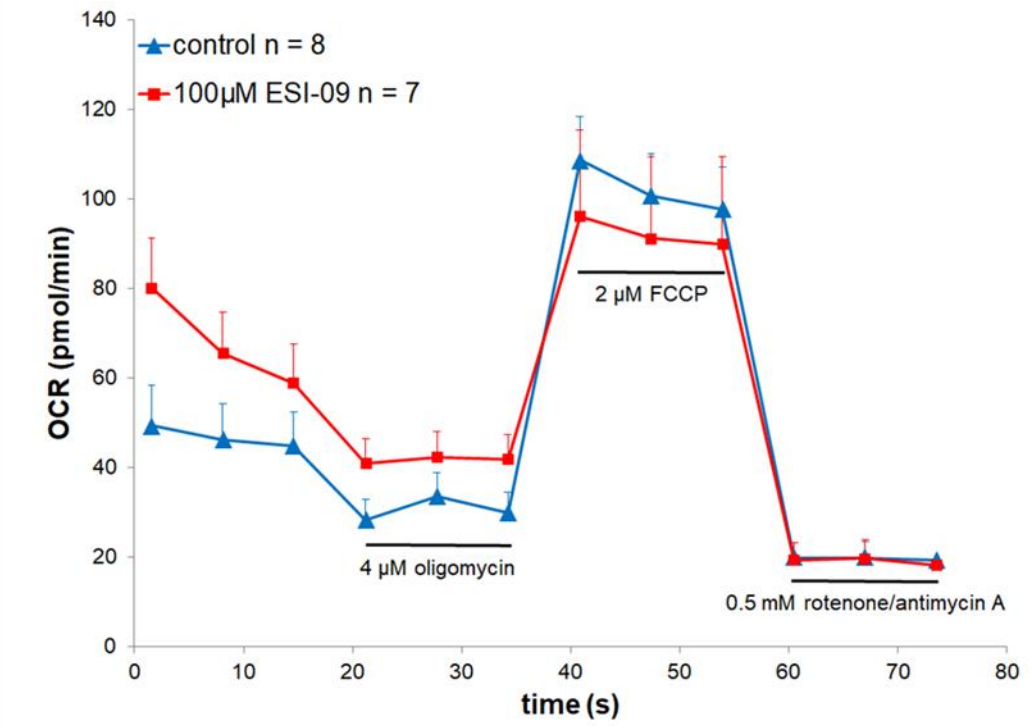

Figure 4.19: The effect of 100 µM ESI-09 vs control upon synaptosome bioenergetics. Treatment of 100 µM of EPACs inhibitor ESI-09 did not significantly affect the bioenergetics of synaptosomes compared to control during a Mito-Stress test ($p = 0.672$). Values represented are the mean plus SEM from 3 independent experiments. The experiments were performed at 37˚C in the Seahorse Xfp flux analyser.

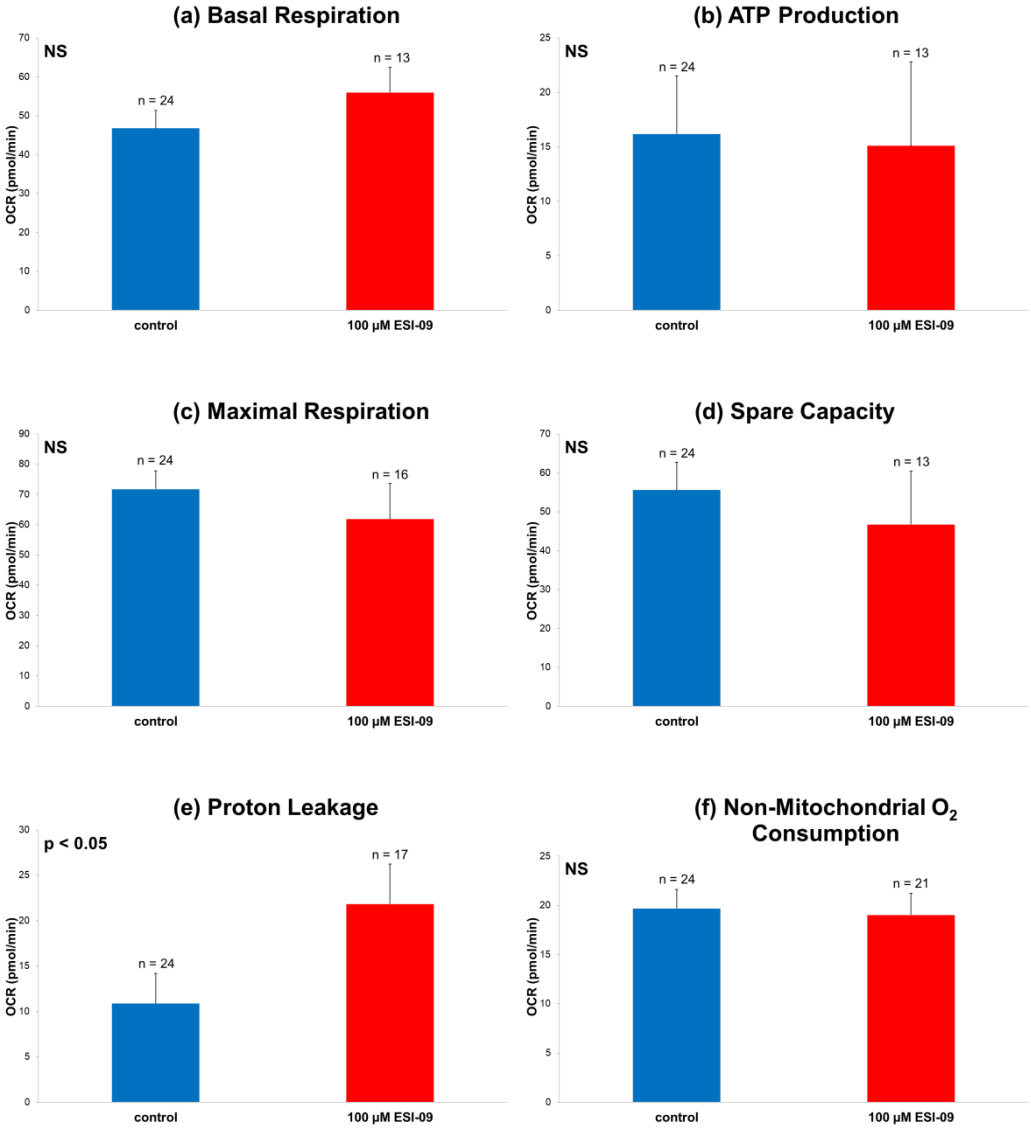

Figure 4.20: The effect of 100 µM ESI-09 vs control upon mitochondrial function. EPACs inhibition with ESI-09 showed no significant change in (a) basal respiration, (b) ATP production, (c) maximum respiration, (d) spare capacity or (f) non-mitochondrial oxygen consumption, compared to non-drug control synaptosomes (these parameters $p > 0.05$). However, for (e) Proton leakage was significantly increased compared to non-drug control synaptosomes ($p < 0.05$). Values represented are the mean plus SEM from 3 independent experiments. *NS*, not significant.

4.6 Discussion

As discussed in Chapter 3, PKA was able to switch the mode of exocytosis differently for each SV pool, and this could be through phospho-regulation of dynamin-1 activity. The binding of cAMP specifically activates PKA, which is synthesised by the transmembrane protein AC (Walsh *et al*., 1968). This chapter discusses the role AC and cAMP have in regulation of amount of Glu release and the mode of SV exocytosis in synaptosomes, as well as another substrate of cAMP, EPAC.

The activity of cAMP has been well established to regulate Ca^{2+} triggered exocytosis by modifying molecular machinery (Chen and Regehr, 1997), and in neurons cAMP has been shown to increase neurotransmitter release and has been implicated in causing long-term potentiation (Weisskopf *et al*., 1994; Huang *et al*., 1995) which is an important factor in synaptic plasticity. However, this may be simply due to activation of PKA; as discussed in Chapter 3, increases in PKA activation enhances neurotransmitter release, unless neurotransmitter release is maximal, such as in the stimulation conditions used in this thesis. Other research conversely demonstrates that increases in cAMP levels cause a disruption to vesicular mobility (Petrov *et al*., 2008) and this could be through activation of both PKA and EPACs (Dao *et al*., 2006; Grandoch *et al*., 2010). Since the discovery of EPACs (de Rooij *et al*., 1998) many PKA-independent cAMP effects have been shown to be the result of EPACs activation (Beaumont *et al*., 2002).

In this chapter AC was inhibited using 9-cp-ade or activated using forskolin, and EPACs were inhibited using ESI-09 to determine how these treatments would affect evoked release of Glu, mode of exocytosis for distinct SV pools and the levels of $[Ca^{2+}]_i$. The Mito-Stress test was used to detect the metabolic viability of synaptosomes after drug treatments.

4.6.1 Discussion of AC inhibition

Inhibition of AC did not modulate the amount of release of Glu from synaptosomes. Glu was released at control levels from the RRP when treated with 9-cp-ade and stimulated with 4AP5C (Figure 4.1a). When stimulated with HK5C (Figure 4.1b) or ION5C (Figure 4.1c), treatment with 9-cp-ade allowed control levels of release of the RRP and the RP. These results showed that the same numbers of SVs were undergoing release in both 9-cp-ade treated and non-drug synaptosomes during stimulation. As no SVs were recycling and only one round of SV release was being studied (see Figure A4 in Appendix A) the inhibition of AC – with a subsequent decrease in intracellular cAMP concentration – did not have a role in regulating release of SV pools from nerve terminals, when stimulated to maximally release SVs from either the RRP or RP.

Inhibition of AC did not modulate the mode of SV exocytosis in synaptosomes. The FM 2-10 dye was released at control levels from the RRP when stimulated with 4AP5C (Figure 4.2a) and from the RRP and RP when stimulated with HK5C (Figure 4.2b) or ION5C (Figure 4.2c). These results showed that reducing intracellular cAMP level did not have a role in switching mode of release of SVs from the RRP or RP.

It was hypothesised that 9-cp-ade inhibition of AC could affect evoked $[Ca^{2+}]_i$ levels without reaching levels sufficient to affect Glu or FM 2-10 dye release; however treatment of 100 µM 9-cp-ade had no significant effect upon $[Ca^{2+}]_i$ levels evoked by any of the three stimuli (Figure 4.3). This may indicate that inhibition of AC and the drop in cAMP levels did not have a role in regulating $[Ca^{2+}]_i$ levels. Although 9-cp-ade treatment had no significant effect upon Glu release, FM 2-10 dye release or evoked $[Ca^{2+}]_i$ levels compared to respective controls, it was shown that 9-cp-ade had effective inhibition of AC, as evidenced by 9-cp-ade being able to negate forskolin's effect on evoked Glu release when used in pre-treatment before forskolin (Figure 4.8).

To ensure that changes in SV mode of exocytosis and amount of SV release was due to specific drug action and not perturbation to synaptosome respiration, the drugs used in this chapter were subjected to the Mito-Stress

test, similarly to the drugs used in Chapter 3. Synaptosomes treated with 100 µM 9-cp-ade for 90 min at 37˚C displayed the same OCR, viability, and mitochondrial function as control synaptosomes (Figure 4.4). Treatment of 9-cp-ade regulated AC without significantly affecting basal respiration, ATP production, maximal respiration, spare capacity, proton leakage or non-mitochondrial respiration (Figure 4.5) (Agilent Technologies, 2019). These results showed that the effects of 9-cp-ade in this model are not due to non-specific effects or perturbation of synaptosome respiration.

4.6.2 Discussion of AC activation

Activation of AC blocked the exocytosis of RP SVs. Amount of Glu released at control levels from the RRP in synaptosomes treated with forskolin and stimulated with 4AP5C (Figure 4.6a) indicating that all RRP SVs were released. However, synaptosomes exhibited a loss of Glu release when treated with forskolin and stimulated with HK5C (Figure 4.6b) or with ION5C (Figure 4.6c). This loss of SV exocytosis must have specifically been from the RP, as forskolin treatment and 4AP5C stimulation did not perturb the RRP.

These results indicated that increase in intracellular cAMP affects the RP but not the RRP using the SV pools' exclusive signalling pathways. Petrov *et al.* (2008) utilised cAMP analogues to activate cAMP dependent proteins and reported a similar disruption to SV mobility and neurotransmitter exocytosis; they concluded that activation of cAMP dependent protein disrupted the transport of vesicles from the 'mobilisation pool' (equivalent to the RP of this thesis).

Forskolin was specifically working on AC as both 100 µM of inactive homologue 1,9-did-forsk (Figure 4.7) or 100 µM 9-cp-ade pre-treatment before 100 µM forskolin (Figure 4.8), demonstrated Glu release at control levels. As no loss of Glu release was seen for PKA activation with cBIMPS as described in Chapter 3 (Figure 3.6), the loss of Glu release from the RP seen when cAMP was raised by AC activation could have been mediated by a different cAMP substrate such as the EPACs, or by a change in $[Ca^{2+}]_i$.

Activation of AC affected mode of SV exocytosis for the RRP. As the RP did not undergo exocytosis during forskolin treatment (Figure 4.6) only the mode of the RRP could be determined using the FM 2-10 dye release assay. Treatment of 100 µM forskolin caused a significant decrease in FM 2-10 dye release when stimulated with 4AP5C (Figure 4.9a) indicating that SVs which release via FF in control conditions had been switched to KR mode by intracellular cAMP level increase. This mode switch was negated by synaptosome pre-treatment with AC inhibitor 9-cp-ade before forskolin treatment, which kept FM 2-10 dye release at control levels (Figure 4.9b). Thus, forskolin activated AC hence increased cAMP levels to switch the mode of RRP SVs to KR mode and blocking AC can negate this effect.

However, it was not established if the RRP mode of release was regulated by downstream activation of EPACs or PKA. As inhibition of PKA with KT5720 produces a majority FF mode of RRP SV exocytosis with 4AP5C stimulation (Figure 3.2a) it was hypothesised that forskolin may work to switch the RRP to KR mode by activating PKA via increased cAMP levels. Thus, synaptosomes were pre-treated with 2 µM PKA inhibitor KT5720 then treated with 100 µM AC activator forskolin with 4AP5C stimulation (Figure 4.10). A significant increase in FM 2-10 dye release was observed indicating a switch to FF mode of exocytosis of the RRP. These results suggested that the mode of the RRP exocytosis was regulated specifically by PKA activity. Intriguingly, the activation of PKA with cBIMPS had no effect upon the RRP mode of exocytosis (Figure 3.7). These results may have revealed that a combination of both PKA and EPACs activation was required for the mode of the RRP to be switched to a KR mode majority. The activation of EPACs is beyond the scope of this thesis' research, as there is no current specific EPAC activator, though how this could modulate mode of release for both the RRP and RP is a relevant experiment for future study.

Treatment with OA also switched RRP SVs to a predominantly FF mode of exocytosis (Figure 4.11a). The OA inhibits PP2A and PP1, dramatically increasing phosphorylation state of numerous proteins (Bialojan and Takai, 1988; Fernández *et al*., 2002), which prevents KR mediated exocytosis (Ashton, 2009; Bhuva, 2015). To discover if OA blocks forskolin action on the RRP, synaptosomes were treated with 0.8 µM OA plus 100 µM forskolin. Significantly

less FM 2-10 dye release was observed when stimulated with 4AP5C, compared to control (Figure 4.11b), similarly to the result of forskolin alone (Figure 4.9a), indicating that forskolin was still able to switch the RRP to KR mode despite wide-ranging phosphorylation changes in synaptosomes. As KT5720 blocked forskolin effects on mode of SV exocytosis but OA did not, this indicated that either forskolin and OA worked on different substrates and pathways, or that forskolin was able to act downstream of OA action.

Activation of AC increased evoked $[Ca^{2+}]_i$ levels. Synaptosomes treated with 100 µM forskolin and stimulated with 4AP5C released Glu at control levels from the RRP (Figure 4.6a) but switched the mode of exocytosis to KR (Figure 4.9a). As previously mentioned a switch to KR mode can be mediated by an increase in evoked $[Ca^{2+}]_i$ levels (Alés *et al*., 1999; Ashton, 2009; Bhuva, 2015), and there was an increase in evoked $[Ca^{2+}]_i$ levels with forskolin treatment and 4AP5C stimulation (Figure 4.12a). This indicated that forskolin may have switched the mode of exocytosis of a proportion of RRP SVs from FF to KR mode by increasing evoked $[Ca^{2+}]_i$ levels via activating AC. This interpretation may explain how no similar switch in RRP mode of exocytosis was observed when PKA was activated directly by cBIMPS treatment (Figure 3.7a), as cBIMPS did not affect $[Ca^{2+}]_i$ levels (Figure 3.8).

However, activation of AC with forskolin and stimulation with HK5C prevented RP SVs undergoing exocytosis (Figure 4.6b). Ashton has previously demonstrated that 4AP5C evoked a lower average $[Ca^{2+}]_i$ level than HK5C in synaptosomes and that is why 4AP5C could not stimulate RP release (see Figure A2 in Appendix A). Therefore, it was possible that forskolin may block RP release by reducing $[Ca^{2+}]_i$ levels during HK5C stimulation. Treatment of 100 µM forskolin caused synaptosomes to have less evoked $[Ca^{2+}]_i$ with HK5C stimulation compared to control (Figure 4.12b), therefore forskolin may block RP release via reduction in evoked $[Ca^{2+}]_i$ levels. Note that during HK5C stimulation there was an initial large increase in $[Ca^{2+}]_i$ localised intracellularly at the AZs which drove RRP SV fusion, and this Ca^{2+} then diffused throughout the terminal which then drove RP mobilisation and fusion at sufficient local concentrations; if this $[Ca^{2+}]_i$ level was reduced then RP SVs would not exocytose. Forskolin treatment increased intracellular cAMP levels which

reduced evoked $[Ca^{2+}]_i$ level below the sensitivity threshold which the RP needed to release.

Synaptosomes treated with 100 µM forskolin for 90 min at 37˚C displayed the same OCR, viability, and mitochondrial function as control synaptosomes (Figure 4.13). Treatment of forskolin regulated AC without significantly affecting basal respiration, ATP production, maximal respiration, spare capacity, proton leakage or non-mitochondrial respiration (Figure 4.14) (Agilent Technologies, 2019). These results showed that the effects of the drug treatments used in this chapter were not due to non-specific effects or perturbation of synaptosome respiration.

4.6.3 Discussion of EPACs inhibition

As cAMP has the targets PKA and EPACs, and PKA stimulation did not perturb Glu release (Figure 3.6) then cAMP may have activated EPACs to block RP release. Inhibition of EPACs with 100 µM ESI-09 did not affect Glu release when stimulated with HK5C (Figure 4.15) but did negate forskolin action from blocking RP release when ESI-09 is used as a pre-treatment before forskolin treatment, restoring evoked Glu release to control levels (Figure 4.16). Although the inhibition of AC, hence reduction of intracellular cAMP levels, didnot regulate the release dynamics of SV pools, the activation of AC and hence increase in cAMP blocked the release of RP SVs specifically through activation of EPACs.

As EPACs activate Rap1 and Rap2 (de Rooij *et al*., 1998; Kawasaki *et al*., 1998) it perhaps could be downstream targets of Rap1 and Rap2 that directly mediated mobilisation of SVs from the RP during stimulation. The Rap proteins have been implicated in synaptic long-term depression (Zhu *et al.,* 2002), the inhibition of glutamatergic synaptic transmission (Imamura *et al*., 2003), inhibition of synaptic transmission at frog neuromuscular junctions (Petrov *et al*., 2008) and indirect disruption of the actin cytoskeleton (Taira *et al*., 2004). Considering that cAMP is a vital secondary messenger, the activation of AC may produce a high enough cAMP concentration to saturate PKA, which binds cAMP in concentration range 5.0-24.6 nM, and activate EPACs thereafter.

These studies may suggest that EPACs have a lower cAMP sensitivity than PKA, allowing for activation either individually or simultaneously (Seino and Shibasaki, 2005; Dao *et al*., 2006).

As forskolin blocked RP release by reducing evoked $[Ca^{2+}]_i$ levels through EPACs activation, it is possible that inhibiting EPACs would cause an increase in evoked $[Ca^{2+}]_i$ levels, especially as ESI-09 treatment can restore RP Glu release from forskolin action. Treatment of 100 µM of EPACs inhibitor ESI-09 caused synaptosomes to increase evoked $[Ca^{2+}]_i$ levels with 4AP5C stimulation (Figure 4.17a) or HK5C stimulation (Figure 4.17b). It appeared that inhibiting EPACs also prevented forskolin action from blocking RP release when used in dual treatments, through increasing evoked $[Ca^{2+}]_i$ levels which reached the sensitivity threshold for release of the RP SVs, during both 4AP5C (Figure 4.18a) or HK5C stimulation (Figure 4.18b).

Synaptosomes treated with 100 µM ESI-09 for 90 min at 37˚C displayed the same OCR, viability, and mitochondrial function as control synaptosomes (Figure 4.19). Treatment with ESI-09 did not significantly affect mitochondrial parameters except an increase in proton leakage (Figure 4.20e) – basal respiration that is not due to ATP production, and excessive proton leakage could be due to mitochondrial damage (Agilent Technologies, 2019). As no other parameter was perturbed, the significance of this result is not understood. Further repeats of ESI-09 treatment could establish whether this is a result of long-term treatment and what could be occurring with the mitochondria. These results nonetheless show that the effects of ESI-09 are not due to non-specific effects or perturbation of synaptosome respiration.

4.7 Conclusion

Increasing cAMP levels inhibits the release of the RP through activation of EPACs which reduces evoked $[Ca^{2+}]_i$ levels, and also switches the RRP mode of exocytosis to KR mode majority, possibly by increased localised Ca^{2+} concentration at the AZs via EPACs action. Therefore, AC can regulate the RRP and RP independently from each other by modulating $[Ca^{2+}]_i$ levels within pre-synaptic terminals, which describes and explains a novel mechanism of synaptic plasticity.

Decreasing cAMP levels does not have any observable effect on SV release, mode of SV exocytosis nor the evoked $[Ca^{2+}]_i$ levels, with this maximal stimulation model. It may be that incubation time of 5-10 min was not sufficient to inhibit all AC present in the synaptosomes or is unable to block all AC subtypes, allowing a smaller amount of cAMP to be produced and continue regulating PKA and EPACs. In concurrence it has been demonstrated that 9-cp-ade does not inhibit AC type II in purified rat and bovine brains *in vitro* (Johnson *et al.*, 1997). Contrastingly, in these studies inhibition of AC prevents forskolin effects when used in dual treatments.

These results also highlight how changes in evoked $[Ca^{2+}]_i$ levels can discretely regulate both the mode of SV exocytosis for individual SV pools and the availability of SV pools to release.

CHAPTER 5:

Actin Modulation Upon SV exocytosis

5.1 Actin Regulation of Synaptic Vesicles

This chapter describes the study into how modulation of cytoskeletal, polymeric actin filaments - using drug-induced depolymerisation or stabilisation - affected the amount of release of Glu and the mode of exocytosis for the RRP and RP of SVs. Such studies have highlighted novel functions of actin filaments in SV mobility, priming and release that contribute to the SV cycle, and provided further evidence about which proteins contribute to the SV machinery by association with or regulation by actin filaments. As NMII is often bound to actin filaments and dynamin can also be associated with these, these studies also attempted to find connections between these two components that are relevant to the NMII or dynamin regulated mode of exocytosis.

5.1.1 Properties of Actin

Actin is globular multi-functional protein of approximately 42 kDa and diameter of 4–7 nm that can form microfilaments which represent a major component of the cytoskeleton. Actin is ubiquitous and abundant in eukaryotic cells, and it is present as either free monomeric G-actin or as part of a linear polymer microfilament called F-actin. Actin is important for many cellular functions such as mobility, shape and contraction of cells, vesicle and organelle movement, cell signalling and it contributes to cell junctions, and cell division. Many of these processes are mediated by extensive interactions of actin with cellular membranes (Doherty and McMahon, 2008).

In vertebrates, three groups of actin isoforms have been identified: α, β and γ. The α-actins are found in muscle tissues as a constituent of the contractile apparatus, β-actins are found at the expanding edge of cells that use structure projection to induce mobility, and γ-actins are found in stress-fibre microfilaments (Scott *et al.*, 2012). The β- and γ-actins coexist in most cell types as cytoskeleton components and as internal cell motility mediators. It is believed that the diverse range of structures, hence functions of actin, are regulated through the binding of the protein tropomyosin along the microfilaments (Vindin and Gunning, 2013).

Cells have the ability to dynamically remodel actin microfilaments to provide dynamic scaffolds that respond to environment and chemical signals, which among its many functions, contributes to intracellular transport of vesicles, including SVs. Although no high-resolution models of actin's filamentous form exists, a more exact model of its structure based on multiple crystals of actin dimers that bind in different places was made (Sawaya *et al.*, 2008); this model was further refined (Oda *et al.*, 2009; von der Ecken *et al.*, 2015).

Actin is an enzyme that slowly hydrolyses ATP. However, ATP is also required to maintain filamentous structural integrity. Actin can carry out more interactions than many proteins, and this property allows it to perform its large variety of functions (Gunning *et al.*, 2015). The G-actin structure features two lobes separated by an 'ATPase fold' cleft which is the centre of enzymatic catalysis: ATP and Mg^{2+} bind here and it is where subsequently ATP is hydrolysed into ADP and P_i. The G-actin is only functional with ATP or ADP in its cleft, but ATP is predominantly present in cells when actin is in its free state. The actin tertiary structure is formed by two domains known as 'large' and 'small', separated by the ATPase fold. Below this is a deeper notch called a 'groove' (Elzinga *et al.*, 1973). The small domain is further identified as subdomain I and II and the large domain is further identified as subdomain III and IV. The exposed areas of subdomains I and III are referred to as the 'barbed' ends and the exposed areas of subdomains II and IV are referred to as the 'pointed' ends. This nomenclature refers to the polarity of subdomain II, which is important in assembly dynamics (Narita *et al.*, 2012).

Two parallel F-actin strands must rotate 166° to lie correctly on top of each other, forming a double-helix structure, which makes up the F-actin microfilaments. These microfilaments are approximately 7 nm in diameter with the helix repeating every 37 nm. However, as F-actin microfilaments are dynamic, they appear with variability; axial translation is constant at 27.5 Å but appear with subunit rotation displacements of up to 10% from its most common position. This variability could be important in the polymerisation process (Reisler and Egelman, 2007). The monomer contact points in the linear chain are between the 'barbed' region of one monomer and the 'pointed' end of the next one. The contact points in adjacent chains that make lateral contact are through projections from subdomain IV, which includes the C-terminus and a

hydrophobic link. This model suggests that microfilaments are formed by monomers in a sheet formation, in which subdomains turn about themselves (Oda *et al.*, 2009). As all microfilament's point to the same end, this gives F-actin polymers polarity – the end that possesses an exposed ATP-binding site is known as the (-) end, whereas the opposite end without an exposed ATP-binding site is known as the (+) end (Scott *et al.*, 2012).

Actin is characterised by a slow ATP hydrolysing rate, which becomes 'active' when actin becomes filamentous, increasing catalysing rate by approximately 40,000 times, at approximately 0.3 s^{-1}. The resulting P_i remains bound next to ADP until it is cooperatively liberated from the filament interior (Vavylonis *et al.*, 2005; Katkar *et al.*, 2018). A 'closed' conformation of the cleft is required for ATP hydrolysis, which is present in F-actin; in G-actin the cleft conformation is 'open' (Reisler and Egelman, 2007).

Nucleating factors are necessary to stimulate actin polymerisation, including the Arp2/3 complex, which mimics a G-actin dimer to stimulate nucleation (formation of the first trimer) of monomeric G-actin. The Arp2/3 also binds to actin microfilaments at 70° to form new actin branches from existing actin microfilaments. The growth of F-actin filaments can be regulated by the actin binding proteins thymosin and profilin; thymosin binds to G-actin to buffer the polymerising process whilst profilin binds to G-actin to exchange ADP for ATP, promoting the monomeric addition to the barbed (+) end of F-actin microfilaments (Alberts *et al.*, 2002).

The structure of F-actin is dynamic because the monomers are linearly bound with non-covalent bonds, and the lateral bonds with neighbouring monomers can be broken with thermal agitation. The weak bonds give the advantage that the filament ends can easily release or incorporate actin monomers, allowing rapid remodelling to change structure in response to appropriate stimulus. Along with the biochemical mechanisms with the factor complexes that incorporate or release actin monomers, this makes the actin microfilaments 'assembly dynamic' (Alberts *et al.*, 2002).

Although actin hydrolyses ATP, this is not required for actin assembly, as hydrolysis takes place inside an already formed filament, and adenosine

diphosphate (ADP) can also allow polymerisation. The actin cycle consists of the energetically preferential addition of G-actin-ATP monomers to a filament's barbed (+) end, and the simultaneous disassembly of F-actin-ADP monomers at the pointed (-) end wherein ADP is converted to ATP, making a feature of actin microfilament dynamics known as 'treadmilling' (Vavylonis *et al.*, 2005). The substrate ATP is hydrolysed rapidly after the addition of G-actin to the end; there are two hypotheses regarding how this occurs. The hydrolysis may happen stochastically, sporadically in a manner that is influenced by neighbouring molecules, or vectorially, in which hydrolysis occurs adjacent to other molecules in which ATP has already been hydrolysed. In either case, the resulting inorganic phosphate (P_i) is not released, and it remains non-covalently bound to neighbouring ADP. This process allows for three species of actin in a microfilament: ATP-actin, ADP+P_i-actin and ADP-actin. The amount of each species in a microfilament depends upon its length: as elongation commences the filament has an approximately equal amount of ATP-actin and ADP+P_i-actin and a small amount of ADP-actin at the (-) end. As stationary length is achieved the situation reverses, with ADP-actin present along the majority of the microfilament and only the (+) end containing ADP+P_i-actin, and ATP-actin at the tip (Ghodsi and Kazemi, 2011).

Comparing the filaments that only contain ADP-actin with those that include ATP, in the former the critical concentrations (C_c) are similar in both ends, while C_c for the other two nucleotides is different. At the (+) end $C_c^+ = 0.1$ µM while at the (-) end $C_c^- = 0.8$ µM which allows the following situations: for G-actin-ATP concentrations less than C_c^+, no microfilament elongation occurs, for G-actin-ATP concentrations less than C_c^- but greater than C_c^+ elongation occurs at the (+) end, and for G-actin-ATP concentrations greater than C_c^- the microfilaments grow at both ends. Therefore, it is possible that the energy produced by hydrolysis is used to provide a 'stationary state' that is in flux, and instead of a simple equilibrium, the microfilament is dynamic and polar. This explanation justifies the energy expenditure as this state is needed for its many functions (Vavylonis *et al.*, 2005).

The configuration of the different monomer species is detected by actin binding proteins, which also controls the microfilament dynamism (Dominguez, 2004). The actin binding proteins include the previously mentioned thymosin and

profilin, as well as gelsolin and cofilin which cut microfilaments while blocking addition of new monomers to (+) ends (Southwick, 2000). The actin binding protein CapZ caps the (+) ends of F-actin depending on the intracellular levels of Ca^{2+}/calmodulin (Caldwell *et al.*, 1989).

Animal cells commonly have a cortex under the PM characterised by containing many microfilaments, which precludes the presence of organelles. Within neuron axons, there are actin rings linked together using spectrin tetramers, which forms a mechanical support for the axon membrane (Xu *et al.*, 2013). Actin can also form microfilament bundles, long microfilaments associated with non-muscle myosins, involved with intracellular substance transport. Actin microfilaments are vital for systems of cellular mechanical support and provide trafficking routes for signal transduction. They function to transport cargo using nonconventional myosins as motors, such as myosin V and VI to carry the cargo. These myosins use ATP hydrolysis to transport cargo, such as vesicles and organelles directly to their target. Myosin V walks towards the barbed (+) end whereas myosin VI walks towards the pointed (-) end. Most actin filaments are arranged with the (+) end towards the cell membrane and the (-) end towards the cell interior. Actin microfilaments are found both in the cytoplasm and the nucleus (Grummt, 2006). Its location is regulated by cell membrane signal transduction pathways that restructure the microfilaments in response to such signalling (Zouwail *et al.*, 2005).

5.1.2 Role of Actin in Nerve Terminals

The dynamic assembly of F-actin has essential roles in pre-synapse protein assembly, SV mobilisation and recycling, and functions in presynaptic plasticity; however, mechanisms that regulate temporal and spatial assembly of presynaptic F-actin are mostly unknown. Similarly to other F-actin rich specialised membranes, presynaptic terminals contain certain molecules that respond to cellular cues and trans-synaptic signals to trigger activity-dependent assembly of F-actin structures. Netrin is a chemotrophic factor that facilitates synapse assembly. Netrin receptor UNC-40 localises to presynaptic regions in response to netrin. The protein UNC-40 interacts with a signalling pathway to

cause lamellipodin (also known as MIG-10) to organise the actin cytoskeleton in presynaptic regions, which is necessary for SV clustering during synapse assembly but is not necessary for subcellular localisation of AZ proteins. Thus, signalling molecules that organise the actin cytoskeleton can be co-opted to organise SV clustering (Stavoe and Colón-Ramos, 2012).

The AZ protein Piccolo is a key regulator of SV release which functions by coordinating activity-dependent assembly of F-actin and the dynamics of key SV cycle proteins including synapsin 1, profilin, Daam1 and calmodulin dependent kinase II. These functions suggest that Piccolo may function as a coordinator of F-actin spatial organisation, directing from the AZ by binding to key actin regulatory proteins (Wagh *et al*., 2015). In presynaptic terminals F-actin is localised predominantly in the AZs and adjacent SV clusters, including docked SVs and populations of recycling SVs. Contrastingly the proximally located vesicle pool has much less surrounding F-actin (Li *et al*., 2010).

In glutamatergic synaptic terminals of the calyx of Held, RP SVs are converted into RRP SVs by an actin-dependent process once the RRP is depleted during stimulation and this involves regulating the proximity of SVs to Ca^{2+} channels. In the early phase of stimulation, RP SVs are converted rapidly into RRP SVs, counteracting short-term depression. However, during late phase stimulation after the pools are exhausted, calmodulin-dependent recruitment of RRP SVs is activated. This shows that RP SVs have a role in short-term plasticity and that RP SVs are converted to RRP SVs via relocation towards Ca^{2+} channels (Lee *et al.*, 2012).

5.1.3 Role of Actin in Endocytosis

The actin cytoskeleton has been implicated in playing a role in CME. Actin cytoskeleton remodelling is not essential for clathrin-coated vesicle assembly but may indirectly affect the nucleation of clathrin-coated pits. Actin depolymerisation using latrunculin A or cytochalasin D reduced the frequency of pit formation by approximately half without affecting maturation into clathrin-coated vesicles (Boucrot *et al*., 2006). Dynamin is part of a protein network that controls nucleation of actin from membranes. At the endocytic sites, dynamin

may couple the fission reaction to the polymerisation of an actin pool that functions in the separation of the endocytic vesicles from the PM(Lee and de Camilli, 2001). Dynamin, actin, and N-BAR proteins cooperatively function to efficiently catalyse membrane scission in clathrin-coated vesicle formation. Dynamin controls its own recruitment to scission events by modulating the kinetics of actin and N-BAR proteins' recruitment to sites of scission whilst conversely actin functions as a dynamic scaffold that concentrates dynamin and N-BAR proteins at these locations (Taylor *et al.*, 2012). Dynamin-1 and -2 knockout mice present actin-nucleating protein, actin, and BAR domain proteins that accumulate at the base of arrested endocytic clathrin-coated pits, where they support the growth of long, tubular necks of endocytosing membranes. Thus, these proteins function in concerted action independently and prior to dynamin's role of membrane scission (Ferguson *et al.*, 2009).

Assembled dynamin, generated through interactions with short actin filaments, may promote actin polymerisation into higher order structures via displacement of the actin capping protein gelsolin (Gu *et al.*, 2010). Clathrin assembly supports formation of mature clathrin-coated pits in the absence of actin polymerisation in many mammalian cells, however actin coating is necessary to complete membrane deformation into a clathrin-coated pit on PMs under tension from osmotic swelling or mechanical stretching. Resistance of the PM to propagation of the clathrin lattice due to membrane tension determines whether CME is actin dependent or actin independent (Boulant *et al.*, 2011).

There is evidence of clathrin independent endocytosis occurring without dynamin, by an actin polymerisation tension induced mechanism in Shiga toxin treated HeLa cell model. Nascent transport intermediates detach from donor membranes by scission, which can occur with or without dynamin in clathrin-independent endocytosis. Scission of Shiga toxin-induced tubular endocytic membrane invaginations is preceded by cholesterol-dependent membrane reorganisation, correlating with the formation of membrane domains on model membranes, suggesting that domain boundary forces are driving tubule membrane constriction. Actin triggers scission by inducing this membrane reorganisation. Tubule occurrence during Shiga toxin treatment is increased upon depletion of the actin nucleator Arp2, and cortical actin shells in liposomes are sufficient to trigger scission of Shiga toxin-induced tubules dependently on

cholesterol but independently of dynamin action. Therefore, scission of tubules by a mechanical mechanism may function independently or in synergy with dynamin complex constriction (Römer *et al.*, 2010).

It has been confirmed in frog neuromuscular junction that ADBE is initiated during sustained tetanic stimulation, and that nerve terminals undergo a maturation process shortly after the end of stimulation. This includes a transient bulging of the PM wherein amount of bulging and size of cisternae formed corresponds to stimulation frequency. Cytochalasin D, an inhibitor of actin polymerisation, hindered both the initiation and maturation process of ADBE, thus also hindering the number of recycled SVs for further neurotransmission (Nguyen *et al.*, 2012).

The role of actin microfilaments in non-neuronal granule release have been substantially more discovered than actin microfilaments' role in SV release. Some of the results above may have analogous implications for acto-NMII mechanisms in SV exocytosis. See Chapter 1.6.2 for further detail of these mechanisms.

5.2 F-actin Depolymerisation Using Latrunculin A on Synaptic Vesicle Release Dynamics

5.2.1 Latrunculin A Treatment on Evoked Glutamate Release

Latrunculin A morphologically alters polymerisation of actin, dissociating existing F-actin filaments into a 1:1 stoichiometric complex between latrunculin A and resulting G-actin (Coué and Brenner, 1987). Latrunculin A is also used extensively to sequester monomeric G-actin in living cells, which prevents formation of new F-actin filaments. It functions by binding with the nucleotide cleft of actin needed for actin filament elongation, which also causes dissociation of the actin from the filament. It has equilibrium dissociation constant (K_d) of 0.2 – 0.4 µM (Yarmola *et al.*, 2000). These properties made latrunculin A ideal for this study involving the exclusion/reduction of F-actin filaments prior to synaptosome stimulation in order to elucidate how actin filaments function in SV release mechanics.

There was no significant change in Glu release from the RRP when synaptosomes were treated with 15 µM latrunculin A with 4AP5C stimulation (Figure 5.1a), although Glu release was decreased with HK5C (Figure 5.1b) and ION5C (Figure 5.1c) stimulation, using latrunculin A treatment.

These results showed that only the RP was blocked from SV release during or after actin depolymerisation with these stimuli. This may have been due to blocked mobilisation of the RP to the AZ to be primed for release, as SV mobilisation required an active actin scaffold for them to precisely translocate.

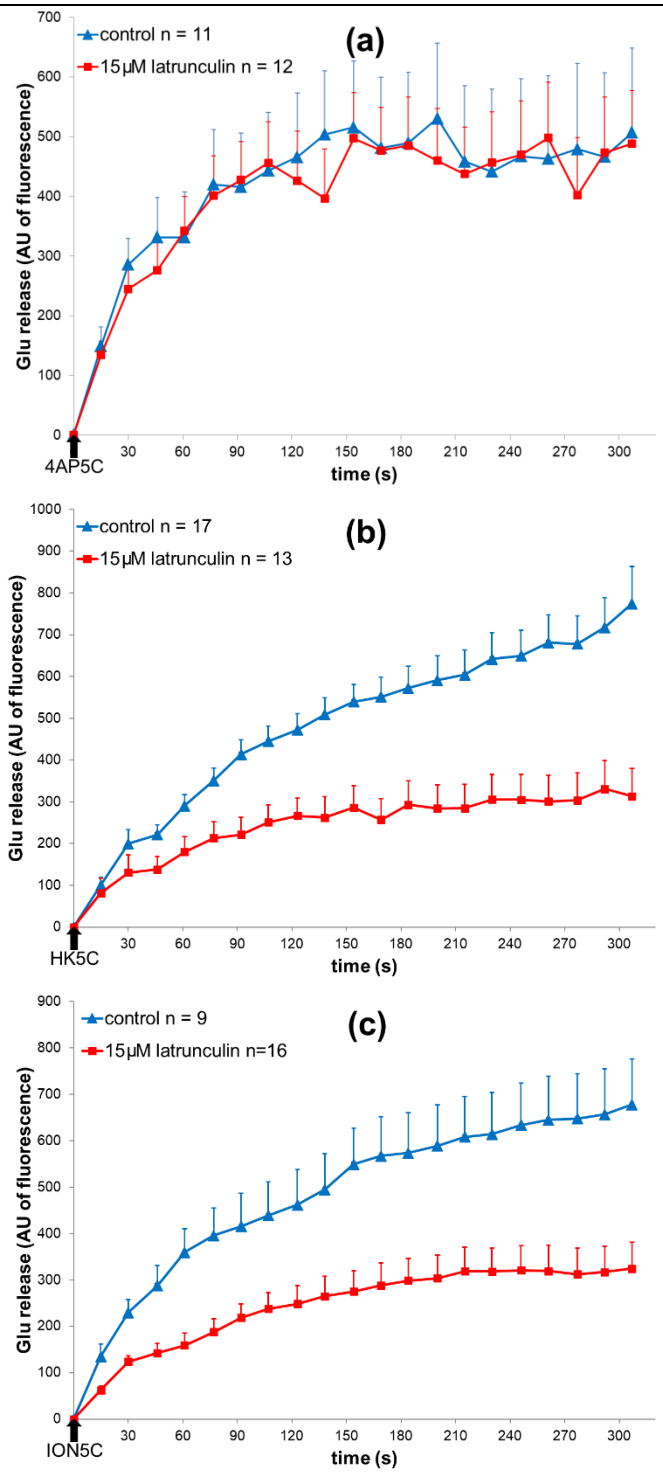

Figure 5.1: The effect of 15 µM latrunculin A vs control upon evoked Glu release. Depolymerisation of F-actin using 15 µM latrunculin A (a) had no significant effect upon 4AP5C evoked Glu release ($p > 0.05$), although significantly decreased Glu release evoked by (b) HK5C stimulation ($p < 0.05$) and (c) ION5C stimulation ($p < 0.05$), compared to non-drug controls. Values represented are the mean plus SEM from 3 (a), 5 (b, c) independent experiments.

5.2.2 Treatment of Latrunculin A Upon FM 2-10 Dye Release

As latrunculin A treatment reduced Glu release during HK5C and ION5C stimulation, showing that the RRP and not RP SVs were released, its effects upon FM 2-10 dye release was investigated. Actin depolymerisation using 15 µM latrunculin A had no apparent effect upon FM 2-10 dye release with HK5C (Figure 5.2a) or ION5C (Figure 5.2b) compared to controls. However, this result was deceiving since normally it is the RP of SVs that undergoes FF and releases FM dye whilst the RRP pool of SVs normally undergo KR and so would not release dye. In order for FM dye release to be apparent in these latrunculin treated terminals, the RRP SVs must be switched to FF mode since there is no RP SVs being released. It is serendipitous that in these rat cerebrocortical synaptosomes the size of the RRP and the RP of SVs are similar (see Chapter 2.4.5) and that is why switching the RRP SVs to FF gave a similar value to release from non-drug treated terminals where the RP only releases FM dye (Figure 5.2a,b). Note that latrunculin did not perturb the total FM content inside the terminals (Figure 5.3). This is important because if latrunculin did perturb the total FM dye content then it would be difficult to observe a change to the pools of SVs.

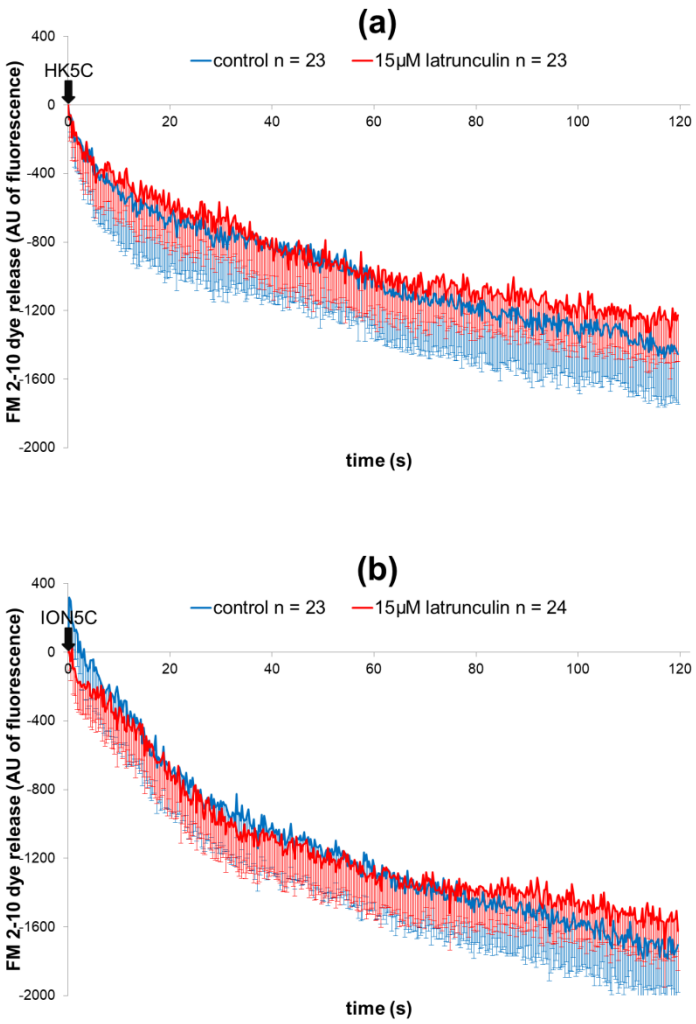

Figure 5.2: The effect of 15 μM latrunculin A vs control upon evoked FM 2-10 dye release. Depolymerisation of F-actin using 15 μM latrunculin A had no significant effect upon FM 2-10 dye release during (a) HK5C stimulation ($p > 0.5$), or (b) ION5C stimulation ($p > 0.7$), compared to non-drug controls. Values represented are the mean plus SEM from 3 independent experiments.

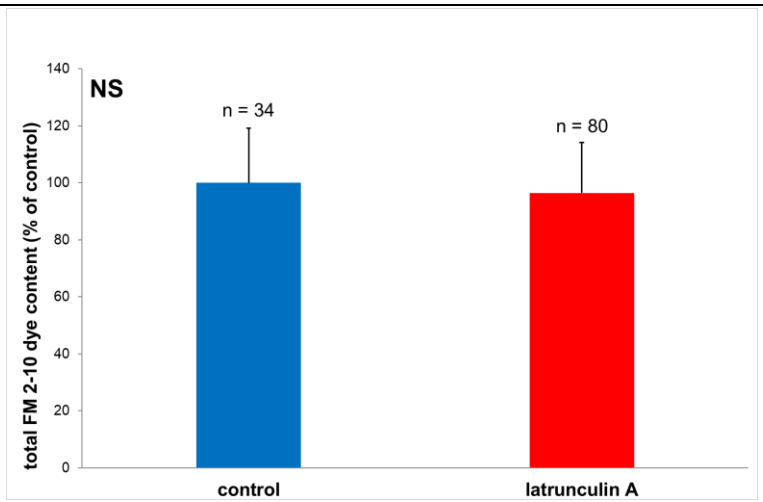

Figure 5.3: The effect of 15 µM latrunculin A treatment upon total FM 2-10 dye content relative to non-drug treated control. There is no significant difference between the FM content in control (n = 34) and latrunculin treated (n = 80) ($p > 0.3$). Values represented are normalised to control, and error bars represent the S.D. from 4 independent experiments.

5.2.3 Dual Treatment of Latrunculin A and Okadaic Acid Upon Evoked Glu and FM 2-10 Dye Release

Previously, the inhibition of PP1 and PP2A using 0.8 µM OA was shown to induce the RRP of SVs to switch from KR to FF mode but such treatment did not perturb the total evoked Glu release from the RRP and RP SVs (Bhuva, 2015; Singh, 2017). This occurred whether the mode of exocytosis was being regulated by dynamin (when ION5C was employed) or when NMII was regulating the pore (when HK5C was used). This result is recapitulated in Figure 5.4a,c which demonstrates that OA did indeed switch the RRP SVs from a KR mode to an FF mode so that there was then more FM dye release compared to control; the control only demonstrated the release of the RP by FF mode. Such treatment did not perturb the total FM dye content so the results could not be explained by changes in the amount of dye inside the SVs in the terminals (Bhuva, 2015; Singh, 2017).

Such OA treatment allowed one to check the hypothesis that latrunculin perturbs the RP release but switches the RRP SV to an FF mode.

Following 15 µM latrunculin A treatment, it was found that the subsequent addition of 0.8 µM OA had no significant effect upon HK5C evoked (Figure 5.4b) or ION5C evoked (Figure 5.4d) FM 2-10 dye release compared to controls. This result was similar to latrunculin A treatment alone (Figure 5.2a, b), where it has been suggested that the RP of SVs is not released but that the RRP SVs are released by an FF mode.

Clearly, this suggestion was backed up by this result because if the latrunculin has switched the RRP to FF mode then OA no longer produced further FM dye release because the RRP had already been switched by OA action. Such dual treatment did not perturb the total FM 2-10 dye content inside the terminals (Figure 5.5). Clearly, latrunculin switched the mode of exocytosis whether the RRP SVs were being regulated by dynamin or NMII.

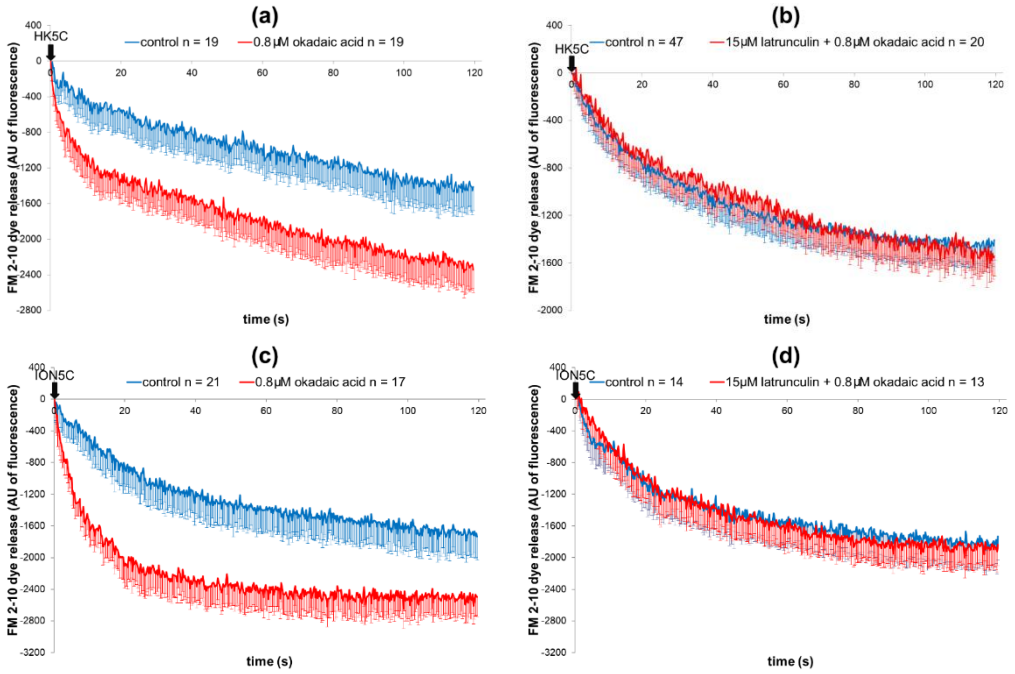

Figure 5.4: The effect upon HK5C or ION5C evoked FM 2-10 dye release of 0.8 µM OA alone or in combination with of 15 µM latrunculin. (a, c) PP1 and PP2A inhibition using 0.8 µM OA significantly increases FM 2-10 dye release compared to non-drug controls with both HK5C and ION5C stimulation ($p < 0.05$). (b, d) Depolymerisation of F-actin using 15 µM latrunculin A and subsequent treatment using 0.8 µM OA has no significant effect upon FM 2-10 dye release, compared to non-drug controls with both HK5C and ION5C stimulation ($p > 0.6$). Values represented are the mean plus SEM from 3 (a, c, d) and 7 (b) experiments.

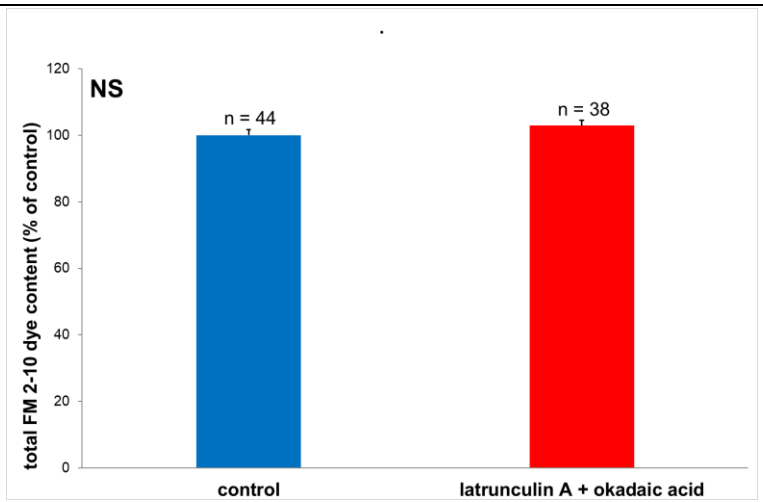

Figure 5.5: The effect of latrunculin plus OA treatment on total FM 2-10 content relative to non-drug treated control. There is no significant difference between the FM content in control (n = 44) and latrunculin plus OA treated terminals (n = 38) ($p > 0.2$) from 4 independent experiments. Values are normalized to control, and error bars represent the SEM.

The interpretation of the results shown in Figure 5.4b and 5.4d assumes that the inclusion of an OA treatment would not prevent latrunculin from inhibiting the release of the RP of Glu containing SVs. Figure 5.6 demonstrates that compared to control the treatment with latrunculin A and OA did indeed block the HK5C (Figure 5.6a) and ION5C (Figure 5.6b) evoked release of the RP such that the Glu release was similar to that found in synaptosomes treated with latrunculin alone (Figure 5.1).

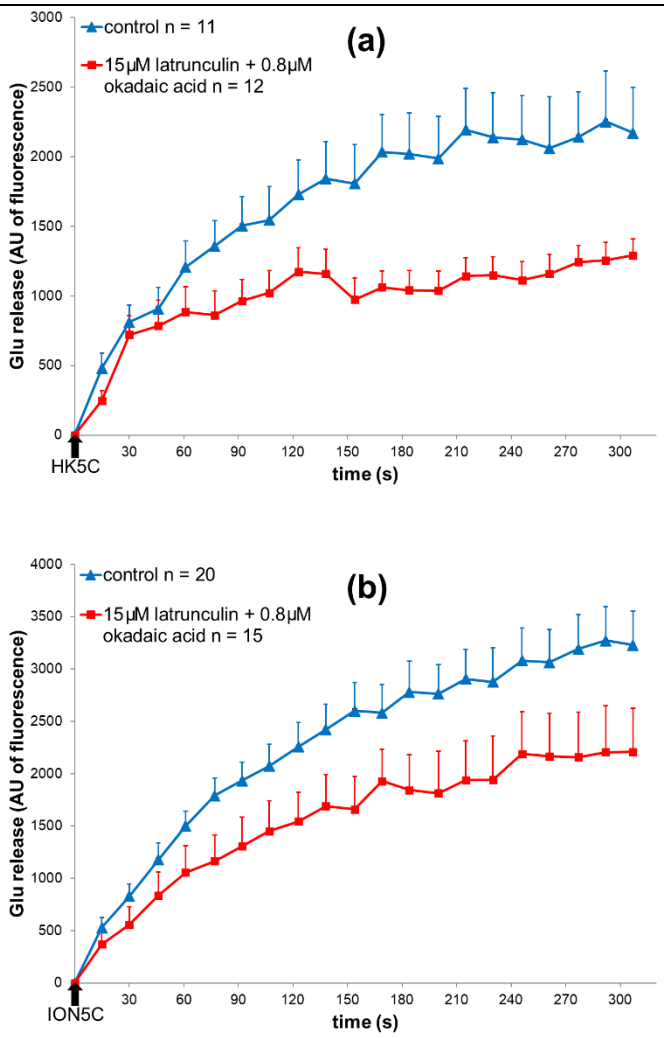

Figure 5.6: The effect of latrunculin A plus OA upon HK5C and ION5C evoked Glu release compared to non-drug treated control. Synaptosomes were treated with 15 µM Latrunculin plus 0.8 µM OA and this induced a significant reduction in release evoked by (a) HK5C or (b) ION5C at later time points ($p < 0.05$) compared to non-drug controls. Values represent mean plus SEM for 3 (a) or 5 (b) independent experiments.

5.2.4 Treatment of Latrunculin A Upon Changes in Intracellular Ca^{2+} Levels

Depolymerisation of actin using 15 µM latrunculin A significantly decreased HK5C evoked $[Ca^{2+}]_i$ levels compared to controls (Figure 5.7a), but such treatment had no effect on ION5C evoked $[Ca^{2+}]_i$ levels (Figure 5.7b).

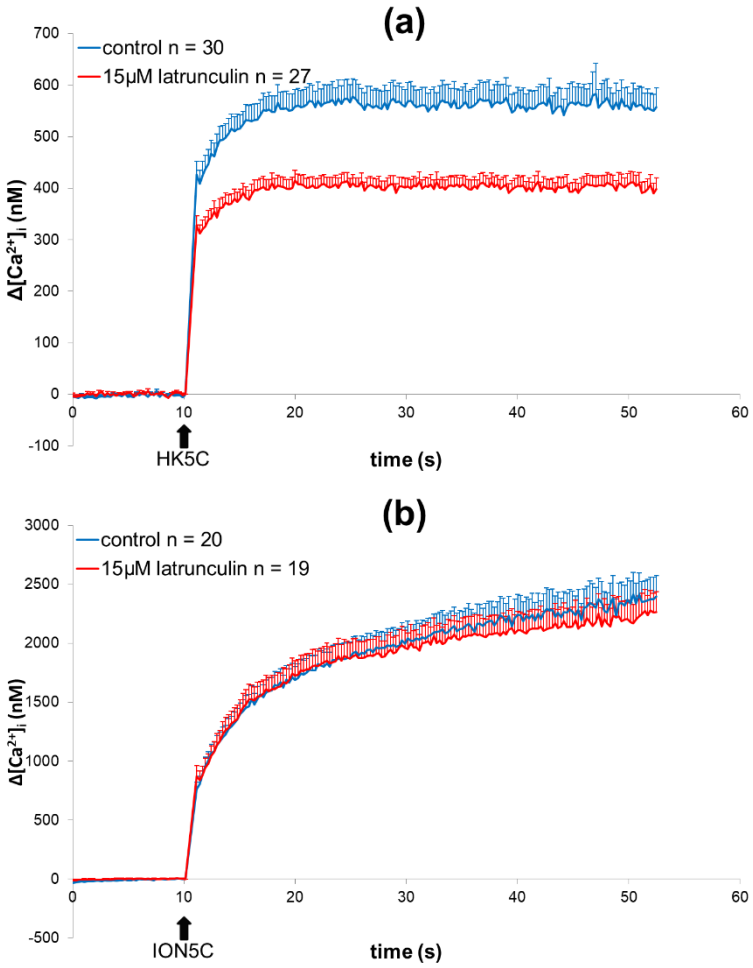

Figure 5.7: The effect of 15 µM latrunculin A vs control upon evoked $[Ca^{2+}]_i$ levels. Depolymerisation of F-actin using 15 µM latrunculin A (a) significantly decreased HK5C evoked $[Ca^{2+}]_i$ levels ($p < 0.05$) but (b) caused no significant change to ION5C evoked $[Ca^{2+}]_i$ levels ($p > 0.3$), compared to non-drug controls. Values represented are the mean plus SEM from 3 (a) and 4 (b) independent experiments.

5.3 Stabilisation of F-actin Using Jasplakinolide Upon Synaptic Vesicle Release Dynamics

5.3.1 Treatment of Jasplakinolide Upon Evoked Glutamate Release

Jasplakinolide is a cyclo-depsipeptide, commonly used to induce actin filament polymerisation and stabilisation by stimulating actin filament nucleation (K_d = 15 nM), and it differs from other actin stabilisers by its membrane permeability properties. Jasplakinolide *in vivo* has been found to disrupt actin filaments and induce polymerisation of monomeric G-actin into amorphous masses, the exact mechanism of which has not been determined (Bubb *et al.*, 2000; Holzinger, 2009).The properties of jasplakinolide to stabilise existing actin filaments, and its prevention of constitutive active reformation, was utilised in this study to investigate SV release mechanics in relation to F-actin changes required before, during and after stimulation.

Following 2.5 µM jasplakinolide treatment, there was no significant change in HK5C (Figure 5.8a) or ION5C (Figure 5.8b) evoked Glu release compared to controls. These results showed that the RRP and RP release were not perturbed by actin stabilisation, whilst there was a block of the release of the RP following F-actin depolymerisation (Figure 5.1). Interestingly, these results also suggested that there was not a normal cycle of disassembly and reassembly of actin microfilaments required for the exocytosis of the RRP and RP SVs because jasplakinolide would prevent this.

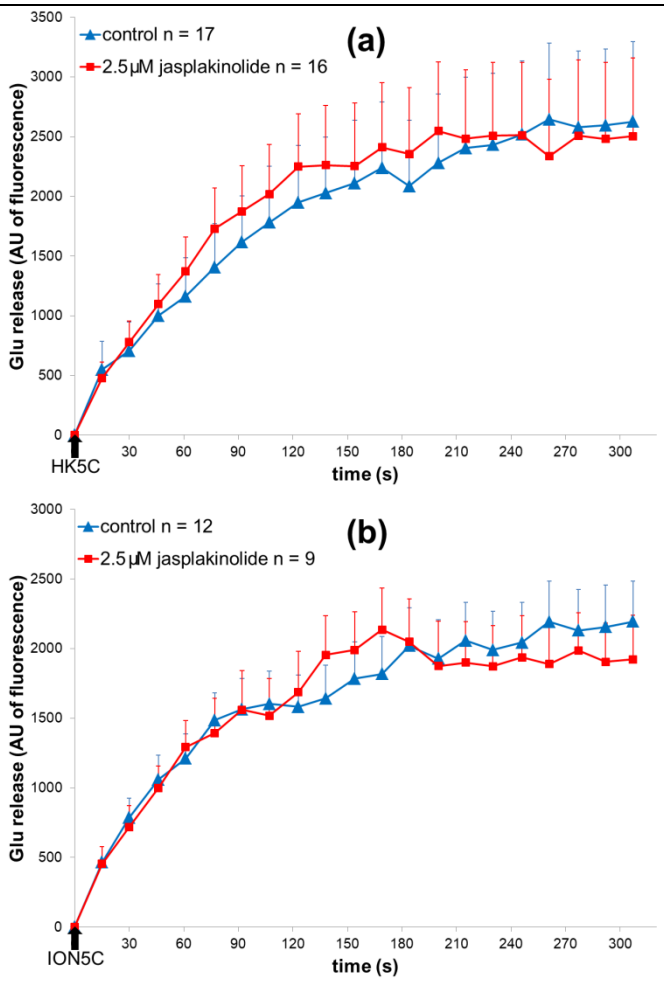

Figure 5.8: The effect of 2.5 µM jasplakinolide upon evoked Glu release. Stabilisation of F-actin using 2.5 µM jasplakinolide had no significant effect upon Glu release during (a) HK5C stimulation ($p > 0.6$) or (b) ION5C stimulation ($p > 0.5$), compared to non-drug controls. Values represented are the mean plus SEM from 4 (a) and 3 (b) independent experiments.

5.3.2 Dual Treatment of Jasplakinolide and Latrunculin A Dual Upon Evoked Glutamate Release

As jasplakinolide treatment did not perturb evoked release of the RRP and RP, then this drug was used to check that latrunculin A was specifically acting on actin microfilaments rather than working non-specifically on another cellular component. This could be done because pre-treatment with jasplakinolide prevents latrunculin A from disassembling actin microfilaments. Therefore, if jasplakinolide action prevents the latrunculin induced inhibition of evoked RP release then the latter must be working by acting on microfilaments.

Compared to non-drug treated control there was no significant change in Glu release during HK5C stimulation (Figure 5.9a) or ION5C stimulation (Figure 5.9b) in synaptosomes treated with 2.5 µM jasplakinolide and then 15 µM latrunculin A. Clearly, jasplakinolide prevented latrunculin A action as both the RRP and RP were released. Conversely, as jasplakinolide prevented the action of latrunculin A, this also showed that jasplakinolide was acting specifically to stabilise the actin microfilaments in the synaptosomes.

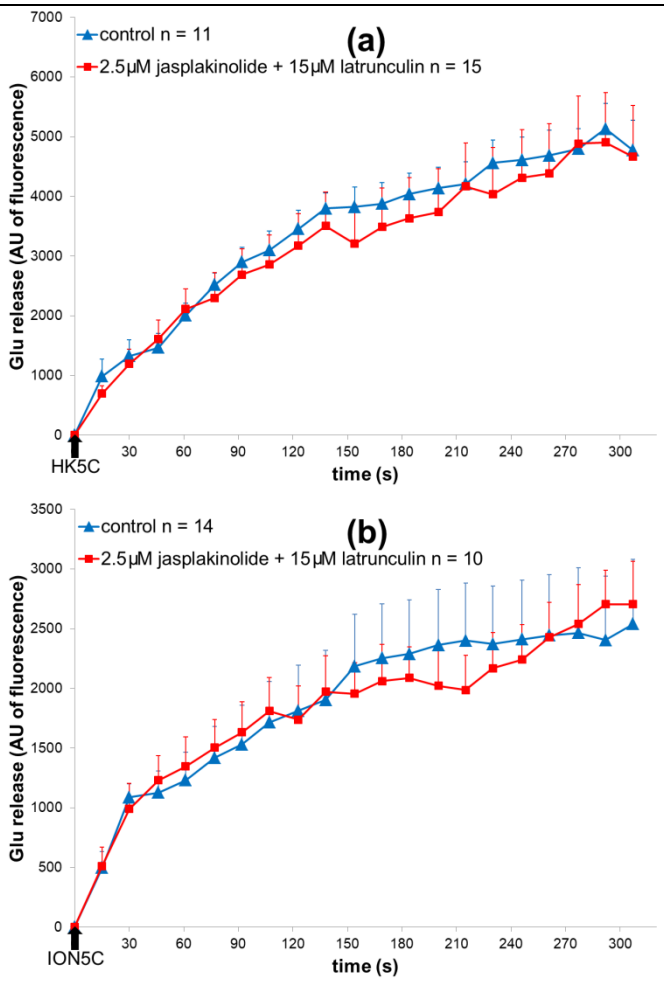

Figure 5.9: The effect of 2.5 µM jasplakinolide plus 15 µM latrunculin A upon evoked Glu release. Stabilisation of F-actin using 2.5 µM jasplakinolide and subsequent treatment using 15 µM latrunculin A had no significant effect upon evoked Glu release using (a) HK5C stimulation ($p > 0.6$), or (b) ION5C stimulation ($p > 0.7$), compared to non-drug controls. Values represented are the mean plus SEM from 3 (a) and 4 (b) independent experiments.

5.3.3 Treatment of Jasplakinolide Upon FM 2-10 Dye Release

Stabilisation of F-actin using 2.5 µM jasplakinolide had no significant effect upon FM 2-10 dye release evoked by HK5C stimulation (Figure 5.10a) or ION5C stimulation (Figure 5.10b), compared to controls. In this case, as jasplakinolide did not prevent the exocytosis of the RRP and RP SVs, then appeared that RRP SVs were still undergoing KR mode and the RP was undergoing FF mode following stabilisation of the microfilaments. Such an assumption would therefore suggest that the normal modes of exocytosis for the RRP and the RP

were not perturbed by jasplakinolide. However, this assumption could be wrong if in fact the RRP was switched to FF mode whilst the RP was switched to KR mode as there were some drugs (e.g., Cys A) that could switch the RP to KR (Figure A15 in Appendix A; Bhuva, 2015). The experiments below indicate that this was not the case.

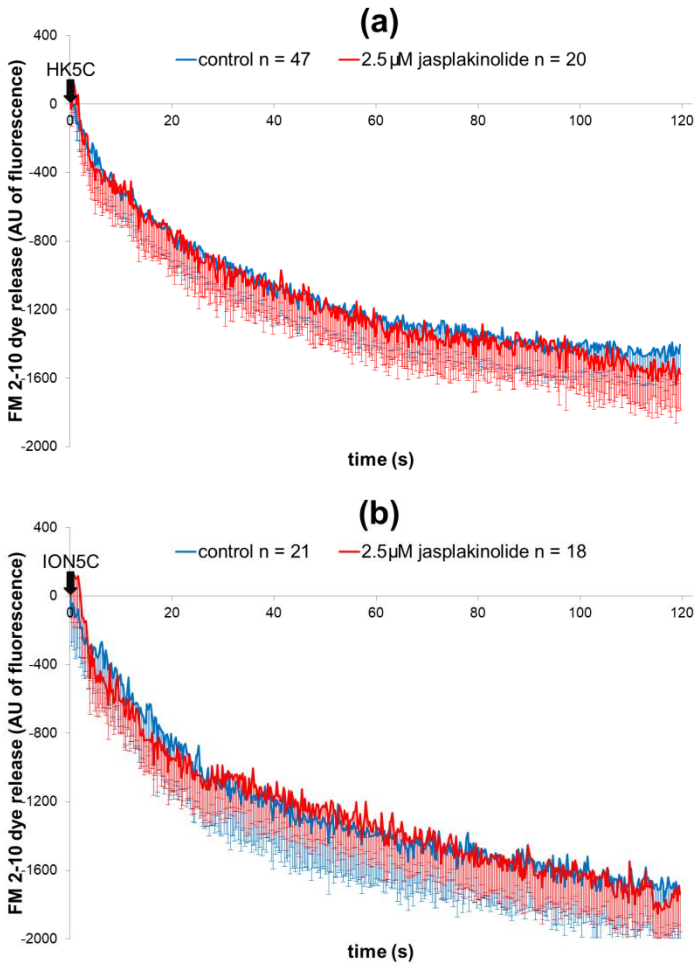

Figure 5.10: The effect of 2.5 µM jasplakinolide upon evoked FM 2-10 dye release. Stabilisation of F-actin using 2.5 µM jasplakinolide had no significant effect upon FM 2-10 dye release during (a) HK5C stimulation ($p > 0.5$) or (b) ION5C stimulation ($p > 0.6$), compared to non-drug controls. Values represented are the mean plus SEM from 7 (a) and 3 (b) independent experiments.

5.3.4 Treatment of Jasplakinolide and Latrunculin A Upon FM 2-10 Dye Release

Dual treatment of 2.5 µM jasplakinolide followed by 15 µM latrunculin A had no significant effect upon FM 2-10 dye release during HK5C stimulation (Figure 5.11a) nor ION5C stimulation (Figure 5.11b), compared to controls. Again, this condition did not prevent the exocytosis for the RRP and RP SVs, but it is not certain whether there were switches in the two modes for the RRP and the RP (see argument in previous paragraph). However, the next experiment shows that the RP must have undergone FF and the RRP must have initially undergone KR.

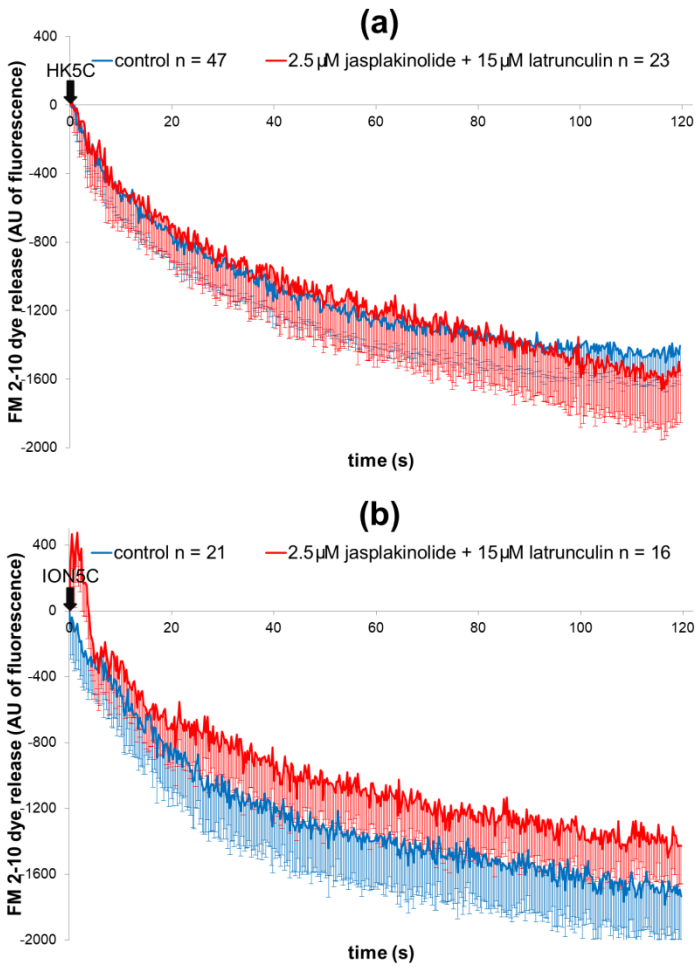

Figure 5.11: The effect of 2.5 µM jasplakinolide plus 15 µM latrunculin A upon evoked FM 2-10 dye release. Stabilisation of F-actin using 2.5 µM jasplakinolide and subsequent treatment using 15 µM latrunculin A had no significant effect upon evoked FM2-10 dye release using (a) HK5C stimulation ($p > 0.5$), or (b) ION5C stimulation ($p > 0.4$), compared to non-drug controls. Values represented are the mean plus SEM from 7 (a) and 3 (b) independent experiments.

5.3.5 Triple Treatment of Jasplakinolide, Latrunculin A and Okadaic Acid Upon FM 2-10 Dye Release and Evoked Glu Release

Following a triple treatment of 2.5 µM jasplakinolide, then 15 µM latrunculin A plus 0.8 µM OA, both HK5C stimulation (Figure 5.12a) and ION5C stimulation (Figure 5.12b) induced a further increase in FM 2-10 dye release compared to the control. This result indicated that jasplakinolide truly prevented the action of latrunculin on the KR mode of the RRP as OA could then work to switch the RRP to FF mode. There was no change in the RP mode as it has been shown previously that OA exclusively worked on the RRP mode (Bhuva, 2015; Singh, 2017). Note that jasplakinolide, jasplakinolide plus latrunculin or jasplakinolide plus latrunculin plus OA did not affect the total FM 2-10 dye content of the synaptosomes and so any results were a reflection upon any changes in the mode of exocytosis (Figure 5.13).

It is important to point out that both the dynamin dependent KR mode of the RRP (stimulated normally by ION5C) and the NMII dependent KR mode of the RRP (stimulated by HK5C) would appear to have been regulated by actin microfilaments such that the KR mode (presumably due to the closure of the fusion pore in < 0.5 s) was prevented when actin microfilaments were disassembled (see discussion). Of course, this interpretation assumes that the triple treatment of jasplakinolide plus latrunculin A plus OA did not perturb the evoked Glu release and it was shown that such treatment did not perturb the HK5C (Figure 5.14a) or ION5C (Figure 5.14b) stimulated exocytosis of Glu containing RRP and RP SVs.

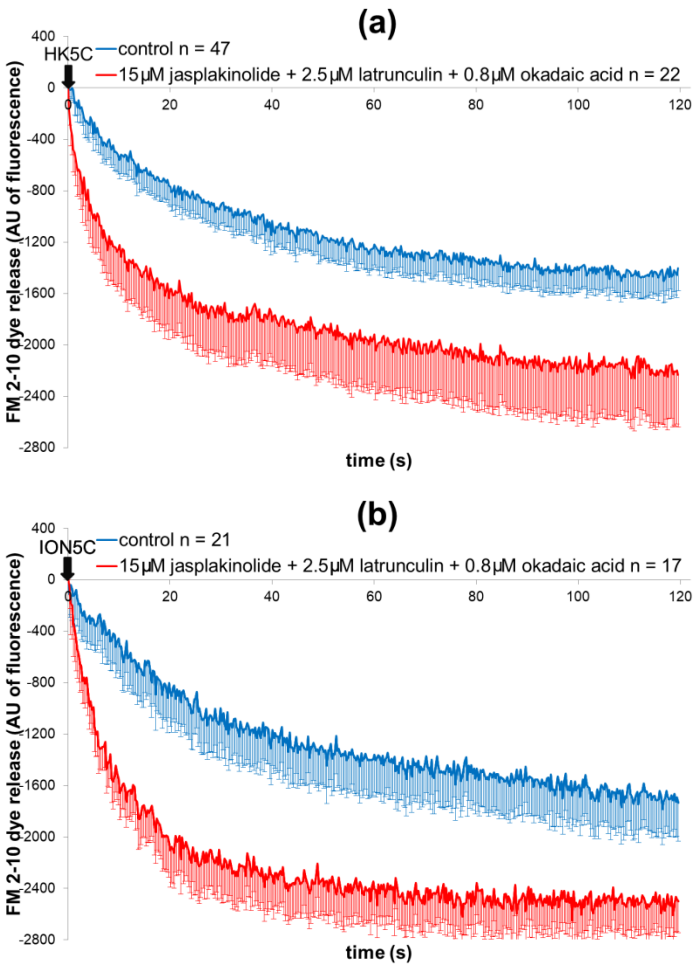

Figure 5.12: The effect of 2.5 µM jasplakinolide plus 15 µM latrunculin A plus 0.8 µM OA upon evoked FM 2-10 dye release. Stabilisation of F-actin using 2.5 µM jasplakinolide with subsequent 15 µM latrunculin A treatment, then 0.8 µM OA treatment significantly increases FM 2-10 dye release with both (a) HK5C stimulation ($p < 0.05$) and (b) ION5C stimulation ($p < 0.05$), compared to non-drug controls. Values represented are the mean plus SEM from 7 (a) and 3 (b) independent experiments.

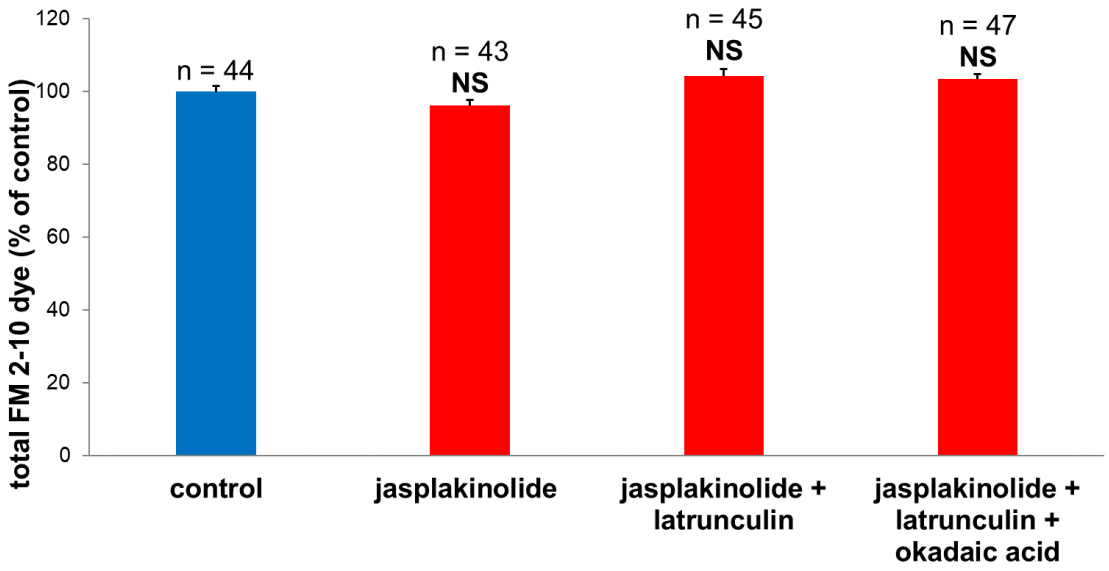

Figure 5.13: The effect of various drug treatments on total FM 2-10 content relative to non-drug treated control. There is no significant difference between the FM content in control and jasplakinolide treated, jasplakinolide plus latrunculin treated or jasplakinolide plus latrunculin plus OA ($p > 0.05$). Values are normalised to control and error bars represent the SEM from 3 independent experiments.

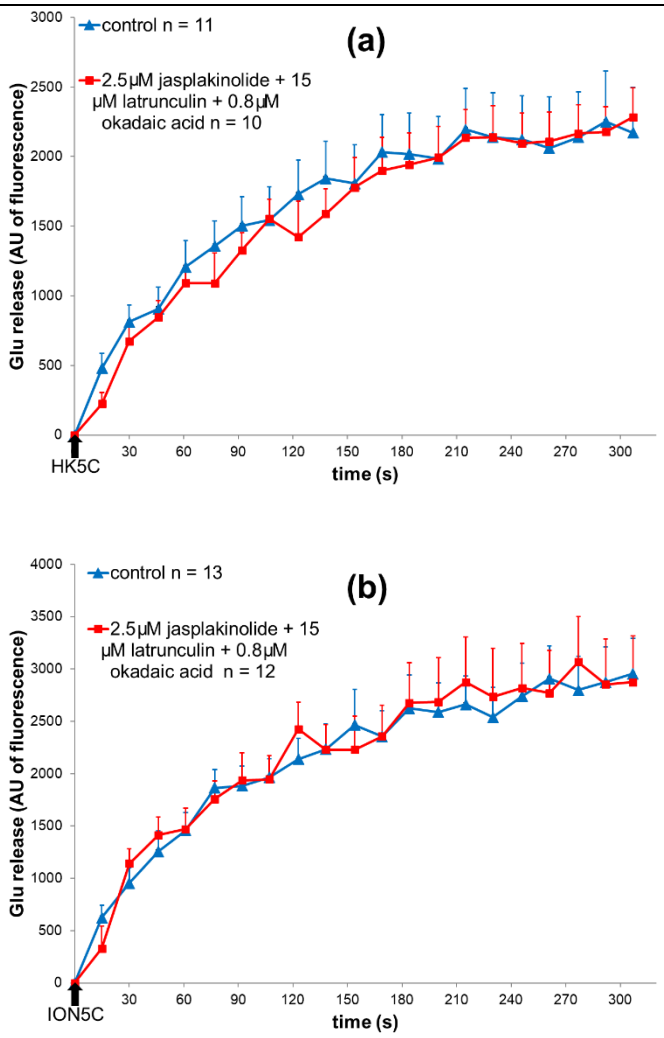

Figure 5.14: The effect of jasplakinolide plus latrunculin A plus OA upon HK5C and ION5C evoked Glu release compared to non-drug treated control.

Synaptosomes were treated with 2.5 µM jasplakinolide plus 15 µM latrunculin plus 0.8 µM OA but such treatment had no significant effect upon evoked Glu release by (a) HK5C ($p > 0.3$) or (b) ION5C ($p > 0.8$) compared to non-drug controls. Values represent mean plus SEM for 3 independent experiments.

5.3.6 Treatment of Jasplakinolide Upon Changes in Intracellular Ca^{2+} Levels

Compared to non-drug treated controls, the stabilisation of F-actin using 2.5 µM jasplakinolide had a small increase effect upon HK5C evoked (Figure 5.15a) but not on ION5C evoked (Figure 5.15b) $[Ca^{2+}]_i$ levels. This result showed that F-actin stabilisation increased evoked $[Ca^{2+}]_i$ levels for HK5C and this might be related to stabilising the localisation of the voltage-gated Ca^{2+} channels at the AZ.

All the results with acute jasplakinolide treatment alone indicated that the stabilisation of microfilaments had no effect on Glu release, the mode of SV exocytosis, or the amount of evoked $[Ca^{2+}]_i$ levels in mature nerve terminals for ION5C and HK5C with the exception that there was a slight increase in HK5C evoked $[Ca^{2+}]_i$ levels.

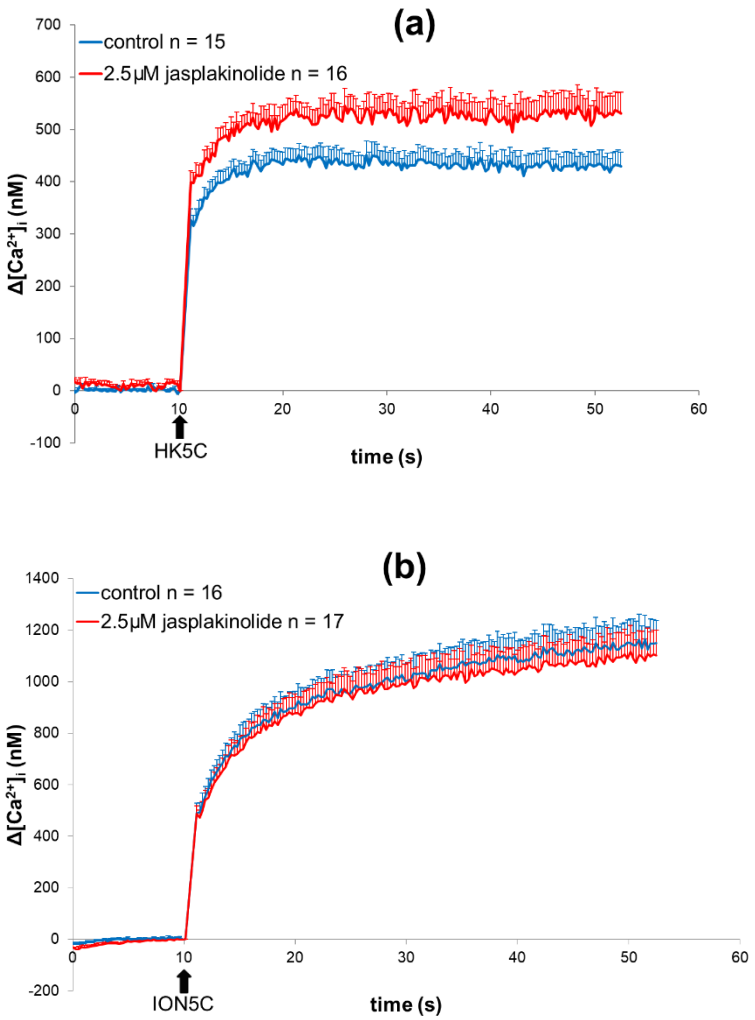

Figure 5.15: The effect of 2.5 μM jasplakinolide upon evoked $[Ca^{2+}]_i$ levels. Stabilisation of F-actin using 2.5 μM jasplakinolide had a significant effect upon evoked $[Ca^{2+}]_i$ levels with (a) HK5C stimulation ($p < 0.05$ for all points tested apart from 14 s and 50 s) but had no significant effect on (b) ION5C stimulation ($p > 0.05$), compared to non-drug controls. Values represented are the mean plus SEM from 3 independent experiments for (a) and (b).

5.3.7 Dual Treatment of Jasplakinolide and Latrunculin A Upon Changes in HK5C Evoked Intracellular Ca^{2+} Levels

Intriguingly, a dual treatment of 2.5 µM jasplakinolide, then 15 µM latrunculin A produced a slight increase in $[Ca^{2+}]_i$ levels following HK5C stimulation compared to controls (Figure 5.16; this experiment was only done twice so statistical analysis was not completed). The increase seen with the two drugs was comparable to the increase seen with jasplakinolide alone (Figure 5.15 a). However, the results in Figure 5.16 are definitely different from the reduction in HK5C evoked $[Ca^{2+}]_i$ levels that latrunculin alone caused (Figure 5.7a) again suggesting that jasplakinolide prevented latrunculin from disassembling actin and that it was indeed such disassembly that led to the reduction in evoked Ca^{2+} changes.

Clearly, this small increase in HK5C evoked $[Ca^{2+}]_i$ (just over 100 nm increase in the presence of jasplakinolide) was not sufficient to convert RRP SVs to a KR mode from their normal FF mode. This was borne by the fact that jasplakinolide increased the HK5C evoked $[Ca^{2+}]_i$ to a similar extent even following latrunculin treatment whilst the RP SVs that were released in this condition were still releasing via an FF mode.

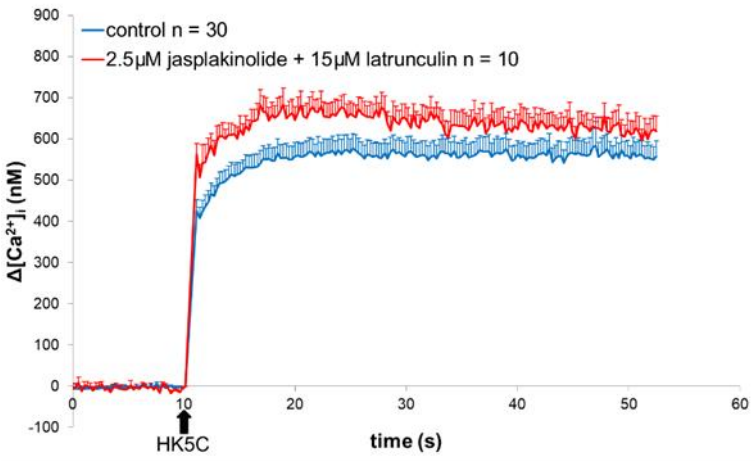

Figure 5.16: The effect of 2.5 μM jasplakinolide plus 15 μM latrunculin A upon evoked $[Ca^{2+}]_i$ levels. Stabilisation of F-actin using 2.5 μM jasplakinolide and subsequent 15 μM latrunculin A treatment had a slight increase effect upon evoked $[Ca^{2+}]_i$ levels with HK5C stimulation compared to non-drug controls. Values represented are the mean plus SEM from 2 independent experiments for drug treatment and 6 independent experiments for control.

The data that has so far been presented in this chapter shows that disassembly of actin microfilaments perturbed the release of the RP, but more interestingly it appeared to switch the RRP mode of release from KR to FF mode for both the HK5C and ION5C stimuli.

Previously, it has been shown that these two stimuli regulate the fusion pore for this KR mode by acting on two distinct proteins (see Appendix A and Bhuva, 2015; Singh, 2017). Stimulation using ION5C stimulated dynamin dependent fusion pore closure whilst HK5C stimulated NMII dependent fusion pore closure. Thus, both dynamin and NMII regulation of the fusion pore may require intact microfilaments such that if these cytoskeletal elements were disassembled the fusion pore was not closed and FF mode may occur.

As latrunculin A treatment did not perturb the ION5C evoked change in $[Ca^{2+}]_i$ then the fusion pore was exposed to the normal stimulated levels of Ca^{2+} that can typically regulate the dynamin dependent KR mode. Thus, it was likely that actin microfilaments may have directly regulated this dynamin dependent process.

However, at least for the HK5C stimulus a different explanation can be put forward. The KR mode could have been switched to FF mode because there was a reduction in the HK5C evoked change in $[Ca^{2+}]_i$ following disassembly of the actin cytoskeleton and this lower $[Ca^{2+}]_i$ may have not supported the KR mode. Therefore, actin microfilaments may have not directly regulated the NMII regulated fusion pore. Experiments outlined below were designed to refute this possibility.

5.4 Stimulation of ION5C Acts on the NMII regulated Kiss-and-Run Mode of RRP Following Activation of Certain PKCs

5.4.1 Treatment of 40 nM PMA Upon ION5C Evoked Glu Release in Latrunculin A and Okadaic Acid Combinations

Previously, it has been shown that the difference between ION5C and HK5C stimulation is that the latter activated specific PKC isoforms; these PKCs inactivated dynamin-1 – such that this could not regulate the KR mode of the RRP SVs – whilst activating NMII which could then activate fusion pore closure producing a KR mode. This conclusion has been further confirmed since ION5C has been made to work through the NMII pathway by using this stimulus in conjunction with activating certain PKCs using 40 nM PMA (Figure A18-19 in Appendix A; Bhuva, 2015; Singh, 2017).

By using 40 nM PMA in conjunction with ION5C, it was investigated whether actin microfilament disassembly could switch the NMII dependent KR mode of RRP SVs without disturbing evoked changes in $[Ca^{2+}]_i$, as HK5C treatment with latrunculin decreased evoked changes in $[Ca^{2+}]_i$ (Figure 5.7a).If results showed that change in $[Ca^{2+}]_i$ after stimulation was not affected, this would have then given further credence to the idea that the NMII regulated KR of the fusion pore might have also had an actin microfilament requirement.

As previously found (Bhuva, 2015; Singh, 2017), the pre-treatment of synaptosomes with 40 nM PMA did not change the amount of ION5C evoked Glu release (Figure 5.17a) such that both the RRP and RP SVs released their content. However, pre-treatment with 15 µM latrunculin A followed by 40 nM

PMA reduced the ION5C evoked release (Figure 5.17b) such that the RP was blocked (similar to the result shown in Figure 5.1c; latrunculin treatment alone) and this amount of ION5C evoked release remained similar with the triple treatment of 15 µM latrunculin A, 40 nM PMA and 0.8 µM OA (Figure 5.17c).

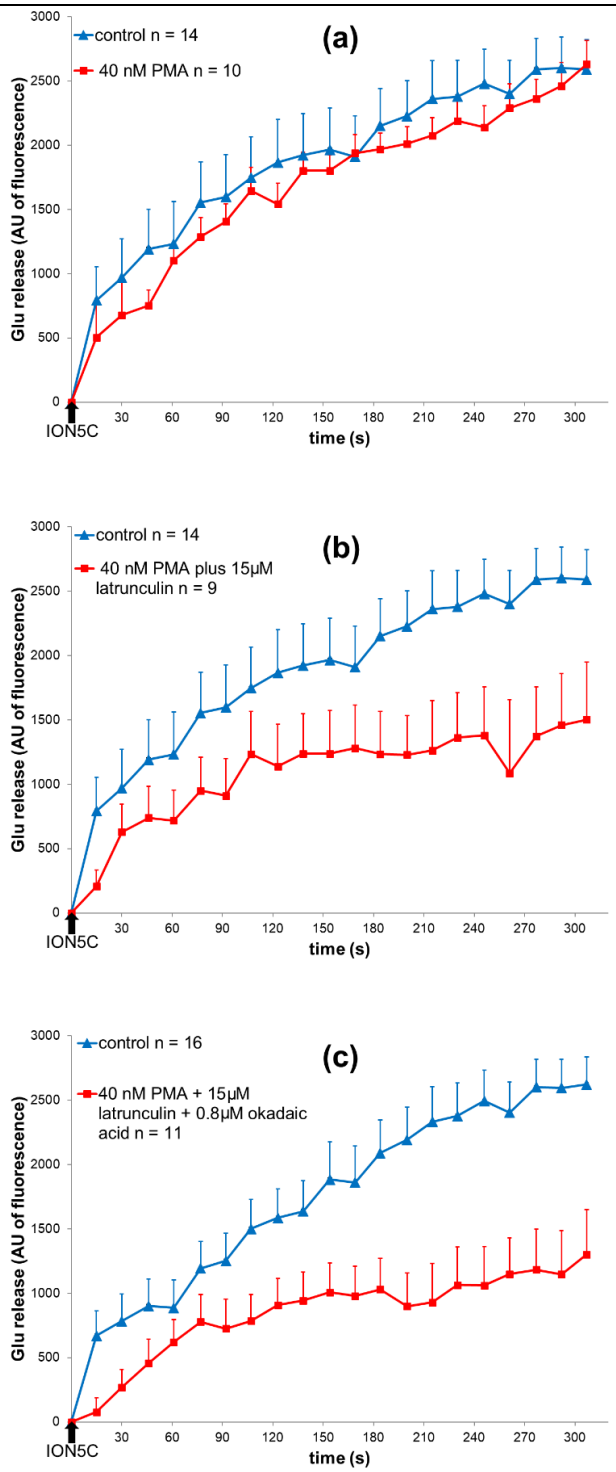

Figure 5.17: The effect of 40 nM PMA, 40 nM PMA plus 15 μM latrunculin A or 40 nM PMA plus 15 μM latrunculin A plus 0.8 μM OA vs control upon ION5C evoked Glu release. (a) 40 nM PMA had no significant effect upon evoked Glu release ($p > 0.05$), whilst (b) pre-treatment with latrunculin A or (c) latrunculin A plus OA in such PMA treated terminals led to a significant reduction ($p < 0.05$) in release at later time points (> 120 s) compared to non-drug controls. Values represented are the mean plus SEM for 6 (control) or 3 (drug treatments) independent experiments.

5.4.2 Treatment of 40 nM PMA Upon ION5C Evoked FM 2-10 Dye Release in Latrunculin A and Okadaic Acid Combinations

As previously noted, (Bhuva, 2015; Singh, 2017), 40 nM PMA treatment did not change the amount of FM dye released by ION5C (Figure 5.18a). Furthermore, the preincubation with latrunculin A followed by PMA revealed the same amount of FM 2-10 dye release as the non-drug treated control when ION5C was added (Figure 5.18b). However, 40 nM PMA did not prevent the latrunculin from switching the RRP SVs to an FF mode, as seen in terminals treated with latrunculin alone (Figure 5.2b). The inclusion of OA with the two other drugs did not induce any further ION5C evoked FM dye release (Figure 5.18c). Treatment of PMA (Figure 5.18a), PMA plus latrunculin (Figure 5.18b) or PMA plus latrunculin plus OA (Figure 5.18c) did not perturb the total FM 2-10 content of the treated synaptosomes compared to non-drug treated controls.

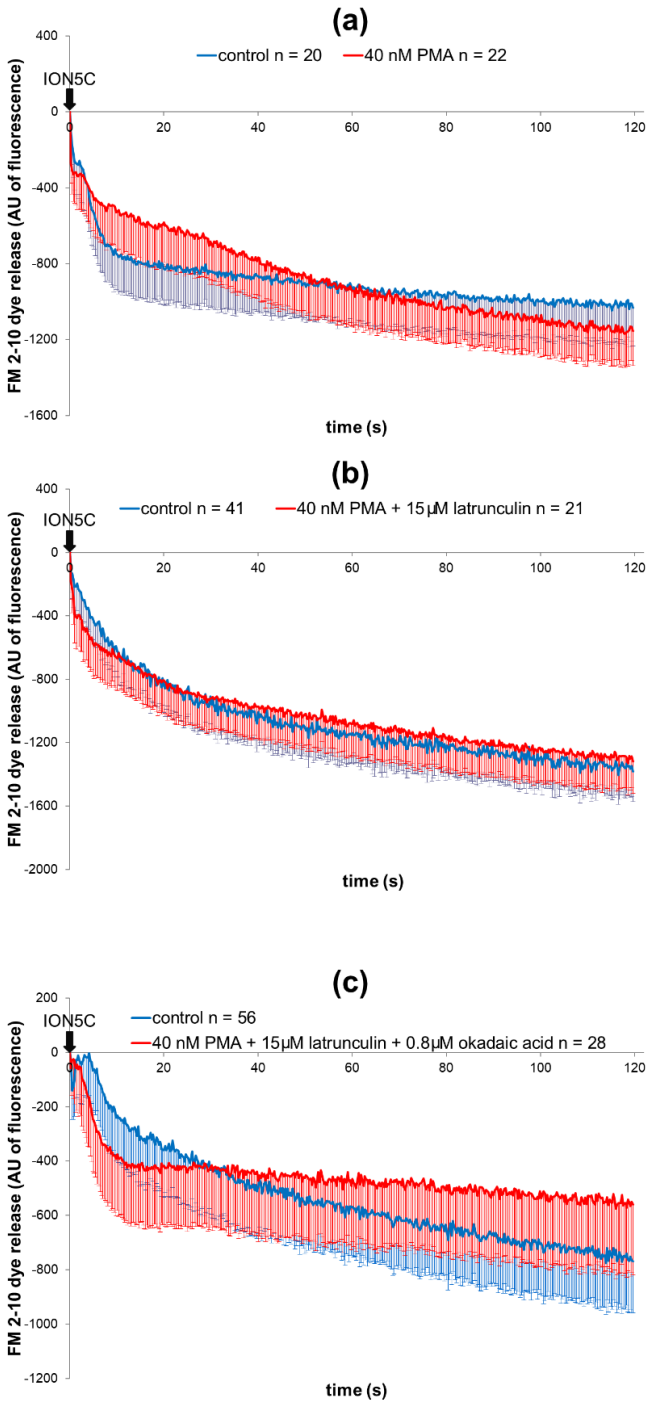

Figure 5.18: The effect of 40 nM PMA, 40 nM PMA plus 15 µM latrunculin A or 40 nM PMA plus 15 µM latrunculin A plus 0.8 µM OA vs control upon ION5C evoked FM2-10 dye release. (a) 40 nM PMA, (b) 40 nM PMA plus depolymerisation of F-actin using 15 µM latrunculin A or (c) 40 nM PMA plus 15 µM latrunculin A and subsequent treatment using 0.8 µM OA had no significant effect upon FM dye release ($p > 0.05$) compared to non-drug treated controls. Values represented are the mean plus SEM for (a) 3 independent experiments for control and PMA treatment, (b) 6 experiments for control and 3 experiments for PMA plus latrunculin A and (c) 7 experiments for control and 4 experiments for PMA plus latrunculin A plus OA.

5.4.3 Treatment of 40 nM PMA Upon ION5C Evoked Changes in Intracellular Ca^{2+} Levels in Latrunculin A and Okadaic Acid Combinations

It has been previously shown that 40 nM PMA did not disturb the ION5C induced $[Ca^{2+}]_i$ change (Singh, 2017). The results in Figure 5.18 could not be explained by any difference in ION5C evoked change in $[Ca^{2+}]_i$ because neither PMA plus latrunculin A (Figure 5.19a) nor PMA plus latrunculin plus OA (Figure 5.19b) perturbed the evoked change in $[Ca^{2+}]_i$, relatively to the non-drug treated control. This is an important finding because ION5C was acting on the NMII dependent KR pathway for the RRP SVs in 40 nM PMA treated synaptosomes and so it was indicated that the perturbation of actin microfilaments could directly switch this particular KR pathway to FF mode without causing differences in the evoked change in $[Ca^{2+}]_i$.

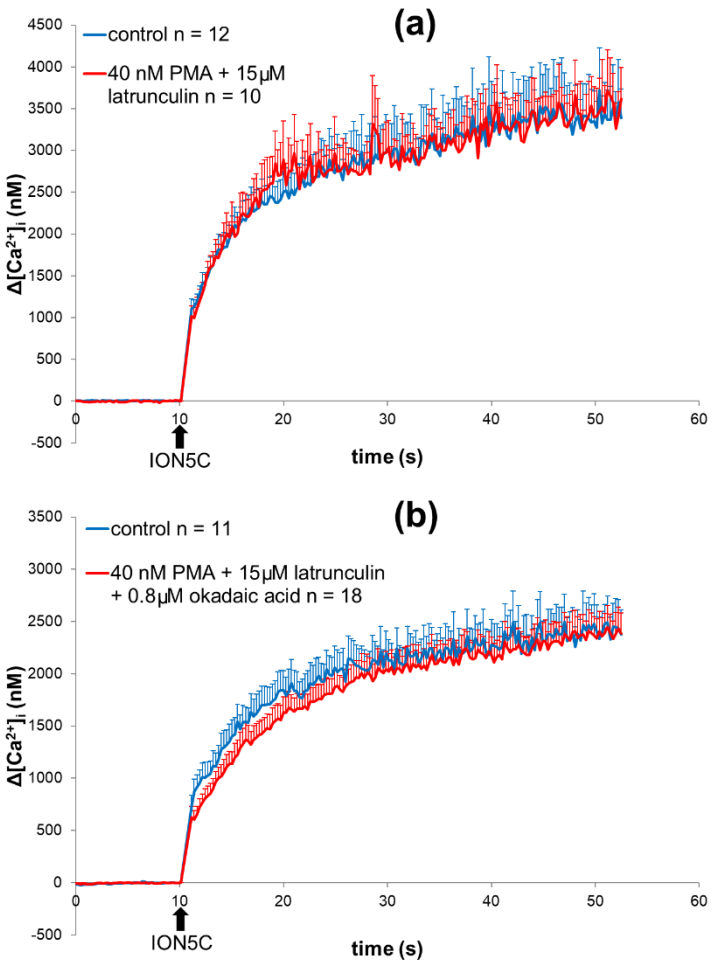

Figure 5.19: The effect of PMA plus latrunculin A or PMA plus latrunculin A plus OA upon ION5C evoked $[Ca^{2+}]_i$ levels compared to control. (a) Depolymerisation of F-actin using 15 µM latrunculin A plus PMA does not perturb evoked changes in $[Ca^{2+}]_i$ levels and (b) there is no significant difference in evoked changes in $[Ca^{2+}]_i$ levels in synaptosomes treated with 40 nM PMA plus 15 µM latrunculin plus 0.8 µM OA compared to non-drug controls ($p > 0.3$). Values represented are the (a) mean plus range (2 independent experiments) and (b) the mean and SEM (3 independent experiments).

5.4.4 Treatment of 40 nM PMA Upon ION5C Evoked Glutamate Release in Jasplakinolide, Latrunculin A and Okadaic Acid Combinations

It is a requisite that one ascertains that, following activation of certain PKCs (with 40 nM PMA), jasplakinolide could still specifically prevent the action of latrunculin A on the release of the RP of Glu containing SVs. Jasplakinolide pre-treatment followed by PMA did not prevent ION5C from releasing the RRP and RP SVs since the amount of Glu exocytosis was similar to non-drug treated control (Figure 5.20a). Furthermore, ION5C evoked the RRP and RP SVs to release in synaptosomes treated with jasplakinolide plus latrunculin A plus PMA (Figure 5.20b) and in synaptosomes treated with jasplakinolide plus latrunculin A plus OA plus PMA (Figure 5.20c). Clearly, both jasplakinolide and latrunculin A were still acting specifically on the actin microfilaments even in 40 nM PMA treated synaptosomes.

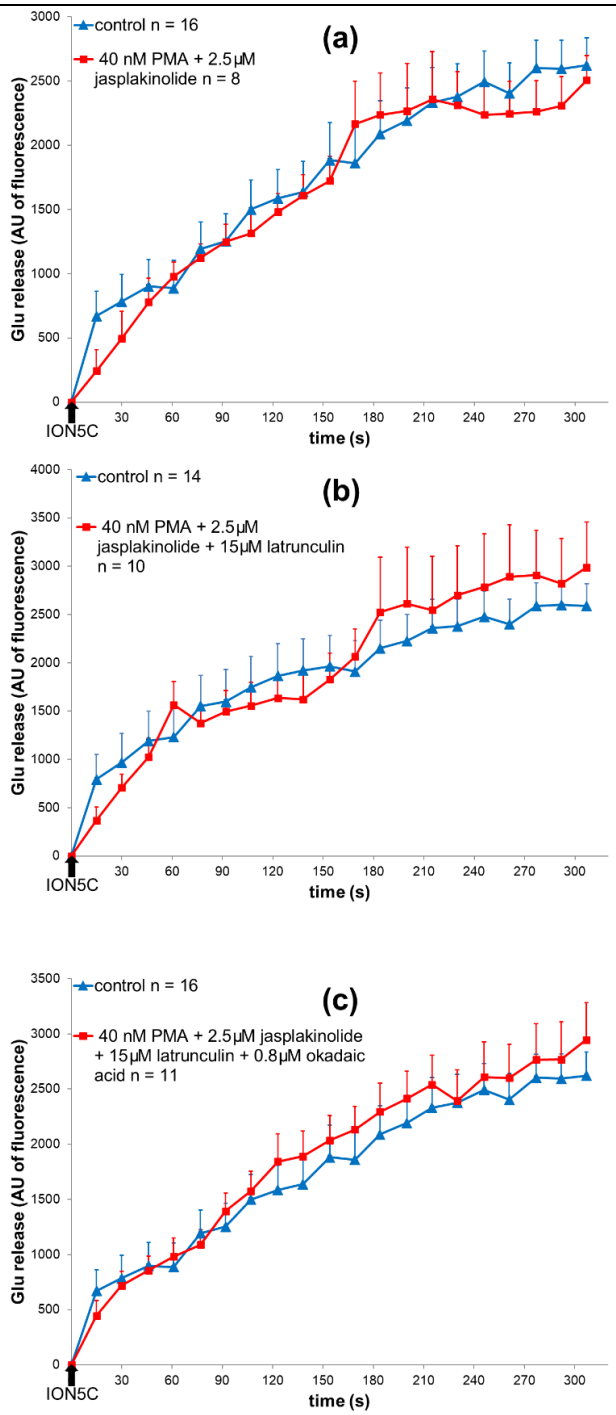

Figure 5.20: The effect of PMA plus jasplakinolide, PMA plus jasplakinolide plus latrunculin A or PMA plus jasplakinolide plus latrunculin A plus OA upon ION5C evoked Glu release compared to non-drug treated control. (a) 40 nM PMA plus 2.5 µM jasplakinolide, (b) 40 nM PMA plus 2.5 µM jasplakinolide plus 15 µM latrunculin A or (c) PMA plus jasplakinolide plus latrunculin A plus 0.8 µM OA had no significant effect upon evoked Glu release ($p > 0.4$) compared to non-drug controls. Values represent mean plus SEM for 6 independent experiments for non-drug treated controls and 3 independent experiments for drug treatments.

5.4.5 Treatment of 40 nM PMA Upon ION5C Evoked FM 2-10 Dye Release in Jasplakinolide, Latrunculin A and Okadaic Acid Combinations

Stimulation using ION5C appeared to evoke the same amount of FM dye release in PMA plus jasplakinolide (Figure 5.21a), or PMA plus jasplakinolide plus latrunculin A treated terminals (Figure 5.21b) as in non-drug treated control. That the amount of dye released represented release from only the RP was shown when release was increased following the addition of OA to PMA plus jasplakinolide plus latrunculin A treated synaptosomes (Figure 5.21c) as in this case the OA treatment was able to switch the RRP SVs from a KR to an FF mode and so dye from such vesicles was also released. None of these treatments perturbed the total FM 2-10 dye content relative to non-drug treated control (Figure 5.25a,b). These results confirm that actin microfilaments played a direct role in the regulation of NMII dependent KR mode of the RRP SVs.

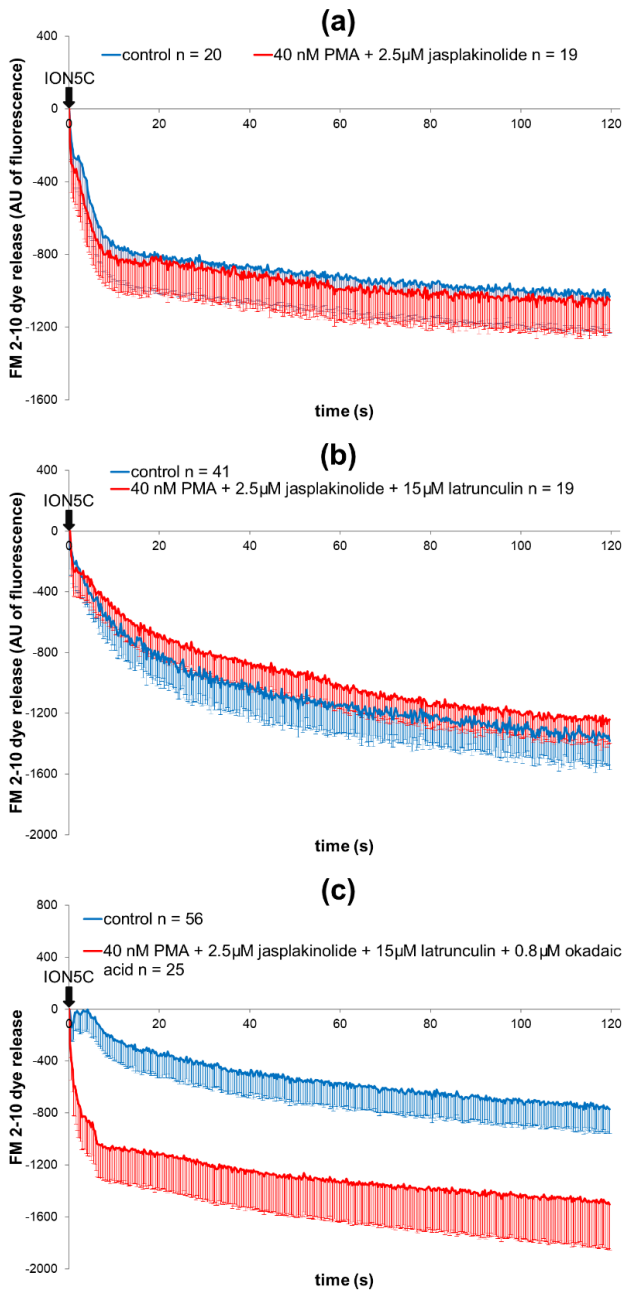

Figure 5.21: The effect of PMA plus jasplakinolide, PMA plus jasplakinolide plus latrunculin A or PMA plus jasplakinolide plus latrunculin A plus OA upon ION5C evoked FM 2-10 dye release compared to non-drug treated control. (a) 40 nM PMA plus 2.5 µM jasplakinolide, or (b) 40 nM PMA plus 2.5 µM jasplakinolide plus 15 µM latrunculin A had no significant effect upon evoked FM dye release ($p > 0.5$) compared to non-drug treated controls. (c) However, synaptosomes treated with PMA plus jasplakinolide plus latrunculin A plus 0.8 µM OA had significantly more FM dye release ($p < 0.05$) compared to non-drug treated controls. Values represent mean plus SEM for (a) 3 independent experiments, 6 independent experiments for control and (b) 3 independent experiments for drug treatment (c) and 7 independent experiments for control and 4 independent experiments for drug treatment.

5.4.6 Treatment of 40 nM PMA Upon ION5C Evoked Changes in Intracellular Ca^{2+} Levels in Jasplakinolide, Latrunculin A and Okadaic Acid Combinations

Compared to the non-drug treated controls, PMA plus jasplakinolide (Figure 5.22a), PMA plus jasplakinolide plus latrunculin A (Figure 5.22b) or PMA plus jasplakinolide plus latrunculin A plus OA (Figure 5.22c) did not perturb the ION5C evoked change in $[Ca^{2+}]_i$ synaptosomes. These results confirmed that any effects of perturbing the actin microfilaments on the KR mode of RRP SVs regulated by NMII did not involve changes in $[Ca^{2+}]_i$.

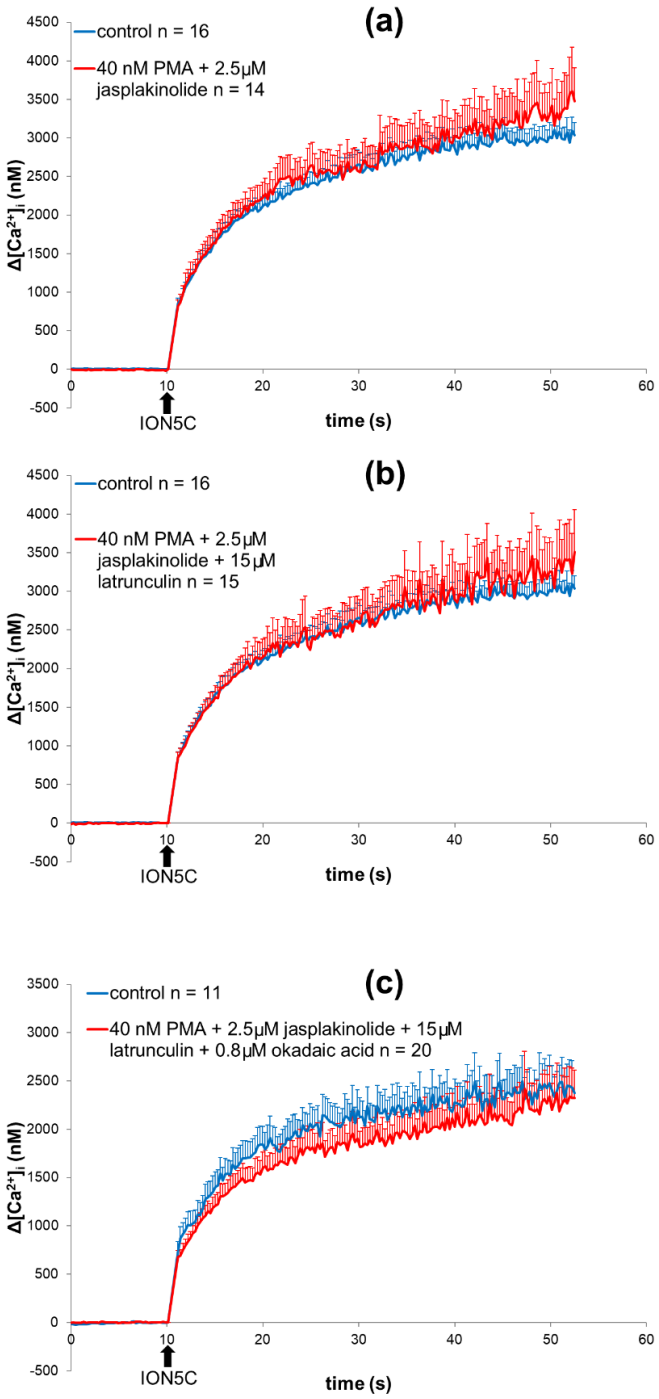

Figure 5.22: The effect of PMA plus jasplakinolide, PMA plus jasplakinolide plus latrunculin A or PMA plus jasplakinolide plus latrunculin A plus OA upon ION5C evoked $[Ca^{2+}]_i$ levels compared to non-drug treated control. (a) 40 nM PMA plus 2.5 µM jasplakinolide, (b) 40 nM PMA plus 2.5 µM jasplakinolide plus 15 µM latrunculin A or (c) PMA plus jasplakinolide plus latrunculin A plus 0.8 µM OA had no significant effect upon evoked changes in $[Ca^{2+}]_i$ levels ($p > 0.25$) compared to non-drug controls. Values represent mean plus SEM for 3 independent experiments for non-drug treated controls and 3 independent experiments for drug treatments.

5.4.7 Treatment of 40 nM PMA Upon ION5C Evoked Glu Release in Jasplakinolide, Latrunculin A and Blebbistatin Combinations

Whether the RRP SV mode was regulated by dynamin-1 (mode switched when dynamin is inhibited by dynasore) or by NMII (mode switched by blebbistatin), neither of these drugs perturbed the exocytosis of Glu from the RRP or RP following stimulation (Figure A12-13 in Appendix A; Bhuva, 2015; Singh, 2017). Stimulation using ION5C acted on the NMII regulated KR mode in terminals treated with 40 nM PMA. Such a KR mode should have been switched to FF if one inhibited NMII ATPase activity but not switched by dynasore, and this was tested using blebbistatin.

Latrunculin A was still able to block the ION5C evoked release of the RP of Glu containing SVs in synaptosomes treated with 40 nM PMA and 50 µM blebbistatin (Figure 5.23a), whereas jasplakinolide blocked latrunculin A action such that both the RRP and the RP Glu containing SVs were released by ION5C in terminals treated with PMA plus jasplakinolide plus latrunculin A plus blebbistatin (Figure 5.23b).

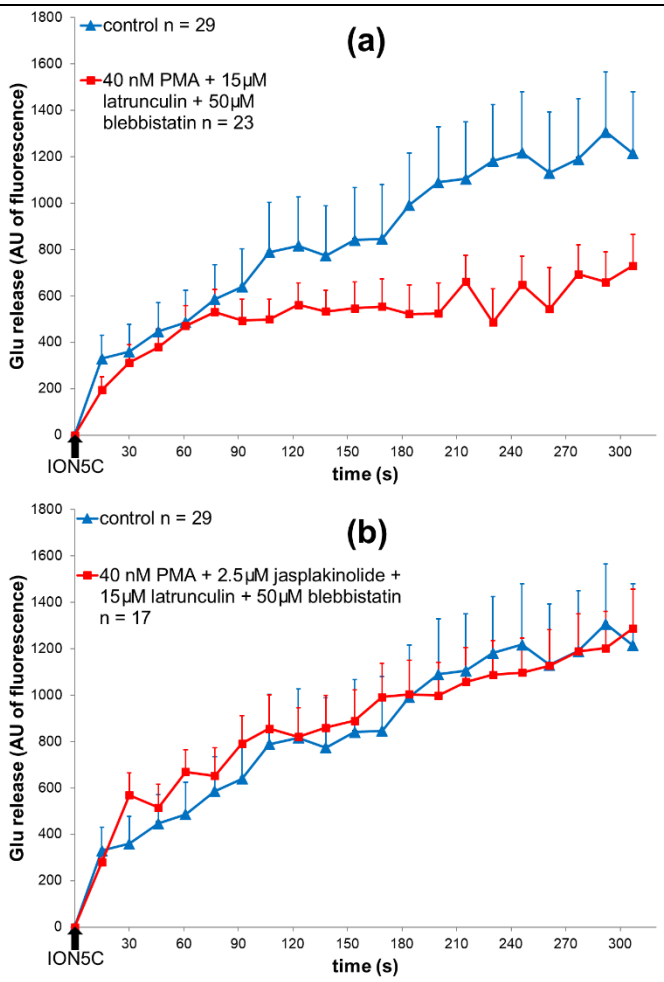

Figure 5.23: The effect of PMA plus latrunculin A plus blebbistatin or PMA plus jasplakinolide plus latrunculin A plus blebbistatin upon ION5C evoked Glu release compared to non-drug treated control. (a) 40 nM PMA plus 15 µM latrunculin A plus 50 µM blebbistatin induced a significant reduction in ION5C evoked Glu release at later time points compared to non-drug treated control whilst (b) PMA plus jasplakinolide plus latrunculin A plus blebbistatin had no significant effect upon evoked Glu release ($p > 0.7$) compared to non-drug controls. Values represent mean plus SEM for 4 independent experiments.

5.4.8 Treatment of 40 nM PMA Upon ION5C Evoked FM 2-10 Dye Release in Jasplakinolide, Latrunculin A and Blebbistatin Combinations

Blebbistatin failed to increase the FM 2-10 dye release from terminals treated with latrunculin A and PMA compared to non-drug treated control (Figure 5.24a). This suggested that, as in earlier experiments, the RRP SVs were already undergoing FF mode (whilst RP was not released) and that blebbistatin could not cause any further changes in dye release. However, following the stabilisation of the actin microfilaments with jasplakinolide so that latrunculin A no longer had effect on the RRP SVs, blebbistatin was able to switch the RRP SVs to an FF mode in 40 nM PMA treated synaptosomes such that there was an increase in FM dye release relative to the non-drug treated control (Figure 5.24b). These drug treatments did not perturb the total FM 2-10 dye content compared to the non-drug treated controls (Figure 5.25b). Such results clearly showed that ION5C was working through the NMII regulated KR pathway of RRP SVs since blebbistatin worked and also emphasised that this pathway may also have been directly regulated by actin microfilaments controlling the properties of the fusion pore.

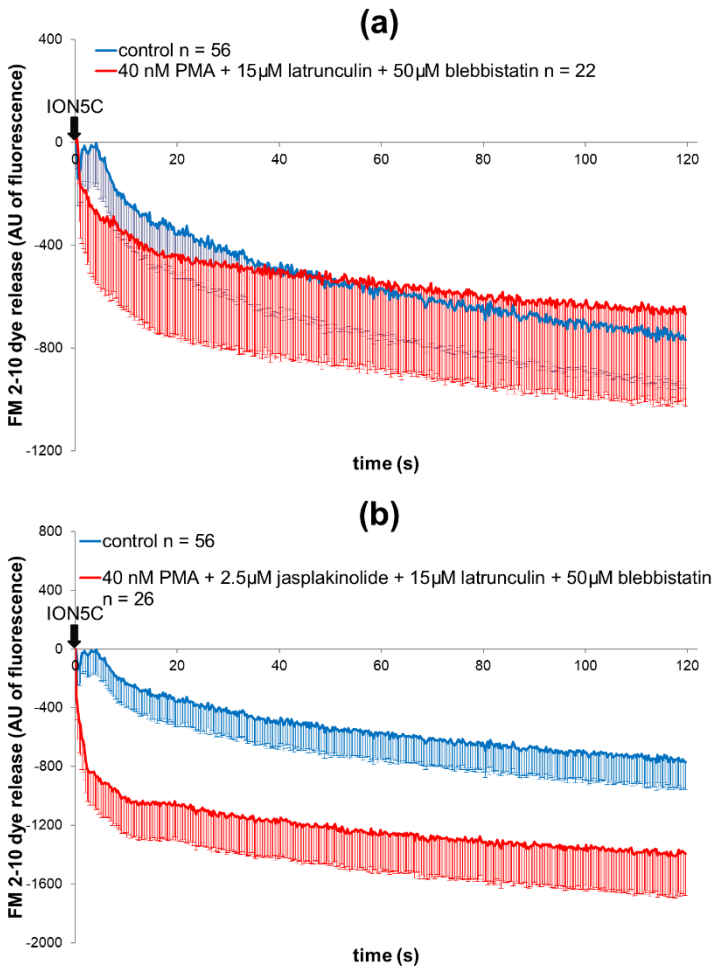

Figure 5.24: The effect of PMA plus latrunculin A plus blebbistatin or PMA plus jasplakinolide plus latrunculin A plus blebbistatin upon ION5C evoked FM 2-10 dye release compared to non-drug treated control. (a) 40 nM PMA plus 15 µM latrunculin A plus 50 µM blebbistatin had no effect on ION5C evoked FM dye release compared to non-drug treated control ($p > 0.7$) whilst (b) PMA plus jasplakinolide plus latrunculin A plus blebbistatin had a significant effect upon evoked FM2-10 dye release compared to non-drug controls ($p < 0.05$). Values represent mean plus SEM for 8 and 4 independent experiments for drug free controls and drug treatments, respectively.

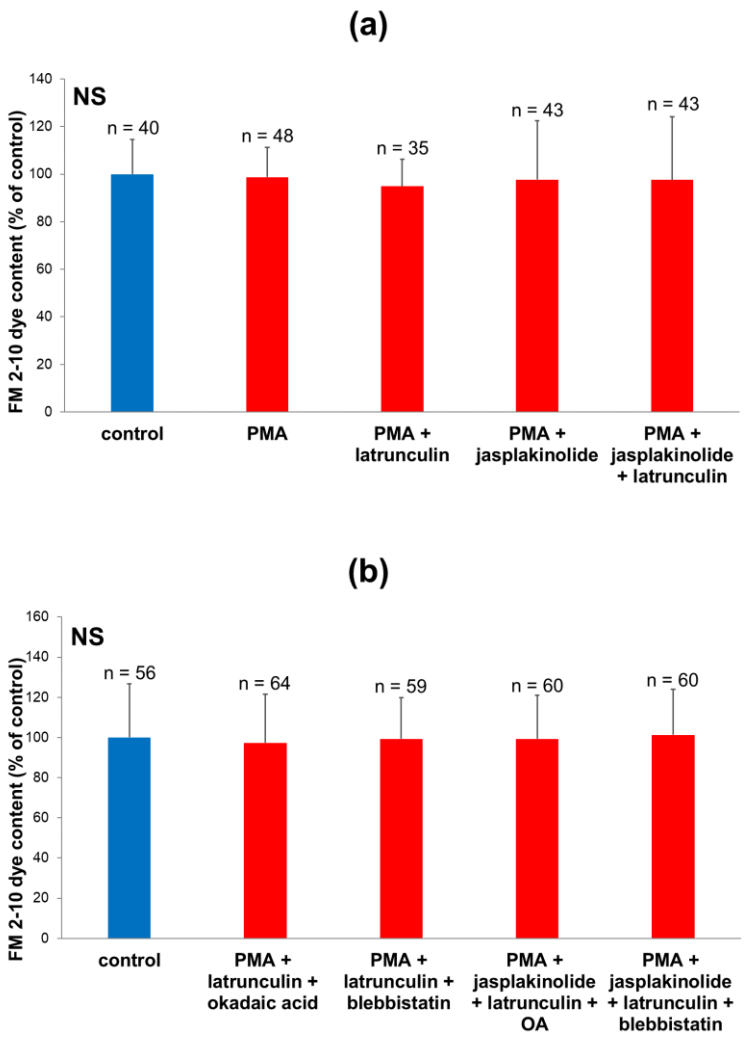

Figure 5.25: The effect of various drug treatments on total FM dye content relative to control non-drug treated samples. In (a) the data was from 3 independent experiments, and in (b) the data was from 4 independent experiments. There was no significant difference between any condition ($p > 0.05$) and the non-drug treated control.

5.5 Discussion

In this chapter actin was depolymerised using latrunculin A or stabilised using jasplakinolide, to determine how these treatments would affect evoked release of Glu, mode of exocytosis for distinct SV pools and the evoked changes in $[Ca^{2+}]_i$. This was done to elucidate what role actin has in SV mobilisation and release, especially in relation to NMII function.

As ION5C showed no changes in evoked $[Ca^{2+}]_i$ compared to control with these drug treatments, ION5C was also switched from dynamin dependent KR mode to NMII dependent KR mode, to check if there was possibly any difference in $[Ca^{2+}]_i$ between these modes during ION5C stimulation with latrunculin A and jasplakinolide. These results would show whether NMII dependent KR of the fusion pore also has an actin microfilament requirement, similarly to dynamin dependent KR.

It would be useful to compare the data from HK5C and ION5C to 4AP5C. Due to time limitations we focussed on the release of both pools; it would be appropriate to compare this to release of the RRP only.

5.5.1 The Effect of F-Actin Depolymerisation on Evoked Glutamate Release

Treating synaptosomes with latrunculin A, which depolymerises actin, blocked release of the RP specifically, as evidenced by a reduction in Glu release with HK5C (Figure 5.1b) and ION5C stimulation (Figure 5.1c). This indicated that mobilisation of the RP to the AZ for priming and release was perturbed although the precise role of the microfilaments in this process could not be discerned from the studies reported herein. However, in synaptosomes with disassembled actin, there was a distinction between the two stimuli's action in regard to evoked changes in $[Ca^{2+}]_i$ levels. The latrunculin A treatment significantly decreased HK5C evoked $[Ca^{2+}]_i$ levels (Figure 5.7a) but had no effect on ION5C evoked $[Ca^{2+}]_i$ levels (Figure 5.7b) when compared to non-drug treated controls.

This difference was probably due to the different mechanisms that these two stimuli employ to increase $[Ca^{2+}]_i$ levels. HK5C acted to depolarise the PM and activate the voltage-gated Ca^{2+} channels at the AZ, and this allowed localised entry of the Ca^{2+} and eventual diffusion of such ions and an increase in the bulk $[Ca^{2+}]_i$ levels. Perturbation of the actin microfilaments may have reduced the Ca^{2+} entry through these Ca^{2+} channels, possibly due to such channels no longer being fixed by the actin cytoskeleton to the precise AZ domain. Whilst the localised Ca^{2+} entry may be still sufficient to drive fusion of the RRP SVs, there may be insufficient build-up of the bulk $[Ca^{2+}]_i$ to induce the release of the RP. The ION5C stimulation worked by inserting into the entire PM– not just acting at the AZs – and allowing transport of Ca^{2+} into the cytosol. Thus, such a stimulus did not have a requirement for voltage-gated Ca^{2+} channels for Ca^{2+} influx, and this could explain why actin microfilaments, which as suggested above may perturb such channels when they are disassembled, did not perturb the ION5C evoked Ca^{2+} entry. Nevertheless, the RP of SVs were prevented from being released by ION5C when actin microfilaments were disassembled.

This indicated that the RP SVs themselves had a requirement for such an intact cytoskeleton in order for them to be released and this could have been due to such microfilaments allowing the RP SVs to reach the appropriate position on the AZs to exocytose following the RRP SVs release. Thus, it could be that the actin microfilaments played several roles in regulating release involving the location of both the RP of SVs and that of the voltage-gated Ca^{2+} channels at the AZ.

5.5.2 The Effect of F-actin Depolymerisation on FM 2-10 Dye Release Reflecting Effects on the Mode of Exocytosis

Latrunculin A treatment switched the RRP mode of release from KR mode to FF mode for both HK5C stimulation (Figure 5.2a) and ION5C stimulation (Figure 5.2b), as although there was less Glu release compared to control in these conditions, the proportion of the RRP usually in KR mode must have been switched to FF mode in order for FM dye release to be similar in amount to control conditions. This was verified using OA treatment. It had been previously found and verified, herein, that inhibition of PP1 and PP2A using OA increased stimulated FM 2-10 dye release with HK5C (Figure 5.4a) or ION5C (Figure 5.4c) compared to controls; this indicated that OA could switch the RRP SV exocytosis to FF mode whether this is regulated by NMII or dynamin. Latrunculin A treatment following OA treatment had results similar to latrunculin A treatment alone on FM 2-10 dye release (Figure 5.4b and 5.4d) and Glu release (compare Figure 5.1b, 5.6a and 5.1c, 5.7b). This indicated that the disassembly of actin had caused the RRP SVs to undergo FF so that OA treatment could not produce any further increase in the FM dye release.

Actin disassembly prevented the release of the RP of SVs evoked by the two stimuli which was independent of any effects this had on evoked $[Ca^{2+}]_i$ levels. However, this change in $[Ca^{2+}]_i$ levels might not apply to the change in mode of exocytosis of the RRP of SVs. This was because as shown previously that it is the high Ca^{2+} concentration achieved at the AZ which may have driven the KR of the RRP (Bhuva, 2015). Therefore, in latrunculin A treated terminals whilst ION5C still induced the same change in $[Ca^{2+}]_i$ levels and so can still induce the dynamin dependent KR mode of the RRP, the lowered HK5C induced change in $[Ca^{2+}]_i$ levels may have caused the NMII dependent KR mode of the RRP SVs to switch to FF mode following disassembly of the actin microfilaments.

5.5.3 The Effect of F-Actin Stabilisation on Evoked Glutamate Release, FM 2-10 Dye Release and Change in Intracellular Ca^{2+}

Stabilisation of F-actin using jasplakinolide caused no change in Glu release evoked by HK5C stimulation (Figure 5.8a) or by ION5C stimulation (Figure 5.8b), compared to controls. Jasplakinolide treatment did not perturb either the RRP or RP SV mode of release induced by HK5C (Figure 5.10a) or ION5C (Figure 5.10b), compared to controls. There was also no reduction of evoked $[Ca^{2+}]_i$ levels during HK5C stimulation (Figure 5.15a; actually, an increase) nor during ION5C stimulation (Figure 5.15b) in terminals with stabilised microfilaments, compared to controls. These results show that stabilised actin microfilaments did not affect SV release mechanisms of the RRP or RP in mature terminals. The SV mobilisation was still able to function to allow RP release, contrarily to latrunculin A treated terminals in which RP release was blocked by the actin depolymerisation. Perhaps the actin matrix supports carrier proteins or mechanical processes that are not affected by F-actin stabilisation but the proteins cannot function during F-actin loss. This suggests that there is not a normal cycle of disassembly and reassembly of actin microfilaments required for the exocytosis of the RRP and RP SVs or for the regulation of the mode of exocytosis because jasplakinolide would prevent such processes.

5.5.4 Specificity of Latrunculin A and Jasplakinolide on Actin Microfilaments

There was no significant difference to controls when synaptosomes were treated with jasplakinolide and latrunculin A when HK5C and ION5C stimulation was utilised to evoke Glu release (Figure 5.9 a,b), FM 2-10 dye release (Figure 5.11 a,b) and evoked $[Ca^{2+}]_i$ levels (Figure 5.16 a,b; jasplakinolide might have caused a slight increase in HK5C evoked $[Ca^{2+}]_i$ levels and latrunculin did not stop this). These results showed that jasplakinolide was able to block latrunculin A action.

It is highly unlikely that both drugs would exhibit a specific action on actin microfilaments but also exhibit similar non-specific actions such that jasplakinolide could prevent the non-specific action of latrunculin. This clearly

indicates that both drugs exhibited effects in nerve terminals that were due to their actions specifically on the actin microfilaments. Thus, we can be sure that this interpretation - that disassembly of actin microfilaments perturbs the release of the RP of Glu containing SVs and the mode of exocytosis of the RRP SV - is correct.

Further evidence that jasplakinolide, by stabilising actin microfilaments, prevents the action of latrunculin is demonstrated in the experiments which involved a triple treatment of jasplakinolide, latrunculin A, and OA. Such conditions did not perturb the HK5C (Figure 5.14a) or ION5C (Figure 5.14b) evoked release of Glu from the RRP and RP SVs but did result in a significant increase in FM 2-10 dye release, showing that RRP and RP SVs are switched to FF mode of release, similarly to OA treatment alone, with both HK5C stimulation (Figure 5.12a) and ION5C stimulation (Figure 5.12b). These results suggested that jasplakinolide blocks latrunculin A action on F-actin, allowing OA effects to have functioned unhindered, as this phenotype is similar to the result of OA treatment alone (Figure 5.4 a, c). Clearly jasplakinolide, by stabilising actin microfilaments did not prevent the action of OA. This suggested that the phosphorylated state of various proteins (including dynamin and NMII) that is produced when OA sensitive phosphatases were blocked was maintained following actin microfilament stabilisation and the application of HK5C or ION5C.

5.5.5 Actin Microfilament Requirement for Dynamin Dependent and NMII Dependent Kiss-and-Run of the RRP Synaptic Vesicles

ION5C evoked dynamin dependent KR of the RRP SVs was switched to FF mode following disassembly of the actin microfilaments. Thus, it is possible the closure of the fusion pore (within < 0.5 s) required the aid of intact microfilaments. This could represent an active process whereby the actin microfilaments may have surrounded the fusion pore and these actin microfilaments may have aided the interaction of dynamin with the neck of the fusion pore such that it contracted and eventually closed. Further, an actin dependent pulling mechanism may have aided in this process.

ION5C evoked NMII dependent KR of the RRP SVs (when 40 nM PMA is used to inactivate dynamin and activate NMII) was also switched to FF mode following disassembly of the actin cytoskeleton. Again, this fusion pore would appear to have required intact microfilaments for the pore to close in < 0.5 s. This could have represented an active process whereby the actin microfilaments may have surrounded the fusion pore and these actin microfilaments may have interacted with the NMII motor proteins such that these pulled on the actin (like a lasso) surrounding the neck of the fusion pore such that it contracted and eventually closed.

The finding that there was no change in $[Ca^{2+}]_i$ levels compared to control in ION5C evoked NMII dependent KR of the RRP with latrunculin or jasplakinolide, unlike HK5C evoked NMII dependent KR of the RRP, is important as this gave evidence that NMII dependent KR of the RRP may have been dependent upon direct actin microfilament action rather than by effects dependent upon changes in evoked $[Ca^{2+}]_i$ levels.

Addition of OA to 40 nM PMA treated ION5C evoked synaptosomes gave the expected result of causing FF of the RRP following jasplakinolide or jasplakinolide plus latrunculin treatment but failed to give any further FM dye release following latrunculin pre-treatment, showing that release dynamics were similar to non-PMA treated synaptosomes. However, in this case ION5C rather than acting on the dynamin dependent KR was acting on the NMII dependent KR. This was demonstrated by the fact that blebbistatin inhibited ION5C evoked NMII dependent release of the RRP with any of the drug combinations used - PMA plus jasplakinolide or PMA plus jasplakinolide plus latrunculin.

Thus, this chapter has established for the first time that the two modes of KR determined for the RRP SVs both depended on intact actin microfilaments to occur.

5.6 Conclusion

Experiments on effects of latrunculin A induced depolymerisation of actin scaffolds on synaptosomes have revealed functions of the actin scaffold on release dynamics of SVs in the synaptosome model. Dynamic actin scaffolds are required to translocate RP SVs to the AZs to exocytose. Actin filaments are also needed for KR mode of exocytosis of the RRP of SVs.

Experiments on latrunculin A and HK5C stimulated $[Ca^{2+}]_i$ levels show that Ca^{2+} influx during stimulation requires intact actin microfilaments for normal SV release. This suggests that PM voltage-gated Ca^{2+} channels may be specifically localised by F-actin at the AZs to raise $[Ca^{2+}]_i$ levels sufficiently for RP mobilisation, priming and release during physiological stimuli. However, as Glu release is reduced similarly in HK5C and ION5C stimulated synaptosomes during latrunculin A treatment, this may also be explained by RP SVs being unable to be translocated to correct position at the AZs due to lack of intact microfilaments.

The studies in this chapter raise questions of further study of the role of both dynamin and NMII at the AZs and their phosphorylation state when actin is acutely perturbed with latrunculin A treatment. Also, the effect of actin scaffolds and dynamics on voltage-gated Ca^{2+} channels and RP SV function may be investigated using voltage-gated Ca^{2+} channel targeted drugs in conjunction with latrunculin A and jasplakinolide.

CHAPTER 6:

General Discussion

Since Ceccarelli *et al.* (1973) reported that SVs can be recycled by the closure of the exocytotic fusion pore without CME - later termed KR (Fesce *et al.*, 1994) - the mechanisms of SV recycling have been an ongoing debate. However, over nearly fifty years since then rather than resolving the issue of FF or KR SV exocytosis, other models for SV recycling have emerged: ADBE and UE. This has raised more questions about which modes are physiologically feasible and under what conditions, and how they may mechanically function in a presynapse (Gan and Watanabe, 2018). Adding to the complexity is that SVs might be functionally heterogenous according to Crawford and Kavalali (2015), defined by different molecular compositions that are likely to be able to change based upon activity-dependent rearrangements.

The essential role of CME in the SV cycle has been questioned, as more recent studies suggest that endocytosis can proceed after knockdown of clathrin heavy chain or its adaptor AP-2 (Kim and Ryan, 2009; Kononenko *et al.*, 2014; Watanabe *et al.*, 2014), pharmacological inhibition (Delvendahl *et al.*, 2016), acute photo-inactivation (Heerssen *et al.*, 2008; Kasprowicz *et al.*¸2008) or using temperature-sensitive clathrin heavy chain mutants (Yu *et al.*, 2018), although in some cases compensatory endocytosis was aberrant and insufficient for regenerating SVs for sustained neurotransmission (Heerssen *et al.*, 2008; Kasprowicz *et al.*, 2008). This lack of an obligatory requirement for CME was found to be most prevalent at physiological temperatures in mammalian neurons. However, in all documented cases of a clathrin requirement during the SV cycle this was either at the PM or at the endosome (Watanabe *et al.*, 2014; Delvendahl *et al.*, 2016; Soykan *et al.*, 2017).

Although KR mode has been established in chromaffin cells, and neurosecretory cells (Elhamdani *et al.*, 2006; Chan *et al.*, 2010 b), its physiological presence and feasibility in neurons is much more debatable due to the difficulty of visualising the phenomenon. Work by Ashton and colleagues have determined that rat cerebrocortical synaptosomes can release glutamatergic SVs via KR mode during particular stimulation conditions, and that the mode of release can be determined using a combination of maximal Glu release and FM 2-10 dye release assays. Furthermore, a major role for intracellular Ca^{2+} has been found to participate in the regulation of exocytotic

mode; increases in $[Ca^{2+}]_i$ can switch SVs which undergo FF to KR mode (Bhuva, 2015; Singh, 2017).

This thesis describes studies to establish the mechanisms that control mode of SV exocytosis, and highlights two phosphoproteins that may be involved. The research described herein, has produced results on two separate topics regarding the RRP and the RP of Glu containing SVs: (i) their release properties; (ii) mechanisms involved in regulating their mode of exocytosis. These are discussed separately.

6.1 Release Properties of the RRP and RP of Synaptic Vesicles

In Chapter 3 it was discovered that neither PKA inhibition nor activation affected the release of the RP SVs stimulated by HK5C or ION5C. However, the experiments with MiTMAB revealed two important points. The RRP and the RP of Glu containing SVs were still released by HK5C when dynamin was prevented from binding to membrane(s). This suggested that exocytosis of such SVs did not require dynamin to bind to membrane(s) unlike this requirement for the recycling (see below).

Previously, it has been ascertained that both the RRP and RP could be stimulated to exocytose by HK5C or ION5C even when the GTPase activity of dynamin was inhibited by dynasore (see Figure A12 in Appendix A). Some dynamin must be associated with some membrane(s) prior to the addition of MiTMAB because the dynamin dependent KR mode can still take place (see below). The second important result was obtained when synaptosomes were pre-treated with MiTMAB before the HK5C pre-stimulation step. Under such circumstances it is known that both the RRP and RP SVs would undergo exocytosis. Thus, one can then study whether their recycling, reloading and re-availability for release was compromised when dynamin was prevented from binding to membrane(s). This experiment produced the exciting result that the RRP SVs could still re-release whilst there was no re-release of the RP SVs, as shown by a decrease in Glu release after the MiTMAB pre-treatment effect on subsequent recycling with ION5C, and not 4AP5C, which releases the RRP only. This fits in with all the predictions from the results about KR and FF mode.

The RRP SVs recycled via a NMII dependent KR mechanism which was not perturbed by MiTMAB. However, the RP SVs underwent FF following the addition of the HK5C pre-stimulation and these had to recycle via CME mechanisms that had a requirement for dynamin to associated with membranes. This was prevented by MiTMAB, so during a second round of stimulation using ION5C, there was no RP SVs to undergo exocytosis. This MiTMAB pre-stimulation experiment result complements earlier studies where similar experiments with dynasore or Pitstop® 2 prevented the re-release of the RP (Singh, 2017).

Pitstop® 2 treatment prevented CME; this was shown to prevent the recycling of the RP following pre-stimulation with HK5C such that subsequent ION5C stimulated release only evoked the RRP SVs to undergo exocytosis (Appendix Figures A5-A8). Dynasore also had a similar effect on pre-stimulation, confirming that CME of the RP SVs requires dynamin for membrane scission at the PM. This pre-stimulation paradigm was able to prevent dynamin binding to the PM. This is because MiTMAB pre-treatment followed by the pre-stimulation paradigm using HK5C prevented the RP SVs recycling such that subsequent application of ION5C only evoked the release of the RRP SVs. This indicates that in order for CME of the RP SVs – such that they recycle – dynamin needs to be recruited to the PM and this blocked by MiTMAB. This is clearly different to the requirements for dynamin in exocytosis wherein some dynamin is already bound and primed at the PM for exocytosis such that MiTMAB has no effect on any of the tested parameters (Singh, 2017).

Thus, three separate drugs – dynasore, Pitstop® 2 and MiTMAB – working via distinct mechanisms indicate that the RP SVs undergo FF mode and recycle by a clathrin and dynamin dependent mechanism.

In Chapter 4, it was shown that an increase in cAMP prevented the release of the RP of SVs. For the HK5C stimulus, this was revealed to be connected to the activation of EPACs, and not PKA. The cAMP increase causing activation of EPAC could possibly have involved a reduction in Ca^{2+} entry through voltage-gated Ca^{2+} channels and such reduction may be sufficient to reduce the overall increase in the terminal $[Ca^{2+}]_i$ such that this level was insufficient to drive the fusion of the RP SVs. However, this does not seem to be the mechanism for

how increased cAMP prevents the release of the RP as this condition also prevented ION5C evoked RP SV release and with this stimulus there was no change in evoked $[Ca^{2+}]_i$. If one assumes that the increase in cAMP actually prevented the release of the RP evoked by HK5C or ION5C by similar mechanisms, then this indicated that changes in Ca^{2+} does not contribute to this pathway. It is possible that increased cAMP could perturb the translocation of the RP SVs to the fusion sites at the PM or that it could perturb the formation of new SNARE complexes including their interaction with the Ca^{2+} sensor required for RP SV fusion. Clearly, this interesting observation will require extensive future experimentation to enable one to elucidate the mechanism

Finally, in Chapter 5 it was established that an intact actin cytoskeleton was required for release of the RP SVs by both ION5C and HK5C. This suggested that a specific located population of microfilaments in the terminal was required to allow the RP SVs to begin priming and translocate to the AZ and be available for release following the release of the RRP. Considering the results from Chapter 4 there is the possibility that the increase in cAMP may have caused the disassembly of the actin microfilaments and so one gets the same phenotype of inhibition of the evoked release of the RP SVs. Alternatively, disassembly of microfilaments may alter the location/properties of AC such that there is an increase in cAMP. Furthermore, the activation/location of EPAC could be changed following disassembly of microfilaments. Future experiments should investigate the relationship between actin, AC and EPAC.

One could investigate whether disassembly of microfilaments leads to an increase in the cAMP levels within the nerve terminals using relevant cAMP assays. One could also use relevant immunocytochemical fluorescence microscopy methods to investigate whether there was a re-localisation of ACs following microfilament disassembly (using fixed tissue, antibodies to ACs and fluorescent secondary anti-bodies) although this would represent a major project which would be particularly challenging in view of the small size of synaptosomes and may require the use of sophisticated light microscopy methods and collaboration with groups with this technology.

Although it appeared that disassembly of microfilaments perturbed Ca^{2+} entry through voltage-gated Ca^{2+} channels, such reduction of levels of $[Ca^{2+}]_i$ cannot explain the role of actin cytoskeleton in release of the RP of SVs as ION5C evoked release of RP SVs was also perturbed and this did not involve any voltage-gated Ca^{2+} channels. Future experiments will be designed to discover whether disassembly of actin cytoskeleton perturbs a particular voltage-gated Ca^{2+} channel type (either L, P/Q or N) by comparing the effect of latrunculin plus inhibitors to each of these channels to see if there is additivity of effect upon HK5C evoked changes in $[Ca^{2+}]_i$ as measured using Fura-2 assay. It may be that there is additive effect for the blockage of some types of the channels with actin disassembly such that there is a larger decrease in evoked $[Ca^{2+}]_i$ whereas there may be no additive effects for a particular Ca^{2+} channel blocker and latrunculin such that alone or together one still only sees the same decrease in evoked $[Ca^{2+}]_i$. This latter condition could indicate that the disassembly of actin perturbs the same channel as the particular Ca^{2+} channel inhibitor. This may indicate that it is this particular Ca^{2+} channel which is perturbed by disassembly of actin microfilaments, and this could be because such a channel is no longer localised to the relevant region of the PM to allow sufficient Ca^{2+} entry to drive fusion of the RP SVs.

From this data, it became apparent that the properties of release of the RP SVs were distinct from the release of the RRP (as suggested previously Ashton and Ushkaryov, 2005). Herein, we have been able to study the RRP in isolation by stimulating with 4AP5C. However, we could only study the RP after we have also measured the release of the RRP SVs. Indeed, it is the conventional wisdom that the RP SVs will only release after the RRP SVs have exocytosed. However, the results reported herein, led Ashton's research group to propose whether it was possible to release the RP SVs without releasing the RRP SVs. The motive for doing this was to try to reproduce the findings for the RP SVs shown here, and elsewhere, without the added complication of the RRP SVs having to be released. Remarkably, in a new project, conditions have been found where apparently only the RP SVs are exocytosing and so the findings produced here can now be checked when studying just the RP SVs. The release of just the RP SVs utilises a low dose of ION, 0.5 µM. This will be insufficient to produce a high enough concentration of intracellular Ca^{2+} at the

AZ for the RRP but it would appear to produce a bulk change in intracellular Ca^{2+} that can allow fusion of the RP SVs which have a lower $[Ca^{2+}]_i$ requirement. For example, if one stimulates Glu release with 0.5 µM ION plus 5 mM Ca^{2+} one gets lower release than when one releases with 5 mM ION plus 5 mM Ca^{2+} and this former release can be completely blocked if one disassembles the actin microfilaments with latrunculin. This is highly suggestive of only the RP SVs being released.

6.2 Regulating the Mode of Exocytosis of the RRP and RP Synaptic Vesicles

When PKA activity was inhibited by KT5720, it was found that the dynamin dependent KR mode of RRP SVs (exhibited in 4AP5C or ION5C evoked release) was switched to FF mode whilst the NMII dependent KR exhibited following HK5C stimulation was unperturbed. This was a very similar phenotype to that seen when dynamin's GTPase activity was directly inhibited by dynasore. This may suggest that endogenous PKA activity may keep dynamin in an active state either through a direct action on this protein or through an interacting partner for dynamin including phosphorylation on a protein phosphatase that regulates dynamin (e.g. PP2B/calcineurin). A relevant experiment that should be performed in the future is to perform a dual treatment of KT5720 and dynasore wherein one would expect that the individual treatments should give a similar effect as the combination treatment as in all cases the RRP SVs would be switched to an FF mode. A different result would mean that one would have to reconsider what was happening.

Contrastingly to affecting the RRP, activation of PKA using cBIMPS led to a switch of the RP of SVs so that some now undergo KR mode. This occurred whether ION5C or HK5C were used as the stimulus. Again, this phenotype is very similar to one seen previously for inhibition of PP2B with Cys A (see Figure A15 in Appendix A). This could suggest that the mode of the RP SVs was regulated by a dynamin dependent process (as suggested previously; Singh, 2017) although this cannot involve the GTPase activity of the dynamin as dynasore itself does not cause the RP SVs to switch to KR mode. Neither can it

involve increases in evoked $[Ca^{2+}]_i$ because whilst Cys A treatment is shown to do this, cBIMPS treatment does not change $[Ca^{2+}]_i$.

Increasing or decreasing cAMP levels within the terminal produced differing effects on the mode of exocytosis of the RRP induced by 4AP5C. Inhibiting AC with 9-cp-ade did not perturb the amount of KR and FF mode release from the RRP vesicles whilst activating AC with forskolin produced more KR mode by switching those SVs undergoing FF to KR. This was an interesting observation and may be due to an increase in 4AP5C evoked $[Ca^{2+}]_i$ as higher Ca^{2+} favours KR mode. Future experiments should investigate whether a Ca^{2+} dose response curve for 4AP evoked Glu release has a lower optimal $[Ca^{2+}]_i$ following forskolin treatment and whether at this lower optimal concentration forskolin does not switch the RRP FF SVs to KR mode.

Further, the effect that forskolin may have on PKC induced changes (see Singh, 2017) in the mode should be researched. OA treatment - which normally switches the RRP SVs to FF mode - cannot switch the SVs induced to undergo KR mode by forskolin and this phenomenon should be further investigated as it may highlight some of the pathways involved in this process and may reveal some important phosphorylation changes that can be studied using western blotting and specific antibodies against specific phosphorylation sites on dynamin (although, this may require such antibodies to immunoprecipitate the phosphorylated protein).

The KR mode of RRP SVs induced by either ION5C or HK5C had a requirement for an intact actin cytoskeleton and disassembled microfilaments led to these RRP SVs switching to FF mode. This was shown by various experiments outlined in Chapter 5 that indicated that both the dynamin and the NMII dependent KR modes for RRP SVs that involved the closure of the initial FP (without complete FP expansion into FF mode) required assembled microfilaments. Future studies are needed to investigate what precise role this cytoskeletal element has in allowing the FP to close such that KR mode is produced. The ineffectiveness of stabilisation of the actin microfilaments - using jasplakinolide - on the dynamin or NMII dependent KR mode is an important result because it showed that there was no requirement for the assembly of new microfilaments to allow the FP to close in < 0.5 s after it was opened.

In Chapter 4, it was decided that as the RP of SVs were blocked by forskolin that the mode of exocytosis of the RRP SVs that were still exocytosed should be studied using 4AP5C which only releases this latter pool. However, 4AP5C worked through the dynamin dependent KR pathway. Thus, the role of increased cAMP on the NMII dependent KR pathway was not studied. Whilst it is clear that using forskolin one can still test the dynamin dependent and NMII dependent KR of the RRP SVs using ION5C and HK5C, we could also in the future test the effect of increases of cAMP on the NMII dependent KR of the RRP using 4AP5C if terminals were also treated with 40 nM PMA which should allow 4AP5C to work on this pathway. Despite the block of release of the RP SVs in latrunculin A treated synaptosomes, the dynamin dependent KR and NMII dependent KR of the RRP SVs were studied using ION5C and HK5C (or ION5C following 40 nM PMA treatment) respectively. This means that future experiments should repeat the results with forskolin but utilise ION5C and HK5C as stimuli.

6.3 Concluding Statement

Understanding subjects vital to neurophysiology such as the little understood sub-cellular mechanisms of modulating neurotransmitter release is paramount to make necessary advancements in this scientific field and may be essential in discovering aetiologies of common neuronal pathologies by comparing the mechanisms of diseased states to healthy states of cells. We cannot understand how the brain works without understanding how the fundamental parts work together. This thesis describes compelling novel evidence that furthers this knowledge using physiologically mature mammalian CNS neurons.

Intriguingly, it was discovered that cAMP levels can regulate SV exocytosis but in ways distinct from activating PKA. Activation of AC induced increases in cAMP that blocked the fusion of the RP SVs whilst it caused all the evoked RRP SVs to undergo KR. The increase in cAMP action on the RP SVs was due to cAMP activation of EPAC as inhibition of this enzyme prevented such a perturbation of the RP. This evidence provides insight to how modulation of AC from extracellular signals could affect neurotransmitter response.

Activation of PKA led to some RP SVs to switch to KR mode whilst blockade of PKA switched dynamin dependent mode of RRP SVs to FF mode. This dynamin dependent mode of exocytosis appears to depend upon membrane bound dynamin – as opposed to translocation of cytosolic dynamin to the membrane – such that it still occurs when non-membrane bound dynamin does not contribute to the first round of release. This interpretation complements emerging evidence of membrane bound dynamin sub-populations within neurons.

Disassembly of actin microfilaments also prevented the release of the RP and future experiments may ascertain whether this has any relationship to the changes in cAMP levels. However, actin disassembly also switched both dynamin dependent KR and NMII dependent KR to FF. This is distinct from results with either PKA activation or cAMP increase. Future experiments should reveal whether the fusion pore closure during KR is associated with actin microfilaments.

LIST OF REFERENCES

Agilent Technologies, Inc. (2019). Agilent Seahorse XF Cell Mito Stress Test Kit: User Guide: 103016-400. Wilmington, DE.

Ahmari, S.E. and Smith, S.J. (2002). 'Knowing a nascent synapse when you see it'. *Neuron*, **34**(3), 333-336.

Alabi, A.A. and Tsien, R.W. (2012). 'Synaptic vesicle pools and dynamics.' *Cold Spring Harb. Perspect. Biol.*, **4**(8):a013680.

Alberts, B., Johnson, A., Lewis, J., Raff, M., Roberts, K., Walter, P., Bray, D. and Watson, J.D. (2002). 'The self-assembly and dynamic structure of cytoskeletal filaments.' In: Molecular Biology of the Cell. 4th ed. New York: Garland Science.

Alés, E., Tabares, L., Poyato, J.M., Valero, V., Lindau, M. and Alvarez de Toledo, G. (1999).' High calcium concentrations shift the mode of exocytosis to the kiss-and-run mechanism.' *Nat. Cell Biol.*, **1**(1), 40-44.

Almahariq, M., Tsalkova, T., Mei, F.C., Chen, H., Zhou, J., Sastry, S.K., Schwede, F. and Cheng, X. (2013). 'A novel EPAC-specific inhibitor suppresses pancreatic cancer cell migration and invasion.' *Mol. Pharacol.*, **83**(1), 122-128.

Anantharam, A., Axelrod, D. and Holz, R.W. (2012). 'Real-time imaging of plasma membrane deformations reveals pre-fusion membrane curvature changes and a role for dynamin in the regulation of fusion pore expansion.' *J. Neurochem.*, **122**(4), 661-671.

Aoki, R., Kitaguchi, T., Oya, M., Yanagihara, Y., Sato, M., Miyawaki, A. and Tsuboi, T. (2010). 'Duration of fusion pore opening and the amount of hormone released are regulated by myosin II during kiss-and-run exocytosis.' *Biochem. J.*, **429**(3), 497-504.

Armbruster, M., Messa, M., Ferguson, S.M., De Camilli, P. and Ryan, T.A. (2013). 'Dynamin phosphorylation controls optimization of endocytosis for brief action potential bursts.' *eLife*, **2**. doi: 10.7554/eLife.00845.

Ashton, A.C. and Ushkaryov, Y.A. (2005). 'Properties of synaptic vesicle pools in mature central nerve terminals.' *J. Biol. Chem.*, **280**(44), 37278-37288.

Ashton, A.C., Patel, M.H. and Sihra, T.S. (2009). 'Changes in protein phosphorylation and calcium regulate switching between distinct modes of synaptic vesicle exocytosis.' *Soc. Neurosci.*

Baba, T., Sakisaka, T., Mochida, S. and Takai, Y. (2005). 'PKA-catalyzed phosphorylation of tomosyn and its implication in Ca^{2+}-dependent exocytosis of neurotransmitter.' *J. Cell. Biol.*, **170**(7), 1113-1125.

Bähring, R. and Covarrubias, M. (2011). 'Mechanisms of closed-state inactivation in voltage-gated ion channels.' *J. Physiol.*, **589**(3), 461-479.

Baldwin, M.L., Rostas, J.A.P. and Sim, A.T.R. (2003). 'Two modes of exocytosis from synaptosomes are differentially regulated by protein phosphatase types 2A and 2B.' *J. Neurochem.*, **85**(5), 1190-1199.

Barclay, J.W., Morgan, A., and Burgoyne, R.D. (2005). 'Calcium-dependent regulation of exocytosis.' *Cell Calcium.,* **38**(3-4), 343-353.

Bauerfeind, R., Takei, K. and De Camilli, P. (1997). 'Amphiphysin I is associated with coated endocytic intermediates and undergoes stimulation-dependent dephosphorylation in nerve terminals.' *J. Biol. Chem.*, **272**(49), 30984-30992.

Beach, J.R., Hussey, G.S., Miller, T.E., Chaudhury, A., Patel, P., Monslow, J., Zheng, Q., Keri, R.A., Reizes, O., Bresnick, A.R., Howe, P.H. and Egelhoff, T.T. (2011). 'Myosin II isoform switching mediates invasiveness after TGF-β-induced epithelial-mesenchymal transition.' *P.N.A.S.*, **108**(44), 17991-17996.

Beaumont, V., Zhong, N., Froemke, R.C., Ball, R.W. and Zucker, R.S. (2002). 'Temporal synaptic tagging by I(h) activation and actin: involvement in long-term facilitation and cAMP-induced synaptic enhancement.' *Neuron*, **33**(4), 601-613.

Berberian, K., Torres, A.J., Fang, Q., Kisler, K. and Lindau, M. (2009). 'F-actin and myosin II accelerate catecholamine release from chromaffin granules.' *J. Neurosci.*, **29**(3), 863-870.

Bethoney, K.A., King, M.C., Hinshaw, J.E., Ostap, E.M. and Lemmon, M.A. (2009). 'A possible effector role for the pleckstrin homology (PH) domain of dynamin.' *P.N.A.S. USA*, **106**(32), 13359-13364.

Bhuva, D. (2015). ‘Dynamins and myosin-II regulate the distinct modes of synaptic vesicle exocytosis in mature cerebrocortical nerve terminals and this involves calcium dependent phosphorylations.’ Doctoral thesis, UCLan, Preston.

Bialojan, C. and Takai, A. (1988). ‘Inhibitory effect of a marine-sponge toxin, okadaic acid, on protein phosphatases. Specificity and kinetics.’ *Biochem. J.*, **256**(1), 283-290.

Biel, M. (2008). ‘Cyclic Nucleotide-regulated Cation Channels.’ *J. Biol. Chem.*, **284**(14), 9017-9021.

Blumenthal, D.K., Takio, K., Hansen, R.S. and Krebs, E.G. ‘Dephosphorylation of cAMP-dependent protein kinase regulatory subunit (type II) by calmodulin-dependent protein phosphatase. Determinants of substrate specificity’. *J. Biol. Chem.*, **261**(18), 8140-8145.

Boczan, J., Leenders, A.G.M. and Sheng, Z.H. (2004). ‘Phosphorylation of syntaphilin by cAMP-dependent protein kinase modulates its interaction with syntaxin-1 and annuls its inhibitory effect on vesicle exocytosis.’ *J. Biol. Chem.*, **279**(18), 18911-18919.

Bos, J.L. (2006). ‘Epac proteins: multi-purpose cAMP targets.’ *Trends. Biochem. Sci.*, **31**(12), 680-686.

Boucrot, E., Saffarian, S., Massol, R., Kirchhausen, T. and Ehrlich, M. (2006). ‘Role of lipids and actin in the formation of clathrin-coated pits.’ *Exp. Cell. Res.*, **312**(20), 4036-4048.

Boulant, S., Kural, C., Zeeh, J., Ubelmann, F. and Kirchhausen, T. (2011). ‘Actin dynamics counteract membrane tension during clathrin-mediated endocytosis.’ *Nat. Cell. Biol.*, **13**(9), 1124-1131.

Breckenridge, M.T., Dulyaninova, N.G. and Egelhoff, T.T. (2009). ‘Multiple regulatory steps control mammalian nonmuscle myosin II assembly in live cells.’ *Mol. Biol. Cell*, **20**(1), 338-347.

Bresnick, A.R. (1999). ‘Molecular mechanisms of nonmuscle myosin-II regulation.’ *Curr. Opin. Cell Biol.*, **11**(1), 26-33.

Bretou, M., Jouannot, O., Fanget, I., Pierobon, P., Larochette, N., Gestraud, P., Guillon, M., Emiliani, V., Gasman, S., Desnos, C., Lennon-Duménil, A.M. and Darchen, F. (2014). ‘Cdc42 controls the dilation of the exocytotic fusion pore by regulating membrane tension.’ *Mol. Biol. Cell*, **25**(20), 3195-3209.

Bubb, M.R., Spector, I., Beyer, B.B. and Fosen, K.M. (2000). 'Effects of jasplakinolide on the kinetics of actin polymerization.' *J. Biol. Chem.*, **275**(7), 5163-5170.

Cabeza, J.M., Acosta, J. and Alés, E. (2010). 'Dynamics and regulation of endocytotic fission pores: role of calcium and dynamin.' *Traffic*, **11**(12), 1579-1590.

Caldwell, J.E., Heiss, S.G., Mermall, V. and Cooper, J.A. (1989). 'Effects of CapZ, an actin capping protein of muscle, on the polymerization of actin.' *Biochem.*, **28**(21), 8506-8514.

Cano, R. and Tabares, L. (2016). 'The active and periactive zone organization and the functional properties of small and large synapses.' *Front Synaptic Neurosci.*, **8**, 12. doi:10.3389/fnsyn.2016.00012.

Ceccarelli, B., Hurlbut, W.P. and Mauro, A. (1973). 'Turnover of transmitter and synaptic vesicles at the frog neuromuscular junction.' *J. Cell. Biol.* **57**(2), 499-524.

a. Chan, L.S., Hansra, G., Robinson, P.J. and Graham, M.E. (2010). 'Differential phosphorylation of dynamin I isoforms in subcellular compartments demonstrates the hidden complexity of phosphoproteomes.' *J. Proteome Res.*, **9**(8), 4028-4037.

b. Chan, S.A., Doreian, B. and Smith, C. (2010). 'Dynamin and myosin regulate differential exocytosis from mouse adrenal chromaffin cells.' *Cell. Mol. Neurobiol.*, **30**(8), 1351-1357.

Chanaday, N.L. and Kavalali E.T. (2017). 'How do you recognize and reconstitute a synaptic vesicle after fusion?' *F1000Res.*, **6**, 1734. doi:10.12688/f1000research.12072.1.

Chandrasekar, I., Huettner, J.E., Turney, S.G. and Bridgman, P.C. (2013). 'Myosin II regulates activity dependent compensatory endocytosis at central synapses.' *J. Neurosci.*, **33**(41), 16131-16145.

Chavez-Noriega, L.E. and Stevens, C.F. (1994). 'Increased transmitter release at excitatory synapses produced by direct activation of adenylate cyclase in rat hippocampal slices.' *J. Neurochem.*, **14**(1), 310-317.

Chen, C. and Regehr, W.G. (1997). 'The mechanism of cAMP-mediated enhancement at a cerebellar synapse.' *J. Neurosci.*, **17**(22), 8687-8694.

Cheng, Q., Yakel, J.L. (2014). ‘Presynaptic α7 nicotinic acetylcholine receptors enhance hippocampal mossy fiber glutamatergic transmission via PKA activation.’ *J. Neurosci.*, **34**(1), 124-133.

Cheung, G. and Cousin, M.A. (2013). ‘Synaptic vesicle generation from activity-dependent bulk endosomes requires calcium and calcineurin.’ *J. Neurosci.*, **33**(8), 3370-3379.

Cheung, G. and Cousin, M.A. (2019). ‘Synaptic vesicle generation from activity-dependent bulk endosomes requires a dephosphorylation-dependent dynamin–syndapin interaction’. *J, Neurochem.*, **151**(5), 570-583.

Cheung, G., Jupp, O.J. and Cousin, M.A. (2010). ‘Activity-dependent bulk endocytosis and clathrin-dependent endocytosis replenish specific synaptic vesicle pools in central nerve terminals.’ *J. Neurosci.*, **30**(24), 8151-8161.

Choi, S.W., Gerencser, A.A. and Nicholls, D.G. (2009). ‘Bioenergetic analysis of isolated cerebrocortical nerve terminals on a microgram scale: spare respiratory capacity and stochastic mitochondrial failure’. *J. Neurochem.*, **109**(4), 1179-1191.

Clayton, E.L. and Cousin, M.A. (2008). ‘Differential labelling of bulk endocytosis in nerve terminals by FM dyes.’ *Neurochem. Int.*, **53**(3-4), 51-55.

Clayton, E.L., Evans, G.J.O. and Cousin, M.A. (2008). ‘Bulk synaptic vesicle endocytosis is rapidly triggered during strong stimulation.’ *J. Neurosci.*, **28**(26), 6627-6632.

Cocucci, E., Gaudin, R. and Kirchhausen, T. (2014). ‘Dynamin recruitment and membrane scission at the neck of a clathrin-coated pit.’ *Mol. Biol. Cell.*, **25**(22), 3595-3609.

Collins, J.H. and Elzinga, M. (1975). ‘The primary structure of actin from rabbit skeletal muscle. Completion and analysis of the amino acid sequence.’ *J. Biol. Chem.*, **250**(15), 5915-5920.

Cotter, K., Stransky, L., McGuire, C. and Forgac, M. (2015) ‘Recent insights into the structure, regulation, and function of the V-ATPases. *Trends Biochem. Sci.*, **40**(10), 611-622.

Coué, M., Brenner, S.L., Spector, I. and Korn, E.D. (1987). ‘Inhibition of actin polymerization by latrunculin A.’ *FEBS Lett.*, **213**(2), 316-318.

Cousin, M.A, and Evans, G.J.O. (2011). ‘Activation of silent and weak synapses by cAMP-dependent protein kinase in cultured cerebellar granule neurons.’ *J. Physiol.*, **589**(8), 1943-1955.

Crawford, D.C. and Kavalali, E.T. (2015) ‘Molecular underpinnings of synaptic vesicle pool heterogeneity.’ *Traffic*.,**16**(4), 338-364.

Damke, H., Binns, D.D., Ueda, H., Schmid, S.L. and Baba, T. (2001). ‘Dynamin GTPase domain mutants block endocytic vesicle formation at morphologically distinct stages.’ *Mol. Biol. Cell.*, **12**(9), 2578-2589.

Dao, K.K., Teigan, K., Kopperud, R., Hodneland, E., Schwede, F., Christensen, A.E., Martinez, A. and Døskeland, S.O. (2006). Epac1 and cAMP-dependent protein kinase holoenzyme have similar cAMP affinity, but their cAMP domains have distinct structural features and cyclic nucleotide recognition.’ *J. Biol. Chem.*, **281**(30), 21500-21511.

Das, S., Gerwin, C. and Sheng, Z.H. (2003). ‘Syntaphilin binds to dynamin-1 and inhibits dynamin-dependent endocytosis.’ **278**(42), 41221-41226.

Davies, S.P., Reddy, H., Caivano, M. and Cohen, P. (2000). ‘Specificity and mechanism of action of some commonly used protein kinase inhibitors.’ *Biochem. J.*, **351**(1), 95-105.

De Robertis, E.D.P. and Bennett, H.S. (1955). ‘Submicroscopic vesicular component in the synapse.’ *Fed. Proc.*, **13**, 35.

De Rooij, J., Rehmann, H., van Triest, M., Cool, R.H., Wittinghofer, A. and Bos, J.L. (2000). ‘Mechanism of regulation of the Epac family of cAMP-dependent RapGEFs.’ *J. Biol. Chem.*, **275**(27), 20829-20836.

De Rooij, J., Zwartkruis, F.J., Verheijen, M.H., Cool, R.H., Nijman, S.M., Wittinghofer, A. and Bos, J.L. (1998). ‘Epac is a Rap1 guanine-nucleotide-exchange factor directly activated by cyclic AMP.’ *Nature*, **396**(6710), 474-477.

Del Castillo, J. and Katz, B. (1954). ‘Quantal components of the end-plate potential.’ *J. Physiol.*, **124**(3), 560-573.

Delvendahl, I., Vyleta, N.P., von Gersdorff, H. and Hallermann, S. (2016). ‘Fast, temperature-sensitive and clathrin-independent endocytosis at central synapses.’ *Neuron*, **90**(3), 492-498.

Denker, A. and Rizzoli, S.O. (2010). ‘Synaptic vesicle pools: an update.’ *Front Synaptic Neurosci.*, **2**, 135. doi: 10.3389/fnsyn.2010.00135.

Denker, A., Kröhnert, K., Bückers, J., Neher, E. and Rizzoli, S.O. (2011). ‘The reserve pool of synaptic vesicles acts as a buffer for proteins involved in synaptic vesicle recycling.’ *P.N.A.S.*, **108**(41), 17183-17188.

Dessauer, C.W., Scully, T.T. and Gilman, A.G. (1997). ‘Interactions of forskolin and ATP with the cytosolic domains of mammalian adenylyl cyclase.’ *J. Biol. Chem.*, **272**(35), 22272-22277.

Doherty, G.J. and McMahon, H.T. (2008). ‘Mediation, modulation, and consequences of membrane-cytoskeleton interactions.’ *Annual Review of Biophysics,* **37**, 65-95.

Dominguez, R. (2004). ‘Actin-binding proteins--a unifying hypothesis.’ *Trends Biochem. Sci.*, **29**(11), 572-578.

Dong, J.M., Leung, T., Manser, E. and Lim, L. (2002). ‘Cdc42 antagonizes inductive action of cAMP on cell shape, via effects of the myotonic dystrophy kinase-related Cdc42-binding kinase (MRCK) on myosin light chain phosphorylation.’ *Eur. J. Cell. Biol.*, **81**(4), 231-242.

Doreian, B.W., Fulop, T.G. and Smith, C.B. (2008). ‘Myosin II activation and actin reorganization regulate the mode of quantal exocytosis in mouse adrenal chromaffin cells.’ *J. Neurosci.*, **28**(17), 4470-4478.

Doreian, B.W., Fulop, T.G., Meklemburg, R.L. and Smith, C.B. (2009). ‘Cortical F-actin, the exocytic mode, and neuropeptide release in mouse chromaffin cells is regulated by myristoylated alanine-rich C-kinase substrate and myosin II.’ *Mol. Biol. Cell*, **20**(13), 3142-3154.

Doussau, F., Schmidt, H., Dorgans, K., Valera, A.M., Poulain, B. and Isope, P. (2017). ‘Frequency-dependent mobilization of heterogeneous pools of synaptic vesicles shapes presynaptic plasticity.’ *eLife*, **6**. doi: 10.7554/eLife.28935.

Dulyaninova, N.G., Malashkevich, V.N., Almo, S.C. and Bresnick, A.R. (2005). ‘Regulation of myosin-IIA assembly and Mts1 binding by heavy chain phosphorylation.’ *Biochemistry*, **44**(18), 6867-6876.

Elhamdani, E., Azizi, F. and Artalejo C.R. (2006). ‘Double patch clamp reveals that transient fusion (kiss-and-run) is a major mechanism of secretion in calf adrenal

chromaffin cells: high calcium shifts the mechanism from kiss-and-run to complete fusion.' *J. Neurosci.*, **26**(11), 3030-3036.

Elzinga, M., Collins, J.H., Kuehl, W.M. and Adelstein, R.S. (1973). 'Complete amino-acid sequence of actin of rabbit skeletal muscle.' *P.N.A.S. USA.*, **70**(9), 2687-2691.

Esposito, G., Clara, A. and Verstreken, P. (2012). 'Synaptic vesicle trafficking and Parkinson's disease.' *Dev. Neurobiol.*, **72**(1), 134-144.

Fasshauer, D., Sutton, R.B., Brunger, A.T. and Jahn, R. (1998). 'Conserved structural features of the synaptic fusion complex: SNARE proteins reclassified as Q- and R-SNAREs', *P.N.A.S.*, **95**(26), 15781-15786.

Fatt, P. and Katz, B. (1952). 'Spontaneous subthreshold activity at motor nerve endings.' *J. Physiol.*, **117**(1), 109-128.

Ferguson, S.M. and De Camilli, P. (2012). 'Dynamin, a membrane-remodelling GTPase.' *Nat. Mol. Cell. Biol.*, **13**(2), 75-88.

Ferguson, S.M., Brasnjo, G., Hayashi, M., Wölfel, M., Collesi, C., Giovedi, S., Raimondi, A., Gong, L.W., Ariel, P., Paradise, S., O'Toole, E., Flavell, R., Cremona, O., Miesenböck, G., Ryan, T.A. and De Camilli, P. (2007). 'A selective activity-dependent requirement for dynamin 1 in synaptic vesicle endocytosis.' *Science*, **316**(5824), 570-574.

Ferguson, S.M., Raimondi, A., Paradise, S., Shen, H., Mesaki, K., Ferguson, A., Destaing, O., Ko, G., Takasaki, J., Cremona, O., O'Toole, E. and De Camilli, P. (2009). 'Coordinated actions of actin and BAR proteins upstream of dynamin at endocytic clathrin-coated pits.' *Dev. Cell*, **17**(6), 811-822.

Fernandes, H.B., Riordan, S., Nomura, T., Remmers, C.L., Kraniotis, S., Marshall, J.J., Kukreja, L., Vassar, R. and Contractor, A. (2015). 'Epac2 mediates cAMP-dependent potentiation of neurotransmission in the hippocampus.' *J. Neurosci.*, **35**(16), 6544-6553.

Fernándes, J.J., Candenas, M.L., Souto, M.L., Trujillo, M.M. and Norte, M. (2002). 'Okadaic acid, useful tool for studying cellular processes.' *Curr. Med. Chem.*, **9**(2), 229-262.

Fernandez-Alfonso, T. and Ryan, T.A. (2008). ‘A heterogeneous "resting" pool of synaptic vesicles that is dynamically interchanged across boutons in mammalian CNS synapses.’ *Brain Cell. Biol.*, **36**(1-4), 87-100.

Ferrero, J.J., Alvarez, A.M., Ramírez-Franco, J., Godino, M.C., Bartolomé-Martín, D., Aguado, C., Torres, M., Luján, R., Ciruela, F. and Sánchez-Prieto, J. (2013). ‘β-adrenergic receptors activate Epac, translocate Munc13-1 and enhance the Rab3A-Rim1α interaction to potentiate glutamate release at cerebrocortical nerve terminals.’ *J. Biol. Chem.*, **288**(43), 31370-31385.

Fesce, R., Grohovaz, F., Valtorta, F. and Meldolesi, J. (1994). ‘Neurotransmitter release: fusion or 'kiss-and-run'?’. *Trends Cell Biol.*, **4**(1), 1-4.

Fioravante, D. and Regehr, W.G. (2011). ‘Short-term forms of presynaptic plasticity’. *Current Opinion in Neurobiology*, **21**(2), 269-274.

Fowler, M.W. and Staras, K. (2015). ‘Synaptic vesicle pools: Principles, properties and limitations.’ *Exp. Cell Res.*, **335**(2), 150-156.

Fulop, T., Doreian, B., Smith, C. (2008). ‘Dynamin I plays dual roles in the activity-dependent shift in exocytic mode in mouse adrenal chromaffin cells.’ *Arch. Biochem. Biophys.*, **477**(1), 146-154.

Gabel, M. and Chasserot-Golaz, S. (2016). ‘Annexin A2, an essential partner of the exocytotic process in chromaffin cells.’ *J.Neurochem.*, **137**(6), 890-896.

Gabel, M., Delavoie, F., Demais, V., Rover, C., Bailly, Y., Vitale, N., Bader, M.F. and Chasserot-Golaz, S. (2015). ‘Annexin A2-dependent actin bundling promotes secretory granule docking to the plasma membrane and exocytosis.’ *J. Cell. Biol.*, **210**(5), 785-800.

Galas, M.C., Chasserot-Golaz, S., Dirrig-Grosch, S. and Bader, M.F. (2000). ‘Presence of dynamin--syntaxin complexes associated with secretory granules in adrenal chromaffin cells.’ *J. Neurochem.*, **75**(4), 1511-1519.

Gan, Q. and Watanabe, S. (2018). ‘Synaptic vesicle endocytosis in different model systems.’ *Front. Cell. Neurosci.,* **28**(12), 171.

Gaydukov, A.E., Tarasova, E.O. and Balezina, O.P. (2013). ‘Calcium-dependent phosphatase calcineurin downregulates evoked neurotransmitter release in neuromuscular junctions of mice.’ *Neurochem. J.*, **7**, 29-33.

Ghodsi, H. and Kazemi, M.T. (2012). 'Elastic properties of actin assemblies in different states of nucleotide binding.' *Cel. Mol. Bioeng.*, **5**, 1-13.

González-Jamett, A.M., Guerra, M.J., Olivares, M.J., Haro- Acuña, V., Baéz-Matus, X., Vásquez-Navarrete, J., Momboisse, F., Martinez-Quiles, N. and Cárdenas, A.M. (2017). 'The F-Actin binding protein cortactin regulates the dynamics of the exocytotic fusion pore through its SH3 domain.' *Front. Cell. Neurosci.*, **11**, 130. doi: 10.3389/fncel.2017.00130.

González-Jamett, A.M., Momboisse, F., Guerra, M.J., Ory, S., Báez-Matus, X., Barraza, N., Calco, V., Houy, S., Couve, E., Neely, A., Martínez, A.D., Gasman, S. and Cárdenas, A.M. (2013). 'Dynamin-2 regulates fusion pore expansion and quantal release through a mechanism that involves actin dynamics in neuroendocrine chromaffin cells.' *PLos One*, **8**(8), e70638.

Gormal, R.S., Nguyen, T.H., Martin, S., Papadopulos, A. and Meunier, F.A. (2015). 'An acto-myosin II constricting ring initiates the fission of activity-dependent bulk endosomes in neurosecretory cells.' *J. Neurosci.*, **35**(4), 1380-1389.

Graham, M.E., Anggono, V., Bache, N., Larsen, M.R., Craft, G.E. and Robinson, P.J. (2007). 'The *in vivo* phosphorylation sites of rat brain dynamin I'. *J. Bio. Chem.*, **282**(20), 14695–14707.

Grandoch, M., Roscioni, S.S. and Schmidt, M. (2010). 'The role of Epac proteins, novel cAMP mediators, in the regulation of immune, lung and neuronal function.' *Br. J. Pharmacol.*, **159**(2), 265-284.

Granseth, B., Odermatt, B., Royle, S.J. and Lagnado, L. (2006). 'Clathrin-mediated endocytosis is the dominant mechanism of vesicle retrieval at hippocampal synapses.' *Neuron*, **51**(6), 773-786.

Gray, E.G. and Whittaker, V.P. (1962). 'The isolation of nerve endings from brain: an electron-microscopic study of cell fragments derived by homogenization and centrifugation.' *J. Anat.*, **96**, 79-88.

Grigliatti, T.A., Hall, L., Rosenbluth, R. and Suzuki, D.T. (1973) 'Temperature-sensitive mutations in *Drosophila melanogaster*. XIV. A selection of immobile adults.' *Mol. Gen. Genet.*, **120**(2), 107-114.

Grummt, I. (2006). 'Actin and myosin as transcription factors.' *Current Opinion in Genetics & Development*, **16**(2), 191-196.

Grynkiewicz, G., Poenie, M. and Tsien, R.Y. (1985). 'A new generation of Ca^{2+} indicators with greatly improved fluorescence properties.' *J. Biol. Chem.*, **260**(6), 3440-3450.

Gu, C., Yaddanapudi, S., Weins, A., Osborn, T., Reiser, J., Pollak, M., Hartwig, J. and Sever, S. (2010). 'Direct dynamin–actin interactions regulate the actin cytoskeleton.' *EMBO J.*, **29**(21), 3593-3606.

Gunning, P.W., Ghoshdastider, U., Whitaker, S., Popp, D. and Robinson, R.C. (2015). 'The evolution of compositionally and functionally distinct actin filaments.' *J. Cell Sci.*, **128**(11), 2009-2019.

Han, X., Li, P., Yang, Z., Huang, X., Wei, G., Sun., Y., Kang, X., Hu, X., Deng, Q., Chen, L., He, A., Huo, Y., Li, D., Betzig, E. and Luo, J. (2017). 'Zyxin regulates endothelial von Willebrand factor secretion by reorganizing actin filaments around exocytic granules.' *Nature Communications*, **8**(14639), doi: 10.1038/ncomms14639.

Hanoune, J. and Defer, N. (2001). 'Regulation and role of adenylyl cyclase isoforms.' *Annu. Rev. Pharmacol. Toxicol.*, **41**, 145-174.

Harata, N.C., Aravanis, A.M. and Tsien, R.W. (2006). 'Kiss-and-run and full-collapse fusion as modes of exo-endocytosis in neurosecretion.' *J. Neurochem.*, **97**(6), 1546-1570.

Harata, N.C., Pyle, J.L., Aravanis, A.M., Mozhayeva, M., Kavalali, E.T. and Tsien, R.W. (2001). 'Limited numbers of recycling vesicles in small CNS nerve terminals: implications for neural signaling and vesicular cycling.' *Trends Neurosci*., **24**(11), 637-643.

He, L., Wu, X.S., Mohan, R. and Wu, L.G. (2006). 'Two modes of fusion pore opening revealed by cell-attached recordings at a synapse.' *Nature*, 444(7115), 102-105.

Heerssen, H., Fetter, R.D. and Davis, G.W. (2008). 'Clathrin dependence of synaptic-vesicle formation at the *Drosophila* neuromuscular junction.' *Curr. Biol.*, **18**(6), 401-409.

Herrero, I. and Sánchez-Prieto, J., (1996). 'cAMP-dependent facilitation of glutamate release by β-adrenergic receptors in cerebrocortical nerve terminals.' *J. Biol. Chem.*, **271**(48), 30554-30560.

Heuser, J.E. and Reese, T.S. (1973). ‘Evidence for recycling of synaptic vesicle membrane during transmitter release at the frog neuromuscular junction.’ *J. Cell. Biol.*, **57**(2), 315-344.

Heuser, J.E., Reese, T.S., Dennis, M.J., Jan, Y., Jan, L. and Evans, L. (1979). ‘Synaptic vesicle exocytosis captured by quick freezing and correlated with quantal transmitter release.’ *J. Cell. Biol.*, **81**(2), 275-300.

Heymann, J.A. and Hinshaw, J.E. (2009). ‘Dynamins at a glance.’ *J. Cell. Sci.* **122**(19), 3427-3431.

Hinshaw, J.E. (2000). ‘Dynamin and its role in membrane fission.’ *Annu. Rev. Cell. Dev. Biol.*, **16**, 483-519.

Holzinger, A. (2009). ‘Jasplakinolide: an actin-specific reagent that promotes actin polymerization.’ *Methods Mol. Biol.*, **586**, 71-87.

Hosoi, N., Holt, M. and Sakaba, T. (2009). ‘Calcium dependence of exo- and endocytotic coupling at a glutamatergic synapse.’ *Neuron*, **63**(2), 216-229.

Huang, Y.Y., Kandel, E.R., Varshavsky, L., Brandon, E.P., Qi, M., Idzerda, R.L., McKnight, G.S. and Bourtchouladze, R. (1995). ‘A genetic test of the effects of mutations in PKA on mossy fiber LTP and its relation to spatial and contextual learning.’ *Cell*, **83**(7), 1211-1222.

Ikeda, K. and Bekkers, J.M. (2009). ‘Counting the number of releasable synaptic vesicles in a presynaptic terminal.’. *P.N.A.S.*, **106**(8), 2945-2950.

Ilouz, R., Lev-Ram, V., Bushong, E.A., Stiles, T.L., Friedmann-Morvinski, D., Douglas, C., Goldberg, J.L., Ellisman, M.H. and Taylor, S.S. (2017). ‘Isoform-specific subcellular localization and function of protein kinase A identified by mosaic imaging of mouse brain.’ *eLife*, **6**. doi: 10.7554/eLife.17681.

Imamura, Y., Matsumoto, N., Kondo, S., Kitayama, H. and Noda, M. (2003). ‘Possible involvement of Rap1 and Ras in glutamatergic synaptic transmission.’ *Neuroreport*, **14**(9), 1203-1207.

Imoto, Y., Raychaudhuri, S., Ma, Y., Fenske, P., Sandoval, E., Itoh, K., Blumrich, E., Matsubayashi, H.T., Mamer, L., Zarebidaki, F., Söhl-Kielczynski, B., Trimbuch, T., Nayak, S., Iwasa, J.H., Liu, J., Wu, B., Ha, T., Inoue, T., Jorgensen, E.M., Cousin,

M.A., Rosenmund, C. and Watanabe, S. (2022). ‘Dynamin is primed at endocytic sites for ultrafast endocytosis’. (2022). *Neuron*, **110**(17), 2815-2835.

Jackson, M.B. and Chapman, E.R. (2006). ‘Fusion pores and fusion machines in Ca^{2+}-triggered exocytosis.’ *Annu. Rev. Biophys. Biomol. Struct.*, **35**(135-160).

Jahn, R. and Fasshauer, D. (2012). ‘Molecular machines governing exocytosis of synaptic vesicles.’ *Nature*, **490**(7419), 201-207.

Jana, S.S., Kim, K.Y., Mao, J., Kawamoto, S., Sellers, J.R. and Adelstein, R.S. (2009). ‘An alternatively spliced isoform of non-muscle myosin II-C is not regulated by myosin light chain phosphorylation.’ *J. Biol. Chem.*, **284**(17), 11563-11571.

Johnson, R.A., Désaubry, L., Bianchi, G., Shoshani, I., Lyons, E., Taussig, R., Watson, P.A., Cali, J., Krupinski, J., Pieroni, J.P. and Iyengar, R. (1997). ‘Isozyme-dependent sensitivity of adenylyl cyclases to P-site-mediated inhibition by adenine nucleosides and nucleoside 3′-polyphosphates.’ *J. Biol. Chem.*, **272**(14), 8962-8966.

Kasatkina, L.A. (2016). ‘4-Aminopyridine sequesters intracellular Ca2+ which triggers exocytosis in excitable and non-excitable cells’. *Sci. Rep.*, **6**, 34749.

Kase, H., Iwahashi, K., Nakanishi, S., Matsuda, Y., Yamada, K., Takahashi, M., Murakata, C., Sato, A. and Kaneko, M. (1987). ‘K-252 compounds, novel and potent inhibitors of protein kinase C and cyclic nucleotide-dependent protein kinases.’ *Biochem. Biophys. Res. Commun.*, **142**(2), 436-440.

Kasprowicz, J., Kuenen, S., Miskiewicz, K., Habets, R.L.P., Smitz, L. and Verstreken, P. (2008). ‘Inactivation of clathrin heavy chain inhibits synaptic recycling but allows bulk membrane uptake.’ *J. Cell. Biol.*, **182**(5), 1007-1016.

Kasula, R., Chai, Y.J., Bademosi, A.T., Harper, C.B., Gormal, R.S., Morrow, I.C., Hosy, E., Collins, B.M., Choquet, D., Papadopulos, A. and Meunier, F.A. (2016). ‘The Munc18-1 domain 3a hinge-loop controls syntaxin-1A nanodomain assembly and engagement with the SNARE complex during secretory vesicle priming.’ *J. Cell. Biol.*, **214**(7), 847-858.

Katkar, H.H., Davtyan, A., Durumeric, A.E.P., Hocky, G.M., Schramm, A.C., De La Cruz, E.M. and Voth, G.A. (2018). ‘Insights into the cooperative nature of ATP hydrolysis in actin filaments.’ *Biophys. J.*, **115**(8), 1589-1602.

Kawasaki, H., Springett, G.M., Mochizuki, N., Toki, S., Nakaya, M., Matsuda, M., Housman, D.E. and Graybiel, A.M. (1998). 'A family of cAMP-binding proteins that directly activate Rap1.' *Science*, **282**(5397), 2275-2279.

Kim, S.H. and Ryan, T.A. (2009). 'Synaptic vesicle recycling at CNS synapses without AP-2.' *J. Neurosci.*, **29**(12), 3865-3874.

Kittel, R.J. and Heckmann, M. (2016). 'Synaptic Vesicle Proteins and Active Zone Plasticity'. *Front. Synaptic Neurosci.*, **8**, 8. doi: 10.3389/fnsyn.2016.00008.

Klingauf, J., Kavalali, E.T. and Tsien, R.W. (1998). 'Kinetics and regulation of fast endocytosis at hippocampal synapses.' *Nature*, **394**, 581-585.

Knighton, D.R., Zheng, J.H., Ten Eyck, L.F., Xuong, N.H., Taylor, S.S. and Sowadski, J.M. (1991). 'Structure of a peptide inhibitor bound to the catalytic subunit of cyclic adenosine monophosphate-dependent protein kinase.' *Science*, **253**(5018), 414-420.

Koenig, J.H. and Ikeda, K. (1989). 'Disappearance and reformation of synaptic vesicle membrane upon transmitter release observed under reversible blockage of membrane retrieval.' *J. Neurosci.*, **9**(11), 3844-3860.

Komatsu, S. and Ikebe, M. (2007). 'The phosphorylation of myosin II at the Ser1 and Ser2 is critical for normal platelet-derived growth factor induced reorganization of myosin filaments.' *Mol. Biol. Cell*, **18**(12), 5081-5090.

Kononenko, N.L., Pechstein, A. and Haucke, V. (2013). 'The tortoise and the hare revisited.' *eLife*, **2**. doi: 10.7554/eLife.01233.

Kononenko, N.L., Puchkov, D., Classen, G.A., Walter, A.M., Pechstein, A., Sawade, L., Kaempf, N., Trimbuch, T., Lorenz, D., Rosenmund, C., Maritzen, T. and Haucke, V. (2014). 'Clathrin/AP-2 mediate synaptic vesicle reformation from endosome-like vacuoles but are not essential for membrane retrieval at central synapses.' *Neuron*, **82**(5), 981-988.

Kovács, M., Thirumurugan, K., Knight, P.J. and Sellers, J.R. (2007). 'Load-dependent mechanism of nonmuscle myosin 2.' *P.N.A.S.*, **104**(24), 9994-9999.

Kovács, M., Tóth, J., Hetényi, C., Málnási-Csizmadia, A. and Sellers, J.R. (2004). 'Mechanism of blebbistatin inhibition of myosin II.' *J. Biol. Chem.*, **279**(34), 35557-35563.

Lazareno, S., Popham, A. and Birdsall, N.J. (2000). 'Allosteric interactions of staurosporine and other indolocarbazoles with N-[methyl-(3)H]scopolamine and acetylcholine at muscarinic receptor subtypes: identification of a second allosteric site.' *Mol. Pharmacol.*, **58**(1), 194-207.

Lee, E. and De Camilli, P. (2002). 'Dynamin at actin tails.' *P.N.A.S. USA*, **99**(1), 161-166.

Lee, J.S., Ho, W. and Lee, S. (2012). 'Actin-dependent rapid recruitment of reluctant synaptic vesicles into a fast-releasing vesicle pool.' *P.N.A.S. USA*, **109**(13), E765-764.

Leenders, A.G.M. and Sheng, Z.H. (2005). 'Modulation of neurotransmitter release by the second messenger-activated protein kinases: Implications for presynaptic plasticity.' *Pharmacol. Ther.*, **105**(1), 69-84.

Li, P., Bademosi, A.T., Luo, J. and Meunier, F.A. (2018). 'Actin remodelling in regulated exocytosis: toward a mesoscopic view.' *Trends Cell Biol.*, **28**(9), 685-697.

Li, Y., Bai, W., Zhou, Li, Sun, L. and Hashikawa, T. (2010). 'Nonhomogeneous distribution of filamentous actin in the presynaptic terminals on the spinal motoneurons.' *The Journal of Comparative Neurology*, **518**(16), 3184-3192.

Li, Y., Lalwani, A.K. and Mhatre, A.N. (2008). 'Alternative splice variants of MYH9.' *DNA Cell Biol.*, **27**(3), 117-125.

Linares-Clemente, P., Rozas, J.L., Mircheski, J., Garcia-Junco-Clemente, P., Martinez-López, J.A., Nieto-González, J.L., Vázquez, M.E., Pintado and C.O., Fernández-Chacón, R. (2015). 'Different dynamin blockers interfere with distinct phases of synaptic endocytosis during stimulation in motoneurones.' *J. Physiol.*, **593**(13), 2867-2888.

Lindau, M. and Alvarez de Toledo, G. (2003). 'The fusion pore.' *Biochem. Biophys. Acta.*, **1641**(2-3), 167-173.

Liu, J.P., Sim, A.T. and Robinson, P.J. (1994). 'Calcineurin inhibition of dynamin I GTPase activity coupled to nerve terminal depolarization.' **265**(5174), 970-973.

Liu, Y.W., Neumann, S., Ramachandran, R., Ferguson, S.M., Pucadyil, T.J. and Schmid, S.L. (2011). 'Differential curvature sensing and generating activities of dynamin isoforms provide opportunities for tissue-specific regulation.' *P.N.A.S.*, **108**(26), 234-242.

Loerke, D., Mettlen, M., Yarar, D., Jaqaman, K., Jaqaman, H., Danuser, G and Schmid, S.L. (2009). 'Cargo and dynamin regulate clathrin-coated pit maturation.' *PLoS Biol.*, **7**(3), e1000057.

Lord, S.J., Velle, K.B., Mullins, R.D. and Fritz-Laylin, L.K. (2020). 'SuperPlots: Communicating reproducibility and variability in cell biology'. *J. Cell. Biol.*, **219**(6): e202001064.

Ludowyke, R.I., Elgundi, Z., Kranenburg, T., Stehn, J.R., Schmitz-Peiffer, C., Hughes, W.E. and Biden, T.J. (2006). 'Phosphorylation of nonmuscle myosin heavy chain IIA on Ser1917 is mediated by protein kinase C beta II and coincides with the onset of stimulated degranulation of RBL-2H3 mast cells.' *J. Immunol.*, **177**(3), 1492-1499.

Machesky, L.M. and Gould, K.L. (1999). 'The Arp2/3 complex: a multifunctional actin organizer.' *Curr. Opin. Cell Biol.*, **11**(1), 117-121.

Macia, E., Ehrlich, M., Massol, R., Boucrot, E., Brunner, C. and Kirchhausen, T. (2006). 'Dynasore, a cell-permeable inhibitor of dynamin.' *Dev. Cell.*, **10**(6), 839-850.

Maeno-Hikichi, Y., Polo-Parada, L., Kastanenka, K. and Landmesser, L.T. (2011). 'Frequency-dependent modes of synaptic vesicle endocytosis and exocytosis at adult mouse neuromuscular junctions.' *J. Neurosci.*, **31**(3), 1093-1105.

Marks, B., and McMahon, H.T. (1998). 'Calcium triggers calcineurin-dependent synaptic vesicle recycling in mammalian nerve terminals.' **8**(13), 740-749.

Marland, J.R., Hasel, P., Bonnycastle, K. and Cousin, M.A. (2015). 'Mitochondrial calcium uptake modulates synaptic vesicle endocytosis in central nerve terminals.' *J. Biol. Chem.*, **291**(5), 2080-2086.

Martinsen, A., Schakman, O., Yerna, X., Dessy, C. and Morel, N. (2014). 'Myosin light chain kinase controls voltage-dependent calcium channels in vascular smooth muscle.' *Pflugers Arch*, **466**(7), 1377-1389.

McMahon, H.T. and Nicholls, D.G. (1991). 'The bioenergetics of neurotransmitter release.' *Biochem. Biophys. Acta.*, **1059**(3), 243-264.

Mellander, L.J., Trouillon, R., Svensson, M.L. and Ewing, A.G. (2012). 'Amperometric post spike feet reveal most exocytosis is via extended kiss-and-run fusion'. *Sci. Rep.*, **2**(907), doi:10.1038/srep00907.

Menegon, A., Bonanomi, D., Albertinazzi, C., Lotti, F., Ferrari, G., Kao, H.T., Benfenati, F., Baldelli, P. and Valtorta, F. (2006). 'Protein kinase A-mediated synapsin I phosphorylation is a central modulator of Ca^{2+}-dependent synaptic activity.' *J. Neurosci.*, **26**(45), 11670-11681.

Merrifield, C.J. (2016). 'Actin puts the squeeze on Drosophila glue secretion.' *Nat. Cell Biol.*, **18**(2), 142-144.

Merrifield, C.J., Feldman, M.E., Wan, L. and Almers, W. (2002). 'Imaging actin and dynamin recruitment during invagination of single clathrin-coated pits.' *Nat. Cell. Biol.*, **4**(9), 691-698.

Meunier, F.A. and Gutiérrez, L.M. (2016). 'Captivating new roles of F-actin cortex in exocytosis and bulk endocytosis in neurosecretory cells.' *Trends Neurosci.*, **39**(9), 605-613.

Michel, K., Müller, J.A., Oprisoreanu, A.M. and Schoch, S. (2015). 'The presynaptic active zone: A dynamic scaffold that regulates synaptic efficacy.' *Exp. Cell. Res.*, **335**(2), 157-164.

Miklavc, P., Ehinger, K., Sultan, A., Felder, T., Paul, P., Gottschalk, K.E. and Frick, M. (2015). 'Actin depolymerisation and crosslinking join forces with myosin II to contract actin coats on fused secretory vesicles.' *J. Cell Sci.*, **128**(6), 1193-1203.

Miklavc, P., Hecht, E., Hobi, N., Wittekindt, O.H., Dietl, P., Kranz, C. and Frick, M. (2012). 'Actin coating and compression of fused secretory vesicles are essential for surfactant secretion – a role for Rho, formins and myosin II.' *J. Cell Sci.*, **125**, 2765-2774.

Narita, A., Mueller, J., Urban, E., Vinzenz, M., Small, J.V. and Maéda, Y. (2012). 'Direct determination of actin polarity in the cell.' *J. Mol. Biol.* **419**(5), 359-368.

Neco, P., Fernández-Peruchena, C., Navas, S., Gutiérrez, L.M., de Toledo, G.A. and Alés, E. (2008). 'Myosin II contributes to fusion pore expansion during exocytosis.' *J. Biol. Chem.*, **283**(16), 10949-10957.

Nguyen, P.V. and Woo, N.H. (2003). 'Regulation of hippocampal synaptic plasticity by cyclic AMP-dependent protein kinases.' *Prog. Neurobiol.*, **71**(6), 401-437.

Nguyen, T.H., Maucort, G., Sullivan, R.K.P., Schenning, M., Lavidis, N.A., McCluskey, A., Robinson, P.J. and Meunier, F.A. (2012). 'Actin- and dynamin-dependent

maturation of bulk endocytosis restores neurotransmission following synaptic depletion.' *PLoS One*, **7**(5), e36913.

Nicholls, D.G., Sihra, T.S. and Sanchez-Prieto, J. (1987). 'Calcium-dependent and -independent release of glutamate from synaptosomes monitored by continuous fluorometry.' *J. Neurochem.*, **49**(1), 50-57.

Nicholson-Fish, J.C., Kokotos, A.C., Gillingwater, T.H., Smilllie, K.J. and Cousin, M.A. (2015). 'VAMP4 is essential cargo molecule for activity-dependent bulk endocytosis.' *Neuron*, **88**(5), 973-984.

Nightingale, T.D., Cutler, D.F. and Cramer, L.P. (2012). 'Actin coats and rings promote regulated exocytosis.' *Trends Cell Biol.*, **22**(6), 329-337.

Nightingale, T.D., White, I.J., Doyle, E.L., Turmaine, M., Harrison-Lavole, K.J., Webb, K.F., Cramer, L.P. and Cutler, D.F. (2011). 'Actomyosin II contractility expels von Willebrand factor from Weibel–Palade bodies during exocytosis.' *J. Cell Biol.*, **194**(4), 613-629.

Nygren, P.J. and Scott, J.D. (2016). 'Regulation of the phosphatase PP2B by protein-protein interactions'. *Biochem, Soc. Trans.*, **44**(5), 1313-1319.

Oda, T., Iwasa, M., Aihara, T., Maéda, Y. and Narita, A. (2009). 'The nature of the globular- to fibrous-actin transition.' *Nature,* **457**, 441-445.

Olivares, M.J., González-Jamett, A.M., Guerra, M.J., Baez-Matus, X., Haro-Acuña, V., Martínez-Quiles, N. and Cárdenas, A.M. (2014). 'Src kinases regulate de novo actin polymerization during exocytosis in neuroendocrine chromaffin cells.' *PLoS One*, **9**(6), e99001. doi: 10.1371/journal.pone.0099001.

Olsen, M.K., Reszka, A.A. and Abraham, I. (1998). 'KT5720 and U-98017 inhibit MAPK and alter the cytoskeleton and cell morphology.' *J. Cell. Physiol.*, **176**(3), 525-536.

Palade, G.E. and Palay, S.L. (1954). 'Electron microscope observations of interneuronal and neuromuscular synapses.' *Anat. Rec.*, **118**(2), 335-336.

Palay, S.L. (1956). 'Synapses in the central nervous system.' *J. Biophys. Biochem. Cytol.* **2**(4 Suppl), 193-202.

Papadopulos, A. (2017). 'Membrane shaping by actin and myosin during regulated exocytosis.' *Mol. Cell. Neurosci.*, **84**, 93-99.

Papadopulos, A., Tomatis, V.M., Kasula, R. and Meunier, F.A. (2015). 'The cortical acto-myosin network: from diffusion barrier to functional gateway in the transport of neurosecretory vesicles to the plasma membrane.' *Front. Endocrinol. (Lausanne)*, **4**, 153, doi: 10.3389/fendo.2013.00153.

Parisiadou, L., Yu, J., Sbobio, C., Chengsong, X., Liu, G., Sun, L., Gu, X.L., Lin, X., Crowley, N.A., Lovinger, D.M. and Cai, H. (2014). 'LRRK2 regulates synaptogenesis and dopamine receptor activation through modulation of PKA activity.' *Nat. Neurosci.*, **17**(3), 367-376.

Park, A.J., Havekes, R., Choi, J.H., Luczak, V., Nie, T., Huang, T. and Abel, T. (2014). 'A presynaptic role for PKA in synaptic tagging and memory.' *Neurobiol. Learn. Mem.*, **114**, 101-112.

Petrov, A.M., Giniatullin, A.R. and Zefirov, A.L. (2008). 'Role of the cAMP cascade in the turnover of synaptic vesicles of the frog motor nerve terminal.' *Neurochem. J.*, **2**, 175-182.

Pinto, C., Hübner, N., Gille, A., Richter, M., Mou, T.C., Sprang, S.R. and Seifert, R. (2009). 'Differential interactions of the catalytic subunits of adenylyl cyclase with forskolin analogs.' *Biochem. Pharmacol.*, **78**(1), 62-69.

Quan, A., McGeachie, A.B., Keating, D.J., van Dam, E.M., Rusak, J., Chau, N., Malladi, C.S., Chen, C., McCluskey, A., Cousin, M.A. and Robinson, P.J. (2007). 'Myristyl trimethyl ammonium bromide and octadecyl trimethyl ammonium bromide are surface-active small molecule dynamin inhibitors that block endocytosis mediated by dynamin I or dynamin II.' *Mol. Pharmacol.*, **72**(6), 1425-1439.

Reisler, E. and Egelman, E.H. (2007). 'Actin structure and function: what we still do not understand.' *J. Biol. Chem.*, **282**(50), 36133-36137.

Rizo, J. and Rosenmund, C. (2008). 'Synaptic vesicle fusion.*' Nat. Struct. Mol. Biol.* **15**(7), 665-674.

Rizzoli, S.O. (2014). 'Synaptic vesicle recycling: steps and principles.' *EMBO J.*, **33**(8), 788-822.

Rizzoli, S.O. and Betz, W.J. (2003). 'All change at the synapse.' *Nature*, **423**, 591-592.

Rizzoli, S.O. and Betz, W.J. (2004). 'The structural organization of the readily releasable pool of synaptic vesicles.' *Science*, **303**(5666), 2037-2039.

Rizzoli, S.O. and Betz, W.J. (2005). ‘Synaptic vesicle pools.’ *Nat. Rev. Neurosci.*, **6**(1), 57-69.

Rizzoli, S.O. and Jahn, R. (2007). ‘Kiss-and-run, collapse and 'readily retrievable' vesicles.’ *Traffic*, **8**(9), 1137-1144.

Robertson, M.J., Horatscheck, A., Sauer, S., von Kleist, L., Baker, J.R., Stahlschmidt, W., Nazaré, M., Whiting, A., Chau, N., Robinson, P.J., Haucke, V. and McCluskey, A. (2016). ‘5-Aryl-2-(naphtha-1-yl)sulfonamido-thiazol-4(5H)-ones as clathrin inhibitors’. *Organic & Biomolecular Chemistry.* **14**(47), 11266-11278.

Robinson, M.S., and Bonifacino, J.S. (2001). ‘Adaptor-related proteins.’ *Curr. Opin. Cell. Biol.*, **13**(4), 444-453.

Robinson, P.J. (1991). ‘Dephosphin, a 96,000 Da substrate of protein kinase C in synaptosomal cytosol, is phosphorylated in intact synaptosomes.’ *FEBS Lett.*, **282**(2), 388-392.

Robinson, P.J., Liu, K.A., Powell, K.A., Fykse, E.M. and Südhof, T.C. (1994). ‘Phosphorylation of dynamin I and synaptic-vesicle recycling.’ *Trends Neurosci.*, **17**(8), 348-353.

Römer, W., Pontani, L., Sorre, B., Rentero, C., Berland, L., Chambon, V., Lamaze, C., Bassereau, P., Sykes, C., Gaus, K. and Johannes, L. (2010). ‘Actin dynamics drive membrane reorganization and scission in clathrin-independent endocytosis.’ *Cell*, **140**(4), 540-553.

Ryan, T.A. (1999). ‘Inhibitors of myosin light chain kinase block synaptic vesicle pool mobilization during action potential firing.’ *J. Neurosci.*, **19**(4), 1317-1323.

Saheki, Y. and De Camilli, P. (2012). ‘Synaptic vesicle endocytosis.’ *Cold Spring Harb. Perspect. Biol.*, **4**(9). doi: 10.1101/cshperspect.a005645.

Sandana, R. and Dessauer, C.W. (2009). ‘Physiological roles for G protein-regulated adenylyl cyclase isoforms: insights from knockout and overexpression studies.’ *Neurosignals*, **17**(1), 5-22.

Sandberg, M., Butt, E., Nolte, C., Fischer, L., Halbrügge, M., Beltman, J., Jahnsen, T., Genieser, H.G., Jastorff, B. and Walter, U. (1991). ‘Characterization of Sp-5,6-dichloro-1-beta-D-ribofuranosylbenzimidazole- 3',5'-monophosphorothioate (Sp-5,6-DCl-

cBiMPS) as a potent and specific activator of cyclic-AMP-dependent protein kinase in cell extracts and intact cells.' *Biochem. J.*, 279(2), 521-527.

Sandquist, J.C. and Means, A.R. (2008). 'The C-terminal tail region of nonmuscle myosin II directs isoform-specific distribution in migrating cells.' *Mol. Biol. Cell*, **19**(12), 5156-5167.

Sawaya, M.R., Kudryashov, D.S., Pahkov, I., Adisetiyo, H., Reisler, E. and Yeates, T.O. (2008). 'Multiple crystal structures of actin dimers and their implications for interactions in the actin filament.' *Acta. Crystallogr. D. Biol. Crystallogr.*, **64**(4), 454-465.

Schikorski, T. and Stevens, C.F. (1997). 'Quantitative ultrastructural analysis of hippocampal excitatory synapses.' *J. Neurosci.*, **17**(15), 5858-5867.

Schmid, S.L. and Frolov, V.A. (2011). 'Dynamin: functional design of a membrane fission catalyst.' *Annu. Rev. Cell. Dev. Biol.*, **27**, 79-105.

Schmidt, M., Dekker, F.J. and Maarsingh, H. (2013). 'Exchange protein directly activated by cAMP (epac): A multidomain cAMP mediator in the regulation of diverse biological functions.' *Pharmacol. Rev.*, **65**(2), 670-709.

Schweizer, F.E. and Ryan, T.A. (2006). 'The synaptic vesicle: cycle of exocytosis and endocytosis.' *Curr. Opin. Neurobiol.*, **16**(3), 298-304.

Seabrooke, S. and Stewart, B.A. (2011). 'Synaptic transmission and plasticity are modulated by nonmuscle myosin II at the neuromuscular junction of *Drosophila*.' *J. Neurophysiol.*, **105**(5), 1966-1976.

Seabrooke, S., Qiu, X. and Stewart, B.A. (2010). 'Nonmuscle Myosin II helps regulate synaptic vesicle mobility at the *Drosophila* neuromuscular junction.' *B.M.C. Neurosci.*, **11**(37).

Seamon, K.B. and Daly, J.W. (1981). 'Forskolin: a unique diterpene activator of cyclic AMP-generating systems.' *J. Cyclic. Nucleotides Res.*, **7**(4), 201-224.

Seino, S. and Shibasaki, T. (2005). 'PKA-dependent and PKA-independent pathways for cAMP-regulated exocytosis.' *Physiol. Rev.*, **85**(4), 1303-1342.

Shi, L., Shen, Q.T., Kiel, A., Wang, J., Wang, H.W., Melia, T.J., Rothman, J.E. and Pincet, F. (2012). 'SNARE proteins: one to fuse and three to keep the nascent fusion pore open.' *Science*, **335**(6074), 1355-1359.

Shu, S., Liu, X. and Korn, E.D. (2005). 'Blebbistatin and blebbistatin-inactivated myosin II inhibit myosin II-independent processes in *Dictyostelium*.' *P.N.A.S.*, **102**(5), 1472-1477.

Shupliakov, O., Bloom, O., Gustafsson, J.S., Kjaerulff, O., Low, P., Tomilin, N., Pieribone, V.A., Greengard, P. and Brodin, L. (2002). 'Impaired recycling of synaptic vesicles after acute perturbation of the presynaptic actin cytoskeleton.' *P.N.A.S.*, **99**(22), 14476-14481.

Shutova, M.S. and Svitkina, T.M. (2018). 'Common and specific functions of nonmuscle myosin II paralogs in cells.' *Biochemistry (Mosc.)*, **83**(12), 1459-1468.

Sihra, T.S. (1997). 'Protein phosphorylation and dephosphorylation in isolated nerve terminals (synaptosomes).' In: Hemmings H.C. (1997). Regulatory protein modification: techniques and protocols. Totowa, NJ: Humana Press.

Sim, A.T., Herd, L., Proctor, D.T., Baldwin, M.L., Meunier, F.A. and Rostas, J.A. (2006). 'High throughput analysis of endogenous glutamate release using a fluorescence plate reader.' *J. Neurosci. Methods*, **153**(1), 43-47.

Singh, D. (2017). 'Phosphorylation sites on specific neuronal proteins can control the mode of synaptic vesicle exocytosis and thereby regulate synaptic transmission.' Doctoral thesis, UCLan, Preston.

Smillie, K.J. and Cousin, M.A. (2005). 'Dynamin I phosphorylation and the control of synaptic vesicle endocytosis.' *Biochem. Soc. Symp.*, (72), 87-97.

Sokac, A.M., Schietroma, C., Gundersen, C.B. and Bement, W.M. (2006). 'Myosin-1c couples assembling actin to membranes to drive compensatory endocytosis.' *Dev. Cell*, **11**(5), 629-640.

Somlyo, A.P. and Somlyo, A.V. (2003). 'Ca^{2+} sensitivity of smooth muscle and nonmuscle myosin II: modulated by G proteins, kinases, and myosin phosphatase.' *Physiol. Rev.*, **83**(4), 1325-1358.

Sone, M., Suzuki, E., Hoshino, M., Hou, D., Kuromi, H., Fukata, M., Kuroda, S., Kaibuchi, K., Nabeshima, Y. and Hama, C. (2000). 'Synaptic development is controlled in the periactive zones of *Drosophila* synapses.' *Development*, **127**(9), 4157-4168.

Song, B.D., Yarar, D. and Schmid, S.L. (2004). 'An assembly-incompetent mutant establishes a requirement for dynamin self-assembly in clathrin-mediated endocytosis *in vivo*.' *Mol. Biol. Cell.*, **15**(5), 2243-2252.

Southwick, F.S. (2000). 'Gelsolin and ADF/cofilin enhance the actin dynamics of motile cells.' *P.N.A.S.*, **97**(13), 6936-6938.

Sovkan, T., Kaempf, N., Sakaba, T., Vollweiter, D., Goerdeler, F., Puchkov, D., Kononenko, N.L. and Haucke, V. (2017). 'Synaptic vesicle endocytosis occurs on multiple timescales and is mediated by formin-dependent actin assembly.' *Neuron*, **93**(4), 854-866.

Stavoe, A.K.H. and Colón-Ramos, D.A. (2012). 'Netrin instructs synaptic vesicle clustering through Rac GTPase, MIG-10, and the actin cytoskeleton.' *J. Cell. Biol.*, **197**(1), 75-88.

Staykova, M., Holmes, D.P., Read, C. and Stone, H.A. (2011). 'Mechanics of surface area regulation in cells examined with confined lipid membranes.' *P.N.A.S.*, **108**(22), 9084-9088.

Ster, J., Bock, F.D., Guérineau, N.C., Janossy, A., Barrère-Lemaire, S., Bos, J.L., Bockaert, J. and Fagni, L. (2007). 'Exchange protein activated by cAMP (Epac) mediates cAMP activation of p38 MAPK and modulation of Ca^{2+}-dependent K^{+} channels in cerebellar neurons.' *P.N.A.S.*, **104**(7), 2519-2524.

Stowell, M.H., Marks, B., Wigge, P. and McMahon, H.T. (1999). 'Nucleotide-dependent conformational changes in dynamin: evidence for a mechanochemical molecular spring.' *Nat. Cell. Biol.*, **1**(1), 27-32.

Südhof, T.C. (2004). 'The synaptic vesicle cycle.' *Annu. Rev. Neurosci.*, **27**, 509-547.

Südhof, T.C. (2013). 'Neurotransmitter release: the last millisecond in the life of a synaptic vesicle.' *Neuron*, **80**(3), 675-690.

Südhof, T.C. and Rizo, J. (2011). 'Synaptic vesicle exocytosis.' *Cold Spring Harb. Perspect. Biol.*, **3**(12). doi: 10.1101/cshperspect.a005637.

Südhof, T.C. and Rothman, J.E. (2009). 'Membrane fusion: grappling with SNARE and SM proteins'. *Science*, **323**(5913), 474-477.

Sunahara, R.K., Dessauer, C.W. and Gilman, A.G. (1996). 'Complexity and diversity of mammalian adenylyl cyclases.' *Annu. Rev. Pharmacol. Toxicol.*, **36**, 461-480.

Taira, K., Umikawa, M., Takei, K., Myagmar, B.E., Shinzato, M., Machida, N., Uezato, H., Nonaka, S. and Kariya, K. (2004). 'The Traf2- and Nck-interacting kinase as a putative effector of Rap2 to regulate actin cytoskeleton.' *J. Biol. Chem.*, **279**(47), 49488-49496.

Takamori, S., Holt, M., Stenius, K., Lemke, E.A., Grønborg, M., Riedel, D., Urlaub, H., Schenck, S., Brügger, B., Ringler, P., Müller, S.A., Rammner, B., Gräter, F., Hub, J.S., De Groot, B.L., Mieskes, G., Moriyama, Y., Klingauf, J., Grubmüller, H., Heuser, J., Wieland, F. and Jahn, R. (2006). 'Molecular anatomy of a trafficking organelle.' *Cell*, **127**(4), 831-846.

Takata, F., Dohgu, S., Nishioku, T., Takahashi, H., Harada, E., Makino, I., Nakashima, M., Yamauchi, A. and Kataoka, Y. (2009). 'Adrenomedullin-induced relaxation of rat brain pericytes is related to the reduced phosphorylation of myosin light chain through the cAMP/PKA signaling pathway.' *Neurosci. Lett.*, **449**(1), 71-75.

Takei, K. and Haucke, V. (2001). 'Clathrin-mediated endocytosis: membrane factors pull the trigger.' *Trends Cell Biol.*, **11**(9), 385-391.

Takei, K., McPherson, P.S., Schmid, S.L. and De Camilli, P. (1995). 'Tubular membrane invaginations coated by dynamin rings are induced by GTP-γS in nerve terminals.' *Nature*, **374**, 186-190.

Tan, J.L., Ravid, S. and Spudich, J.A. (1992). 'Control of nonmuscle myosins by phosphorylation.' *Annu. Rev. Biochem.*, **61**, 721-759.

Tan, Y.Q., Li, J. and Chen, H.W. (2022). 'Epac, a positive or negative signaling molecule in cardiovascular diseases'. *Biomedicine & Pharmacotherapy*, **148**, 112726.

Tang, W.J. and Hurley, J.H. (1998). 'Catalytic mechanism and regulation of mammalian adenylyl cyclases.' *Mol. Pharmacol.*, **54**(2), 231-240.

Taylor, M.J., Lampe, M. and Merrifield, C.J. (2012). 'A feedback loop between dynamin and actin recruitment during clathrin-mediated endocytosis.' *PLoS Biol.*, **10**(4), e1001302.

Tibbs, G.R., Barrie, A.P., Van Mieghem, F.J., McMahon, H.T. and Nicholls, D.G. (1989). 'Repetitive action potentials in isolated nerve terminals in the presence of 4-

aminopyridine: effects on cytosolic free Ca^{2+} and glutamate release.' *J. Neurochem.*, **53**(6), 1693-1699.

Trudeau, L.E., Emery, D.G. and Haydon, P.G. (1996). 'Direct modulation of the secretory machinery underlies PKA-dependent synaptic facilitation in hippocampal neurons.' *Neuron*, **17**(4), 789-797.

Tzounopoulos, T., Janz, R., Südhof, T.C., Nicoll, R.A. and Malenka, R.C. (1998). 'A role for cAMP in long-term depression at hippocampal mossy fiber synapses.' *Neuron*, **21**(4), 837-845.

Vavylonis, D., Yang, Q. and O'Shaughnessy, B. (2005). 'Actin polymerization kinetics, cap structure, and fluctuations.' *P.N.A.S.*, **102**(24), 8543-8548.

Vicente-Manzanares, M., Ma, X., Adelstein, R.S. and Horwitz, A.R. (2009). 'Non-muscle myosin II takes centre stage in cell adhesion and migration.' *Nat. Rev. Mol. Cell Biol.*, **10**(11), 778-790.

Vicente-Manzanares, M., Zareno, J., Whitmore, L., Choi, C.K. and Horwitz, A.F. (2007). 'Regulation of protrusion, adhesion dynamics, and polarity by myosins IIA and IIB in migrating cells.' *J. Cell Biol.*, **176**(5), 573-580.

Villanueva, J., Torregrosa-Hetland, C.J., García-Martínez, V., del Mar Francés, M., Viniegra, S. and Gutiérrez, L.M. (2012). 'The F-actin cortex in chromaffin granule dynamics and fusion: a minireview.' *J. Mol. Neurosci.*, **48**, 323-327.

Vindin, H. and Gunning, P. (2013). 'Cytoskeletal tropomyosins: choreographers of actin filament functional diversity.' *J. Muscle. Res. Cell Motil.*, **34**(3-4), 261-274.

Volynski, K.E. and Krishnakumar, S.S. (2018). 'Synergistic control of neurotransmitter release by different members of the synaptotagmin family'. *Curr Opin Neurobiol*., **51**, 154-162.

Von der Ecken, J., Müller, M., Lehman, W., Manstein, D.J., Penczek, P.A. and Raunser, S. (2015). 'Structure of the F-actin-tropomyosin complex.' *Nature,* **519**(7541), 114-117.

Von Kleist, L., Stahlschmidt, W., Bulut, H., Gromova, K., Puchkov, D., Robertson, M.J., MacGregor, K.A., Tomilin, N., Pechstein, A., Chau, N., Chircop, M., Sakoff, J., von Kries, J.P., Saenger, W., Kräusslich, H.G., Shupliakov, O., Robinson, P.J., McCluskey,

A. and Haucke, V. (2011). ‘Role of the clathrin terminal domain in regulating coated pit dynamics revealed by small molecule inhibition.’ *Cell*, **146**(3), 471-484.

Wagh, D., Terry-Lorenzo, R., Waites, C.L., Leal-Ortiz, S.A., Maas, C., Reimer, R.J. and Garner, C.C. (2015). ‘Piccolo directs activity dependent F-actin assembly from presynaptic active zones via Daam1.’ *PLoS One*, **10**(4), e0120093.

Waites, C.L. and Garner, C.C. (2011). ‘Presynaptic function in health and disease.’ *Trends Neurosci.*, **34**(6), 326-337.

Walsh, D.A., Perkins, J.P. and Krebs, E.G. (1968). ‘An adenosine 3',5'-monophosphate-dependent protein kinase from rabbit skeletal muscle.’ *J. Biol. Chem.*, **243**(13), 3763-3765.

Wang, A., Ma, X., Conti, M.A. and Adelstein, R.S. (2011). ‘Distinct and redundant roles of the non-muscle myosin II isoforms and functional domains.’ *Biochem. Soc. Trans.*, **39**(5), 1131-1135.

Wang, H. and Sieburth, D. (2013). ‘PKA controls calcium influx into motor neurons during a rhythmic behavior.’ *PloS. Genet.*, **9**(9):e1003831.

Watanabe, S. and Boucrot, .E. (2017). ‘Fast and ultrafast endocytosis.’ *Curr. Opin. Cell Biol.*, **47**, 64-71.

Watanabe, S., Liu, Q., Davis, M.W., Hollopeter, G., Thomas, N., Jorgensen, N.B. and Jorgensen, E.M. (2013). ‘Ultrafast endocytosis at Caenorhabditis elegans neuromuscular junctions’. *eLife* **2**, e00723. https://doi.org/10.7554/eLife.00723.

Watanabe, S., Rost, B.R., Camacho-Pérez, M., Davis, M.W., Söhl-Kielczynski, B., Rosenmund, C. and Jorgenson, E.M. (2013). ‘Ultrafast endocytosis at mouse hippocampal synapses.’ *Nature*, **504**(7479), 242-247.

Watanabe, S., Trimbuch, T., Camacho-Pérez, M., Rost, B.R., Brokowski, B., Söhl-Kielczynski, B., Felies, A., Davis, M.W., Rosenmund, C. and Jorgenson, E.M. (2014). ‘Clathrin regenerates synaptic vesicles from endosomes.’ *Nature*, **515**(7526), 228-233.

Weisskopf, M.G., Castillo, P.E., Zalutsky, R.A. and Nicoll, R.A. (1994). ‘Mediation of hippocampal mossy fiber long-term potentiation by cyclic AMP.’ *Science*, **265**(5180), 1878-1882.

Wen, P.J., Grenklo, S., Arpino, G., Tan, X., Liao, H., Heureaux, J., Peng, S., Chiang, H., Hamid, E., Zhao, W., Shin, W., Näreoja, T., Evergren, E., Jin, Y., Karlsson, R., Ebert, S.N., Jin, A., Liu, A.P., Shupliakov, O. and Wu, L. (2016). 'Actin dynamics provides membrane tension to merge fusing vesicles into the plasma membrane.' *Nature Communications*, **7**(12604), doi: 10.1038/ncomms12604.

Wendt, T., Taylor, D., Trybus, K.M. and Taylor, K. (2001). 'Three-dimensional image reconstruction of dephosphorylated smooth muscle heavy meromyosin reveals asymmetry in the interaction between myosin heads and placement of subfragment 2.' *P.N.A.S.*, **98**(8), 4361-4366.

Whittaker, V.P. (1959). 'The isolation and characterization of acetylcholine containing particles from brain.' *Biochem. J.*, **72**, 694-705.

Whittaker, V.P., Michaelson, I.A. and Kirkland, R.J.A. (1964). 'The separation of synaptic vesicles from nerve-ending particles ('Synaptosomes').' *Biochem. J.*, **90**(2), 293-303.

Wilhelm, B.G., Mandad, S., Truckenbrodt, S., Kröhnert, K., Schäfer, C., Rammner, B., Koo, S.J., Claßen, G.A., Krauss, M., Haucke, V., Urlaub, H. and Rizzoli, S.O. (2014). 'Composition of isolated synaptic boutons reveals the amounts of vesicle trafficking proteins.' *Science*, **344**(6187), 1023-1028.

Wu, W. and Wu, L.G. (2007). 'Rapid bulk endocytosis and its kinetics of fission pore closure at a central synapse.' *P.N.A.S.*, **104**(24), 10234-10239.

Xu, K., Zhong, G. and Zhuang, X. (2013). 'Actin, spectrin, and associated proteins form a periodic cytoskeletal structure in axons.' *Science*, **339**(6118), 452-456.

Yamashita, T., Hige, T. and Takahashi, T. (2005). 'Vesicle endocytosis requires dynamin-dependent GTP hydrolysis at a fast CNS synapse.' *Science*, **307**(5706), 124-127.

Yarmola, E.G., Somasundaram, T., Boring, T.A., Spector, I. and Bubb, M.R. (2000). 'Actin-latrunculin A structure and function. Differential modulation of actin-binding protein function by latrunculin A.' *J. Biol. Chem.*, **275**(36), 28120-28127.

Yoshihara, M., Suzuki, K. and Kidokoro, Y. (2000). 'Two independent pathways mediated by cAMP and protein kinase A enhance spontaneous transmitter release at *Drosophila* neuromuscular junctions.' *J. Neurosci.*, **20**(22), 8315-8322.

Yu, H.Y. and Bement, W.M. (2007). ‘Control of local actin assembly by membrane fusion-dependent compartment mixing.’ *Nat. Cell Biol.*, **9**(2), 149-159.

Yu, S.C., Jánosi, B., Liewald, J.F., Wabnig, S. and Gottschalk, A. (2018). ‘Endophilin A and B join forces with clathrin to mediate synaptic vesicle recycling in *Caenorhabditis elegans*.’ *Front. Mol. Neurosci.*, **11**(196).

Zhang, Q., Li, Y. and Tsien, R.W. (2009). ‘The dynamic control of kiss-and-run and vesicular reuse probed with single nanoparticles.’ *Science*, **323**(5920), 1448-1453.

Zhong, H., Sia, G.M., Sato, T.R., Gary, N.W., Mao, T., Khuchua, Z., Huganir, R.L. and Svoboda, K. (2009). ‘Subcellular dynamics of type II PKA in neurons.’ *Neuron*, **62**(3), 363-374.

Zhong, Y. and Wu, C.F. (1991). ‘Altered synaptic plasticity in *Drosophila* memory mutants with a defective cyclic AMP cascade.’ *Science* **251**(4990), 198-201.

Zhou, Q., Lai, Y., Bacaj, T., Zhao, M., Lyubimov, A.Y., Uervirojnangkoorn, M., Zeldin, O.B., Brewster, A.S., Sauter, N.K., Cohen, A.E., Soltis, S.M., Alonso-Mori, R., Chollet, M., Lemke, H.T., Pfuetzner, .R.A., Choi, U.B., Weis, W.I., Diao, J., Südhof, T.C. and Brunger, A.T. (2015). ‘Architecture of the synaptotagmin–SNARE machinery for neuronal exocytosis.’ *Nature*, **525**(7567), 62-67.

Zhu, J.J., Qin, Y., Zhao, M., Van Aelst, L. and Malinow R. (2002). ‘Ras and Rap control AMPA receptor trafficking during synaptic plasticity.’ *Cell*, **110**(4), 443-455.

Zouwail, S., Pettitt, T.R., Dove, S.K., Chibalina, M.V., Powner, D.J., Haynes, L., Wakelam, M.J.O. and Insall, R.H. (2005). ‘Phospholipase D activity is essential for actin localization and actin-based motility in *Dictyostelium*.’ *Biochem. J.,* **389**(1), 207-214.

APPENDIX A: Review of Previous Results

A Review of Previous Research

Results in Appendix A are from previous research carried out by Ashton's group. These results were created whilst establishing optimal experimental conditions for use with the synaptosome model and are displayed here to aid understanding of new and original data presented and discussed in the main text of this thesis. Note that these experiments are not original to this thesis and represent unpublished work as of this submission. I did not take part in these experiments.

A.1 Maximal Glutamate Release

For a direct comparison between FM 2-10 dye and Glu release assays it was necessary that the stimuli employed in this thesis produced a maximal level of Glu release. To determine this, synaptosomes were treated with the three stimuli (HK, ION and 4AP) – see Chapter 2 for further details – in the presence of a range of extracellular Ca^{2+} concentrations ($[Ca^{2+}]_e$) (Figure A1). It can be observed that 5 mM $[Ca^{2+}]_e$ produced maximal Glu release for all stimuli, and a further increase in $[Ca^{2+}]_e$ to 10 mM had no effect on HK evoked Glu release (Figure A1a), and possibly decreased Glu release with ION and 4AP (Figure A1b, A1c). For all experiments in this study a concentration of 5 mM $[Ca^{2+}]_e$ was therefore used with each of the three stimuli to maximally release Glu from synaptosomes.

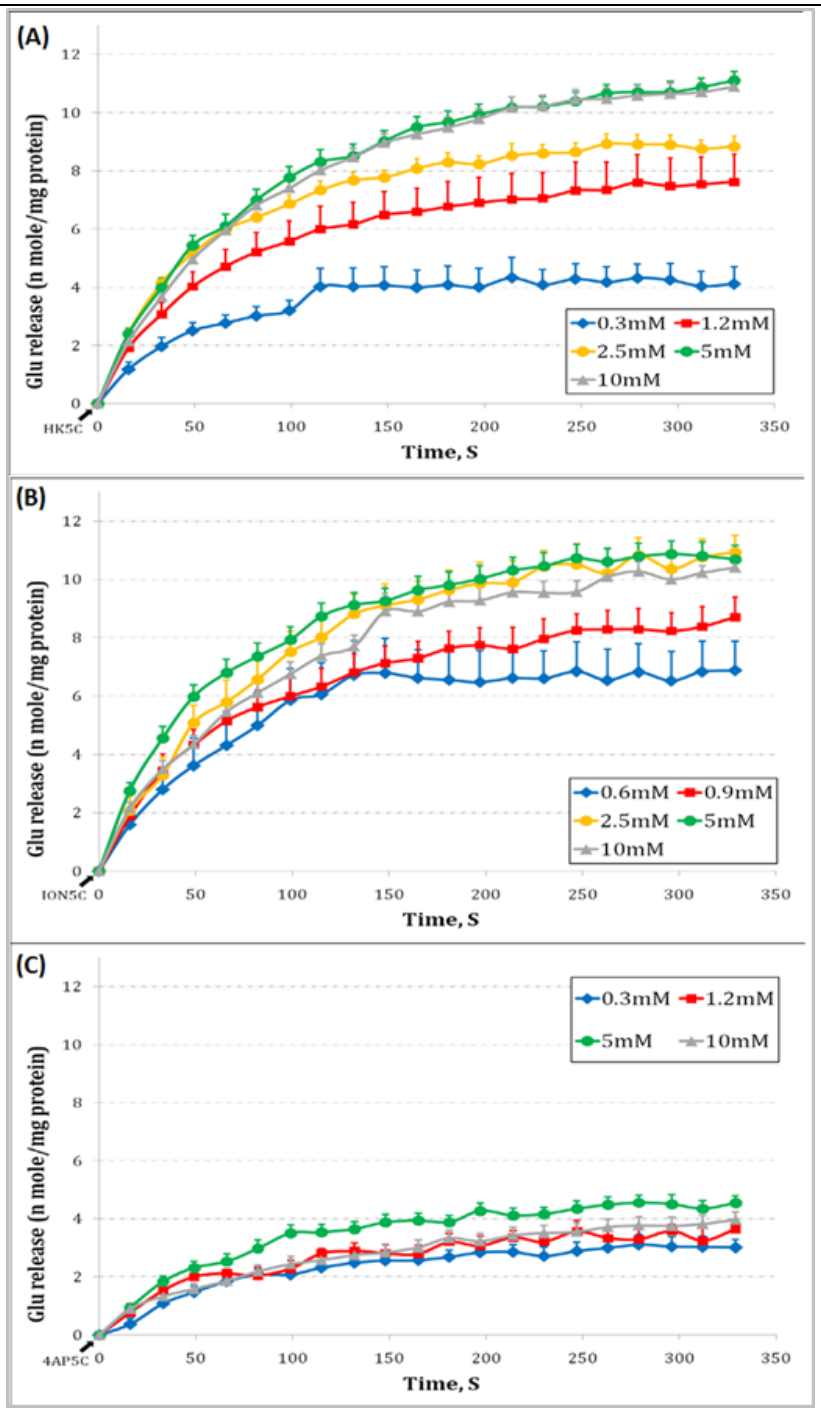

Figure A1: Effect of a range of $[Ca^{2+}]_e$ upon evoked Glu release. Stimulation in the presence of 5 mM $[Ca^{2+}]_e$ induces maximal Glu release for (a) HK, (b) ION and (c) 4AP. Values represented are the mean plus SEM from 4 independent experiments (Ashton and colleagues, unpublished results).

Stimulation with 4AP5C produced a lower maximal Glu release (4.5 mol/mg of protein) (Figure A1c) compared to HK5C (10.8 mol/mg of protein) ($p < 0.05$) (Figure A1a) or ION5C (11 mol/mg of protein) ($p < 0.05$) (Figure A1 B) with 5 mM $[Ca^{2+}]_e$. An explanation for this can be found when looking at the different

changes in $[Ca^{2+}]_i$ produced by each stimulus (Figure A2). 4AP5C produces a lower, more gradual change in $[Ca^{2+}]_i$ (180 ± 20 nM Ca^{2+}) than either HK5C or ION5C (370 ± 25 nM Ca^{2+}) ($p < 0.05$), which is interpreted as 4AP5C only being able to release the RRP of SVs whilst HK5C and ION5C can release both the RRP and the RP of SVs.

Though HK5C and ION5C achieved an equivalent level of $[Ca^{2+}]_i$, this is mediated by different kinetics (Figure A2). HK5C produced much of the $[Ca^{2+}]_i$ increase upon the application of stimulation, plateauing rapidly (< 10 s), potentially due to voltage-gated Ca^{2+} channel desensitisation (Bähring and Covarrubias, 2011), whilst ION5C produced a more gradual increase in $[Ca^{2+}]_i$ which plateaus later (~40 s) (Figure A2). This speed of achieving maximum increase in $[Ca^{2+}]_i$ applies in every experiment that has been performed in this thesis and over 10 years of research. However, it appears that distinct batches of ionomycin may achieve higher maximum $[Ca^{2+}]_i$ although maximum release is not altered (Ashton, unpublished observation).

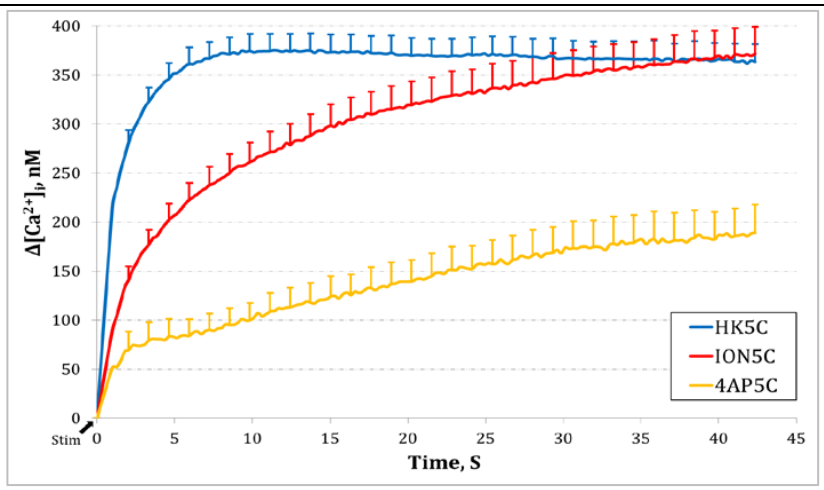

Figure A2: Effect of stimuli upon cytosolic free calcium $[Ca^{2+}]_i$. All three stimuli employed in this study produce a change in $[Ca^{2+}]_i$ via different kinetics. 4AP5C evokes a significantly lower $[Ca^{2+}]_i$ change than HK5C or ION5C ($p < 0.05$). No significant difference was observed between HK5C and ION5C ($p > 0.05$) in this set of experiments. Values represented are the mean plus SEM from 3 independent experiments (Ashton and colleagues, unpublished results).

A.2 Expression of Glutamate release

There are several ways to express the Glu release and all these still show the relevant properties and can be employed. To show the similarity between the different plots, below shows a comparison between HK5C and ION5C evoked Glu release for 5 independent experiments. The simplest way is to plot Glu release as arbitrary units of fluorescence (Figure A3a). This is the method mainly employed throughout the thesis. Because the sensitivity of the assay is measured in every experiment by adding 10 nmol of Glu then one can convert arbitrary fluorescence units to nmol of Glu (Figure A3b). Every experiment uses approximately the same amount of synaptosome material for release and this can be determined by a protein assay so the results can be expresses as nmol of Glu per mg of protein (Figure A3c). Finally, one can expressed the results relative to the maximum control release: herein, we have used HK5C maximum release as the 100% control (Figure A3d). Some results in the thesis are expressed in this manner.

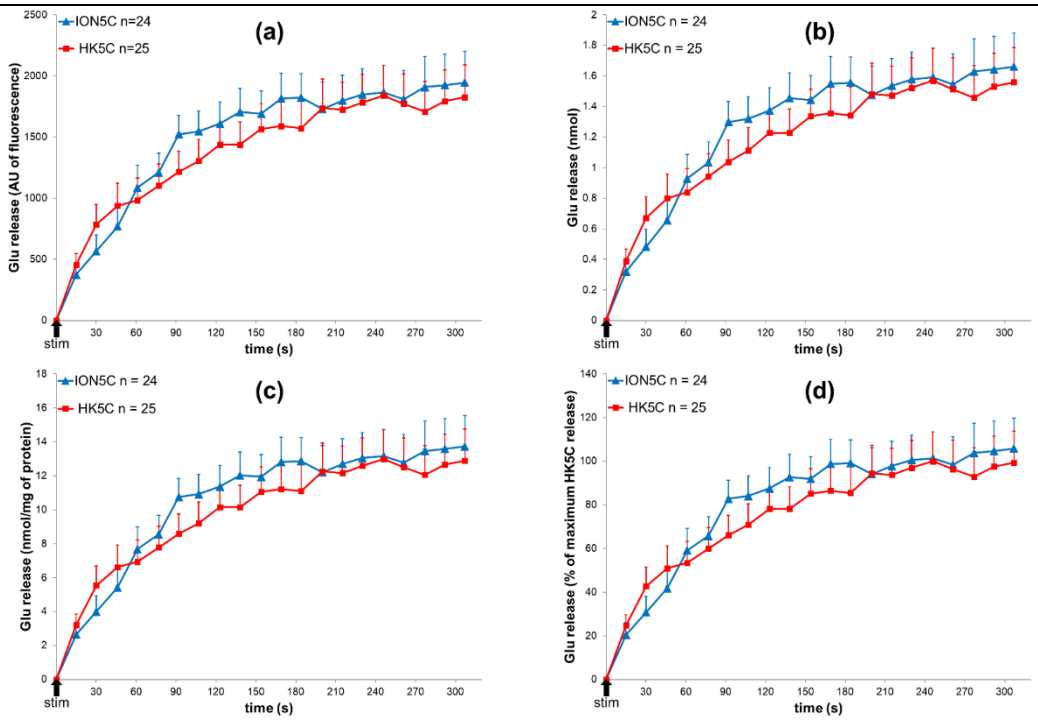

Figure A3: Different expressions of Glu release data. The Glu release result data can be interpreted and presented as (a) arbitrary units (AU) of fluorescence (b) moles of Glu released, (c) moles of Glu per mass of synaptosomal protein or (d) percentage of maximum value. Values represented are the mean plus SEM from 5 independent experiments (Ashton and colleagues, unpublished results).

A.3 A Single Round of Exocytosis

Due to the kinetics of the FM 2-10 dye and Glu release assays, synaptosomes in this study are subject to long stimulation periods (between 60-300 s). Due to this long duration of stimulation, there is a possibility that SVs could undergo multiple rounds of recycling, refilling with and re-releasing Glu, leading to an erroneous interpretation of Glu release. Further, it is possible that SV releasing via KR could retain its FM 2-10 dye label while undergoing several rounds of KR recycling, or SV could lose its FM 2-10 dye and release additional Glu without a link to dye fluorescence. To accurately compare Glu and FM 2-10 dye release, it is essential to establish that SVs are only undergoing one round of release during the stimulation and measurement period.

In order to ensure recycling was not occurring during stimulation and measurement, synaptosomes were acutely treated with 1 µM of the selective

vacuolar H^+ ATPase (V-ATPase) inhibitor bafilomycin A1. The V-ATPase pump is a complex found on SVs that is responsible for re-acidification of the vesicular lumen after endocytosis, which is vital for SVs to be refilled with Glu (Cotter *et al.*, 2015). Such acute bafilomycin A1 treatment has no effect upon the Glu content of non-exocytosed SVs and does not impede their release upon stimulation (Ikeda and Bekkers, 2008). An acute treatment of 1 µM bafilomycin A1 did not significantly affect Glu release compared with untreated controls, regardless of stimulation (Figure A4) ($p > 0.05$). If SVs were undergoing multiple rounds of recycling, the level of Glu release would be expected to decrease with the bafilomycin A1 treatment.

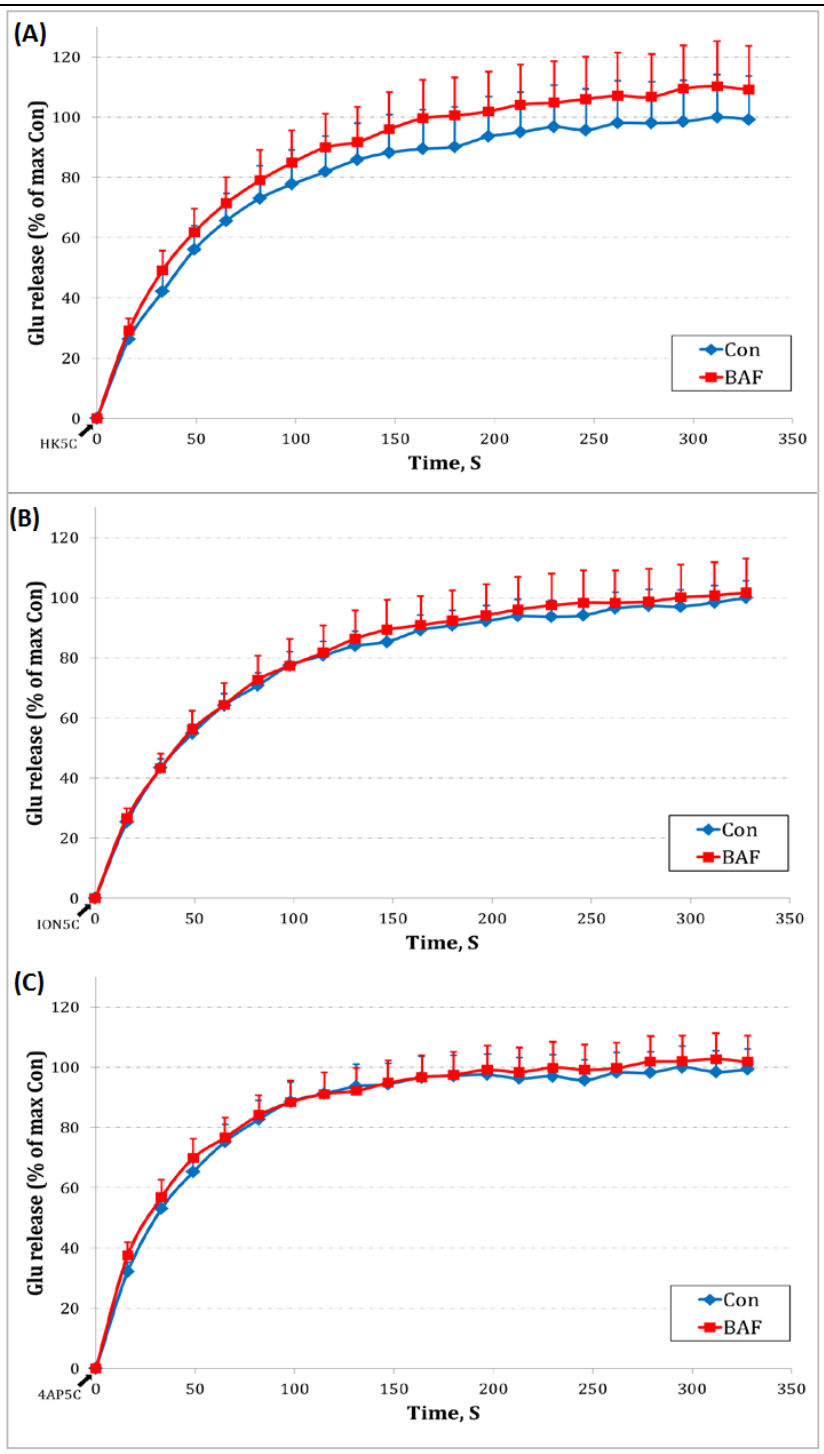

Figure A4: Effect of 1 µM bafilomycin A1 upon evoked Glu release. Treatment with 1 µM bafilomycin A1 does not significantly affect Glu release when stimulated with (a) HK5C, (b) ION5C or (c) 4AP5C compared to untreated controls ($p > 0.05$ for all). Values represented are the mean plus SEM from 4 independent experiments (Ashton and colleagues, unpublished results).

In order to demonstrate that during a first round of SV exocytosis involving both the RRP and the RP, there was no clathrin dependent recycling and re-release of some of these SVs, synaptosomes were treated normally (including the HK5C pre-stimulation; FM dye was included in this pre-loading for FM dye release measurements) and following recovery synaptosomes were incubated for 10 mins with DMSO solvent (control) or 15 µM Pitstop® 2 at 37ºC (Von Kleist *et al.*, 2011; Robertson *et al.*, 2016). Following a relevant washing step, SV release was evoked utilising ION5C for either the measurement of Glu (Figure A5) or FM 2-10 dye (Figure A6). Pitstop® 2 treatment did not perturb the total amount of Glu release indicating that both the RRP and the RP SVs were exocytosed and neither pool had a clathrin requirement. Similarly, there was no difference between control and Pitstop® 2 treatment for FM 2-10 dye release and this indicates that the RRP SVs still underwent KR exocytosis whilst the RP SVs release their FM dye content due to undergoing FF. This deduction was further confirmed because a joint drug treatment with Pitstop® 2 and dynasore did switch the RRP SVs to an FF mode (not shown).

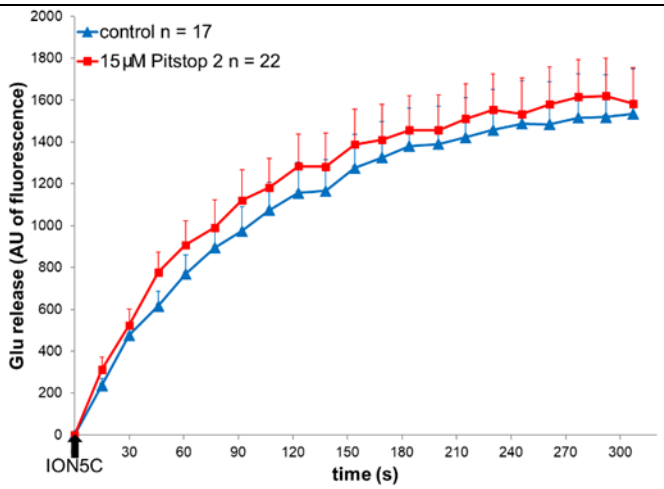

Figure A5: Effect of 15 µM Pitstop® 2 vs control upon ION5C evoked Glu release. Clathrin inhibition using 15 µM Pitstop® 2 caused no significant difference to ION5C evoked Glu release compared to non-drug controls ($p > 0.05$). Values represented are the mean plus SEM from 5 independent experiments (Ashton and colleagues, unpublished results).

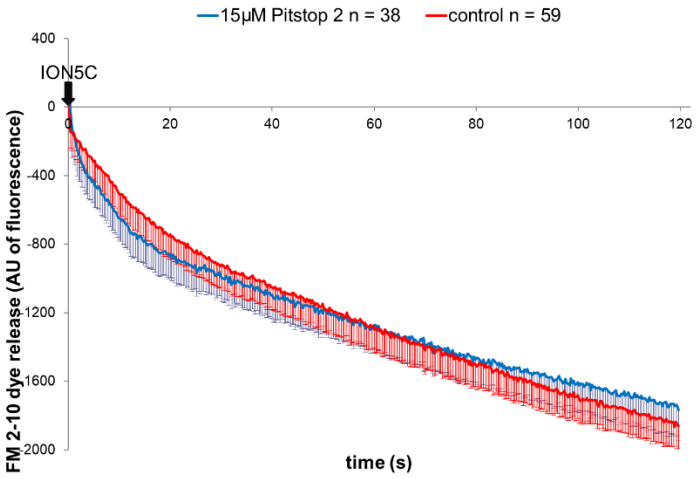

Figure A6: Effect of 15 μM Pitstop® 2 vs control upon ION5C evoked FM 2-10 dye release. Clathrin inhibition using 15 μM Pitstop® 2 caused no significant difference to ION5C evoked FM 2-10 dye release compared to non-drug controls ($p > 0.05$). Values represented are the mean plus SEM from 5 independent experiments (Ashton and colleagues, unpublished results).

These results suggested that a first round of exocytosis of RRP and RP SVs had no clathrin dependent requirement. However, we were able to investigate whether the recycling of the RRP or recycling of the RP for subsequent rounds of release had a clathrin requirement. We did this by simply pre-treating synaptosomes with 15 μM Pitstop® 2 prior to the initial HK5C pre-stimulation. Under such conditions, HK5C would release the RRP and RP but if such SVs had a clathrin requirement for recycling then these would not recycle and so would no longer be available for release during a second round of stimulation with ION5C. Figure A7 indicated that whilst there was a large amount of Glu release with ION5C in control treated terminals, there was a great reduction in the ION5C evoked release in the Pitstop® 2 pre-treated synaptosomes. That the reduction was due to loss of the RP SVs was shown when control and Pitstop® 2 treated synaptosomes were stimulated with 4AP5C which only released the RRP SVs (Figure A8). There was no significant difference between control and drug treated terminals indicating that perturbing clathrin did not affect the recycling and re-release of the RRP. Thus, these results indicate that the RRP SVs recycle by a clathrin independent mechanism whilst the RP SV recycles via a clathrin dependent process. These results complement the idea that the RRP recycles via a KR mechanism during normal physiological neurotransmitter release (which when using HK5C is dynamin and clathrin

independent) whilst the RP undergoes FF and then recycles via a clathrin dependent process.

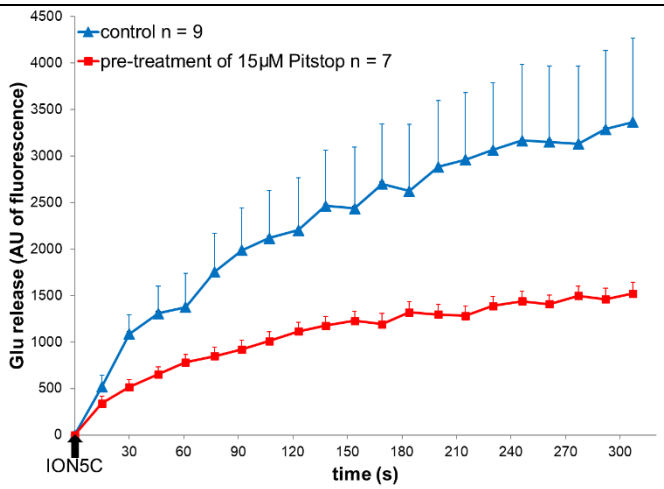

Figure A7: Effect of 15 μM Pitstop® 2 pre-treatment vs control upon ION5C evoked Glu release. Clathrin inhibition using 15 μM Pitstop® 2, treated before HK5C pre-stimulation, decreased ION5C evoked Glu release compared to non-drug controls from 60 s onwards ($p < 0.05$). Values represented are the mean plus SEM from 3 independent experiments (Ashton and colleagues, unpublished results).

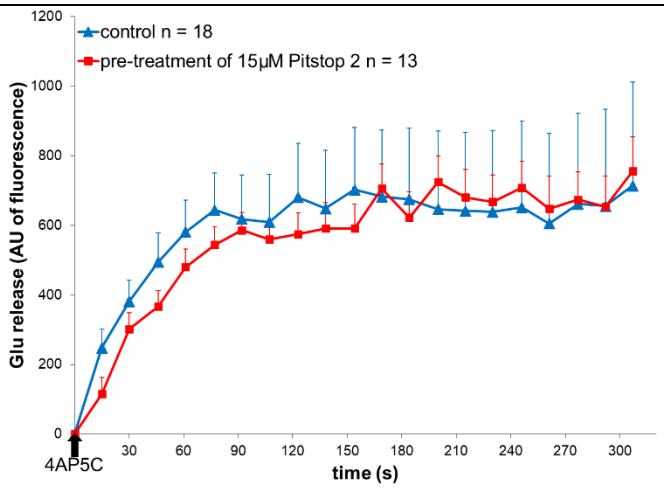

Figure A8: Effect of 15 μM Pitstop® 2 pre-treatment vs control upon 4AP5C evoked Glu release. Clathrin inhibition using 15 μM Pitstop® 2, treated before HK5C pre-stimulation, caused no significant difference to 4AP5C evoked Glu release compared to non-drug controls ($p > 0.05$). Values represented are the mean plus SEM from 4 independent experiments (Ashton and colleagues, unpublished results).

A.4 Maximal Labelling of Synaptic Vesicles with FM 2-10 Dye

Styryl dyes, such as FM 2-10, have been used extensively to label lipid membranes and in particular vesicular trafficking and recycling. In all experiments a concentration of 100 μM FM 2-10 dye was utilised, as many researchers have employed the same concentration (Baldwin, *et al.*, 2003; Cheung, *et al.*, 2010). Clayton and Cousin (2008) however, have previously suggested that the labelling of SVs, especially via bulk endocytosis, is dependent upon the concentration of FM 2-10 dye, and 1 mM but not 100 μM will fully label all SVs (Clayton and Cousin, 2008).

In order to ensure that all SVs are fully labelled with FM 2-10 dye, synaptosomes were incubated with 1 mM or 100 μM and evoked to release during a drug treatment (160 μM dynasore) which has been observed to increase exocytosis via FF mode (Figure A9). In this model system there was no significant difference in FM 2-10 dye release seen between synaptosomes loaded with 1 mM or 100 μM ($p > 0.05$), and drug treatment had no significant impact upon labelling or release of SVs ($p > 0.05$). If 100 μM FM 2-10 dye had been failing to label all releasable SVs, then a reduced amount of dye would be released.

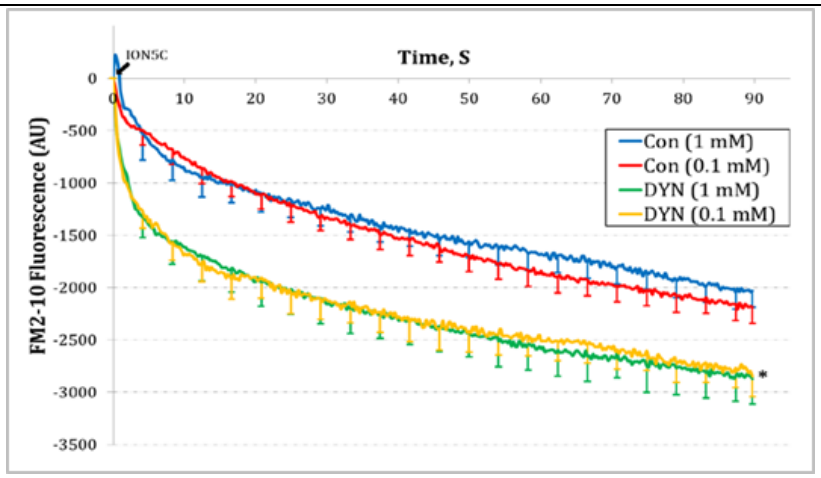

Figure A9: Difference between SVs loaded with 1 mM or 100 µM FM 2-10 dye. SVs loaded with 1 mM (blue) or 100 µM (red) release equivalent levels of FM 2-10 dye following stimulation ($p > 0.05$). Drug treatment, 160 µM dynasore, increases FM 2-10 dye release by a corresponding amount, regardless of amount of FM 2-10 dye loaded, following stimulation (green vs yellow) ($p > 0.05$). Values represented are the mean minus SEM from 4 independent experiments (Ashton and colleagues, unpublished results).

A.5 The Mode of Exocytosis is Stimulation Dependent

Each of the stimuli used in this thesis have been shown to evoke release through distinct $[Ca^{2+}]_i$ kinetics (Figure A2), and changes in $[Ca^{2+}]_i$ have been linked to regulating the mode of exocytosis of distinct pools (Alés, *et al.*, 1999), therefore each stimulus could evoke release of SV pools via unique modes. As the RRP is suggested to be released within 2 s of stimulation (Rizzoli and Betz, 2005), this time period was studied during FM 2-10 dye release for all stimuli (Figure A10a).

Interestingly HK5C and ION5C did not cause any significantly release of FM 2-10 dye in this period ($p > 0.05$), unlike 4AP5C ($p < 0.05$) (Figure A10a). It could be argued that this indicates no SVs are being release during this time period, however when the experiment was repeated with a pre-treatment of 0.8 µM OA (Figure A10b), an inhibitor of PP1 and PP2A which is known to convert all RRP SVs to FF mode of release (Ashton, *et al.*, 2011), an increase in FM 2-10 dye release was noted for all stimuli, that was not significantly different between

stimuli at 2 s ($p > 0.05$). Comparison of these results are interpreted as HK5C and ION5C releasing the RRP via KR mode under control conditions, while 4AP5C releases roughly half the RRP via KR and half by FF mode. All three stimuli release an equivalent amount of FM 2-10 dye during this period (2 s), suggesting it is the RRP being released.

In order to determine the exocytic mode of the RRP and RP, the fluorescence value of FM 2-10 dye release during control conditions was subtracted from the fluorescence value achieved during OA treatment (Figure A11). HK5C stimulation caused all RRP SVs to undergo KR mode within the first 2 s (Figure A11a), and all RP SVs to release via FF mode (after 2 s; Figure A11b). Stimulation with 4AP5C releases all RRP SVs, some via KR and some by FF mode, with fluorescence subtraction demonstrating that both modes contribute equally (Figure A11c). RP SVs do not release when synaptosomes are stimulated with 4AP5C, as this stimulus induced a lower average $[Ca^{2+}]_i$ compared to HK5C and ION5C, and this is unable to drive RP fusion (see Figure A1c and Figure A2).

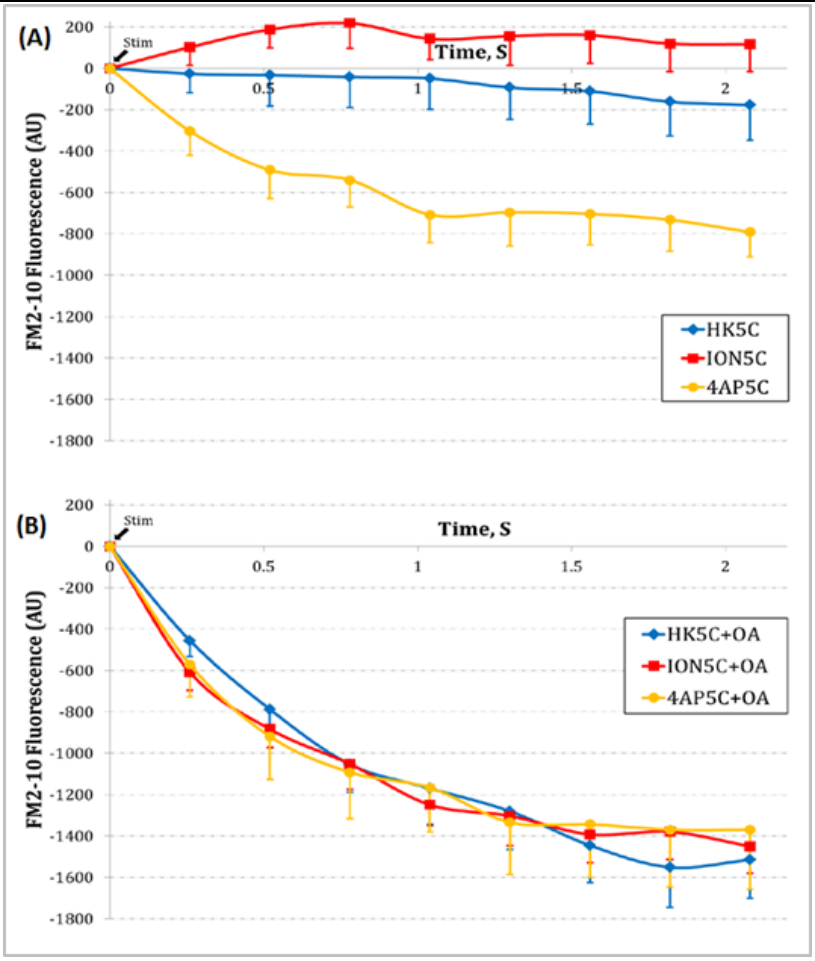

Figure A10: Mode of RRP release during control and 0.8 µM OA treatment. (a) Measurement of control levels of FM 2-10 dye release after stimulation during first 2 s. Only 4AP5C releases a significant amount of dye ($p < 0.05$). (b) Treatment with OA induces equivalent release of FM 2-10 dye regardless of stimulation over first 2 s ($p > 0.05$). Values represented are the mean plus SEM from 3 independent experiments (Ashton and colleagues, unpublished results).

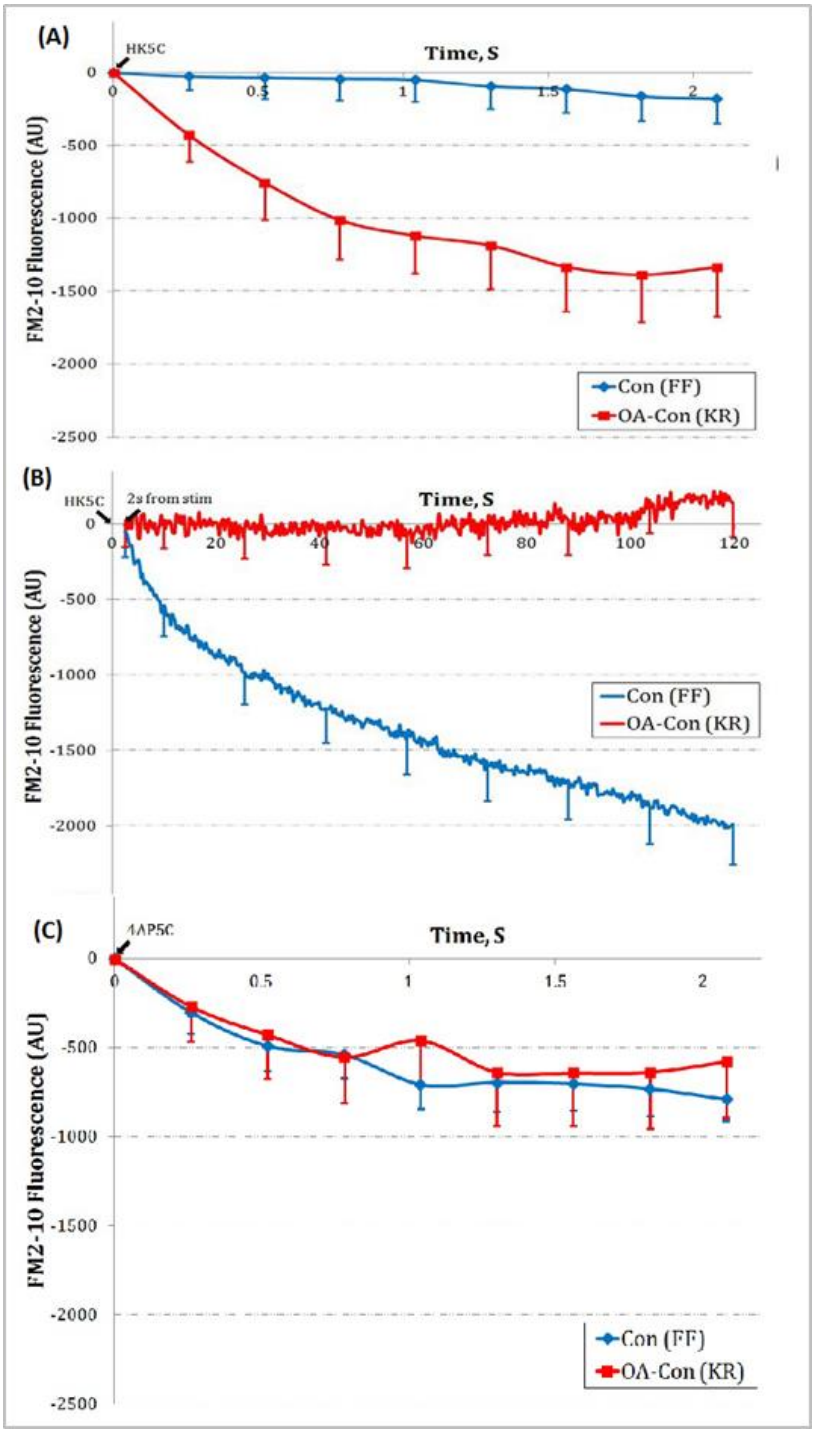

Figure A11: Mode of RRP and RP release during control and 0.8 µM OA treatment. When FM 2-10 dye fluorescence of control was subtracted from OA conditions, it was found that (a) all SVs release via KR during initial 2 s of HK5C stimulation and (b) remaining SVs are released via FF after 2 s. (c) During 4AP5C stimulation, all SVs are released by a combination of KR and FF for initial 2 s. Values represented are the mean plus SEM from 3 independent experiments (from Bhuva, 2015; Ashton and colleagues, unpublished results).

A.6 Presynaptic Proteins Regulating Exocytosis

Dynamin-1 could have a role in modulating the mode of exocytosis at the fusion pore. Previous research undertaken by Ashton group has demonstrated that inhibition of dynamin-1 GTPase activity with 160 µM dynasore did not perturb Glu release with any stimuli (Figure A12a-c) ($p > 0.05$), but significantly increased FM 2-10 dye release with ION5C and 4AP5C (Figure A12e-f) ($p < 0.05$). These results were interpreted as ION5C and 4AP5C having a dynamin-1 dependence to release the RRP via KR mode, while HK5C was able to release the RRP independent of dynamin-1.

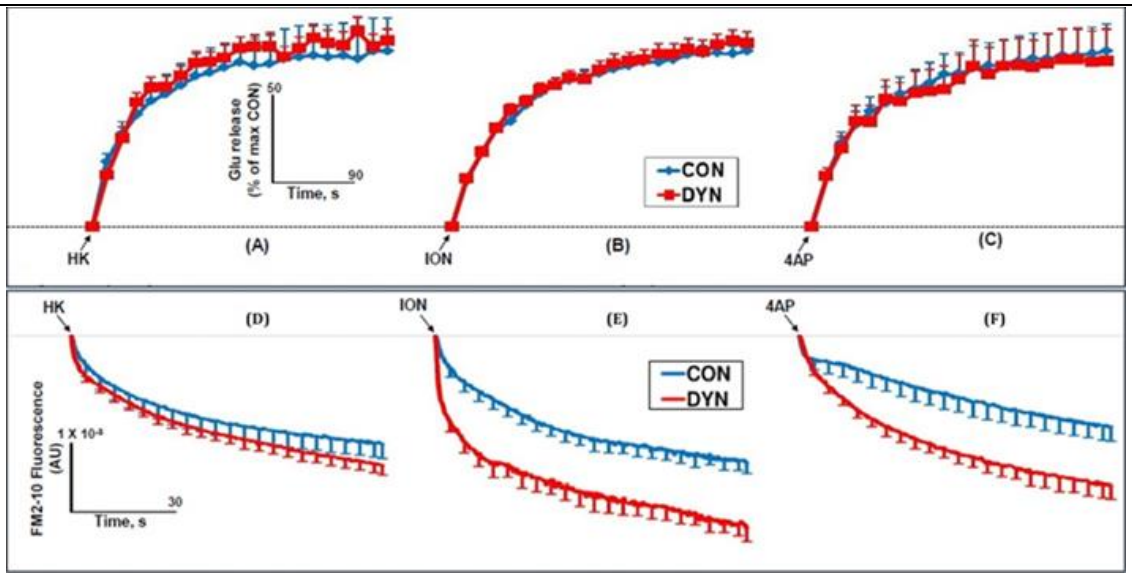

Figure A12: Effect of 160 µM dynasore vs control upon evoked Glu and FM 2-10 dye release. Treatment with 160 µM dynasore does not perturb Glu release evoked by (a) HK5C, (b) ION5C or (c) 4AP5C ($p > 0.05$). 160 µM dynasore (d) had no significant effect of HK5C evoked FM dye release ($p = 0.508$), (e) but increased ION5C ($p = 0.014$) and (f) increased 4AP5C evoked FM dye release ($p = 0.034$). Values represented are mean plus SEM from 4 experiments (Ashton and colleagues, unpublished results).

NMII has also been implicated in regulating the mode of exocytosis at the fusion pore (Neco, *et al.*, 2008; Berberian, *et al.*, 2009; Chan, *et al.*, 2010). Since no change in FM 2-10 dye release was observed when dynamin-1 was inhibited with dynasore during HK5C stimulation (Figure A12d), it was hypothesised that NMII could be responsible for regulating the fusion pore during this mode of exocytosis. Thus, NMII was blocked with 50 µM blebbistatin, a selective, high

affinity small molecule which blocks NMII by inhibiting ATPase activity (Shu, *et al.*, 2005; Kovacs, *et al.*, 2004).

A treatment of 50 µM blebbistatin did not perturb Glu release with any stimuli ($p > 0.05$) (Figure A13) but did significantly increase FM 2-10 dye release with HK5C stimulation only ($p < 0.05$) (Figure A14a). These data may suggest that NMII is able to close the fusion pore during HK5C stimulation, when the $[Ca^{2+}]_i$ level at the AZ is high (Figure A2), as Ca^{2+} is required to regulate NMII phosphorylation and activation (Martinsen, *et al.*, 2014). These data may also suggest that the $[Ca^{2+}]_i$ level achieved at the active zone during ION5C and 4AP5C stimulation may not be high enough to activate NMII, but satisfactory to activate dynamin-1 to regulate the exocytosing fusion pore (Figure A12e-f).

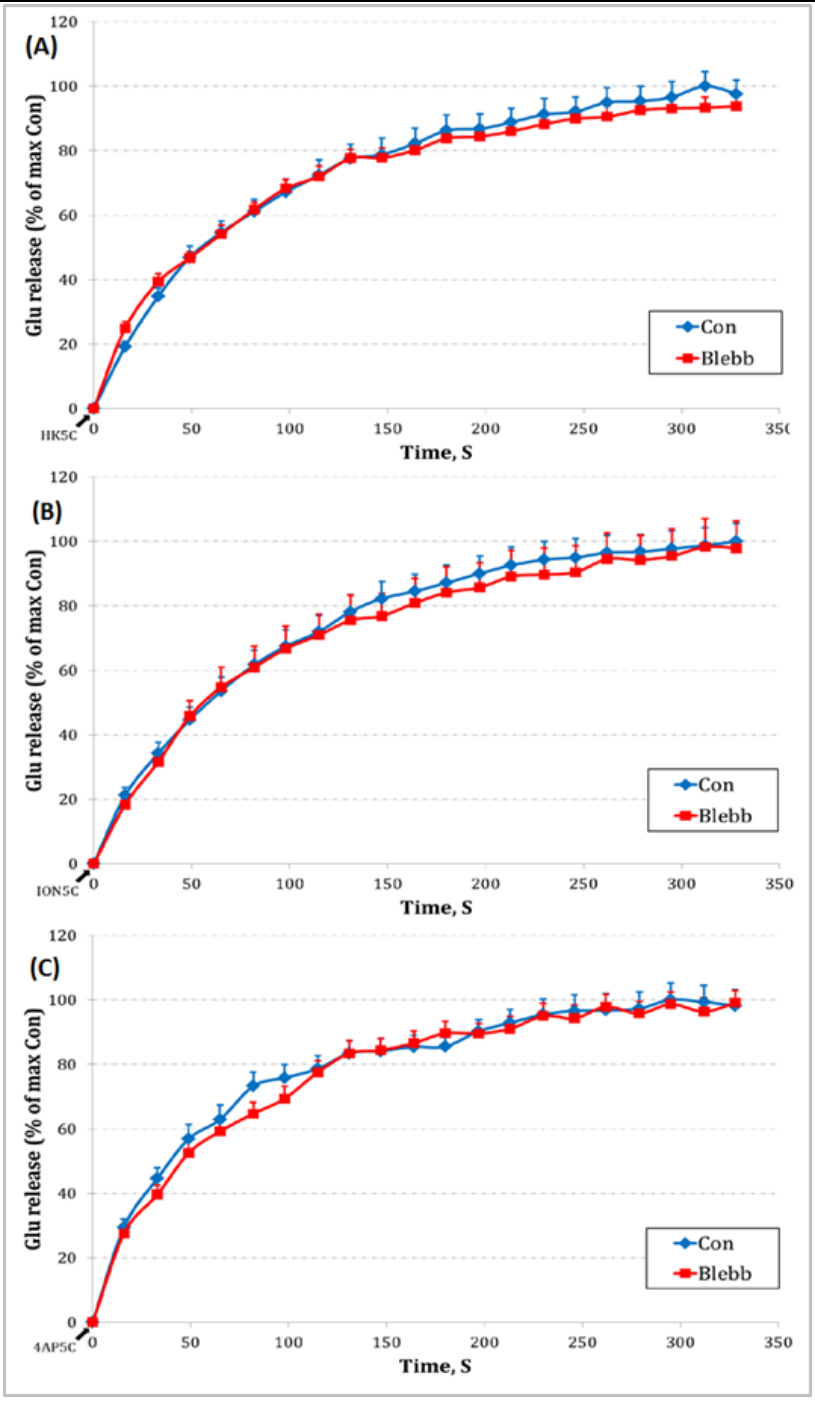

Figure A13: Effect of 50 µM blebbistatin upon evoked Glu release. Treatment with 50 µM blebbistatin (Blebb) did not significantly affect Glu release when stimulated with (a) HK5C, (b) ION5C or (c) 4AP5C ($p > 0.05$). Values represented are the mean plus SEM from 4 independent experiments (Ashton and colleagues, unpublished results).

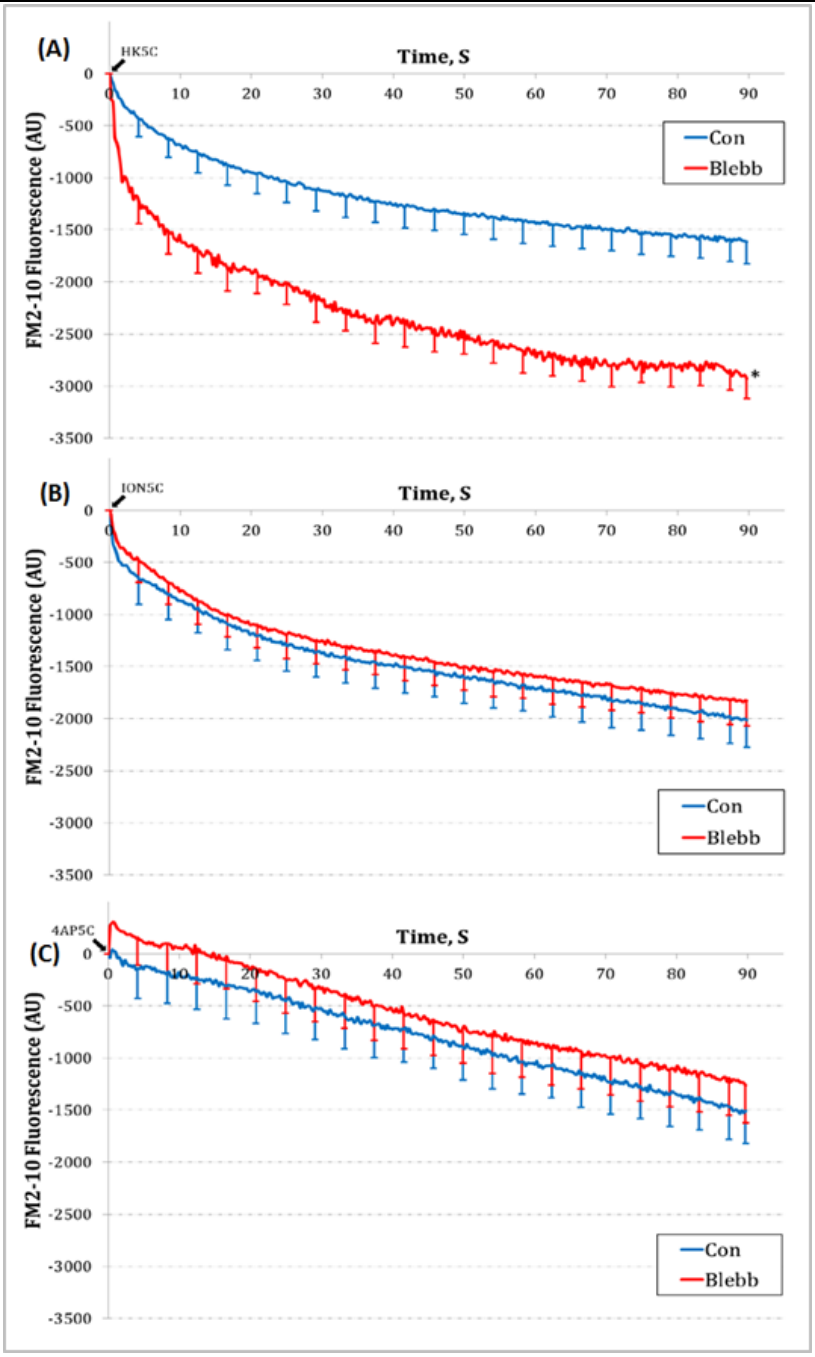

Figure A14: Effect of 50 µM blebbistatin upon evoked FM 2-10 dye release. Treatment with 50 µM blebbistatin (Blebb) significantly increased FM 2-10 dye release when stimulated with (a) HK5C ($p < 0.05$) but had no effect when stimulated with (b) ION5C ($p = 0.716$) or (c) 4AP5C ($p = 0.642$). Values represented are the mean plus SEM from 3 independent experiments (Ashton and colleagues, unpublished results).

The Ca^{2+}-dependent phosphatase PP2B may also have a role in regulating proteins which participate in exocytosis, as PP2B rapidly dephosphorylates many presynaptic proteins upon terminal depolarisation (Robinson, *et al.*, 1994). Inhibition of PP2B with 1 µM Cys A did not significantly affect Glu release (Figure A15a-c) ($p > 0.05$), but significantly decreased FM 2-10 dye release when stimulated with HK5C and ION5C (Figure A15e-f, respectively) ($p < 0.05$). This differs with some studies that have shown Cys A treatment increases Glu release (Gaydukov, *et al.,* 2013), but in the context of this model this further indicates maximal Glu release is being observed under these conditions already (i.e. with 5 mM $[Ca^{2+}]_e$ Figure A1).

When the effects of PP2B inhibition with 1 µM Cys A were investigated upon $[Ca^{2+}]_i$ levels, a significant increase was noted with all three stimuli (Figure A15g-i) ($p < 0.05$). These data are interpreted as the inhibition of PP2B causing more SVs to release via a KR mode of exocytosis, which could be due to the increased $[Ca^{2+}]_i$ level attained during Cys A treatment (Figure A15g-i). The lack of effect upon 4AP5C evoked Glu and FM 2-10 dye, even during an increase in $[Ca^{2+}]_i$ could suggest PP2B inhibition only affects the RP, since 4AP5C does not release the RP (Figure A1c, and Figure A2), and the RRP is already releasing via KR mode with both HK5C and ION5C stimuli (Figure A10a).

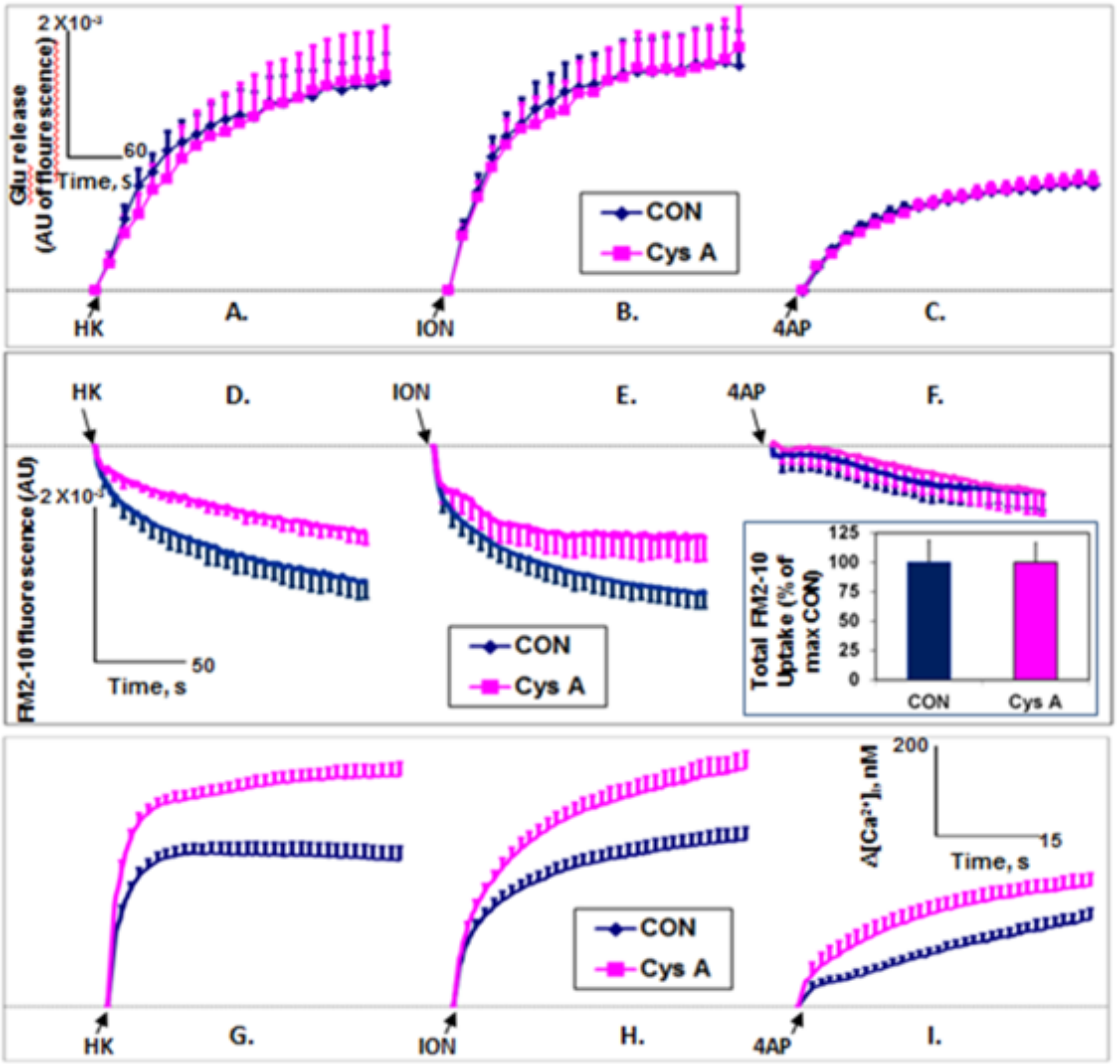

Figure A15: Effect of 1 µM Cys A upon evoked Glu and FM 2-10 dye release. 1 µM Cys A did not perturb Glu release evoked by (a) HK5C, (b) ION5C or (c) 4AP5C ($p > 0.05$ for all). 1 µM Cys A significantly decreased (d) HK5C ($p < 0.025$) and (e) ION5C ($p < 0.023$) evoked FM 2-10 dye release but (f) had no effect upon 4AP5C ($p = 0.985$) evoked FM 2-10 dye release. 1 µM Cys A significantly increased $[Ca^{2+}]_i$ levels with (g) HK5C ($p < 0.001$), (h) ION5C ($p < 0.044$) and (i) 4AP5C ($p < 0.049$) stimulation, compared to controls. Values represented are the mean plus SEM from 4 experiments (Ashton and colleagues, unpublished results).

A.7 Switching of HK5C Evoked Synaptic Vesicle Exocytosis From NMII Dependent KR to Dynamin Dependent KR

Ashton and colleagues have deciphered that HK5C activates PKCs that inactivate dynamin-1 but that activate NMII. Thus, one can make HK5C action switch from the NMII dependent pathway to the dynamin dependent pathway by inhibiting PKCs with Go 6983. Neither pre-treatment with Go 6983 followed by the addition of blebbistatin (Figure A16a) or dynasore (Figure A16b) perturbed the HK5C evoked Glu release indicating that these conditions did not perturb SV from exocytosing and releasing their neurotransmitter.

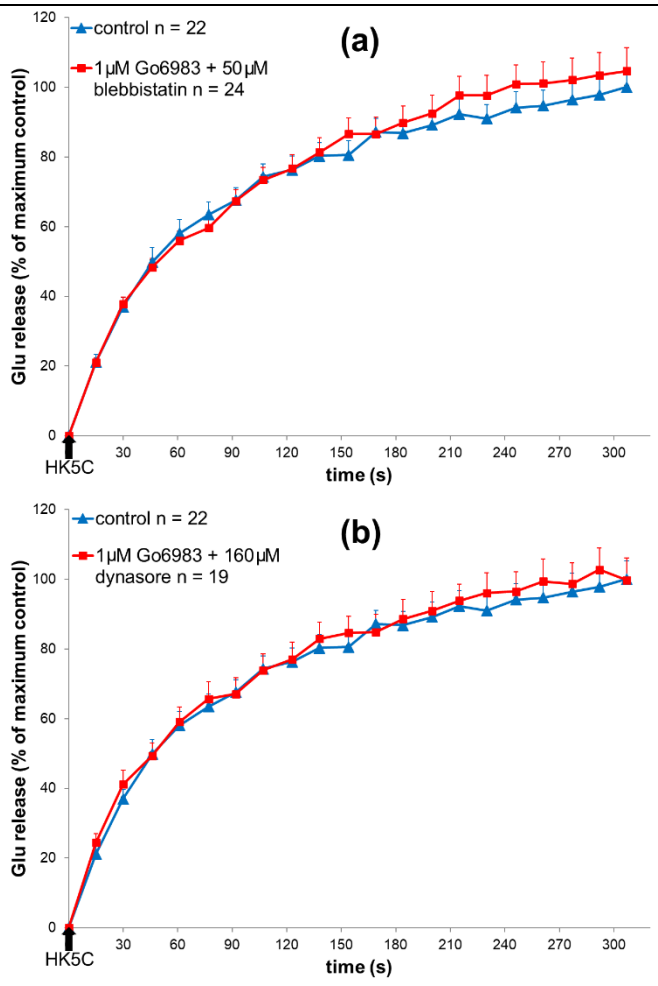

Figure A16: **Effect of 1 µM Go 6983 plus 50 µM blebbistatin or 160 µM dynasore upon evoked Glu release.** (a) 1 µM Go 6983 plus 50 µM blebbistatin did not significantly affect Glu release evoked by HK5C stimulation compared to non-drug controls. (b) 1 µM Go 6983 plus 160 µM dynasore did not significantly affect HK5C stimulation compared to non-drug controls. Values represented are the mean plus SEM from 4 experiments (Ashton and colleagues, unpublished results).

However, following pre-treatment with Go 6983, blebbistatin no longer switched the HK5C evoked RRP SVs to an FF mode as there was not an increase in FM dye release compared to the control (Figure A17a). Remarkably, such Go 6983 treatment now allowed dynasore to act on the HK5C evoked RRP SVs and these did switch to a FF mode (Figure A17b).

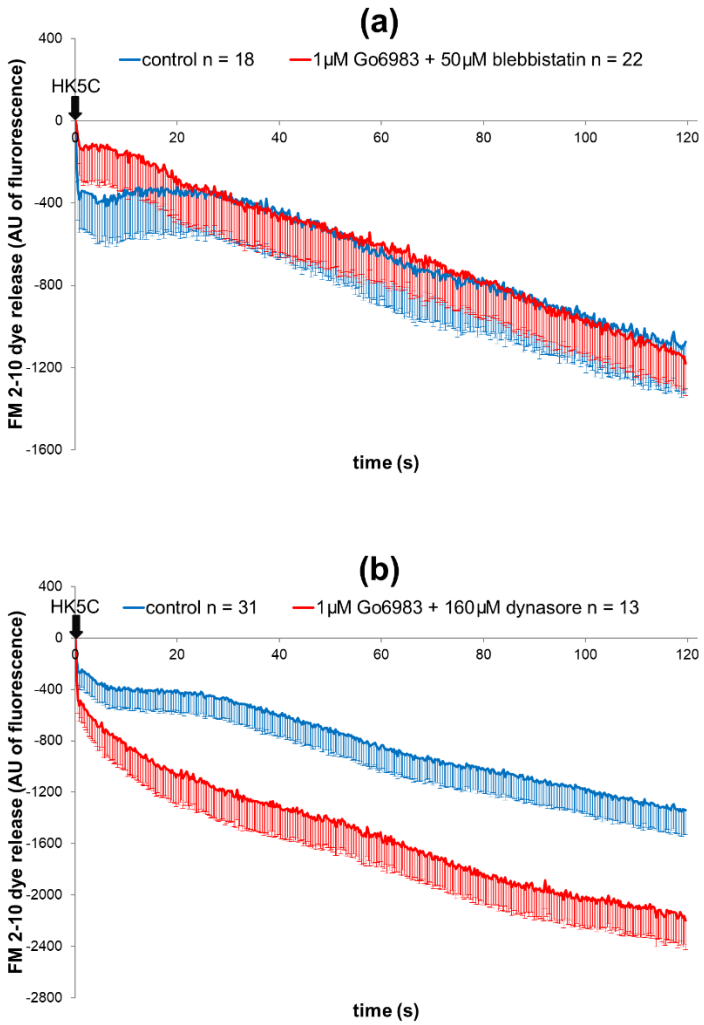

Figure A17: Effect of 1 µM Go 6983 plus 50 µM blebbistatin or 160 µM dynasore upon evoked FM 2-10 dye release. (a) 1 µM Go 6983 plus 50 µM blebbistatin did not significantly affect FM 2-10 dye release evoked by HK5C stimulation compared to non-drug controls. (b) 1 µM Go 6983 plus 160 µM dynasore significantly increased FM 2-10 dye release evoked by HK5C stimulation compared to non-drug controls. Values represented are the mean plus SEM from 3 experiments (Ashton and colleagues, unpublished results).

A.8 Switching of ION5C Evoked Synaptic Vesicle Exocytosis From Dynamin Dependent KR to NMII Dependent KR

Not only can one switch the HK5C stimulus to act on the dynamin dependent KR exocytosis, but one can also switch the ION5C stimulus to act through the NMII dependent pathways. This is achieved by using a low concentration of 40 nM PMA, an active phorbol ester, that can activate certain PKCs within the synaptosomes. Note that this concentration does not switch the RRP KR to FF mode alone although a higher concentration (1 µM PMA) does. However, neither 40 nM PMA plus blebbistatin (Figure A18a) treatment or 40 nM plus dynasore (Figure A18b) treatment perturbs the ION5C evoked Glu release. This indicates that the RRP and RP SVs are still undergoing exocytosis and releasing their neurotransmitter content.

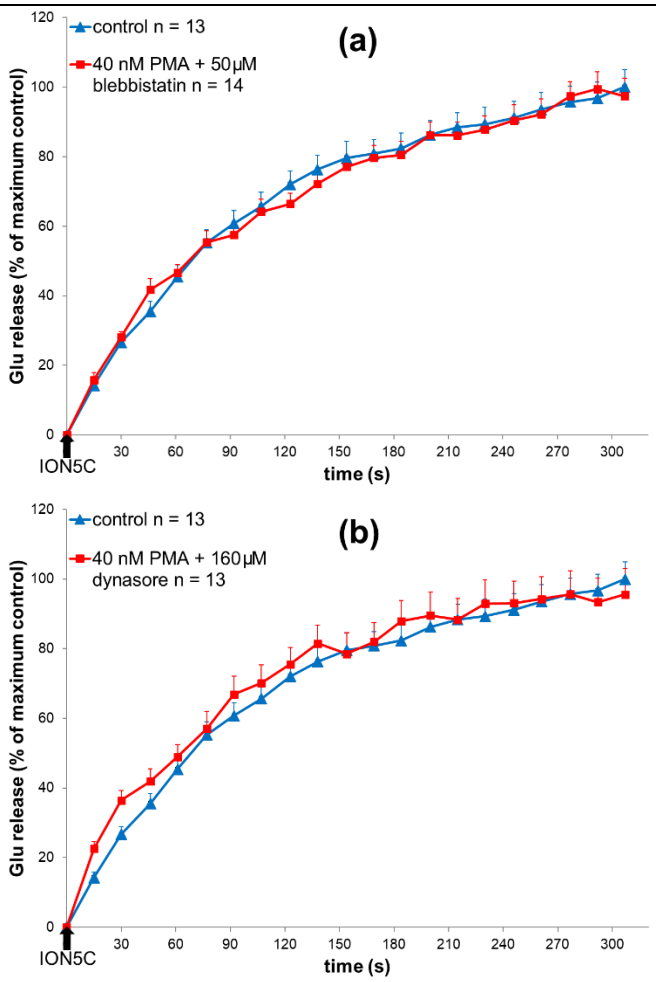

Figure A18: Effect of 40 nM PMA plus 50 µM blebbistatin or 160 µM dynasore upon evoked Glu release. (a) 40 nM PMA plus 50 µM blebbistatin did not significantly affect Glu release evoked by ION5C stimulation compared to non-drug controls. (b) 40 nM PMA plus 160 µM dynasore did not significantly affect Glu release evoked by ION5C stimulation compared to non-drug controls. Values represented are the mean plus SEM from 3 experiments (Ashton and colleagues, unpublished results).

However, following pre-treatment with 40 nM PMA, blebbistatin was able to switch the ION5C evoked RRP SVs to a FF mode as there was now an increase in FM dye release compared to the control (Figure A19a). Remarkably, such 40 nM PMA treatment now prevented dynasore acting on the ION5C evoked RRP SVs and these remained undergoing a KR mode such that there was no extra FM dye release (Figure A19b).

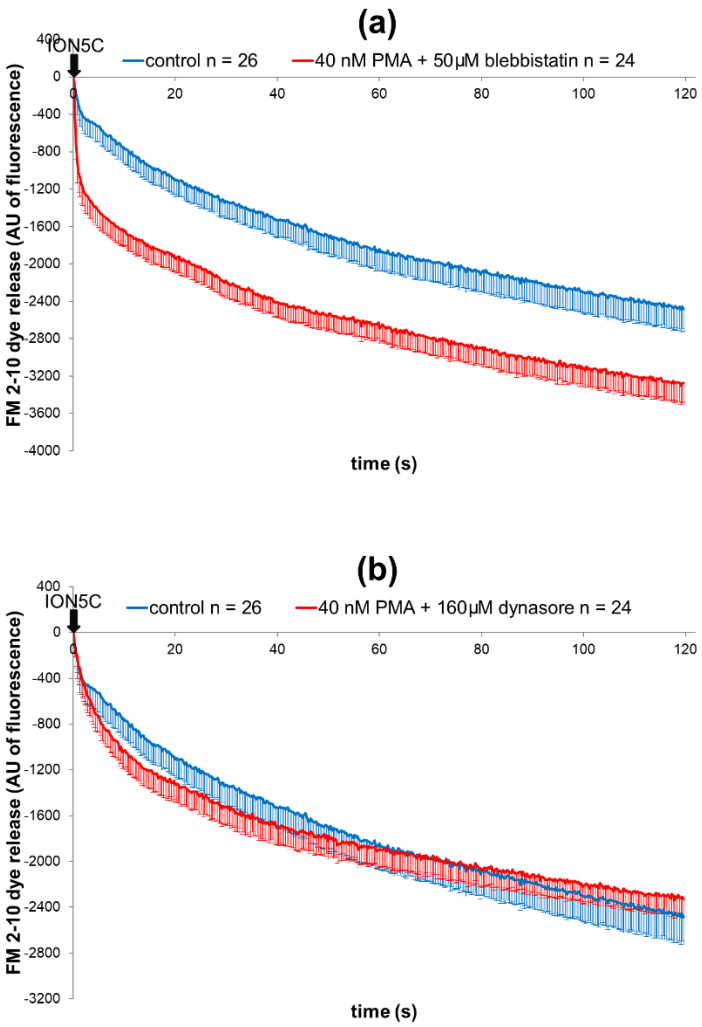

Figure A19: Effect of 40 nM PMA plus 50 µM blebbistatin or 160 µM dynasore upon evoked Glu release. (a) 40 nM PMA plus 50 µM blebbistatin significantly increased FM 2-10 dye release evoked by ION5C stimulation compared to non-drug controls. (b) 40 nM PMA plus 160 µM dynasore did not signiicantly affect FM 2-10 dye release evoked by ION5C stimulation compared to non-drug controls. Values represented are the mean plus SEM from 4 experiments (Ashton and colleagues, unpublished results).

APPENDIX B: Beeswarm Superplots of Results in This Thesis

B Beeswarm Superplots to Show Validity of Results

B.1 Beeswarm Introduction

Superplots are used to display data in graphs that highlight experimental robustness and experiment run-to-run variability. Superplots are so named as they display the distribution of the entire dataset, and report statistics (in this thesis this includes means, standard deviation error bars and p values) that address the reproducibility of the findings by colour-coding individual replicated runs of an experiment on top of means from different plate rows. Superplots are increasingly displayed to ensure that experimental models make statistical sense and show reproducible trends (Lord *et al.*, 2020).

The results for Glu release and FM dye release are calculated from many separate experiments in which the average basal is subtracted from the average stimulated (either HK5C, or ION5C) to get a measure of Ca^{2+} dependent release. There are 21 time points for Glu release whilst there are actually 461 time points measured for FM dye release. To allow the reader an idea of the spread of the data points, the last time point for Glu or FM release has been plotted for every individual measurement of a particular condition. This has been done using a beeswarm plot. In order to do this one has to plot both the stimulated values and the basal values and these are shown on the same plot.

All the Glu release in the chapters is corrected for the sensitivity of the assay for Glu. However, in the beeswarm plot the raw - uncorrected for Glu sensitivity - data has been plotted. This was done to show that in many cases the results still hold even without the sensitivity corrections factors. For FM dye experiments, the results used were those that were corrected to the same starting FM dye content as this varies depending on the exact amount of synaptosomes that are used and, without this correction, the statistics can be incorrect due to large differences in content leading to large errors. For both Glu and FM dye, the Ca^{2+} dependent release (mean and SEM) can be calculated by subtracting the average basal from the average stimulated values. These Ca^{2+} dependent release values can then be compared between the control non-drug

treated samples and the drug treated samples and the significant difference between these obtained. These are shown in the relevant tables.

In the beeswarm plots the individual stimulated values are shown as circles and the individual basal values are shown as triangles. These are colour coded for the individual experiments (shown as dates). The average of each individual experiment is given as a larger circle or triangle of the relevant colour (date) which are shown in the midpoint on the x-axis of the beeswarm plot for stimulated and for basal. Finally, the average of all the means are shown as a line and the error bar shows ± standard deviation (SD) at this midpoint of the stimulated and basal beeswarm plot. The whole plot represents a superplot.

The labelling of the beeswarm/superplots represent the number of the figure in the result chapter and the drug treatment that it applies to e.g. KT5720 treated Figure A3.1a indicates that this is the data taken from the KT5720 data shown in Figure 3.1a in Chapter 3. The control non-drug treated Ca^{2+} dependent value for both Glu and FM may represent the control for several of the drug treatments and so this control is labelled with the figures that it covers in the relevant chapter. This is the control that the drug treatment is related to in the relevant comparison statistical tables that are shown.

B.2 Beeswarm Superplots for Chapter 3

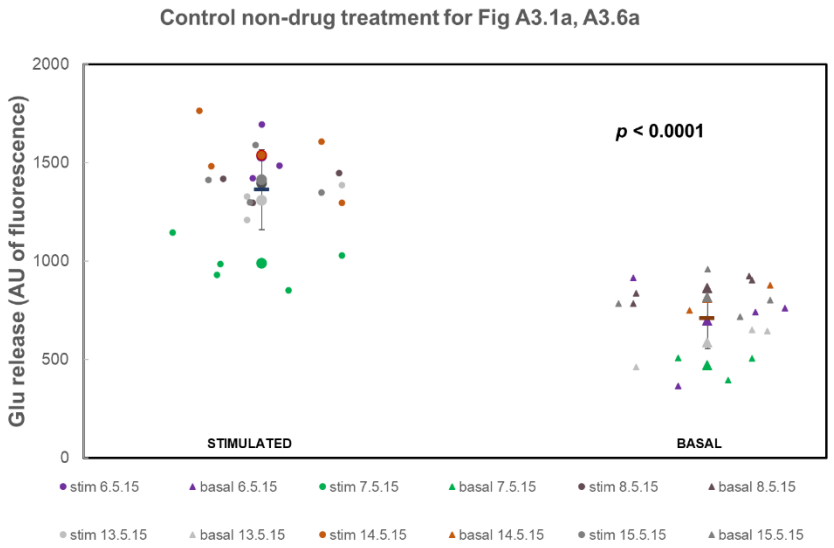

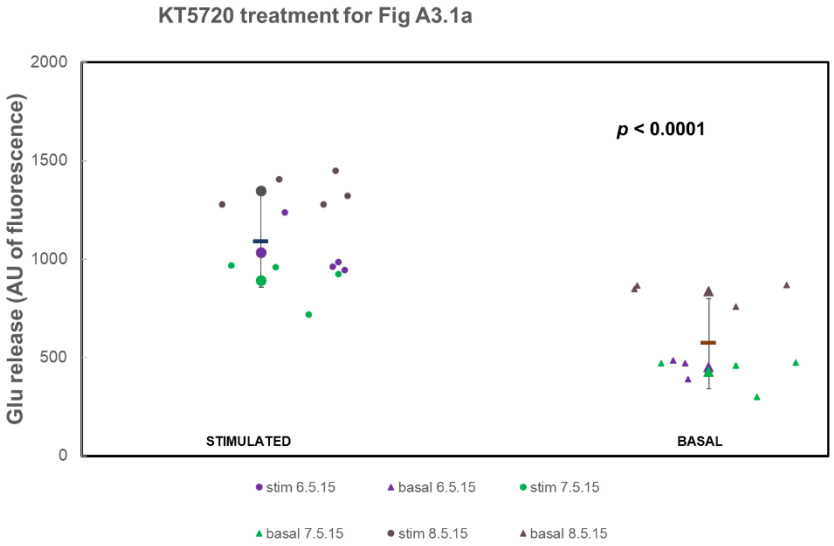

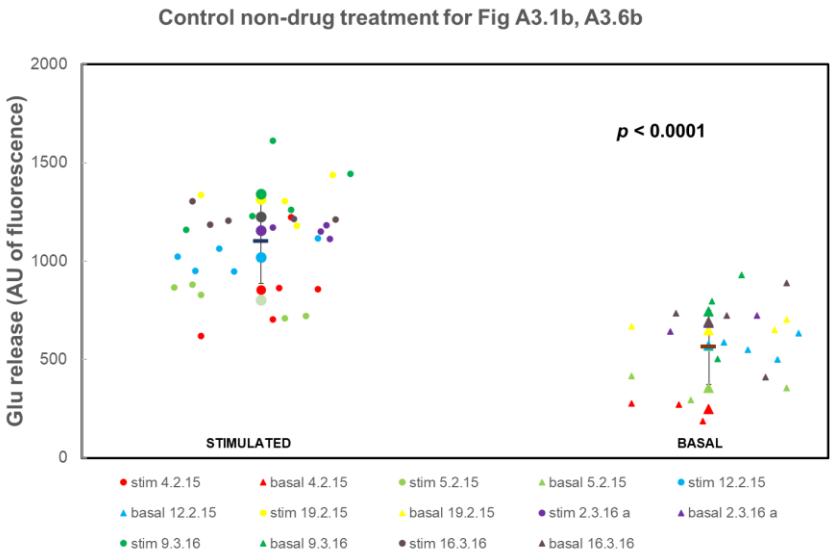

KT5720 treatment for Fig A3.1b

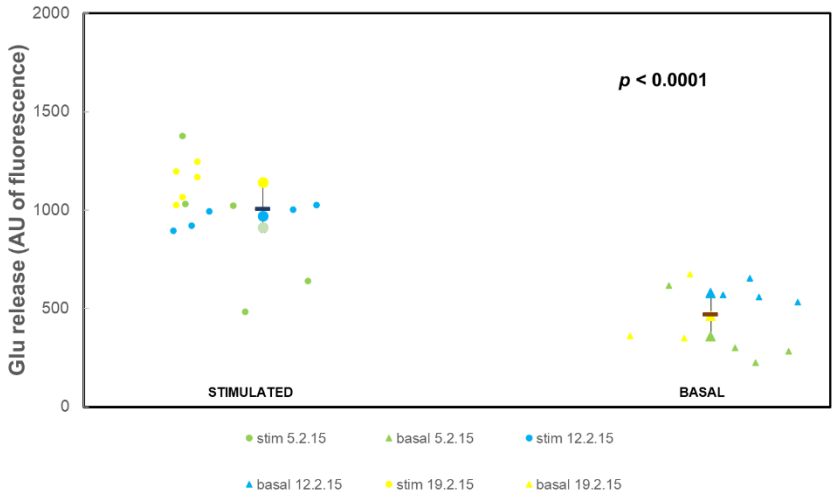

Control non-drug treatment for Fig A3.1c, A3.6c

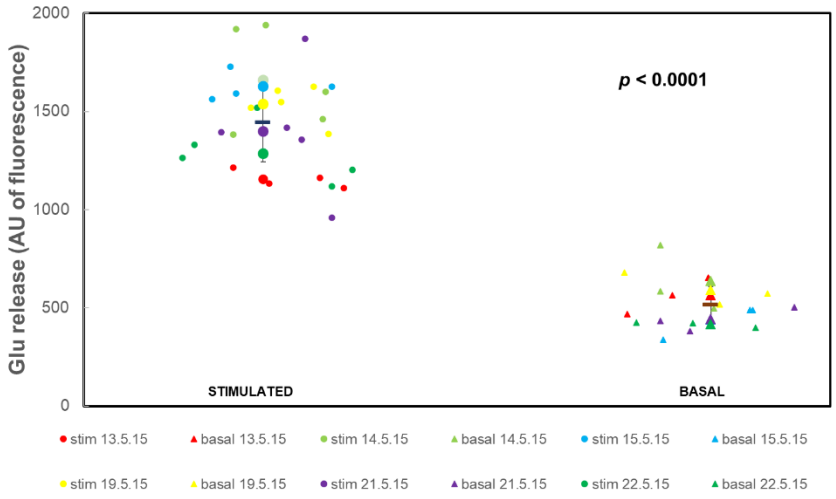

KT5720 treatment for Fig A3.1c

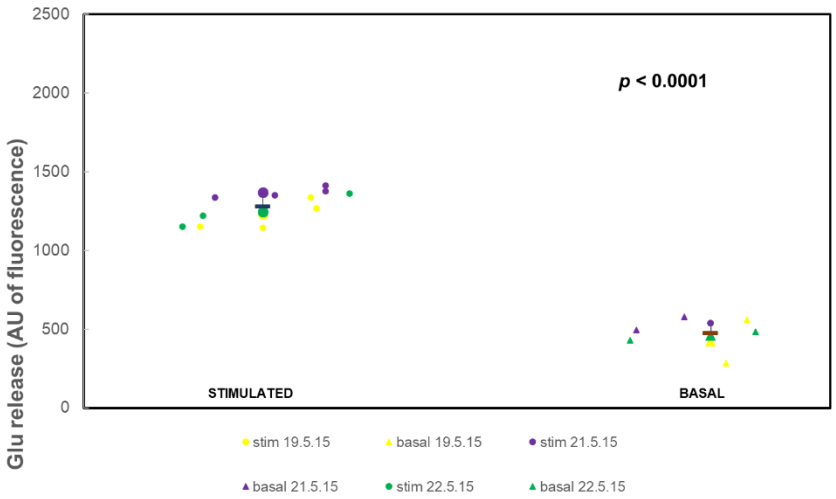

Control non-drug treatment for Fig A3.2a

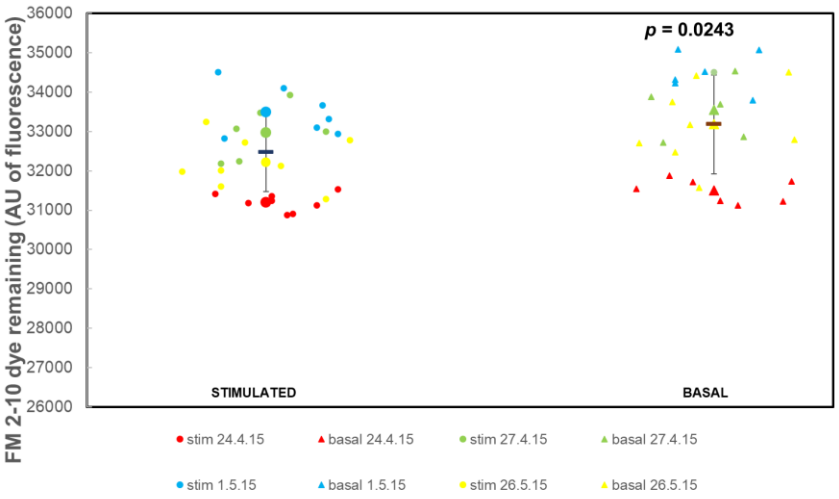

KT5720 treatment for Fig A3.2a

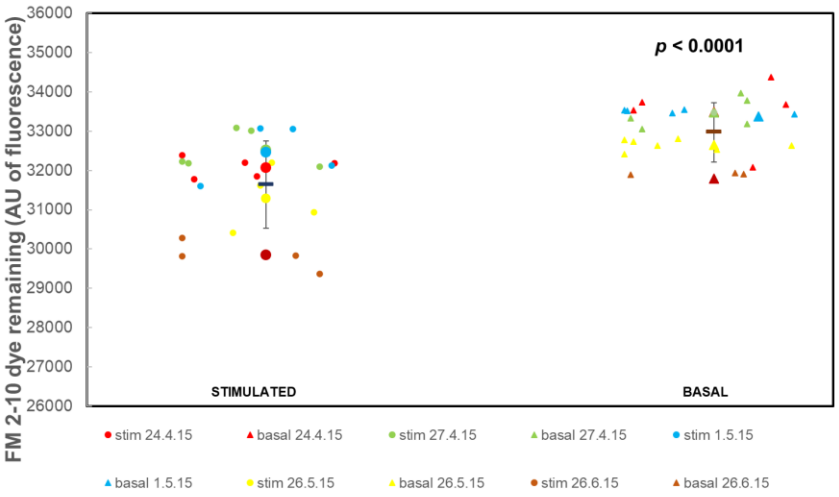

Control non-drug treatment for Fig A3.2b, A3.7b, A3.11a

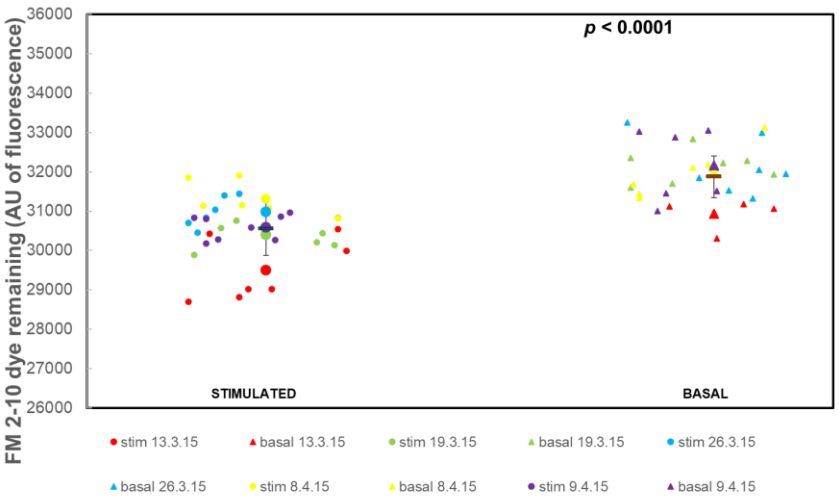

KT5720 treatment for Fig A3.2b

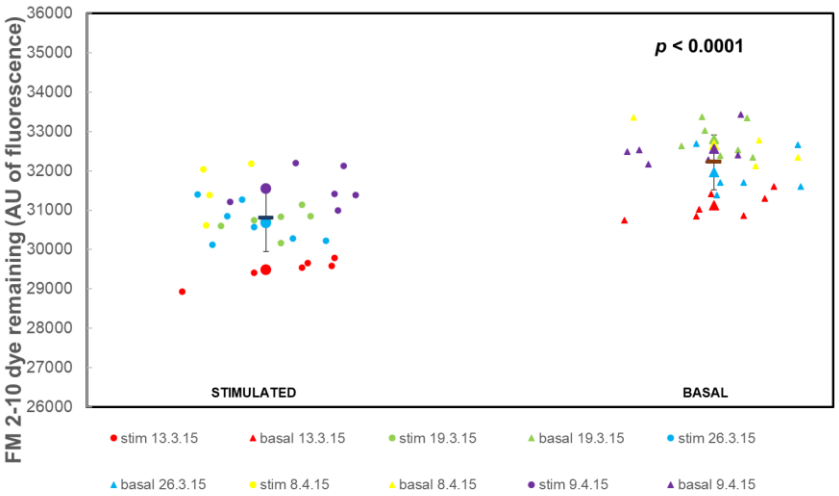

Control non-drug treatment for Fig A3.2c, A3.7c, A3.11b

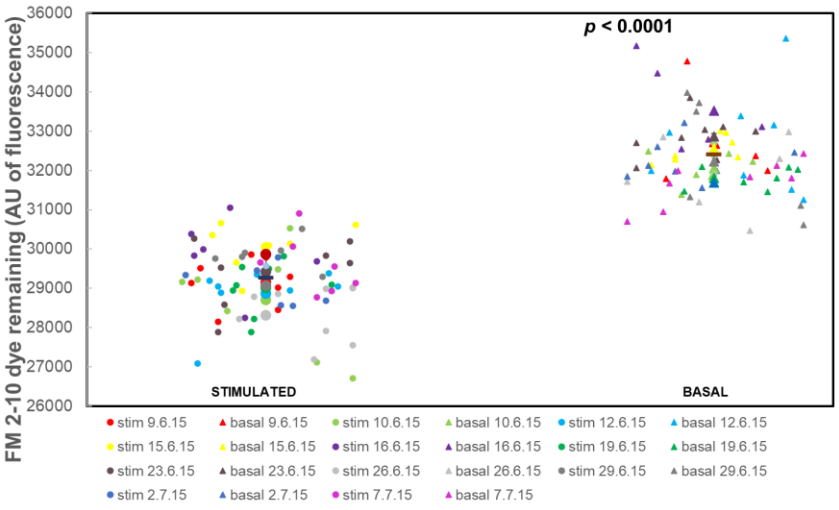

KT5720 treatment for Fig A3.2c

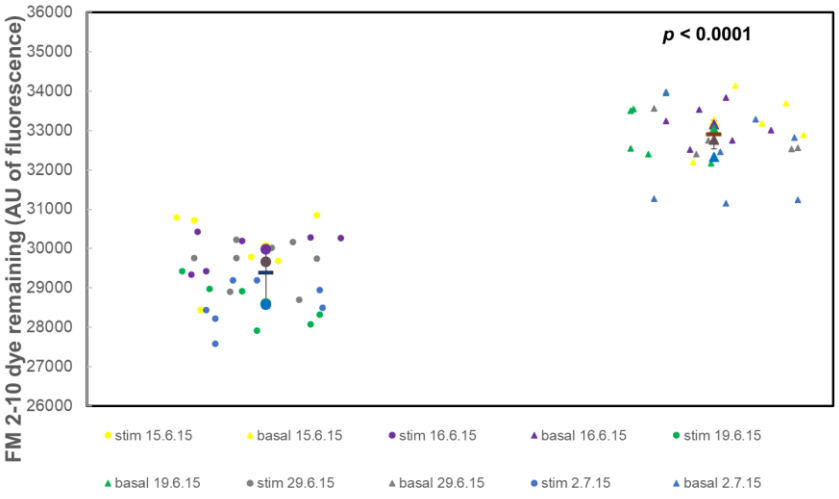

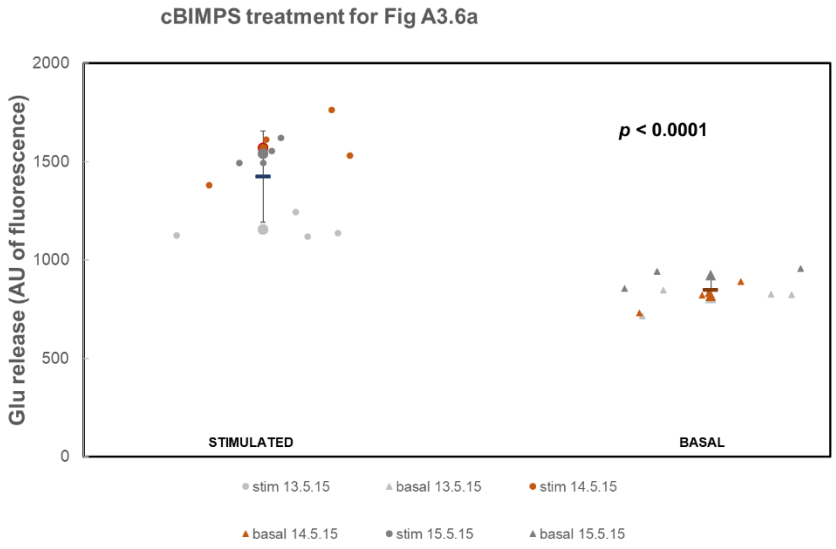
cBIMPS treatment for Fig A3.6a
Glu release (AU of fluorescence)
2000
1500
1000
500
0
p < 0.0001
STIMULATED
BASAL
stim 13.5.15
basal 13.5.15
stim 14.5.15
basal 14.5.15
stim 15.5.15
basal 15.5.15

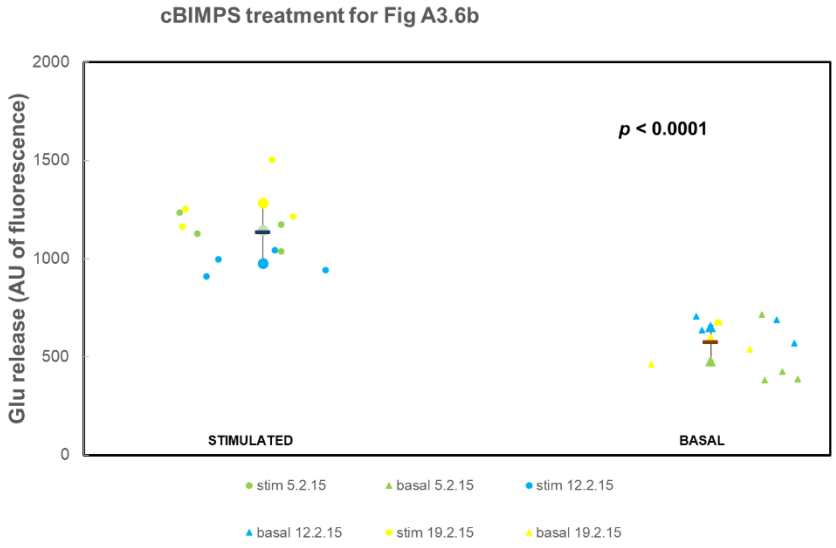
cBIMPS treatment for Fig A3.6b
Glu release (AU of fluorescence)
2000
1500
1000
500
0
p < 0.0001
STIMULATED
BASAL
stim 5.2.15
basal 5.2.15
stim 12.2.15
basal 12.2.15
stim 19.2.15
basal 19.2.15

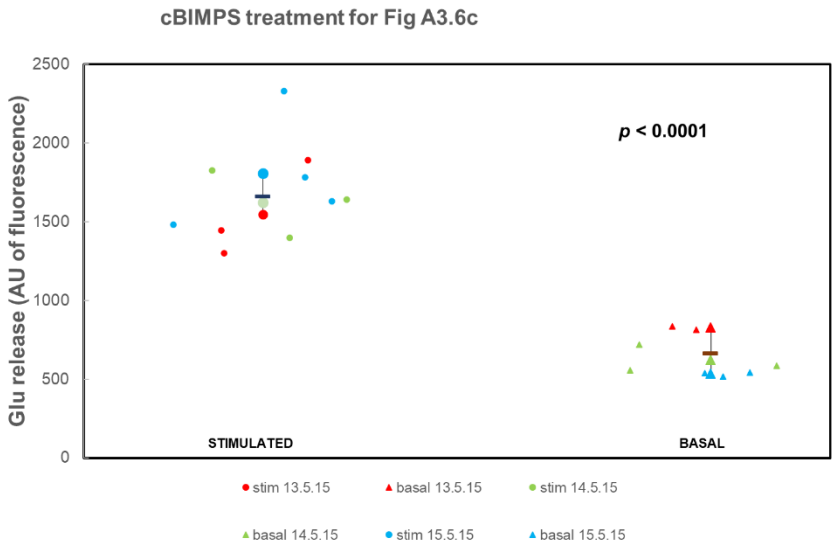
cBIMPS treatment for Fig A3.6c
Glu release (AU of fluorescence)
2500
2000
1500
1000
500
0
p < 0.0001
STIMULATED
BASAL
stim 13.5.15
basal 13.5.15
stim 14.5.15
basal 14.5.15
stim 15.5.15
basal 15.5.15

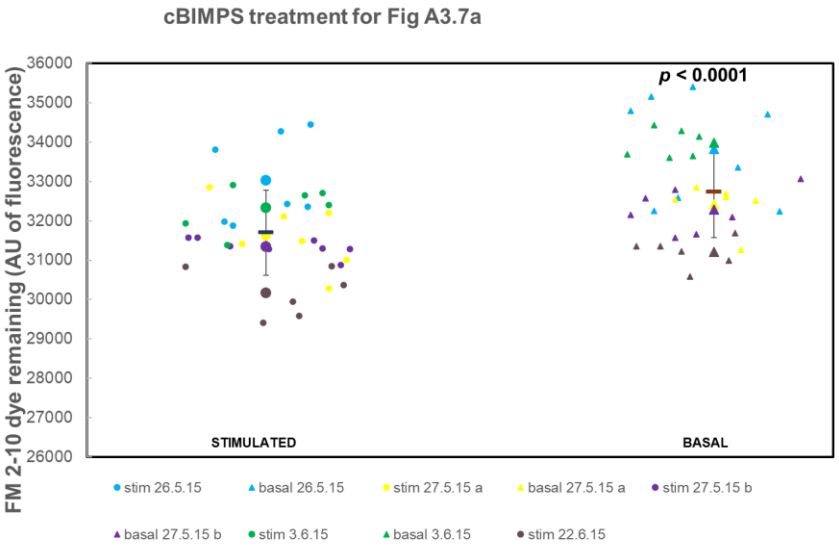
cBIMPS treatment for Fig A3.7a
FM 2-10 dye remaining (AU of fluorescence)
36000
35000
34000
33000
32000
31000
30000
29000
28000
27000
26000
p < 0.0001
STIMULATED
BASAL
stim 26.5.15
basal 26.5.15
stim 27.5.15 a
basal 27.5.15 a
stim 27.5.15 b
basal 27.5.15 b
stim 3.6.15
basal 3.6.15
stim 22.6.15

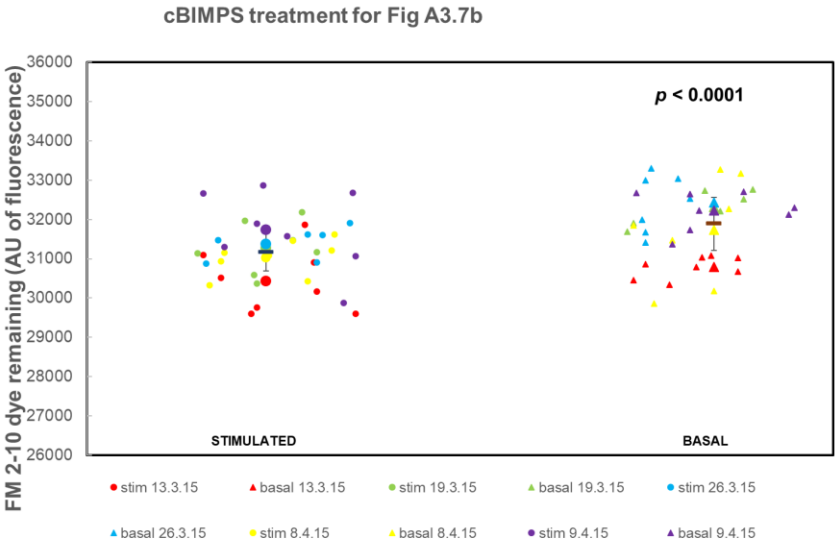
cBIMPS treatment for Fig A3.7b
FM 2-10 dye remaining (AU of fluorescence)
36000
35000
34000
33000
32000
31000
30000
29000
28000
27000
26000
p < 0.0001
STIMULATED
BASAL
stim 13.3.15
basal 13.3.15
stim 19.3.15
basal 19.3.15
stim 26.3.15
basal 26.3.15
stim 8.4.15
basal 8.4.15
stim 9.4.15
basal 9.4.15

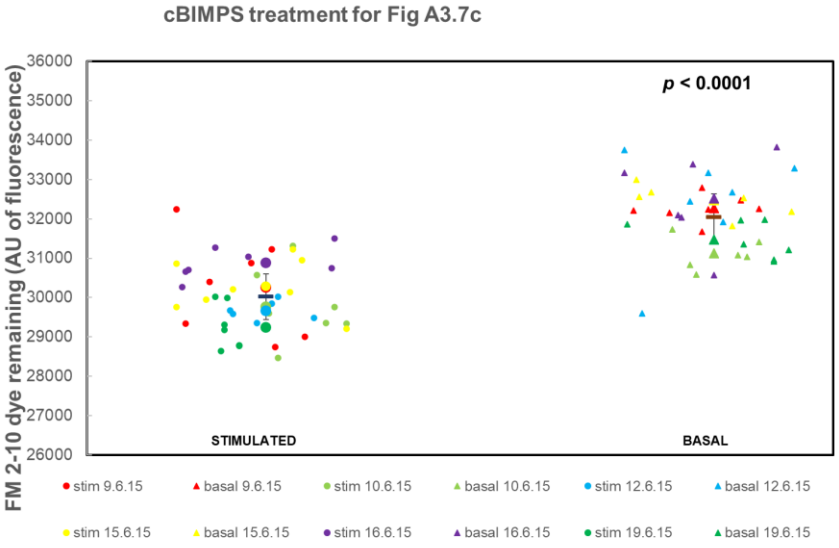
cBIMPS treatment for Fig A3.7c
FM 2-10 dye remaining (AU of fluorescence)
36000
35000
34000
33000
32000
31000
30000
29000
28000
27000
26000
p < 0.0001
STIMULATED
BASAL
stim 9.6.15
basal 9.6.15
stim 10.6.15
basal 10.6.15
stim 12.6.15
basal 12.6.15
stim 15.6.15
basal 15.6.15
stim 16.6.15
basal 16.6.15
stim 19.6.15
basal 19.6.15

KT5720 + cBIMPS treatment for Fig A3.11a

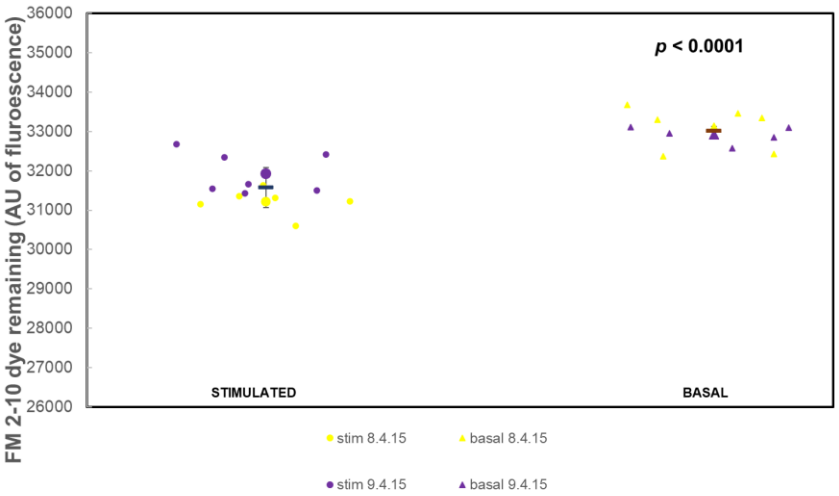

KT5720 + cBIMPS treatment for Fig A3.11b

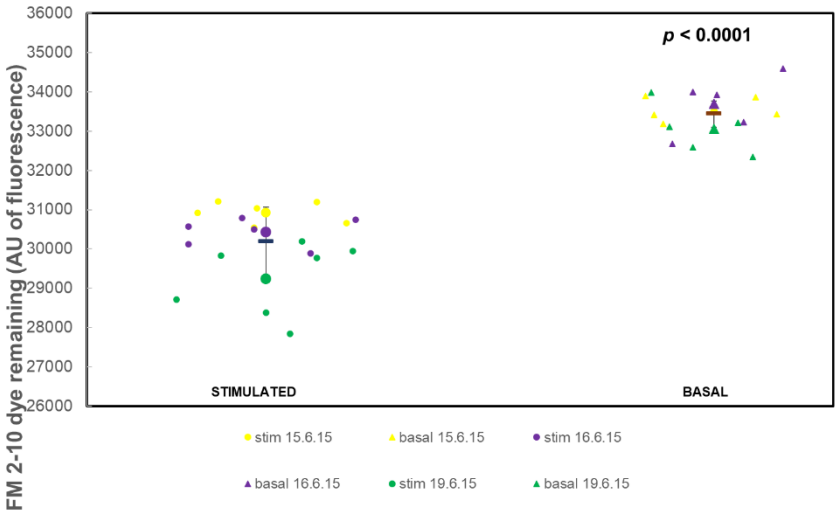

Control non-drug treatment for Fig A3.12a

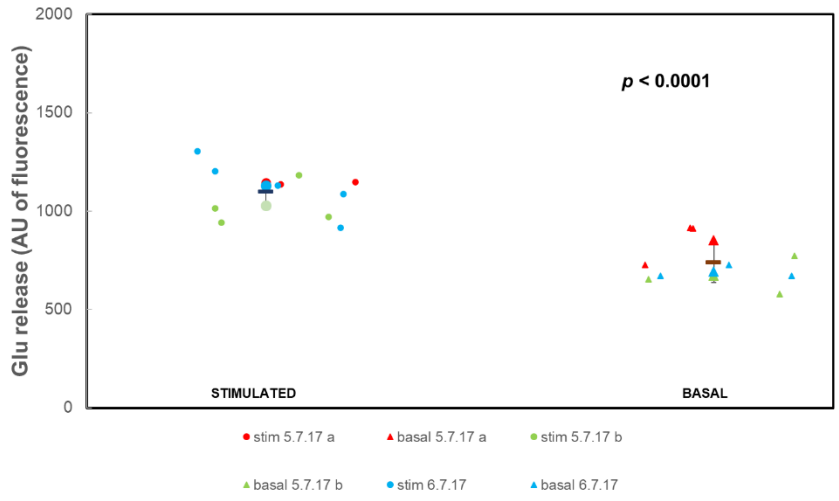

MiTMAB treatment for Fig A3.12a

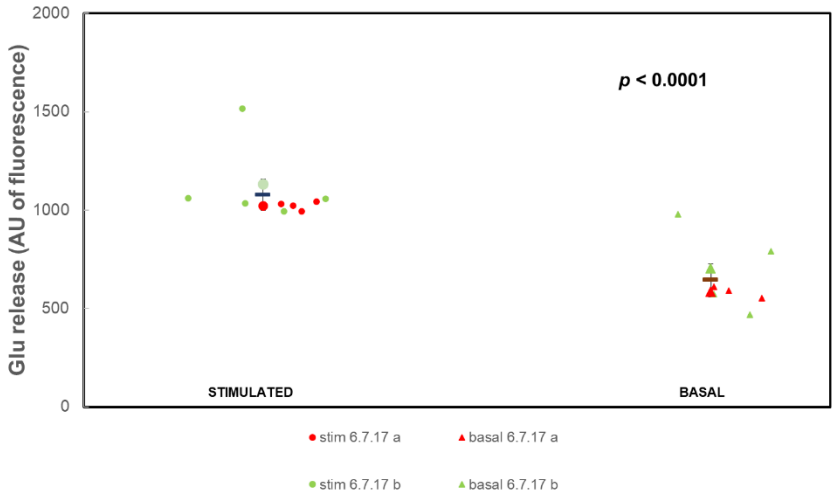

Control non-drug treatment for Fig A3.12b

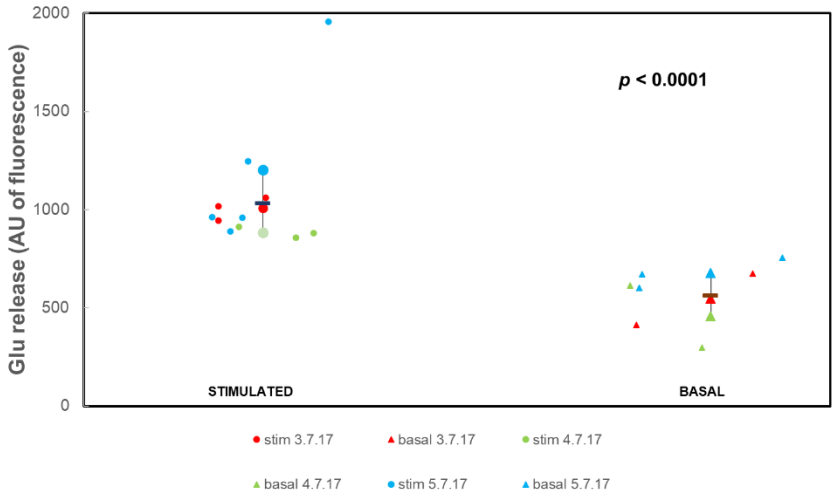

MiTMAB treatment for Fig A3.12b

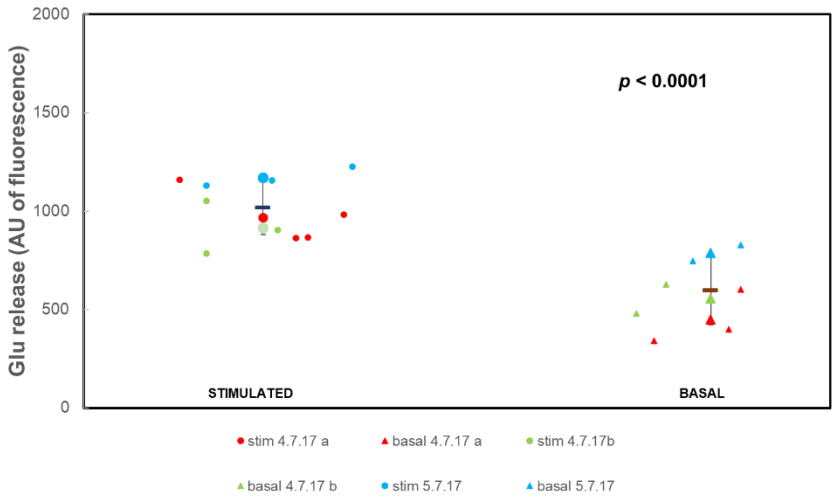

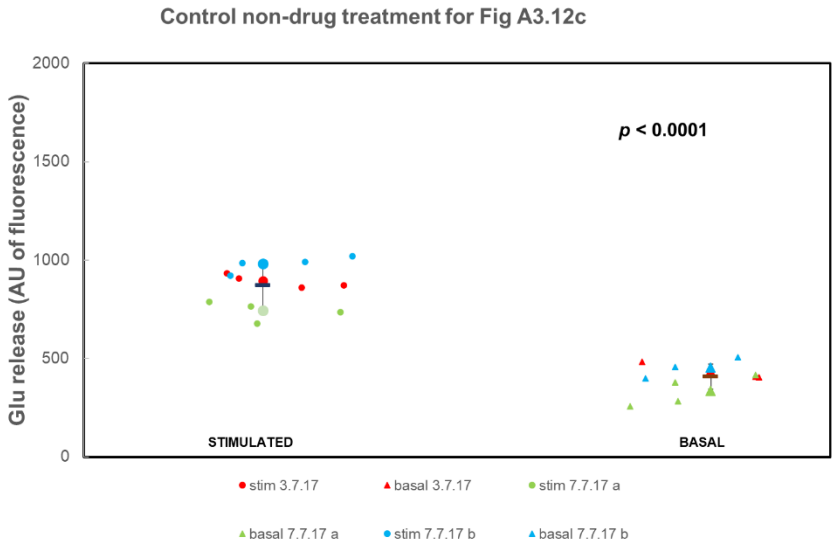
Control non-drug treatment for Fig A3.12c
Glu release (AU of fluorescence)
2000
1500
1000
500
0
p < 0.0001
STIMULATED
BASAL
stim 3.7.17
basal 3.7.17
stim 7.7.17 a
basal 7.7.17 a
stim 7.7.17 b
basal 7.7.17 b

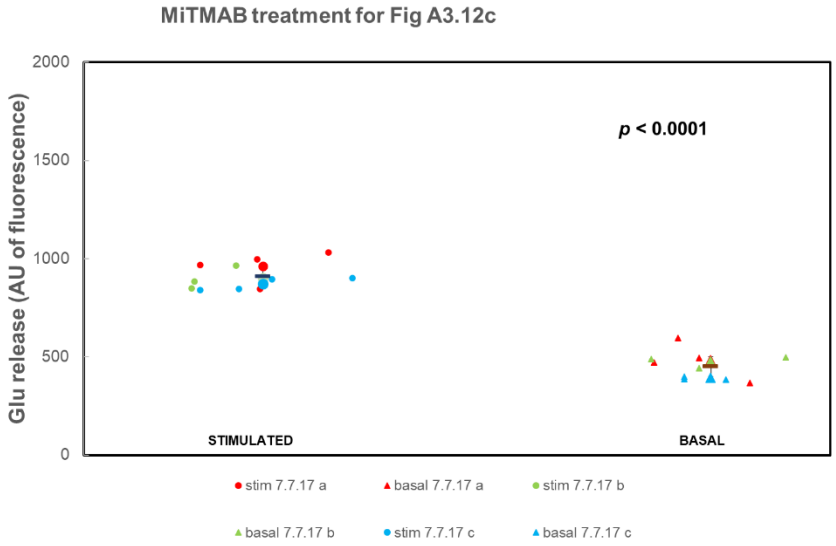
MiTMAB treatment for Fig A3.12c
Glu release (AU of fluorescence)
2000
1500
1000
500
0
p < 0.0001
STIMULATED
BASAL
stim 7.7.17 a
basal 7.7.17 a
stim 7.7.17 b
basal 7.7.17 b
stim 7.7.17 c
basal 7.7.17 c

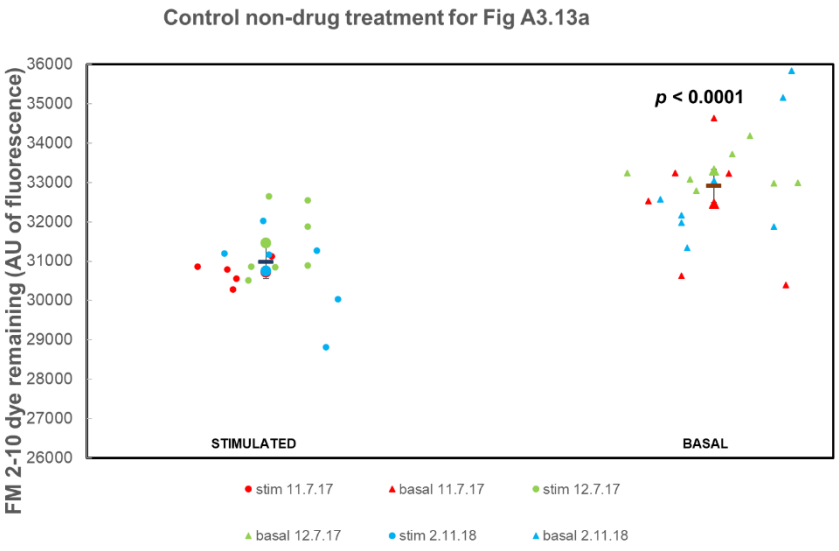
Control non-drug treatment for Fig A3.13a
FM 2-10 dye remaining (AU of fluorescence)
36000
35000
34000
33000
32000
31000
30000
29000
28000
27000
26000
p < 0.0001
STIMULATED
BASAL
stim 11.7.17
basal 11.7.17
stim 12.7.17
basal 12.7.17
stim 2.11.18
basal 2.11.18

MiTMAB treatment for Fig A3.13a

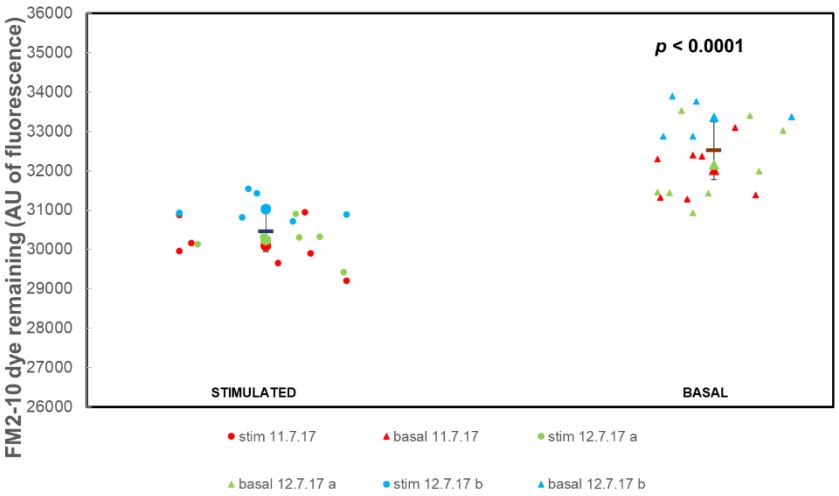

Control non-drug treatment Fig A3.13b

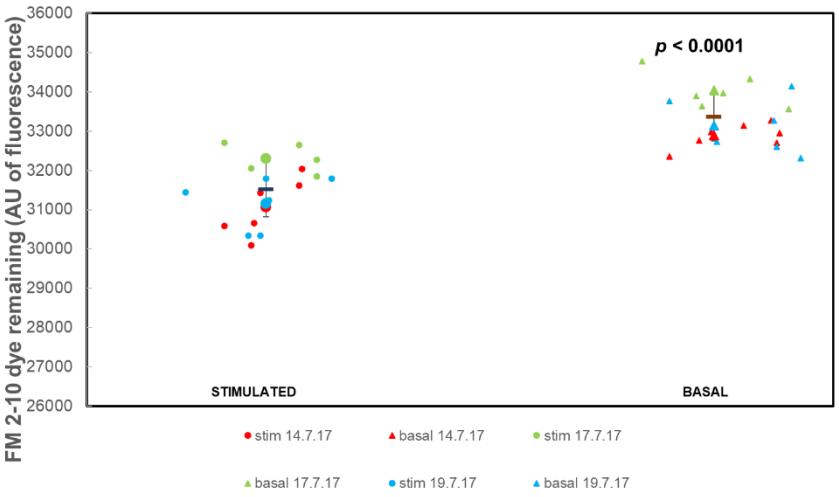

MiTMAB treatment for Fig A3.13b

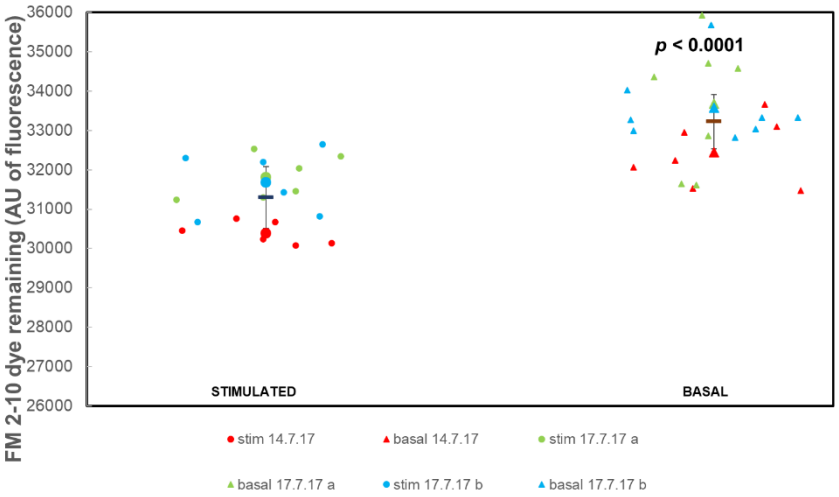

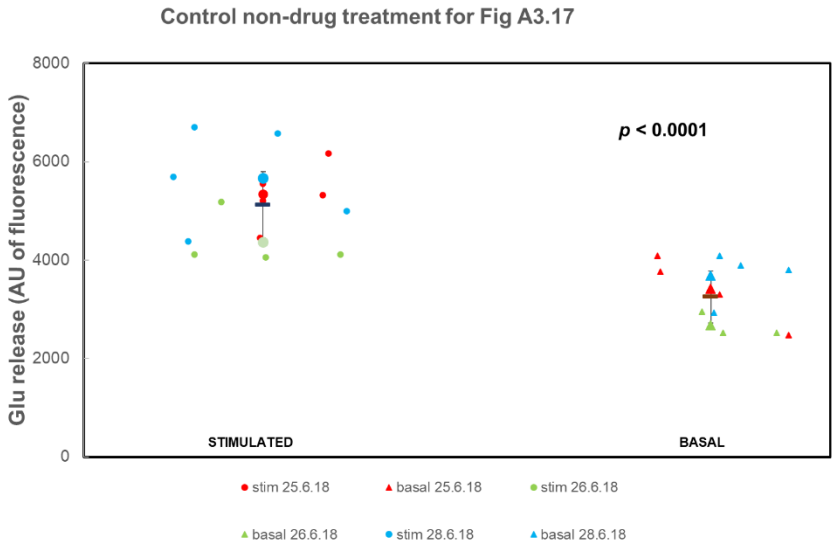
Control non-drug treatment for Fig A3.17
Glu release (AU of fluorescence)
8000
6000
4000
2000
0
p < 0.0001
STIMULATED
BASAL
stim 25.6.18
basal 25.6.18
stim 26.6.18
basal 26.6.18
stim 28.6.18
basal 28.6.18

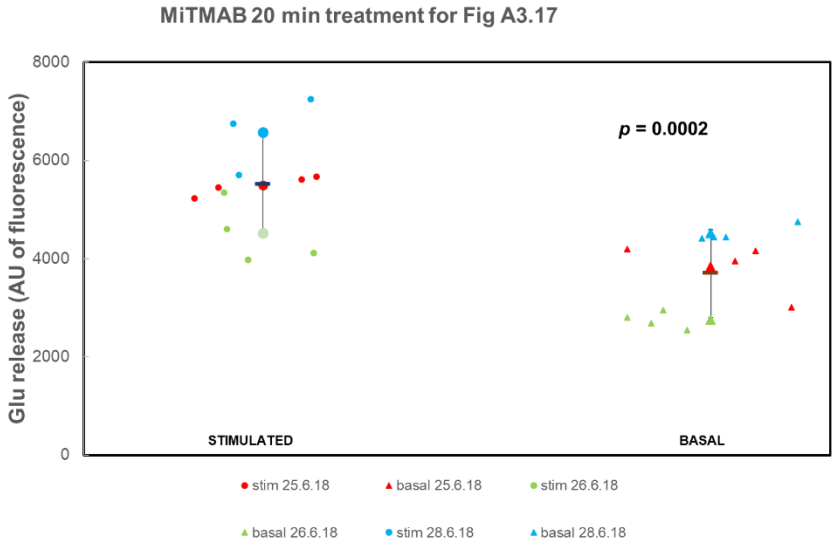
MiTMAB 20 min treatment for Fig A3.17
Glu release (AU of fluorescence)
8000
6000
4000
2000
0
p = 0.0002
STIMULATED
BASAL
stim 25.6.18
basal 25.6.18
stim 26.6.18
basal 26.6.18
stim 28.6.18
basal 28.6.18

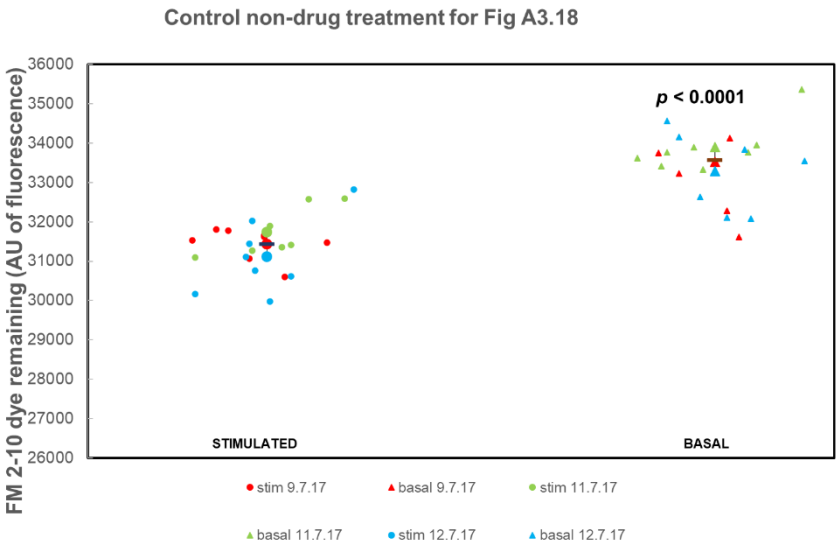
Control non-drug treatment for Fig A3.18
FM 2-10 dye remaining (AU of fluorescence)
36000
35000
34000
33000
32000
31000
30000
29000
28000
27000
26000
p < 0.0001
STIMULATED
BASAL
stim 9.7.17
basal 9.7.17
stim 11.7.17
basal 11.7.17
stim 12.7.17
basal 12.7.17

MiTMAB 20 min treatment for Fig A3.18

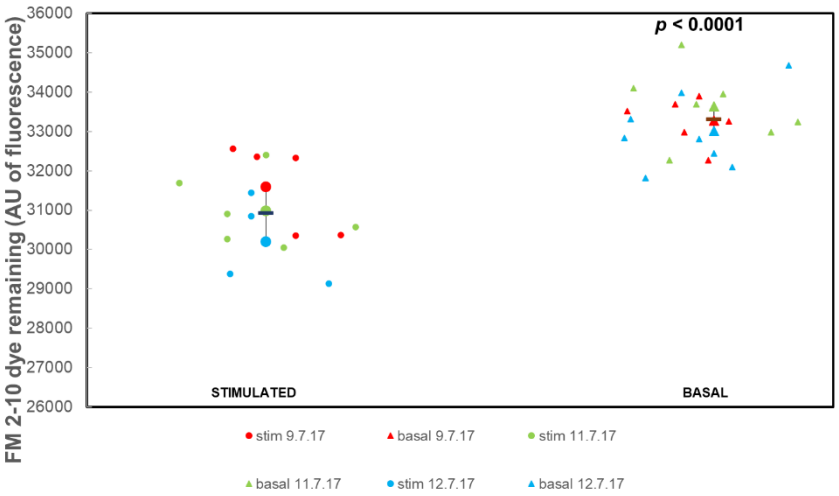

Control non-drug treatment for Fig A3.19a

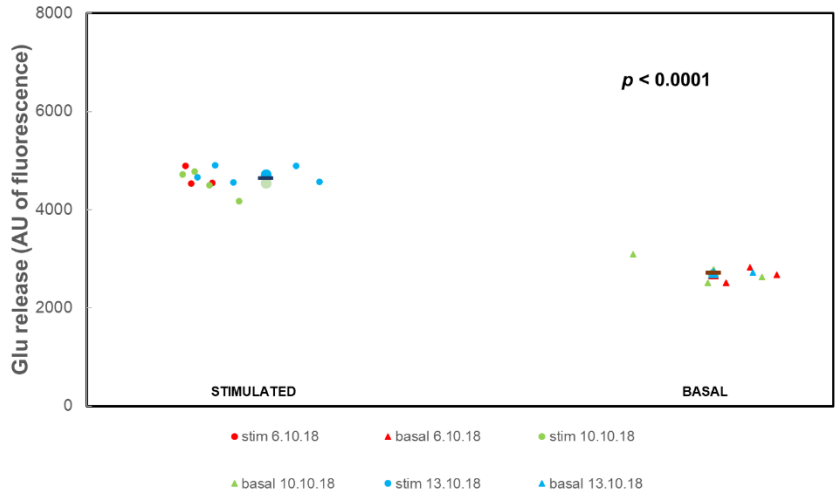

MiTMAB pretreatment for Fig A3.19a

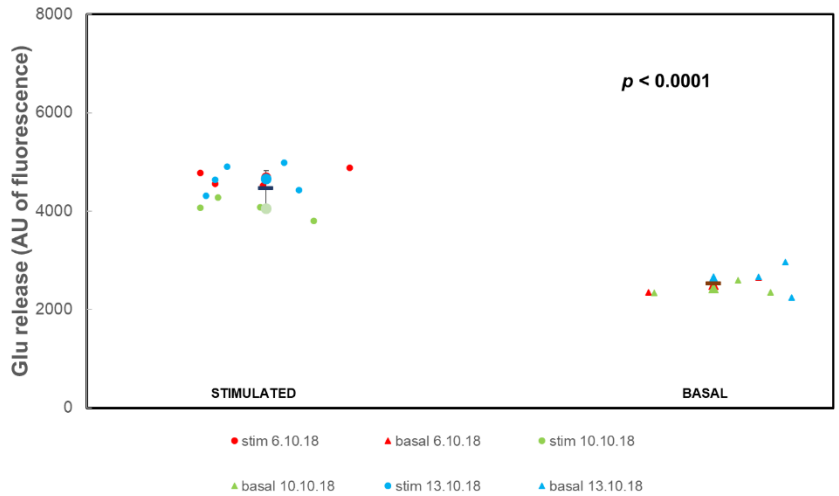

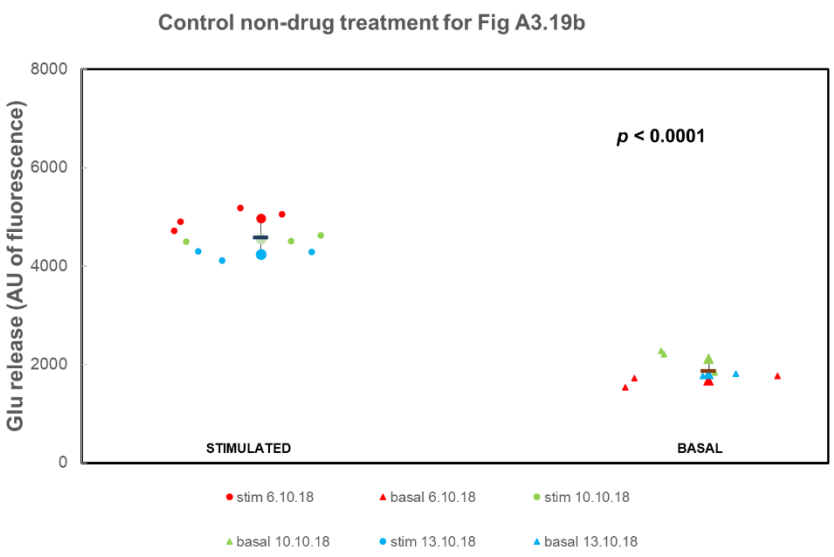
Control non-drug treatment for Fig A3.19b
Glu release (AU of fluorescence)
8000
6000
4000
2000
0
p < 0.0001
STIMULATED
BASAL
stim 6.10.18
basal 6.10.18
stim 10.10.18
basal 10.10.18
stim 13.10.18
basal 13.10.18

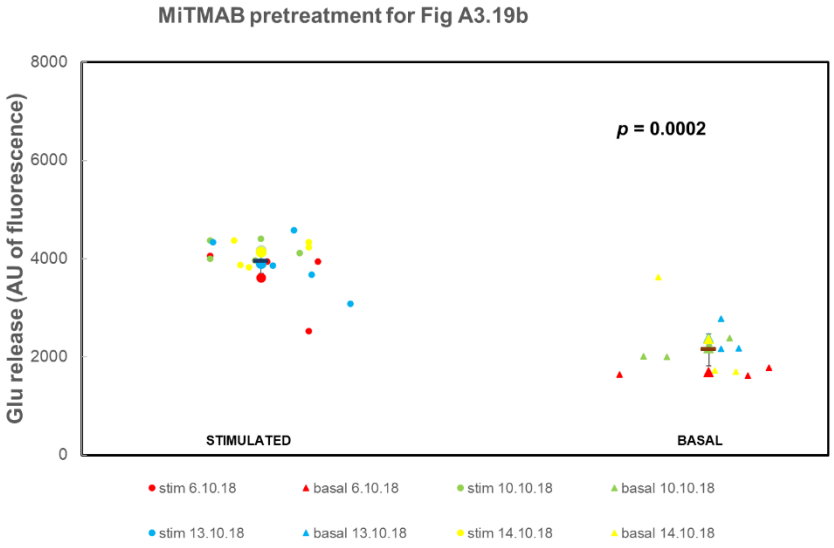
MiTMAB pretreatment for Fig A3.19b
Glu release (AU of fluorescence)
8000
6000
4000
2000
0
p = 0.0002
STIMULATED
BASAL
stim 6.10.18
basal 6.10.18
stim 10.10.18
basal 10.10.18
stim 13.10.18
basal 13.10.18
stim 14.10.18
basal 14.10.18

B.3 Tabulated Statistical Differences Between Conditions Calculated From the Superplot Data for Chapter 3

The Glu release data (Tables B3.1 to B3.3) utilise the raw data and not the corrected for sensitivity data, but the statistics for the superplots showed the same results as found in Chapter 3.

For 4AP5C evoked Glu release, neither cBIMPS or KT5720 induced any change in release of the RRP relative to the control (Table B3.1). However, there was some extra FM dye release for KT5720 treatment (Table B3.4) although with the superplot calculation this was not yet significantly different.

For HK5C evoked release of Glu containing RRP and RP SVs neither cBIMPS treatment or KT5720 treatment affected this release (Table B3.2). However, cBIMPS reduced the amount of FM dye release due to switching some RP SVs to KR mode (Table B3.5) and this was specific for PKA as KT5720 prevented this (Table B3.5) whilst this latter drug alone did not affect the dye release (Table B3.5).

ION5C evoked Glu release was not changed by pre-treatment with either KT5720 or cBIMPS so the same number of SVs were exocytosing as the control (Table B3.3). The superplot data for FM dye release gave exactly the same statistical significant results as found in Chapter 3. Thus, activation of PKA with cBIMPS reduced FM dye release by switching some of the RRP SVs to KR mode (Table B3.6) and this reduction was blocked by inhibiting PKA first with KT5720 (Table B3.6). For ION5C, like 4AP5C but unlike HK5C, the KT5720 actually induced more FM dye release (Table B3.6) due to switching the RRP SVs to FF mode.

Condition	Mean	SEM	n	*p* relative to control	Significance
4AP5C control	655.3593	54.28096	22	-	-
4AP5C KT5720	519.7667	94.48774	12	0.1893	not significant
4AP5C cBIMPS	575.8611	69.32595	12	0.3817	not significant

Table B3.1: 4AP5C Glu release control vs drug treatments statistics using superplot data.

Condition	Mean	SEM	n	*p* relative to control	Significance
HK5C control	539.2476	54.16584	28	-	-
HK5C KT5720	540.6833	45.22422	13	0.9867	not significant
HK5C cBIMPS	560.8333	51.41738	12	0.8111	not significant

Table B3.2: HK5C Glu release control vs drug treatments statistics using superplot data

Condition	Mean	SEM	n	*p* relative to control	Significance
ION5C control	930.6676	45.93072	23	-	-
ION5C KT5720	807.0764	32.7369	9	0.118	not significant
ION5C cBIMPS	998.0675	67.27259	9	0.4326	not significant

Table B3.3: ION5C Glu release control vs drug treatments statistics using superplot data.

Condition	Mean	SEM	n	*p* relative to control	Significance
4AP5C control	-704.776	305.5437	28	-	-
4AP5C KT5720	-1328.48	263.7753	26	0.131	not significant
Condition	**Mean**	**SEM**	**n**	***p* relative to control**	**Significance**
4AP5C control	-1124.94	138.9882	89	-	-
4AP5C cBIMPS	-1036.73	271.1523	34	0.7535	not significant

Table B3.4: 4AP5C FM 2-10 release control vs drug treatments statistics using superplot data.

Condition	Mean	SEM	n	*p* relative to control	Significance
HK5C control	-1307.93	153.7692	32	-	-
HK5C cBIMPS	-720.221	136.5736	37	0.0055	significant difference
HK5C KT5720	-1416.33	197.1089	31	0.665	not significant
HK5C KT5720 + cBIMPS	-1432.06	151.8849	12	0.6467	not significant

Table B3.5: HK5C FM 2-10 release control vs drug treatments statistics using superplot data.

Condition	mean	SEM	n	*p* relative to control	Significance
ION5C control	-3133.69	86.92914	78	-	-
ION5C cBIMPS	-2018.65	129.6893	41	< 0.0001	significant difference
ION5C KT5720	-3518.36	146.9277	31	0.0224	significant difference
ION5C KT5720 + cBIMPS	-3231.54	219.476	18	0.6409	not significant

Table B3.6: ION5C FM 2-10 release control vs drug treatments statistics using superplot data.

Treating synaptosomes with MiTMAB for 5 min at 37ºC did not perturb the Glu release stimulated by 4AP5C, HK5C or ION5C (Table B3.7) and neither did this drug, by preventing dynamin-1 binding to membranes, change the amount of evoked FM dye produced by these stimuli (Table B3.8). These beeswarm plot determined results are the same as those found in Chapter 3.

An incubation for 20 min at 37ºC with MiTMAB did not disturb the amount of HK5C evoked Glu (Table B3.9) or FM dye (Table B3.10).

Finally, using the calculations from the beeswarm plots, it can be seen that the 4AP5C evoked Glu release from the RRP SVs was not pertubed even if the synaptosomes were pretreated with MiTMAB prior to the pre-stimulation by HK5C (Table B3.11): this indicates that the RRP SVs are being recycled by a dynamin independent pathway. However, the ION5C evoked Glu release was reduced by this MiTMAB pretreatment to the level of release of just the RRP

SVs (Table B3.11) and this indicates that the RP SVs normally recycle by a dynamin dependent process and this is blocked by MiTMAB.

Fig	Condition	Mean	SEM	n	*p* relative to control	Significance
12a	**4AP5C control**	362.1111	37.15139	10	-	-
	4AP5C MiTMAB	434.05	40.53009	8	0.2105	not significant
Fig	**Condition**	**Mean**	**SEM**	**n**	***p* relative to control**	**Significance**
12b	**HK5C control**	472.1889	52.46543	9	-	-
	HK5C MiTMAB	421.0278	73.45519	9	0.5787	not significant
Fig	**Condition**	**Mean**	**SEM**	**n**	***p* relative to control**	**Significance**
12c	**ION5C control**	465.1667	40.94118	11	-	-
	ION5C MiTMAB	460.25	20.66003	11	0.9134	not significant

Table B3.7: Evoked Glu release control vs 5 min MiTMAB treatment statistics using superplot data.

Fig	Condition	Mean	SEM	n	*p* relative to control	Significance
13a	**HK5C control**	-1930.59	136.74	19	-	-
	HK5C MiTMAB	-2051.52	199.49	20	0.6235	not significant
Fig	**Condition**	**Mean**	**SEM**	**n**	***p* relative to control**	**Significance**
13b	**ION5C control**	-1838.14	216.19	18	-	-
	ION5C MiTMAB	-1927.97	233.44	20	0.7808	not significant

Table B3.8: Evoked FM 2-10 release control vs 5 min MiTMAB treatment statistics using superplot data.

Fig	Condition	Mean	SEM	n	*p* relative to control	Significance
3.17	**HK5C control**	1875.19	237.47	13	-	-
	HK5C MiTMAB	1824.94	392.46	12	0.9122	not significant

Table B3.9: HK5C Glu release control vs 20 min MiTMAB treatment statistics using superplot data.

Fig	Condition	Mean	SEM	n	*p* relative to control	Significance
3.18	**HK5C control**	-2126.32	93.45	22	-	-
	HK5C MiTMAB	-2375.2	180.99	18	0.2057	not significant

Table B3.10: HK5C evoked FM 2-10 release control vs 20 min MiTMAB treatment statistics using superplot data.

Fig	Condition	Mean	SEM	n	*p* relative to control	Significance
3.19a	**4AP5C control**	1930.76	28.91	11	-	-
	4AP5C MiTMAB	1947.11	111.01	11	0.8881	not significant
Fig	**Condition**	**Mean**	**SEM**	**n**	***p* relative to control**	**Significance**
3.19b	**ION5C control**	2718.81	143.57	9	-	-
	ION5C MiTMAB	1809.45	102.63	16	<0.0001	significant difference

Table B3.11: Evoked Glu release control vs MiTMAB pre-treatment statistics using superplot data.

B.4 Beeswarm Superplots for Chapter 4

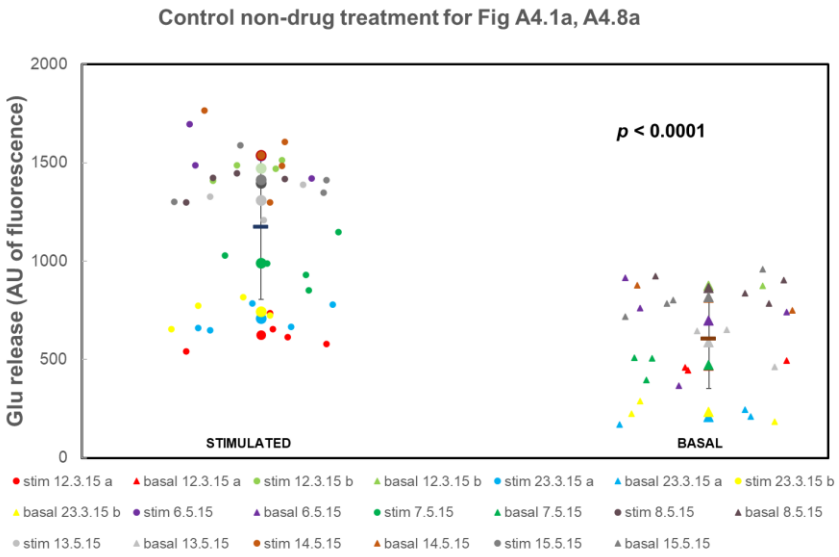

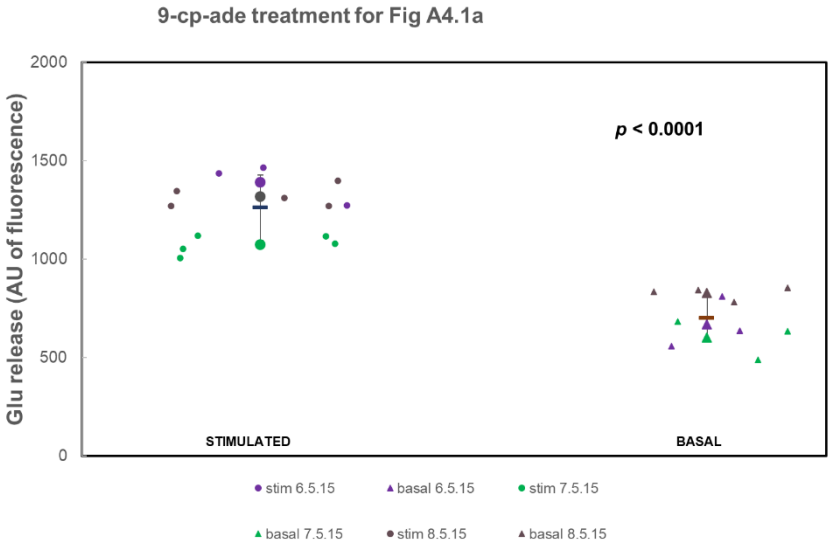

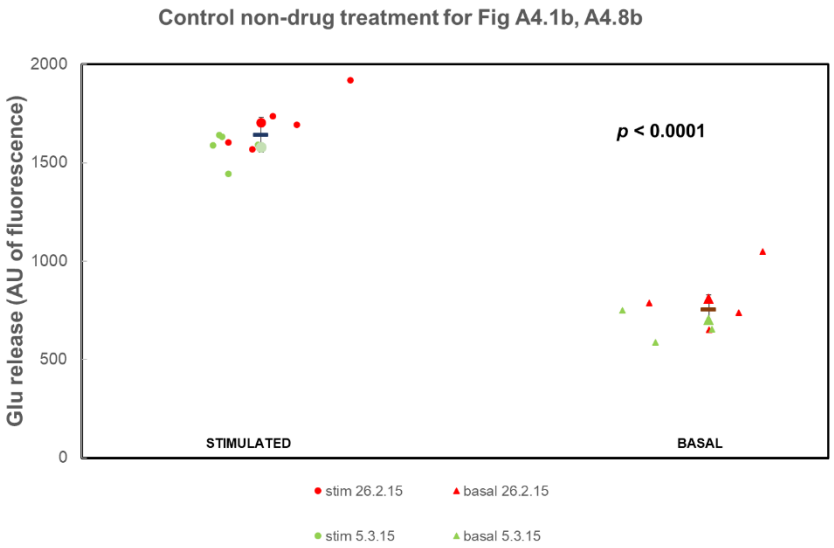

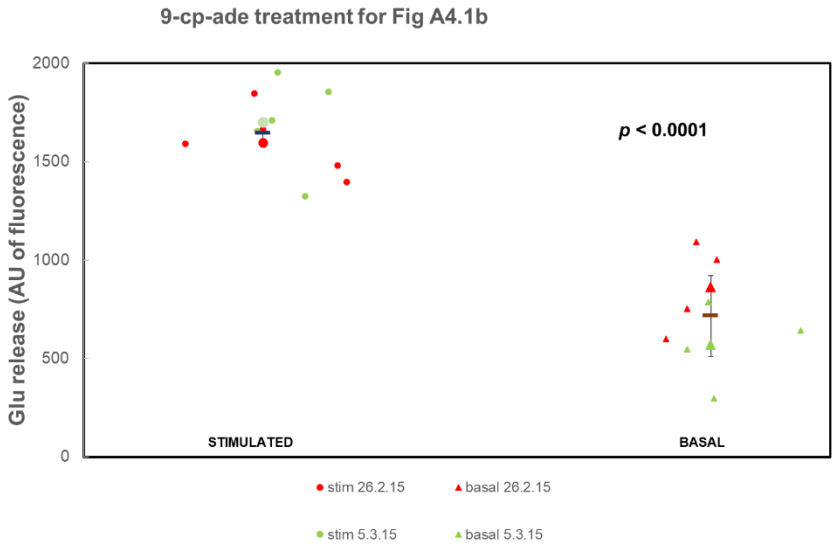
9-cp-ade treatment for Fig A4.1b
Glu release (AU of fluorescence)
2000
1500
1000
500
0
p < 0.0001
STIMULATED
BASAL
stim 26.2.15
basal 26.2.15
stim 5.3.15
basal 5.3.15

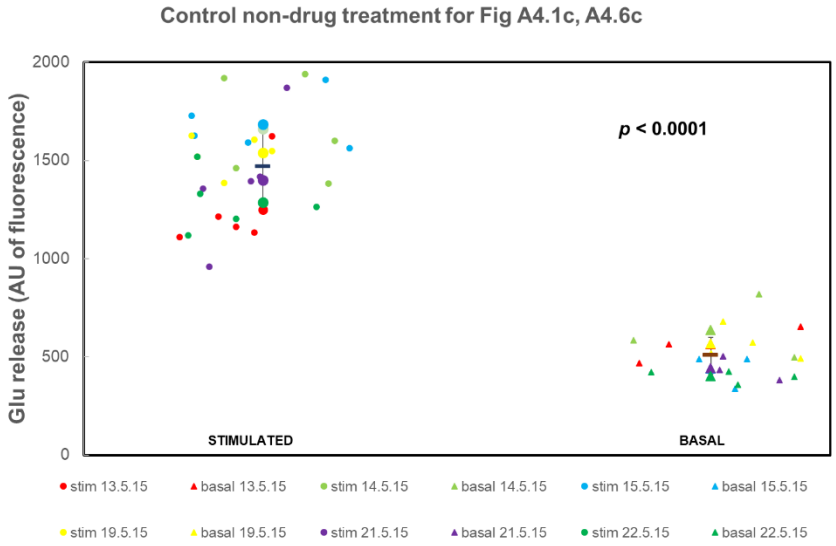
Control non-drug treatment for Fig A4.1c, A4.6c
Glu release (AU of fluorescence)
2000
1500
1000
500
0
p < 0.0001
STIMULATED
BASAL
stim 13.5.15
basal 13.5.15
stim 14.5.15
basal 14.5.15
stim 15.5.15
basal 15.5.15
stim 19.5.15
basal 19.5.15
stim 21.5.15
basal 21.5.15
stim 22.5.15
basal 22.5.15

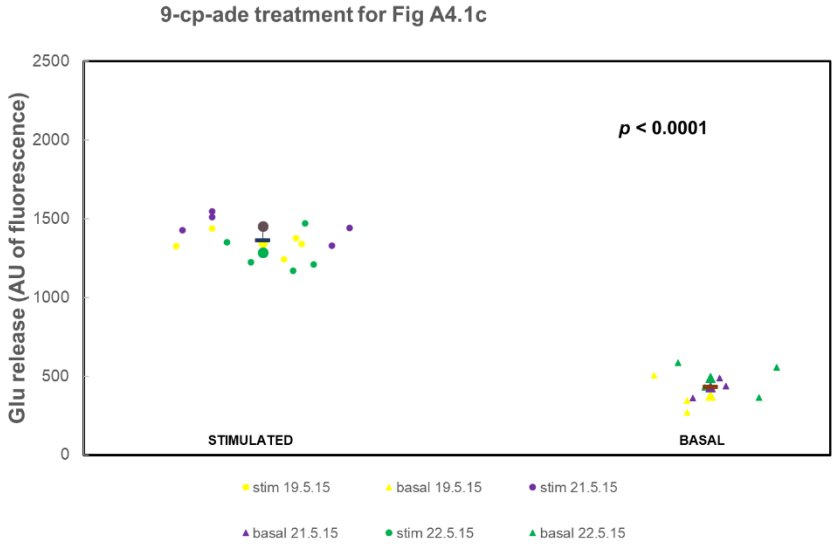
9-cp-ade treatment for Fig A4.1c
Glu release (AU of fluorescence)
2500
2000
1500
1000
500
0
p < 0.0001
STIMULATED
BASAL
stim 19.5.15
basal 19.5.15
stim 21.5.15
basal 21.5.15
stim 22.5.15
basal 22.5.15

Control non-drug treatment for Fig A4.2a, A4.9b, A4.10

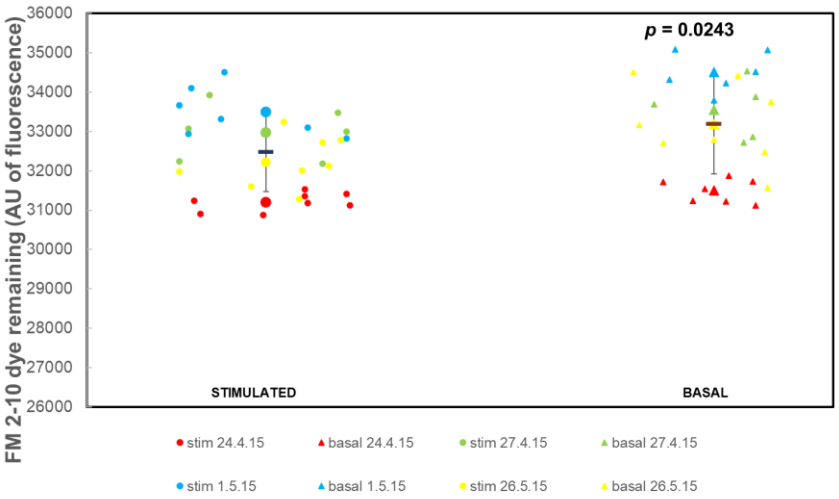

9-cp-ade treatment for Fig A4.2a

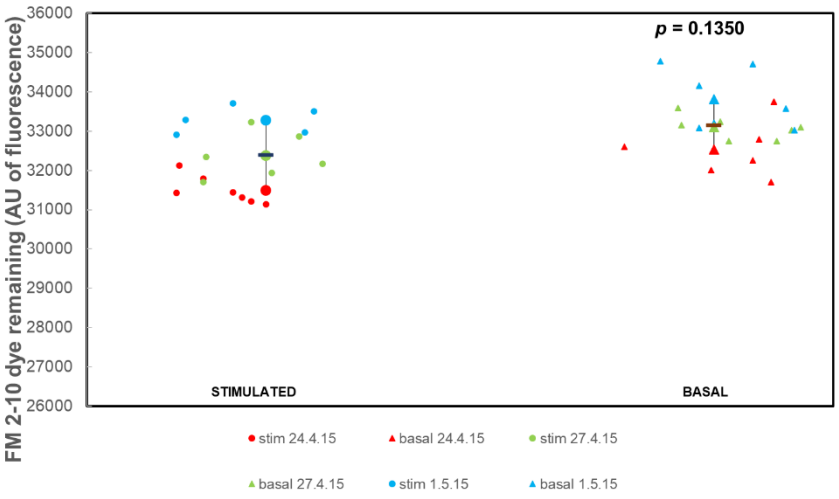

Control non-drug treatment for Fig A4.2b

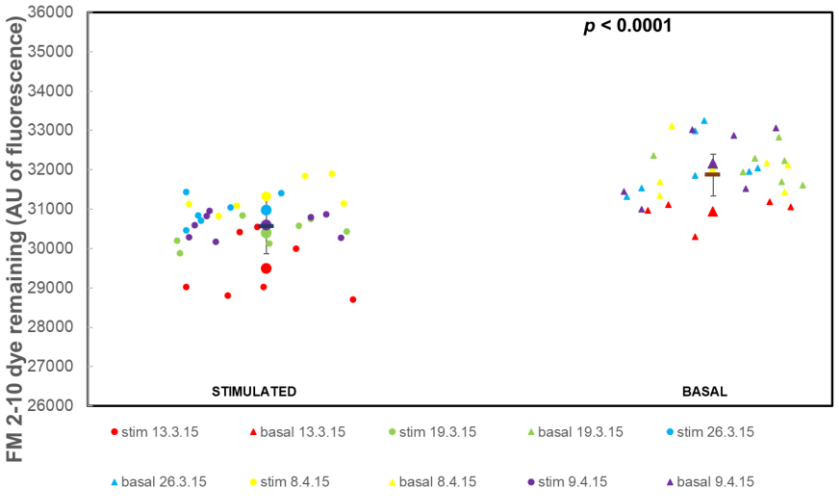

9-cp-ade treatment for Fig A4.2b

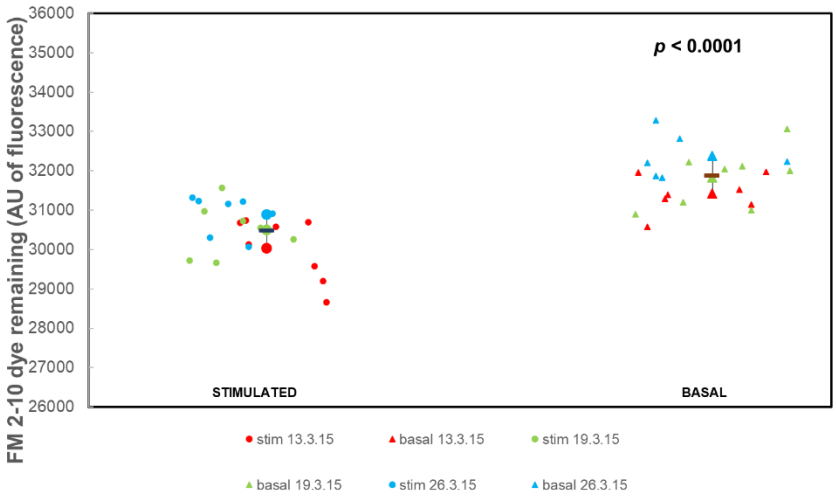

Control non-drug treatment for Fig A4.2c

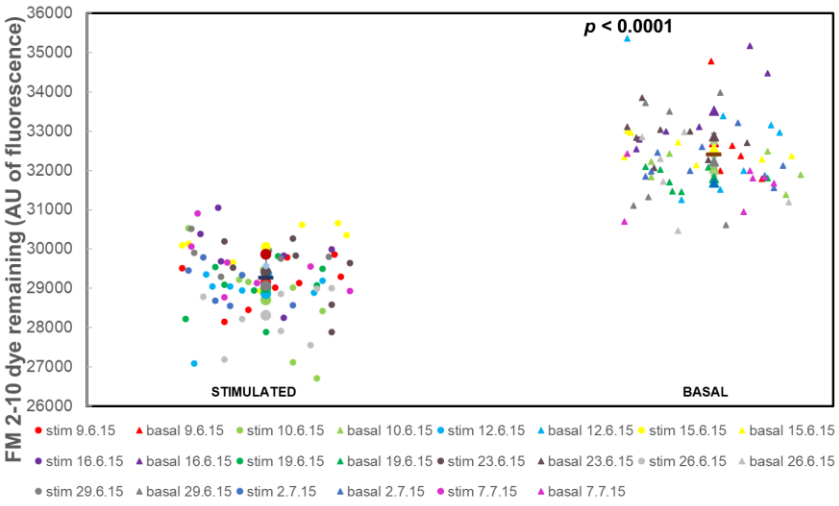

9-cp-ade treatment for Fig A4.2c

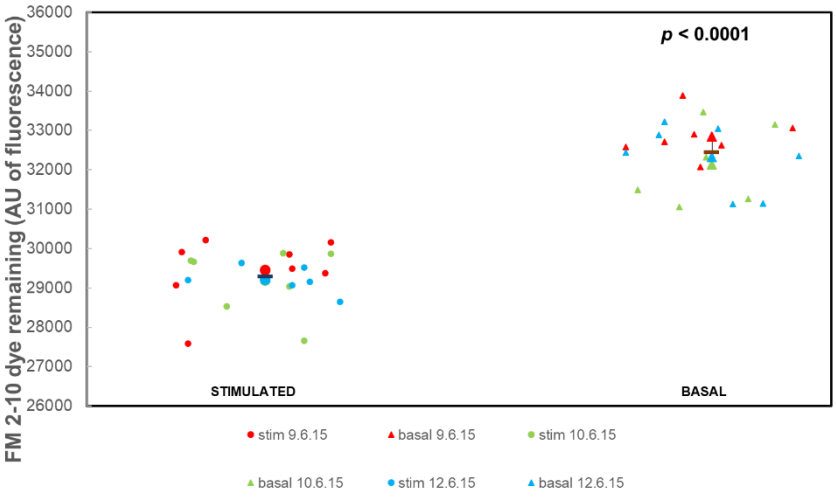

Control non-drug treatment for Fig A4.6a

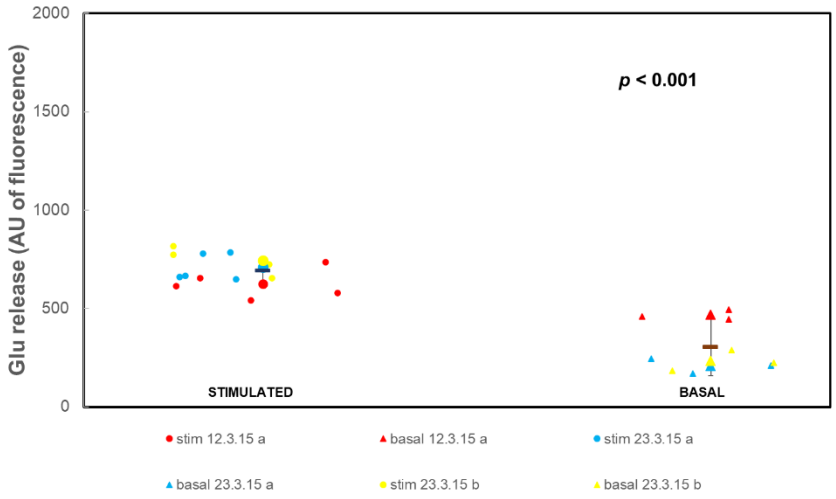

Forskolin treatment for Fig A4.6a

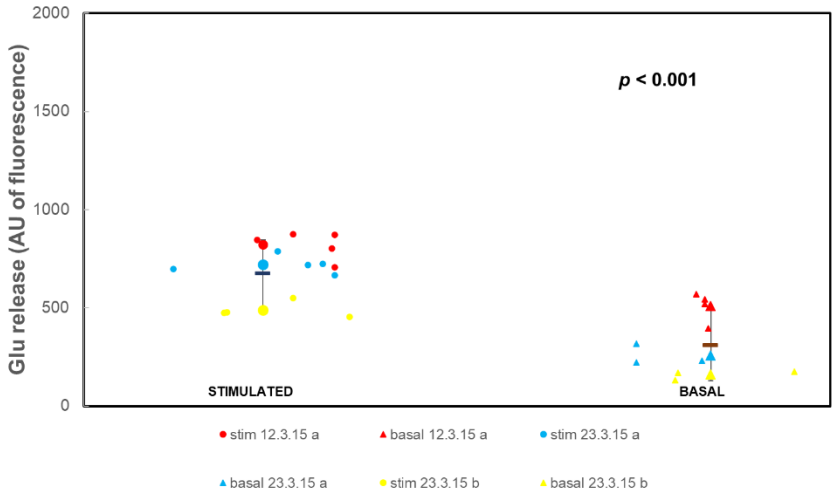

Control non-drug treatment for Fig A4.6b

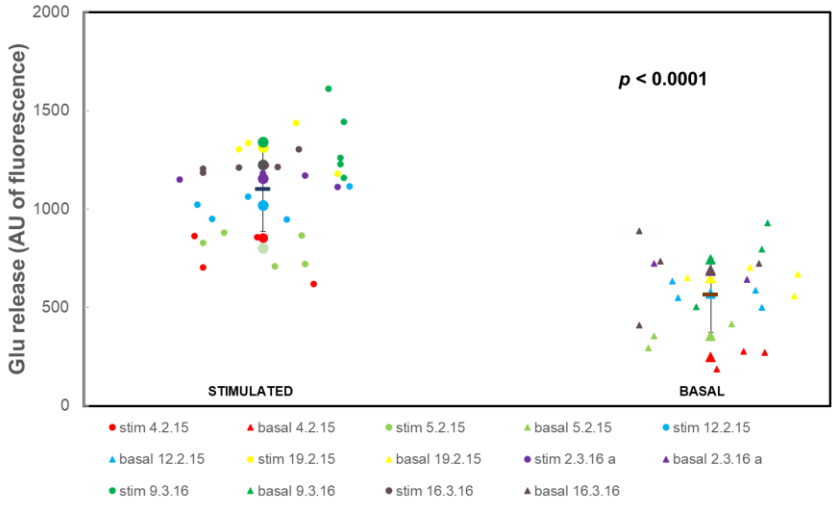

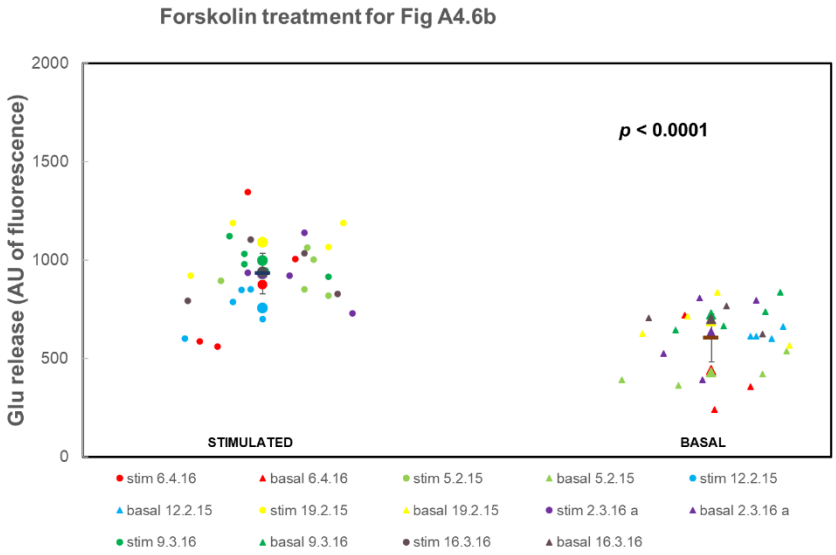
Forskolin treatment for Fig A4.6b
Glu release (AU of fluorescence)
2000
1500
1000
500
0
p < 0.0001
STIMULATED
BASAL
stim 6.4.16
basal 6.4.16
stim 5.2.15
basal 5.2.15
stim 12.2.15
basal 12.2.15
stim 19.2.15
basal 19.2.15
stim 2.3.16 a
basal 2.3.16 a
stim 9.3.16
basal 9.3.16
stim 16.3.16
basal 16.3.16

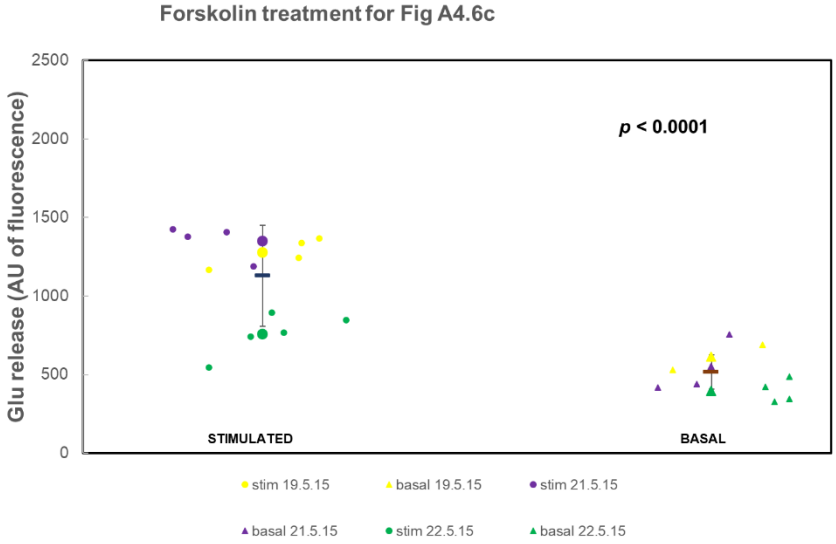
Forskolin treatment for Fig A4.6c
Glu release (AU of fluorescence)
2500
2000
1500
1000
500
0
p < 0.0001
STIMULATED
BASAL
stim 19.5.15
basal 19.5.15
stim 21.5.15
basal 21.5.15
stim 22.5.15
basal 22.5.15

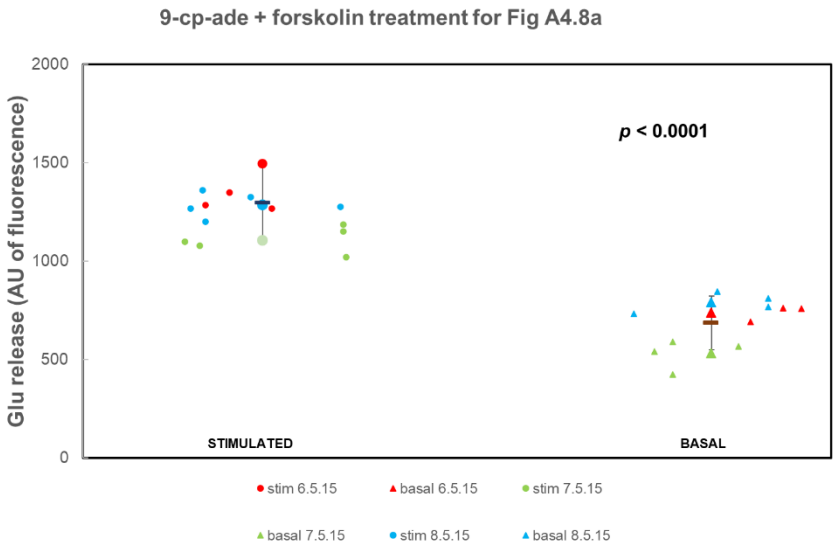
9-cp-ade + forskolin treatment for Fig A4.8a
Glu release (AU of fluorescence)
2000
1500
1000
500
0
p < 0.0001
STIMULATED
BASAL
stim 6.5.15
basal 6.5.15
stim 7.5.15
basal 7.5.15
stim 8.5.15
basal 8.5.15

9-cp-ade + forskolin treatment for Fig A4.8b

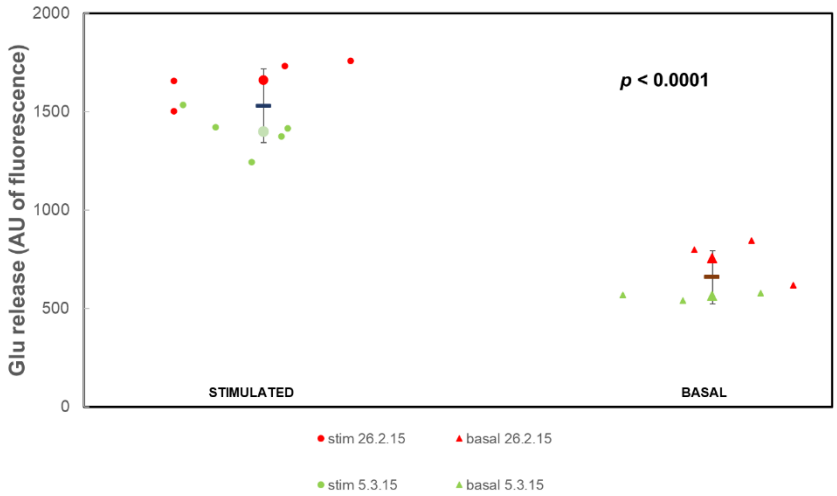

Control non-drug treatment for Fig A4.9a, A4.11a, A4.11b

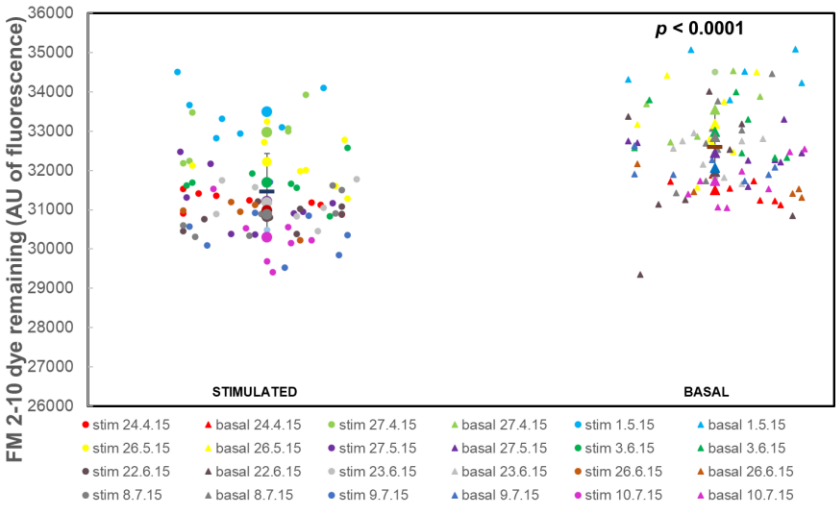

Forskolin treatment Fig A4.9a

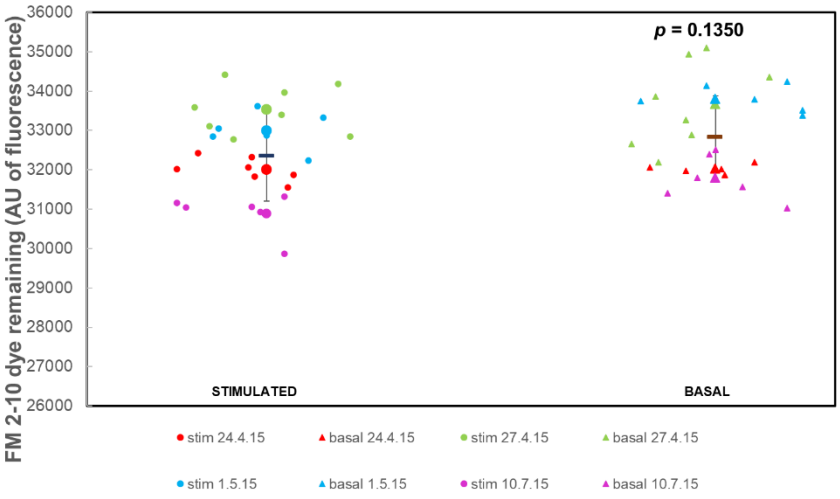

9-cp-ade + forskolin treatment for Fig A4.9b

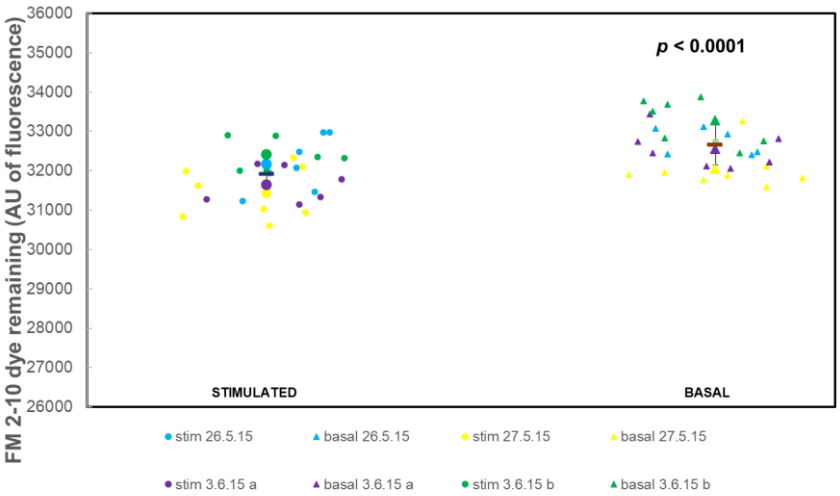

KT5720 + forskolin treatment for Fig A4.10

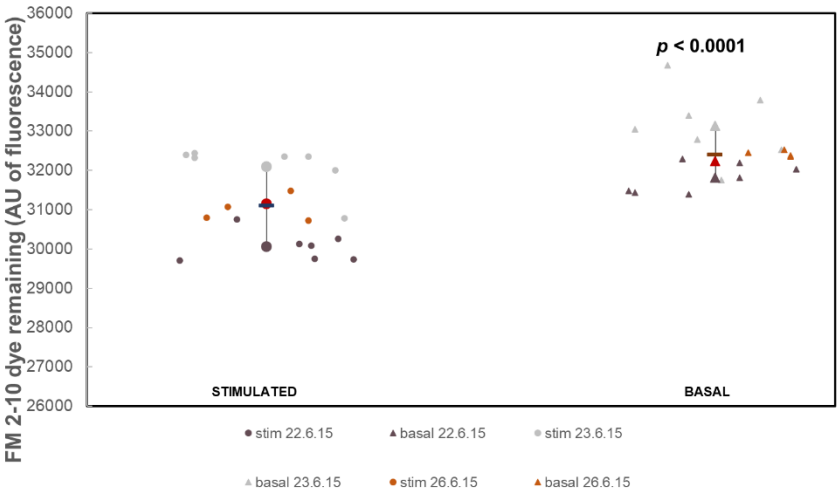

OA treatment for Fig A4.11a

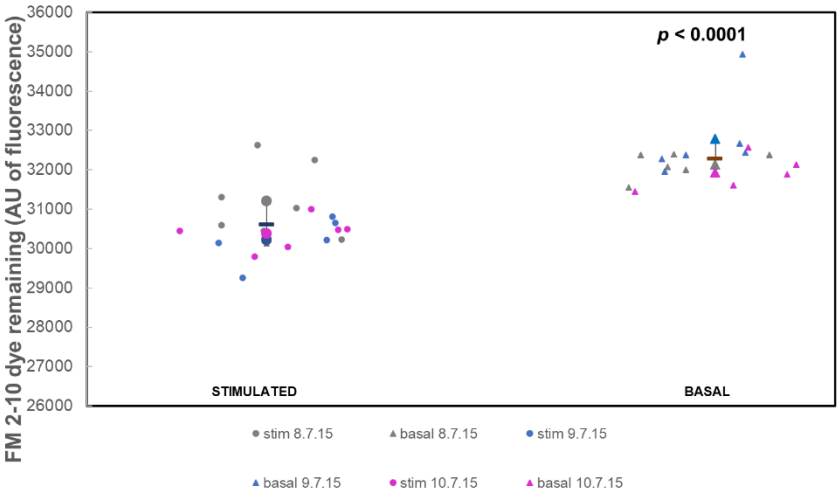

OA + forskolin treatment for Fig A4.11b

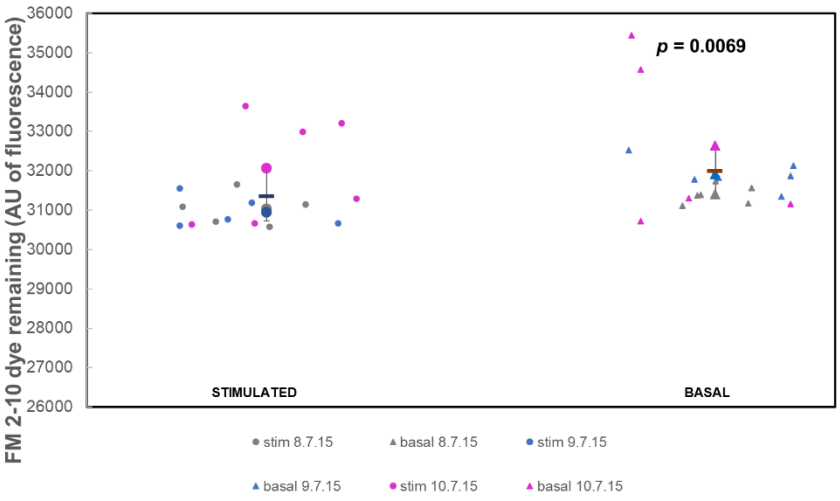

ESI-09 treatment for Fig A4.15

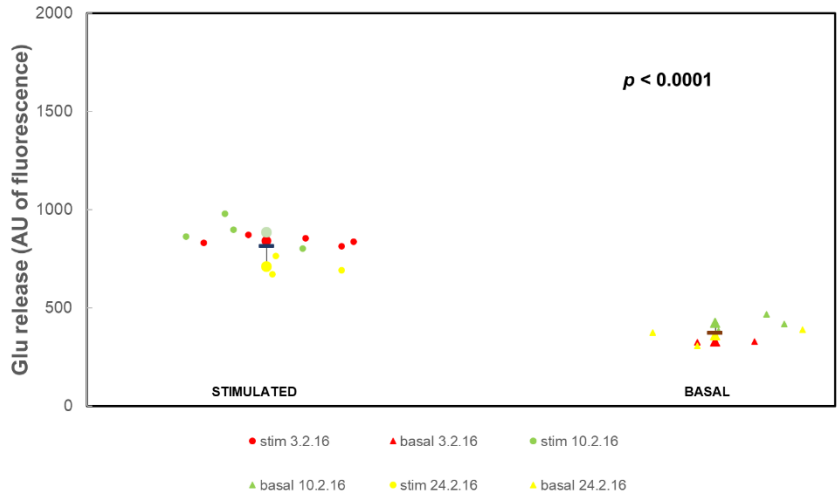

Control non-drug treatment for Fig A4.15, A4.16

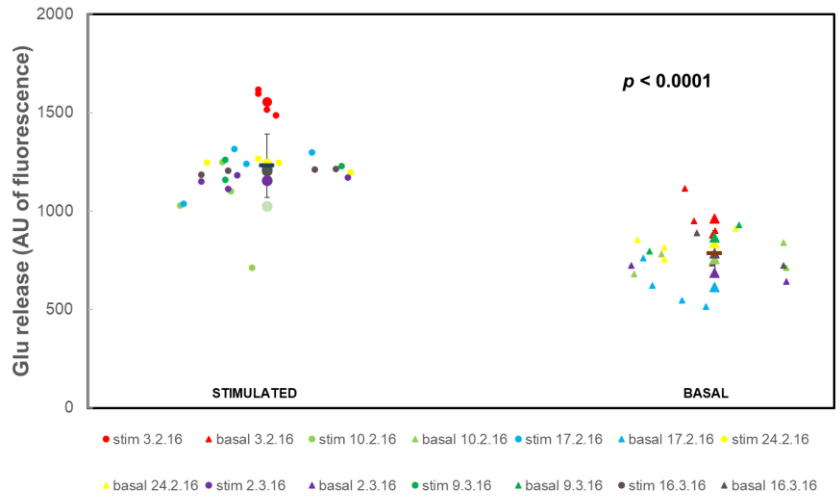

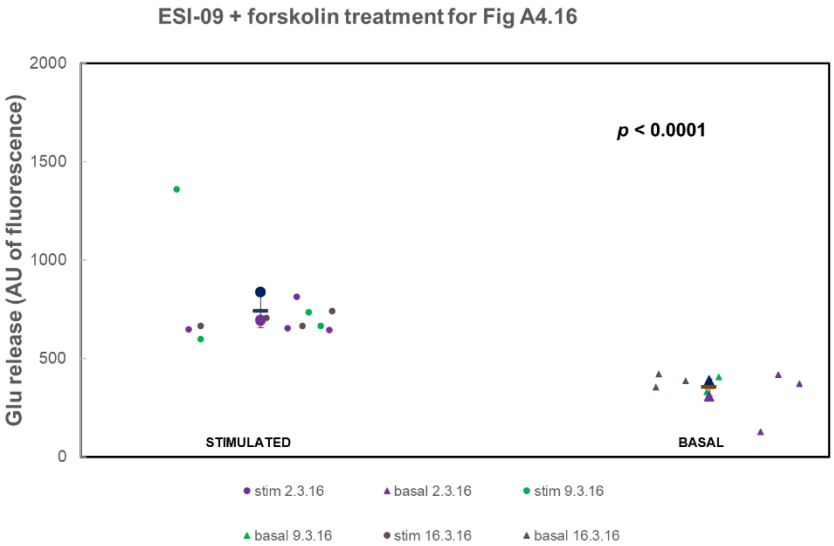
ESI-09 + forskolin treatment for Fig A4.16
Glu release (AU of fluorescence)
2000
1500
1000
500
0
p < 0.0001
STIMULATED
BASAL
stim 2.3.16
basal 2.3.16
stim 9.3.16
basal 9.3.16
stim 16.3.16
basal 16.3.16

B.5 Tabulated Statistical Differences Between Conditions Calculated from the Superplot Data for Chapter 4

Even though the Glu release data (Tables A4.1 to A4.3) utilise the raw data – not the corrected for sensitivity data – the statistics for the superplots still showed the same results as found in Chapter 4. Thus, forskolin inhibited the release of the RP so that Glu release was reduced (see Tables A4.2 and A4.3) whilst it did not effect 4AP5C release which only evoked the RRP SV to exocytose. Similarly, inhibiting AC with 9-cp-ade did not perturb the Glu release for any of the stimuli (Tables A4.1 to A4.3) whilst by blocking AC using 9-cp-ade prevented the action of forskolin on the RP (Table B4.2). Finally, whilst inhibition of EPAC with ESI-09 did not prevent HK5C evoked Glu release, it prevented the action of forskolin (Table B4.2).

Forskolin induced more KR release evoked by 4AP5C (Table B4.4) so that there was significantly less FM dye release. The superplot data also showed that whilst OA increased the FM dye release (as it switched all SVs to FF mode: this was nearly significant and results suggest more experiments could be done, Table B4.4) it was clear that forskolin treatment prevented this OA induced extra release (Table B4.4). However, whilst OA did not stop forskolin action, KT5720 did prevent forskolin action (again this was nearly significant and more results could be done). Inhibition of AC using 9-cp-ade did not prevent the normal release of Glu FM2-10 dye evoked by 4AP5C (Table B4.4), HK5C (Table B4.5) or ION5C (Table B4.6) but pre-treatment with this drug prevented the action of foskolin (Table B4.4). Thus, in most cases the beeswarm plot calculations produced the same statitical findings as that in Chapter 4.

Condition	Mean	SEM	n	*p* relative to control	Significance
4AP5C control	569.3956	74.17339	36	-	-
4AP5C 9-cp-ade	562.3278	56.34558	13	0.9564	not significant
4AP5C 9-cp-ade + forskolin	610.9861	66.09901	13	0.7509	not significant
Condition	**Mean**	**SEM**	**n**	***p* relative to control**	**Significance**
4AP5C control	388.6	44.85255	12	-	-
4AP5C forskolin	367.8556	71.26119	12	0.8077	not significant

Table B4.1: 4AP5C Glu release control vs drug treatments statistics using superplot data.

Condition	Mean	SEM	n	*p* relative to control	Significance
HK5C control	888.65	38.89537	9	-	-
HK5C 9-cp-ade	932.05	73.07686	9	0.6073	not significant
HK5C 9-cp-ade + forskolin	871.675	81.63915	8	0.8481	not significant
Condition	**Mean**	**SEM**	**n**	***p* relative to control**	**Significance**
HK5C control	539.2476	54.16584	28	-	-
HK5C forskolin	327.3346	29.55707	29	0.001	significant difference
Condition	**Mean**	**SEM**	**n**	***p* relative to control**	**Significance**
HK5C control	445.869	39.66714	25	-	-
HK5C ESI-09	442.3389	32.89753	10	0.958	not significant
HK5C ESI-09 + forskolin	387.6667	30.07042	10	0.3839	not significant

Table B4.2: HK5C Glu release control vs drug treatments statistics using superplot data.

Condition	Mean	SEM	n	*p* relative to control	Significance
ION5C control	962.1648	41.65487	25	-	-
ION5C 9-cp-ade	931.1333	28.00026	13	0.6168	not significant
ION5C forskolin	613.2333	102.6398	11	0.006	significant difference

Table B4.3: ION5C Glu release control vs drug treatments statistics using superplot data.

Condition	Mean	SEM	n	*p* relative to control	Significance
4AP5C control	-1124.94	138.9882	89	-	-
4AP5C OA	-1676.07	159.4098	19	0.0788	not significant
4AP5C forskolin	-459.3	302.5441	27	0.0296	significant difference
4AP5C OA + forskolin	-629.551	214.2436	17	0.1389	should be significant
Condition	**Mean**	**SEM**	**n**	***p* relative to control**	**Significance**
4AP5C control	-704.776	305.5437	28	-	-
4AP5C 9-cp-ade	-752.684	245.1471	20	0.8267	not significant
4AP5C 9-cp-ade + forskolin	-737.783	128.5265	28	0.921	not significant
4AP5C KT5720 + forskolin	-1471.89	292.9168	18	0.0904	should be significant
Condition	**Mean**	**SEM**	**n**	***p* relative to OA**	**Significance**
4AP5C OA	-1676.07	159.4098	19	-	-
4AP5C OA + forskolin	-629.551	214.2436	17	0.0004	significant difference

Table B4.4: 4AP5C FM 2-10 release control vs drug treatments statistics using superplot data.

Condition	Mean	SEM	n	*p* relative to control	Significance
HK5C control	-1307.93	153.7692	32	-	-
HK5C 9-cp-ade	-1394.94	137.85	22	0.6915	not significant

Table B4.5: HK5C FM 2-10 release control vs drug treatments statistics using superplot data.

Condition	mean	SEM	n	p relative to control	Significance
ION5C control	-3133.69	86.92914	78	-	-
ION5C 9-cp-ade	-3144.84	86.79527	21	0.949	not significant

Table B4.6: ION5C FM 2-10 release control vs drug treatments statistics using superplot data.

B.6 Beeswarm Superplots for Chapter 5

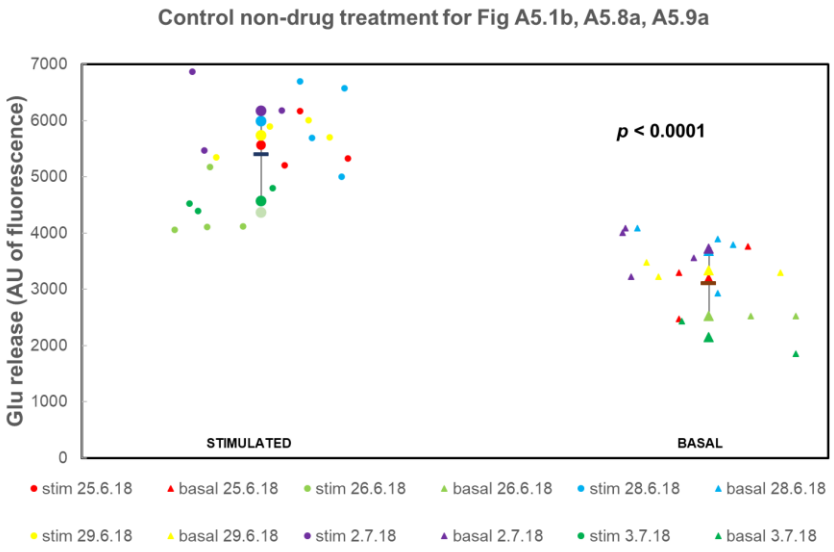

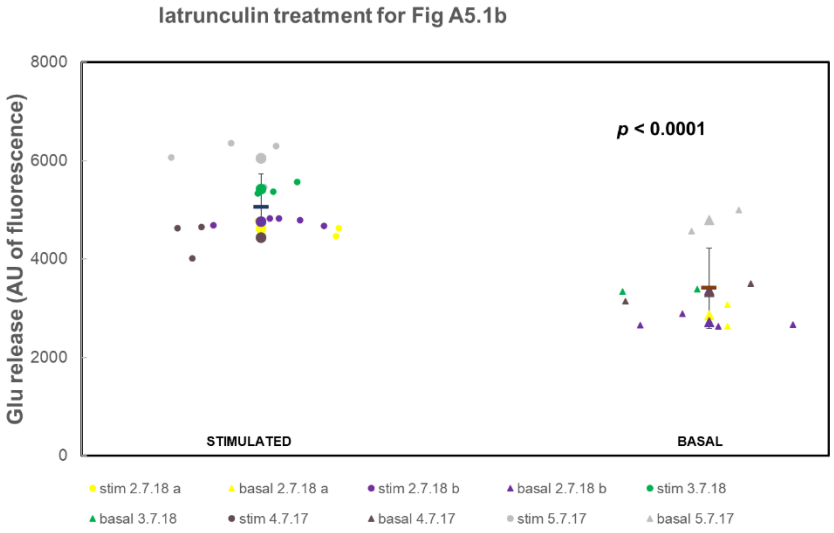

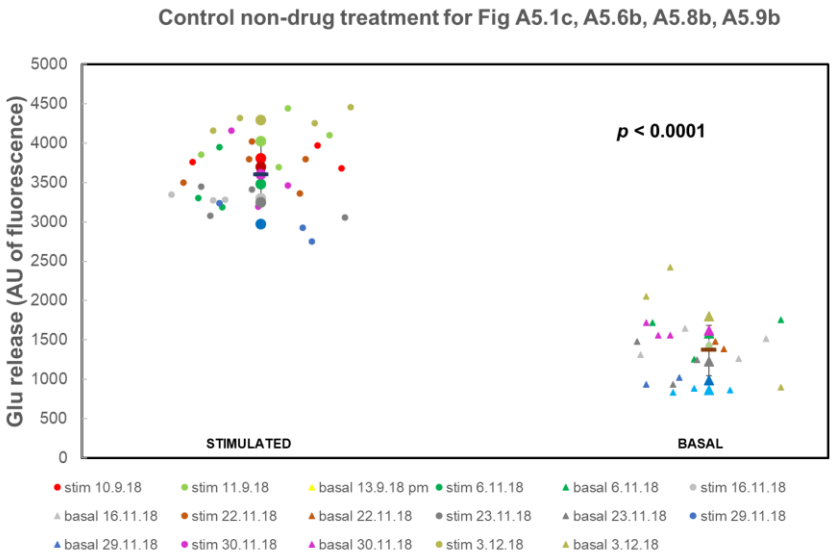

latrunculin for Fig A5.1c

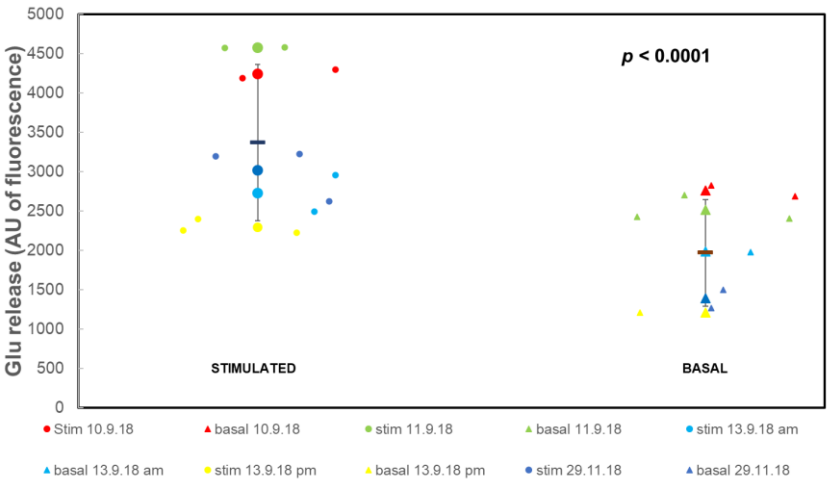

Control non-drug treatment for Fig A5.2a, A5.4a, A5.4b, A5.10a, A5.11a, A5.12a

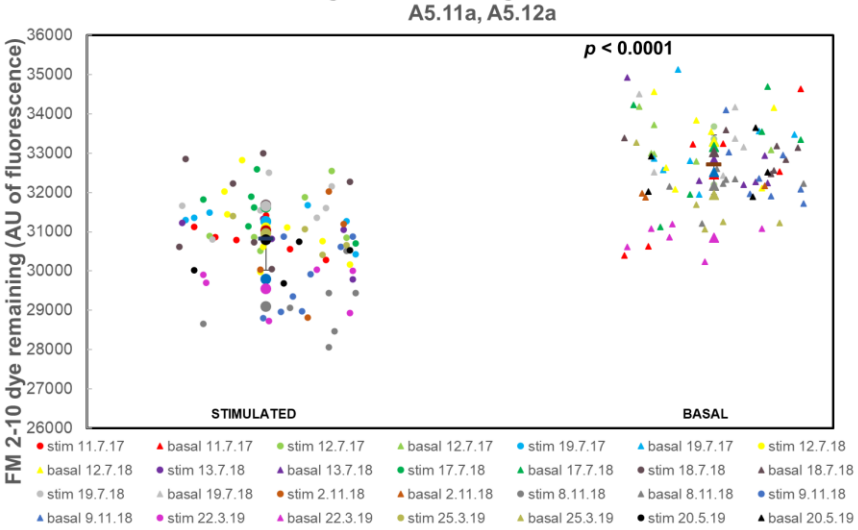

latrunculin treatment for Fig A5.2a

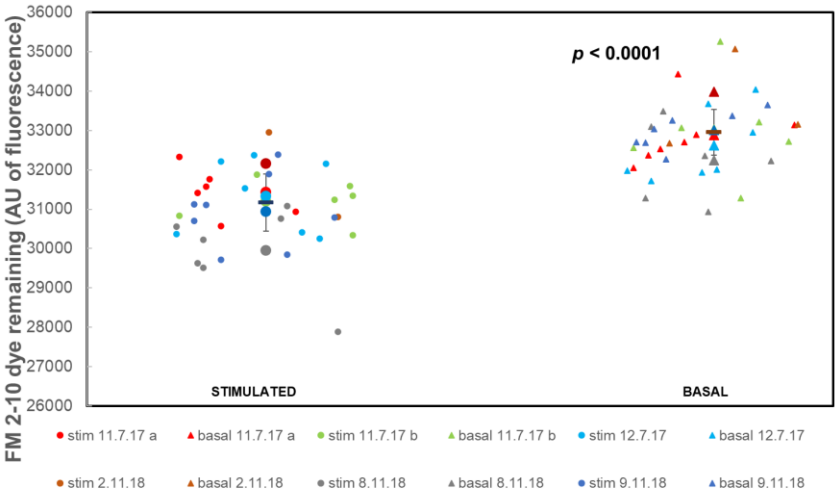

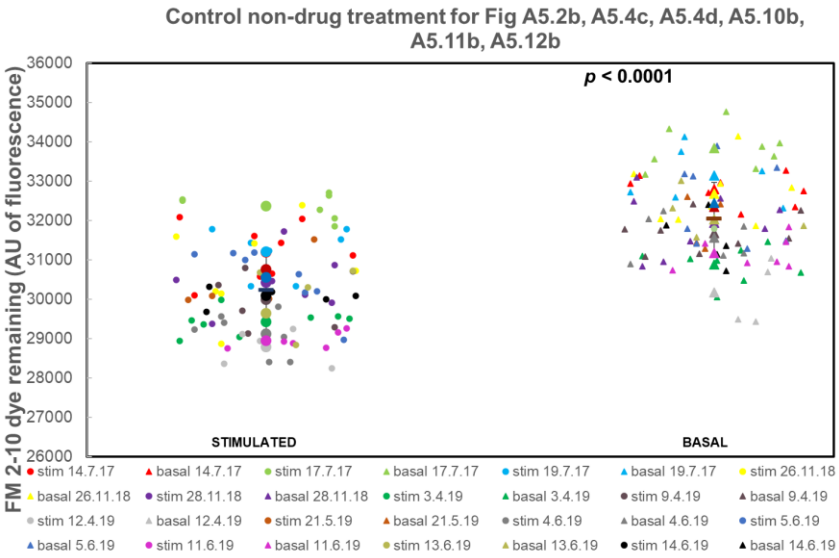
Control non-drug treatment for Fig A5.2b, A5.4c, A5.4d, A5.10b, A5.11b, A5.12b
p < 0.0001
FM 2-10 dye remaining (AU of fluorescence)
36000
35000
34000
33000
32000
31000
30000
29000
28000
27000
26000
STIMULATED
BASAL
stim 14.7.17
basal 14.7.17
stim 17.7.17
basal 17.7.17
stim 19.7.17
basal 19.7.17
stim 26.11.18
basal 26.11.18
stim 28.11.18
basal 28.11.18
stim 3.4.19
basal 3.4.19
stim 9.4.19
basal 9.4.19
stim 12.4.19
basal 12.4.19
stim 21.5.19
basal 21.5.19
stim 4.6.19
basal 4.6.19
stim 5.6.19
basal 5.6.19
stim 11.6.19
basal 11.6.19
stim 13.6.19
basal 13.6.19
stim 14.6.19
basal 14.6.19

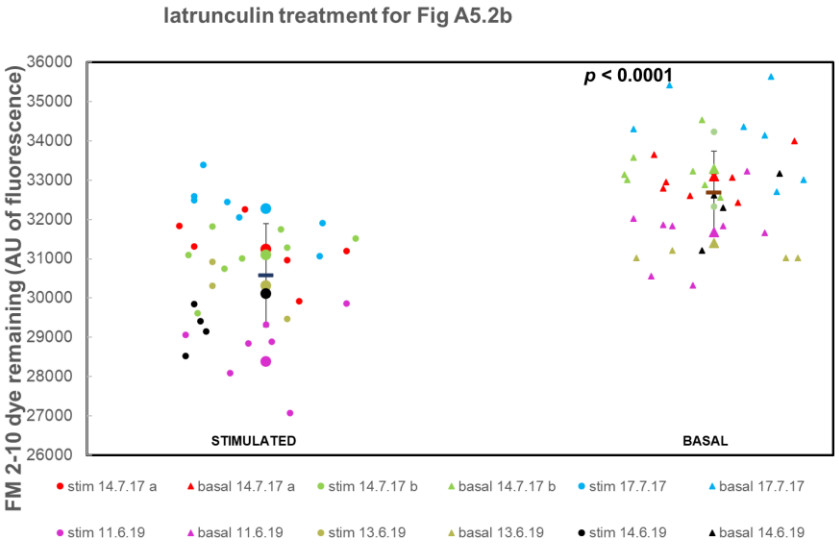
latrunculin treatment for Fig A5.2b
p < 0.0001
FM 2-10 dye remaining (AU of fluorescence)
36000
35000
34000
33000
32000
31000
30000
29000
28000
27000
26000
STIMULATED
BASAL
stim 14.7.17 a
basal 14.7.17 a
stim 14.7.17 b
basal 14.7.17 b
stim 17.7.17
basal 17.7.17
stim 11.6.19
basal 11.6.19
stim 13.6.19
basal 13.6.19
stim 14.6.19
basal 14.6.19

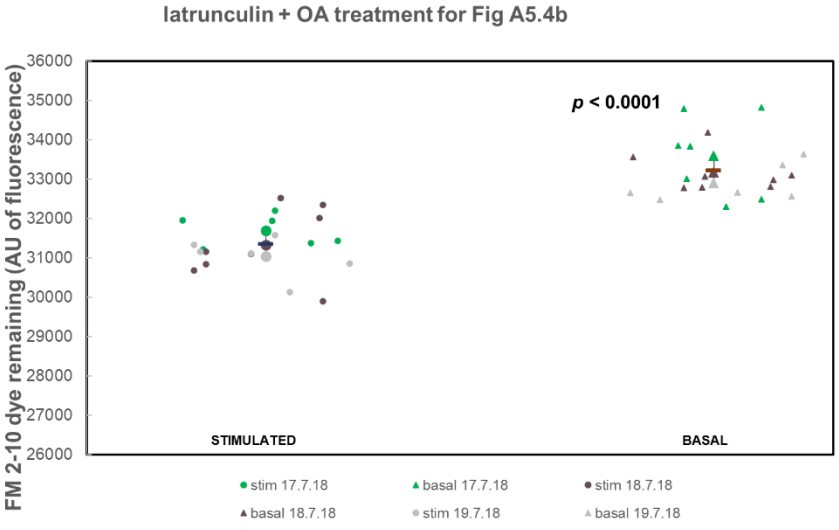
latrunculin + OA treatment for Fig A5.4b
p < 0.0001
FM 2-10 dye remaining (AU of fluorescence)
36000
35000
34000
33000
32000
31000
30000
29000
28000
27000
26000
STIMULATED
BASAL
stim 17.7.18
basal 17.7.18
stim 18.7.18
basal 18.7.18
stim 19.7.18
basal 19.7.18

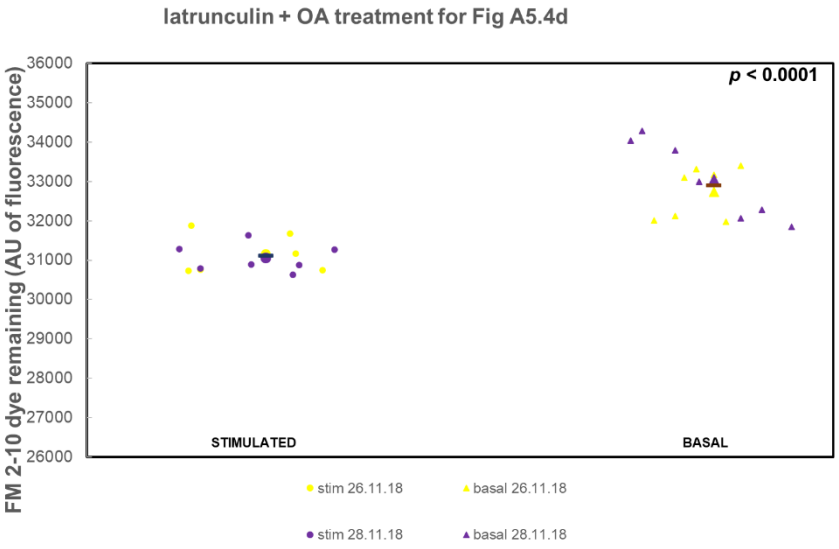
latrunculin + OA treatment for Fig A5.4d
FM 2-10 dye remaining (AU of fluorescence)
36000
35000
34000
33000
32000
31000
30000
29000
28000
27000
26000
p < 0.0001
STIMULATED
BASAL
stim 26.11.18
basal 26.11.18
stim 28.11.18
basal 28.11.18

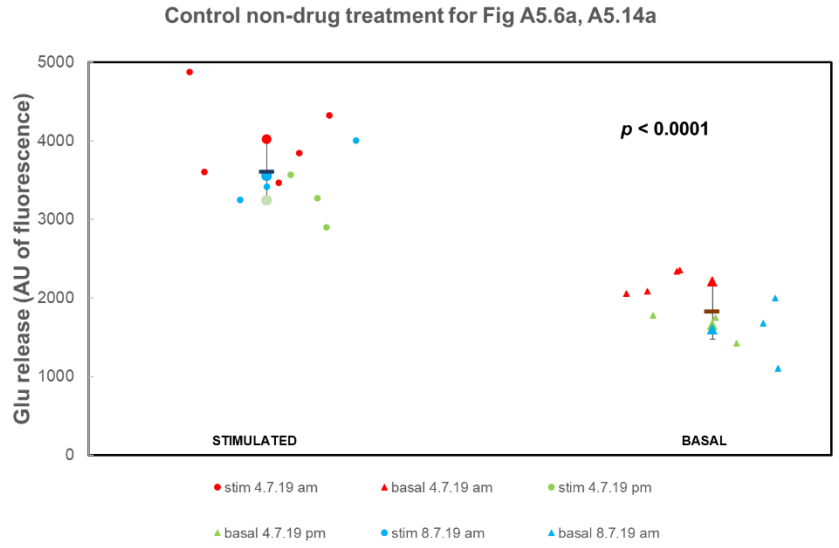
Control non-drug treatment for Fig A5.6a, A5.14a
Glu release (AU of fluorescence)
5000
4000
3000
2000
1000
0
p < 0.0001
STIMULATED
BASAL
stim 4.7.19 am
basal 4.7.19 am
stim 4.7.19 pm
basal 4.7.19 pm
stim 8.7.19 am
basal 8.7.19 am

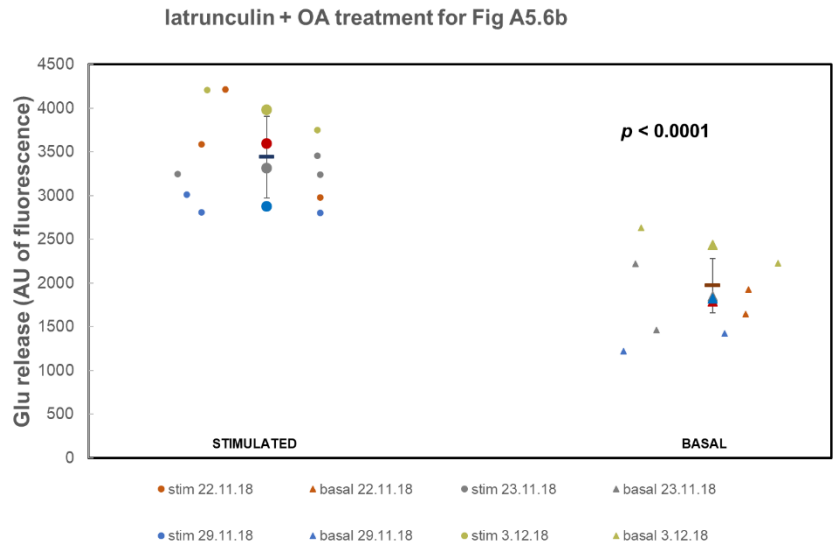
latrunculin + OA treatment for Fig A5.6b
Glu release (AU of fluorescence)
4500
4000
3500
3000
2500
2000
1500
1000
500
0
p < 0.0001
STIMULATED
BASAL
stim 22.11.18
basal 22.11.18
stim 23.11.18
basal 23.11.18
stim 29.11.18
basal 29.11.18
stim 3.12.18
basal 3.12.18

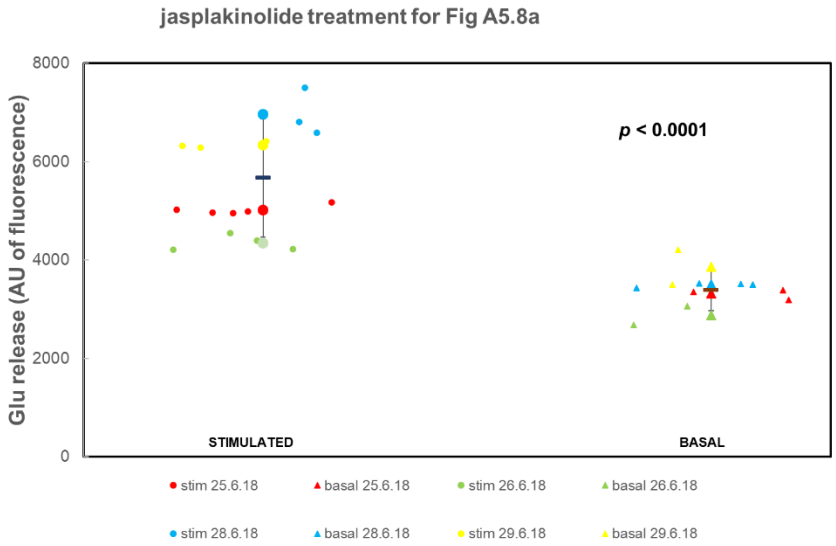
jasplakinolide treatment for Fig A5.8a
Glu release (AU of fluorescence)
8000
6000
4000
2000
0
p < 0.0001
STIMULATED
BASAL
stim 25.6.18
basal 25.6.18
stim 26.6.18
basal 26.6.18
stim 28.6.18
basal 28.6.18
stim 29.6.18
basal 29.6.18

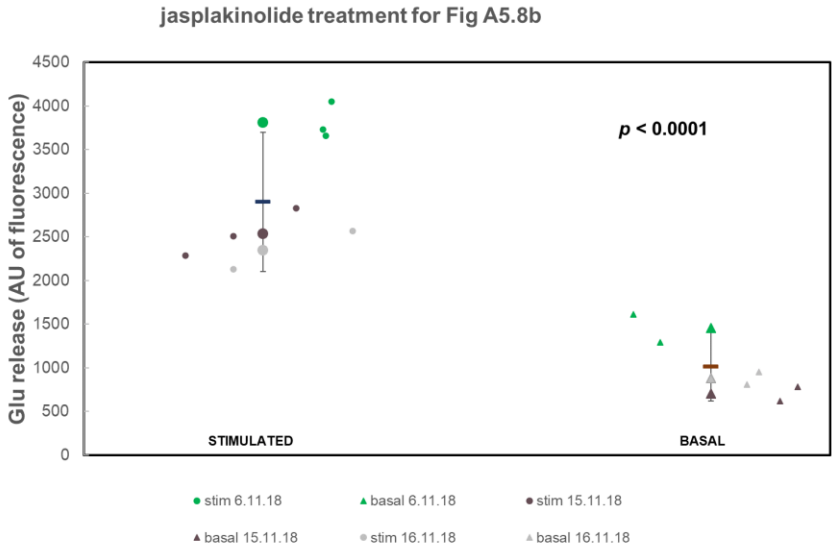
jasplakinolide treatment for Fig A5.8b
Glu release (AU of fluorescence)
4500
4000
3500
3000
2500
2000
1500
1000
500
0
p < 0.0001
STIMULATED
BASAL
stim 6.11.18
basal 6.11.18
stim 15.11.18
basal 15.11.18
stim 16.11.18
basal 16.11.18

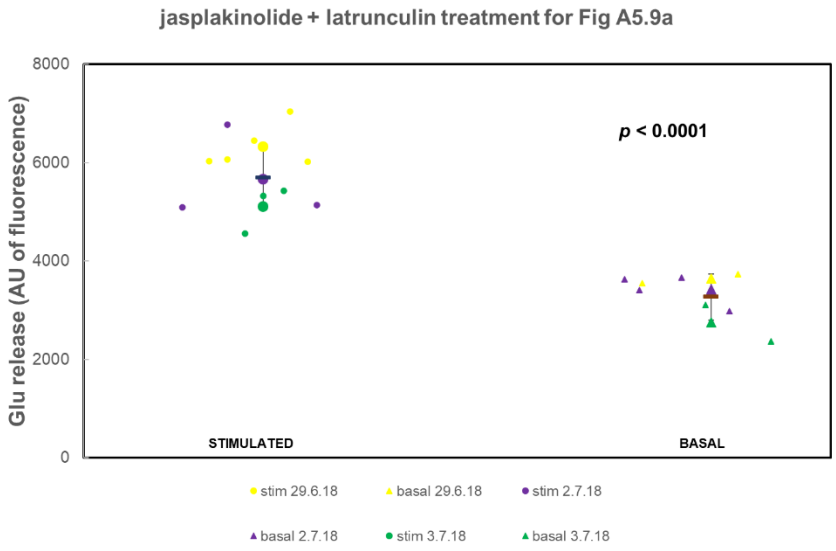
jasplakinolide + latrunculin treatment for Fig A5.9a
Glu release (AU of fluorescence)
8000
6000
4000
2000
0
p < 0.0001
STIMULATED
BASAL
stim 29.6.18
basal 29.6.18
stim 2.7.18
basal 2.7.18
stim 3.7.18
basal 3.7.18

jasplakinolide + latrunculin for Fig A5.9b

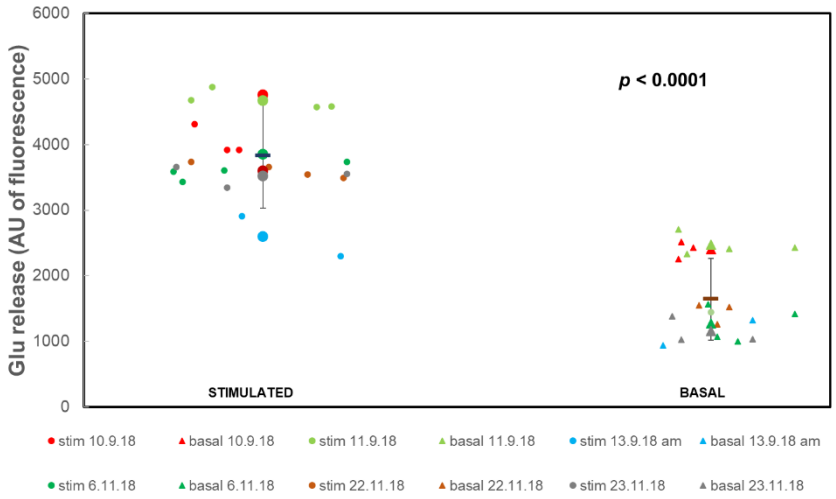

jasplakinolide treatment for Fig A5.10a

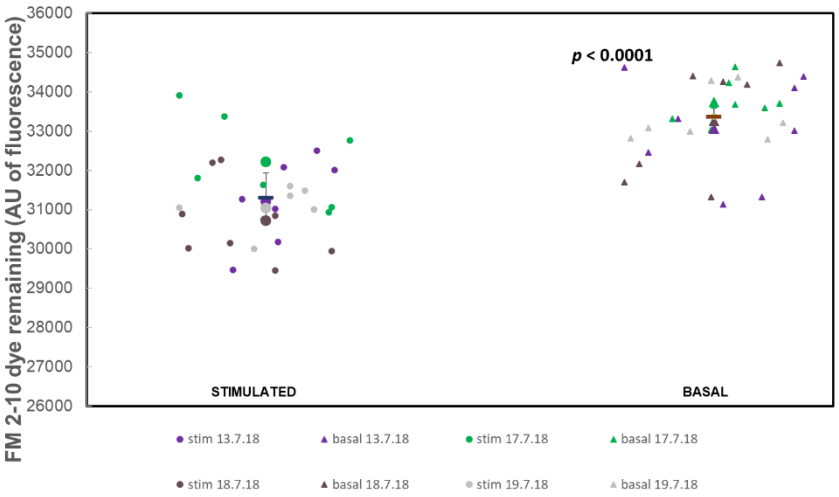

jasplakinolide treatment for Fig A5.10b

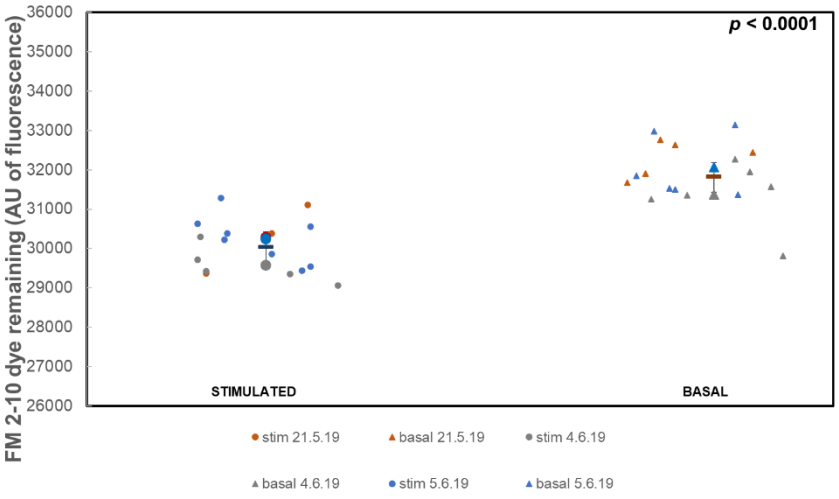

jasplakinolide + latrunculin for Fig A5.11a

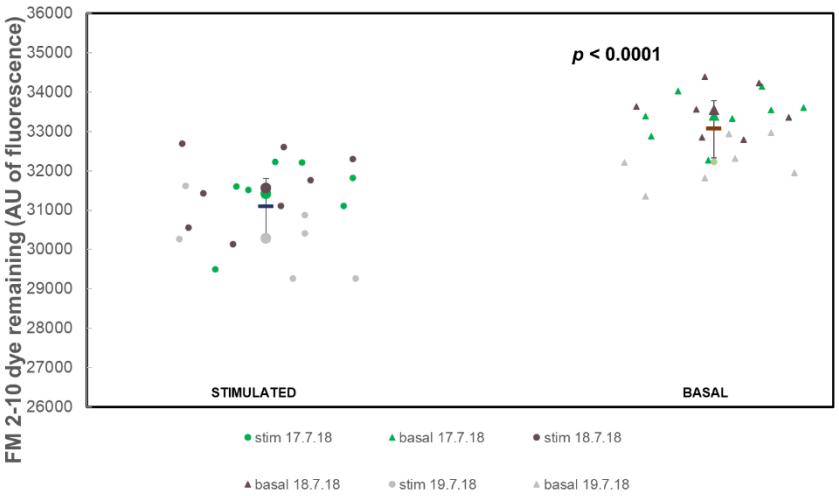

jasplakinolide + latrunculin for Fig A5.11b

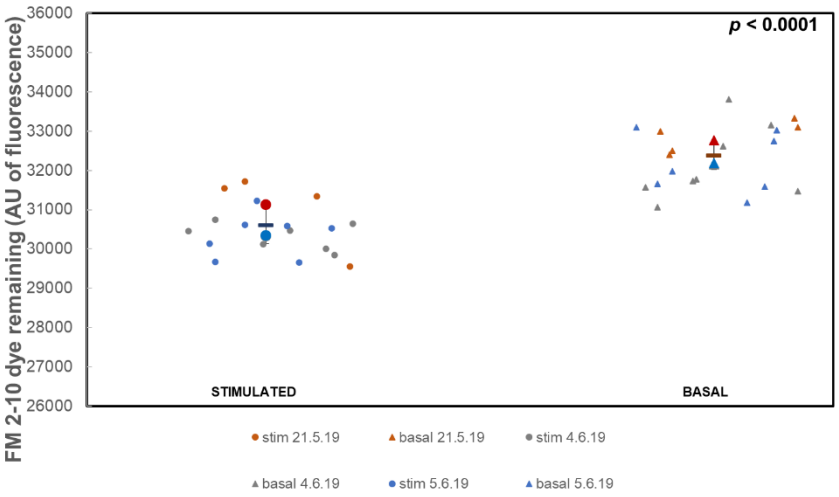

jasplakinolide + latrunculin + OA for Fig A5.12a

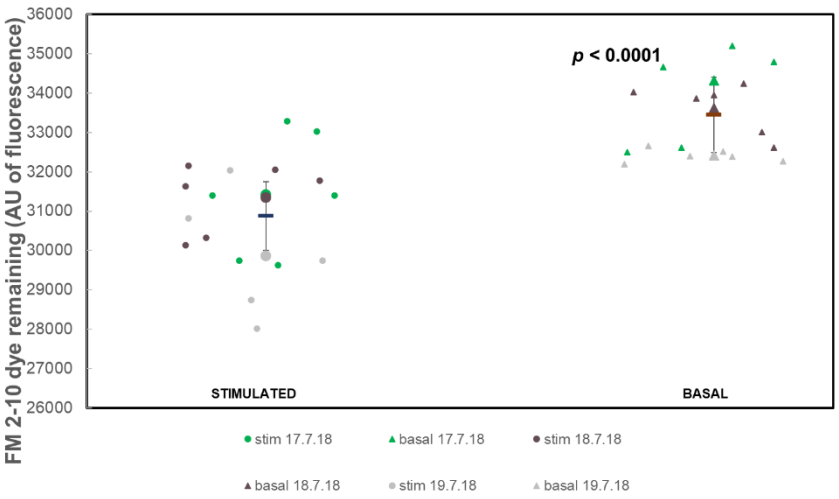

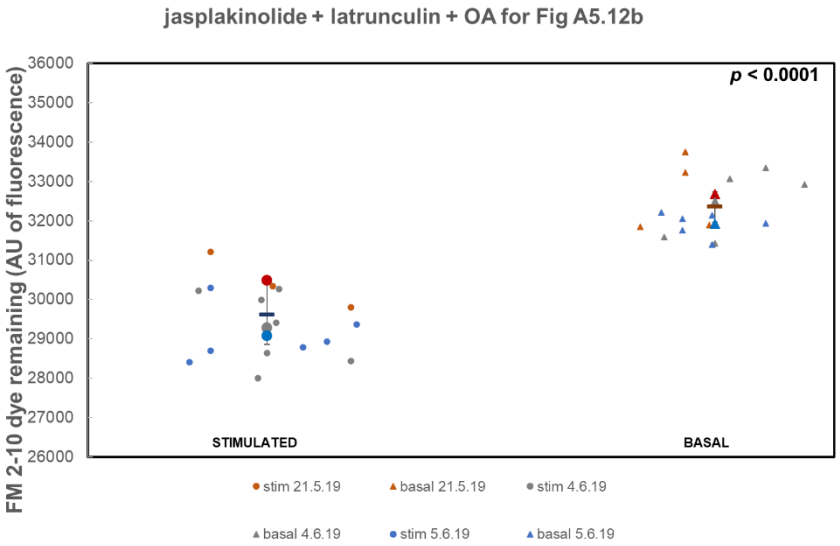
jasplakinolide + latrunculin + OA for Fig A5.12b
FM 2-10 dye remaining (AU of fluorescence)
36000
35000
34000
33000
32000
31000
30000
29000
28000
27000
26000
p < 0.0001
STIMULATED
BASAL
stim 21.5.19
basal 21.5.19
stim 4.6.19
basal 4.6.19
stim 5.6.19
basal 5.6.19

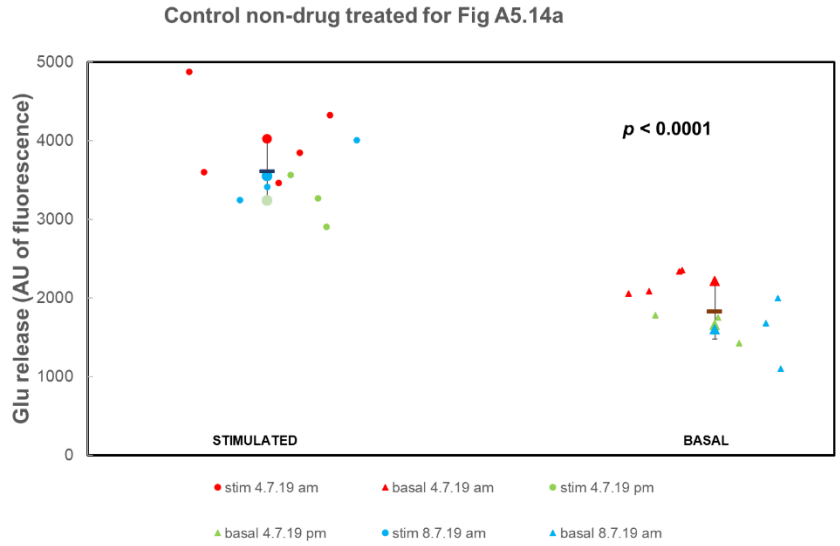
Control non-drug treated for Fig A5.14a
Glu release (AU of fluorescence)
5000
4000
3000
2000
1000
0
p < 0.0001
STIMULATED
BASAL
stim 4.7.19 am
basal 4.7.19 am
stim 4.7.19 pm
basal 4.7.19 pm
stim 8.7.19 am
basal 8.7.19 am

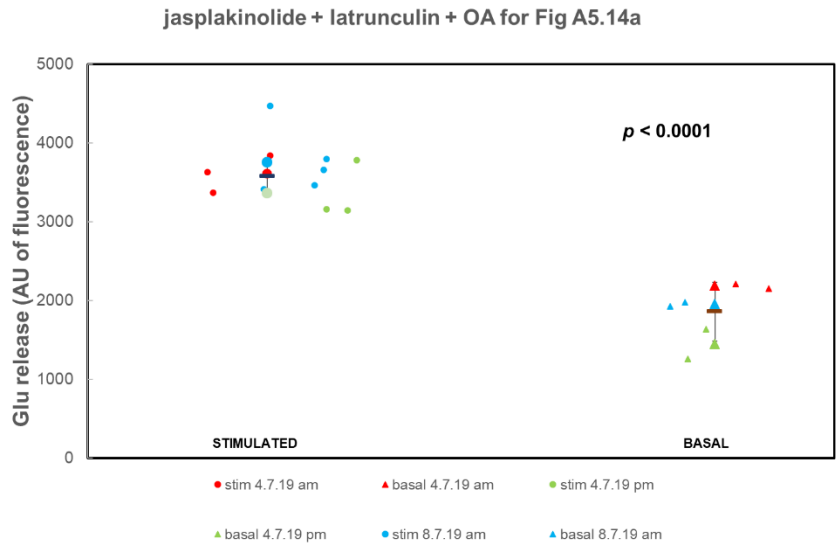
jasplakinolide + latrunculin + OA for Fig A5.14a
Glu release (AU of fluorescence)
5000
4000
3000
2000
1000
0
p < 0.0001
STIMULATED
BASAL
stim 4.7.19 am
basal 4.7.19 am
stim 4.7.19 pm
basal 4.7.19 pm
stim 8.7.19 am
basal 8.7.19 am

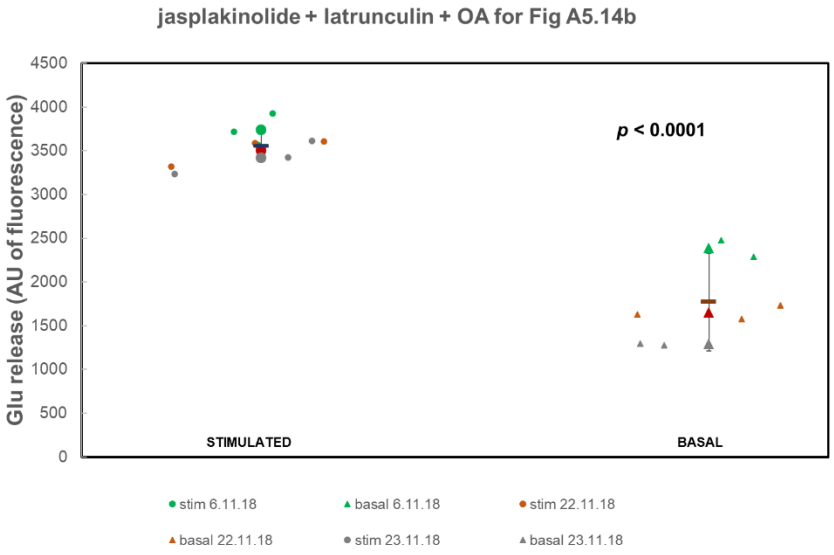
jasplakinolide + latrunculin + OA for Fig A5.14b
Glu release (AU of fluorescence)
4500
4000
3500
3000
2500
2000
1500
1000
500
0
p < 0.0001
STIMULATED
BASAL
stim 6.11.18
basal 6.11.18
stim 22.11.18
basal 22.11.18
stim 23.11.18
basal 23.11.18

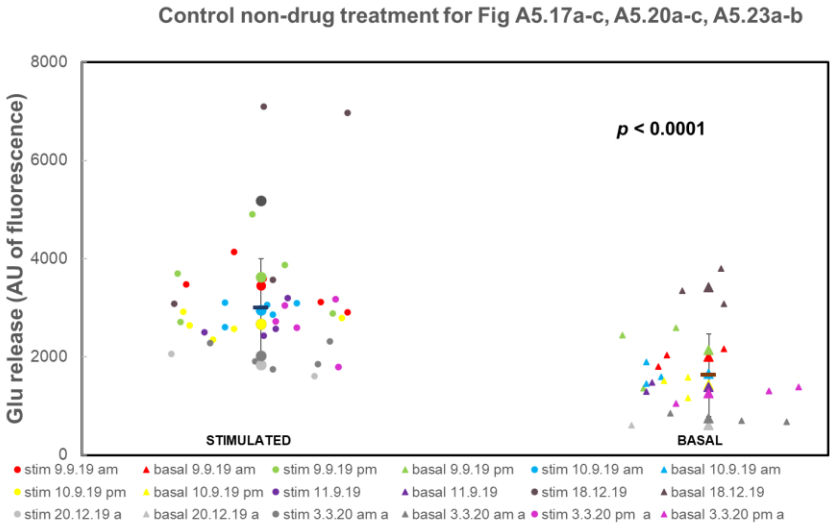
Control non-drug treatment for Fig A5.17a-c, A5.20a-c, A5.23a-b
Glu release (AU of fluorescence)
8000
6000
4000
2000
0
p < 0.0001
STIMULATED
BASAL
stim 9.9.19 am
basal 9.9.19 am
stim 9.9.19 pm
basal 9.9.19 pm
stim 10.9.19 am
basal 10.9.19 am
stim 10.9.19 pm
basal 10.9.19 pm
stim 11.9.19
basal 11.9.19
stim 18.12.19
basal 18.12.19
stim 20.12.19 a
basal 20.12.19 a
stim 3.3.20 am a
basal 3.3.20 am a
stim 3.3.20 pm a
basal 3.3.20 pm a

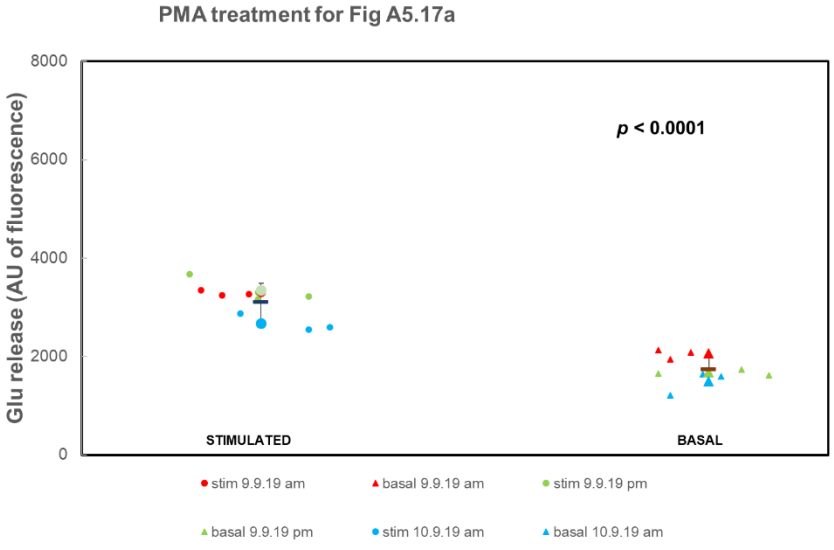
PMA treatment for Fig A5.17a
Glu release (AU of fluorescence)
8000
6000
4000
2000
0
p < 0.0001
STIMULATED
BASAL
stim 9.9.19 am
basal 9.9.19 am
stim 9.9.19 pm
basal 9.9.19 pm
stim 10.9.19 am
basal 10.9.19 am

PMA plus latrunculin treatment for Fig A5.17b

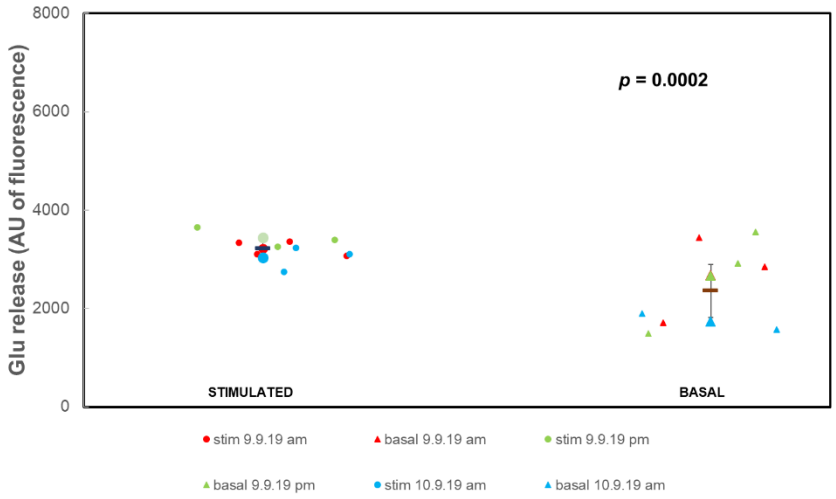

PMA + latrunculin + OA treatment for Fig A5.17c

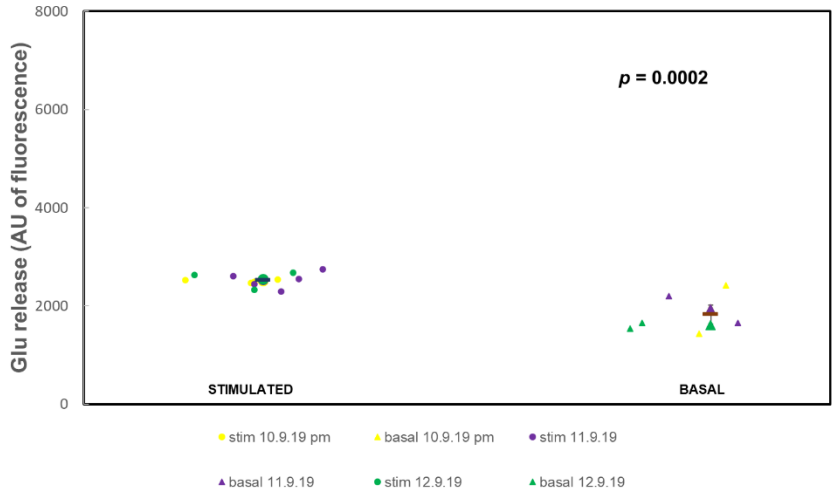

Control non-drug treatment for Fig A5.18a-c, A5.21a-c, A5.24a-b

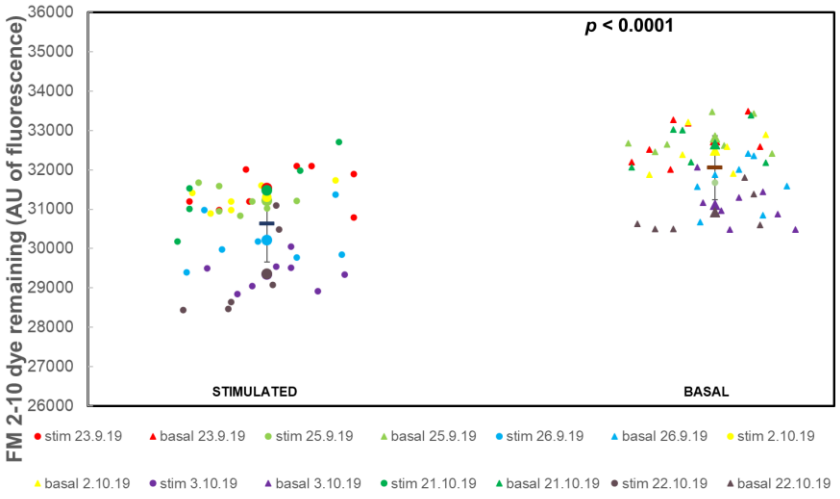

PMA treatment for Fig A5.18a

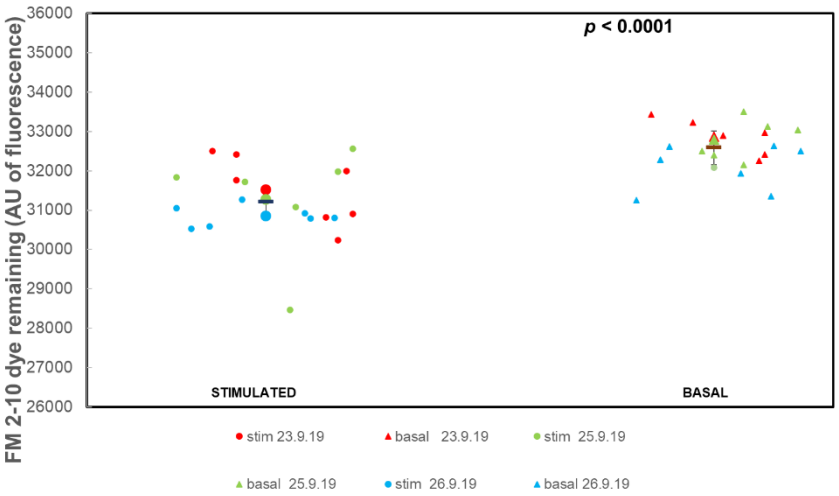

PMA + latrunculin treatment for Fig A5.18b

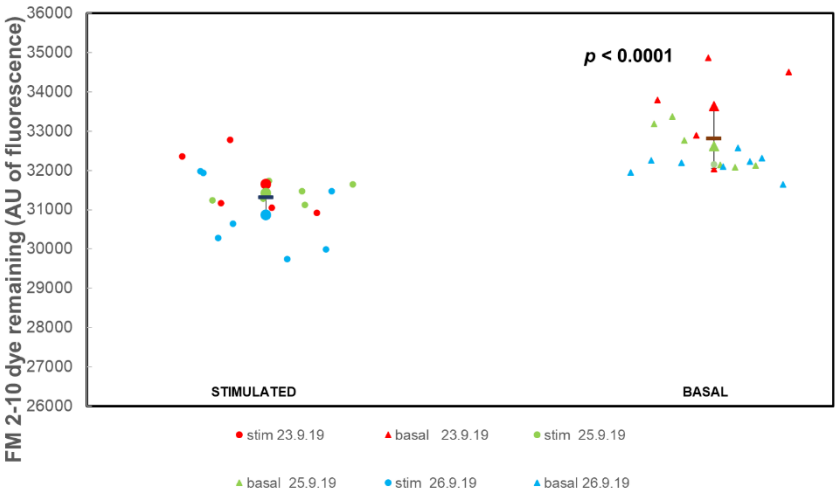

PMA + latrunculin + OA treatment for Fig A5.18c

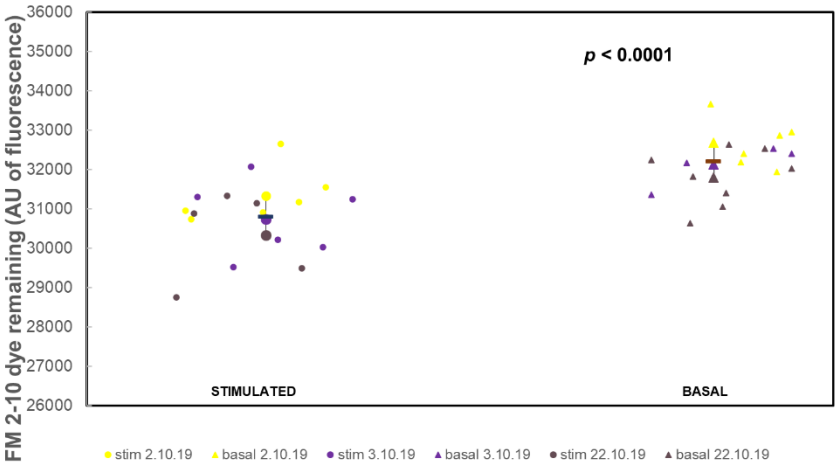

PMA + jasplakinolide treatment for Fig A5.20a

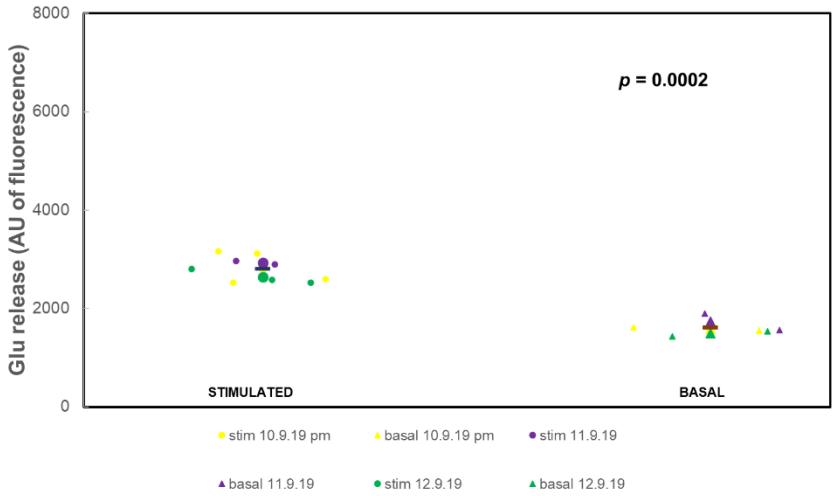

PMA + jasplakinolide + latrunculin treatment for Fig A5.20b

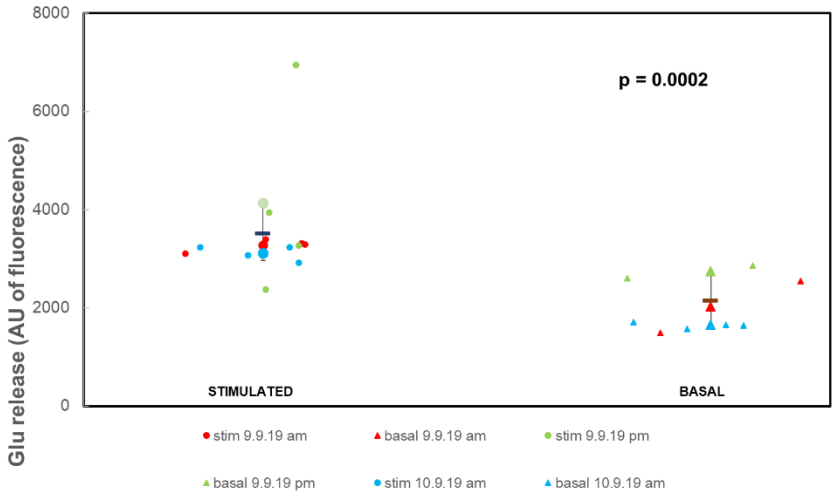

PMA + jasplakinolide + latrunculin + OA treatment for Fig A5.20c

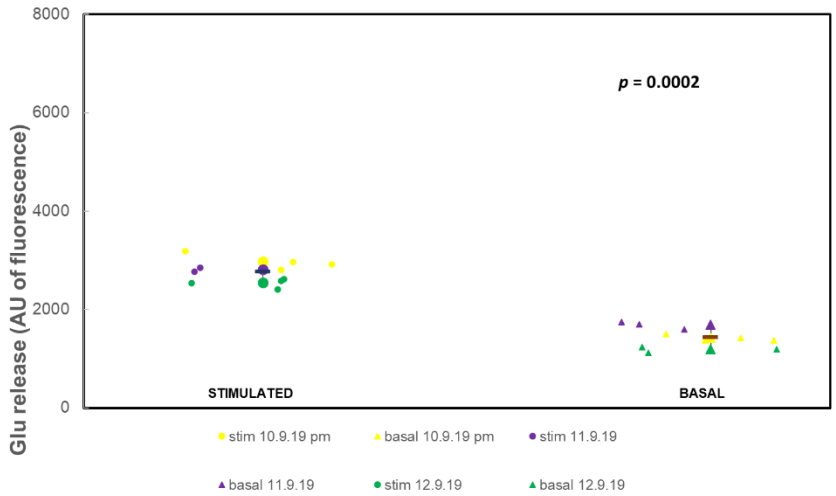

PMA + jasplakinolide treatment for Fig A5.21a

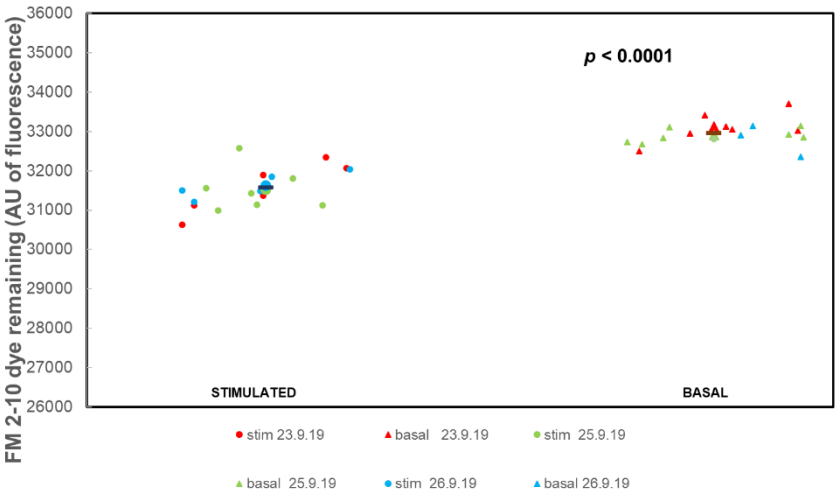

PMA + jasplakinolide + latrunculin treatment for Fig A5.21b

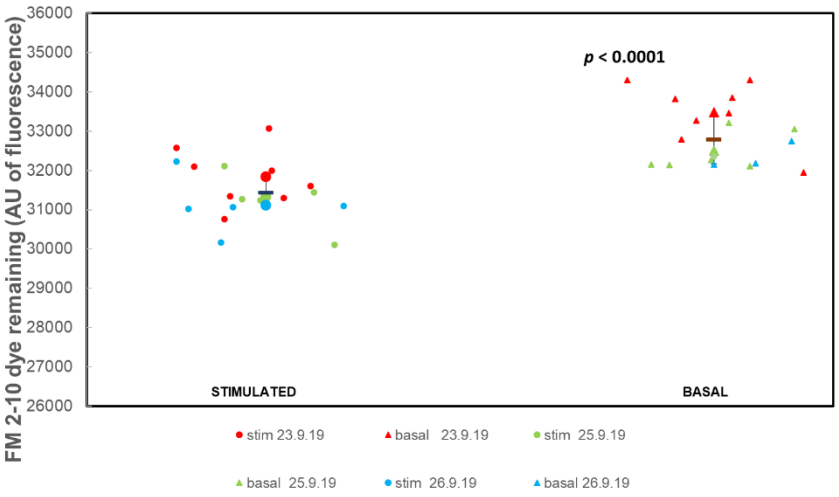

PMA + jasplakinolide + latrunculin + OA treatment for Fig A5.21c

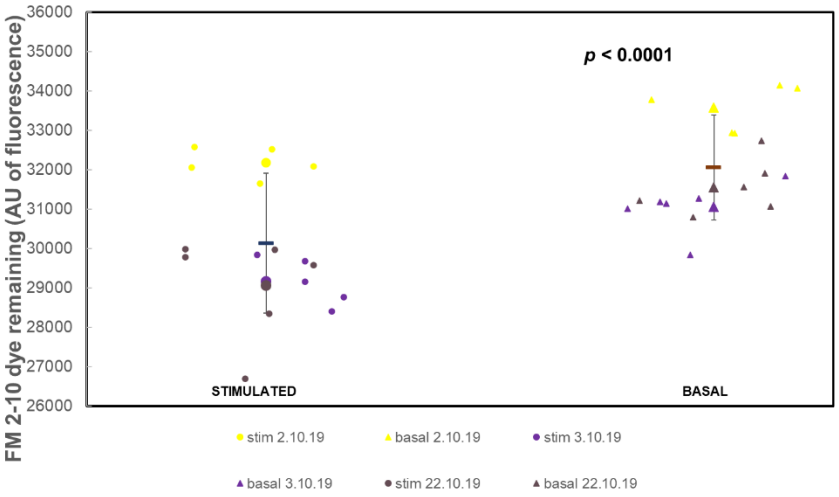

PMA + latrunculin + blebbistatin treatment for Fig A5.23a

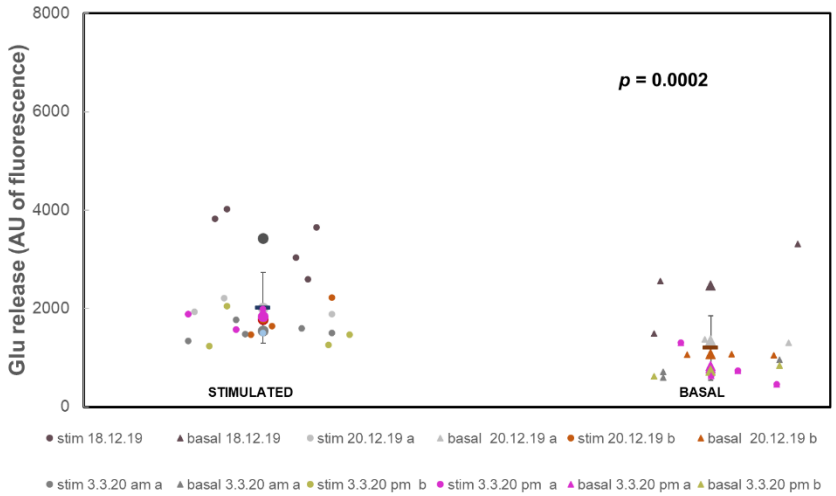

PMA + jasplakinolide + latrunculin + blebbistatin pretreatment for Fig A5.23b

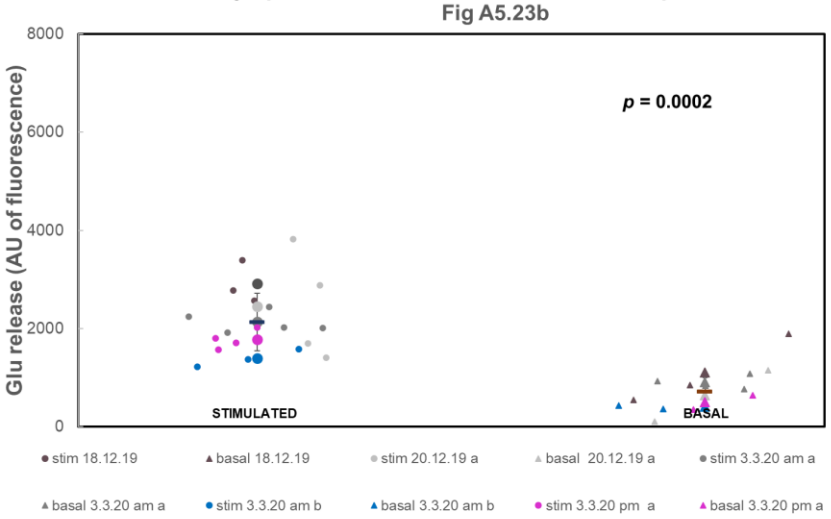

PMA + latrunculin + blebbistatin treatment for Fig A5.24a

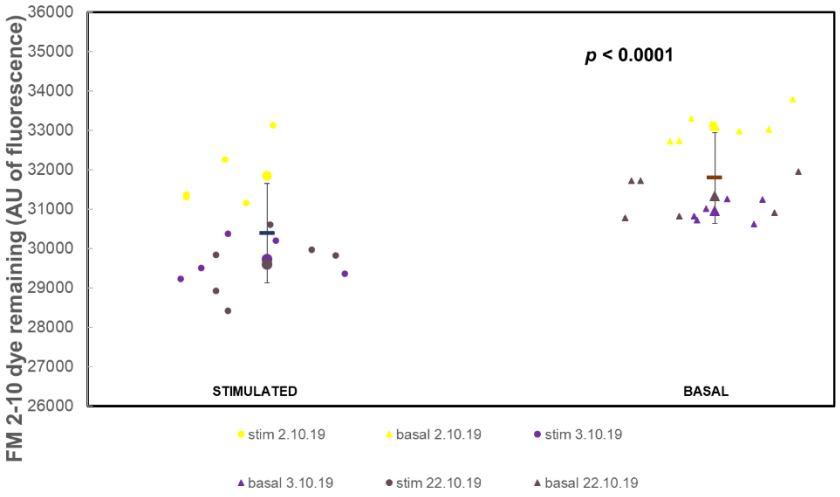

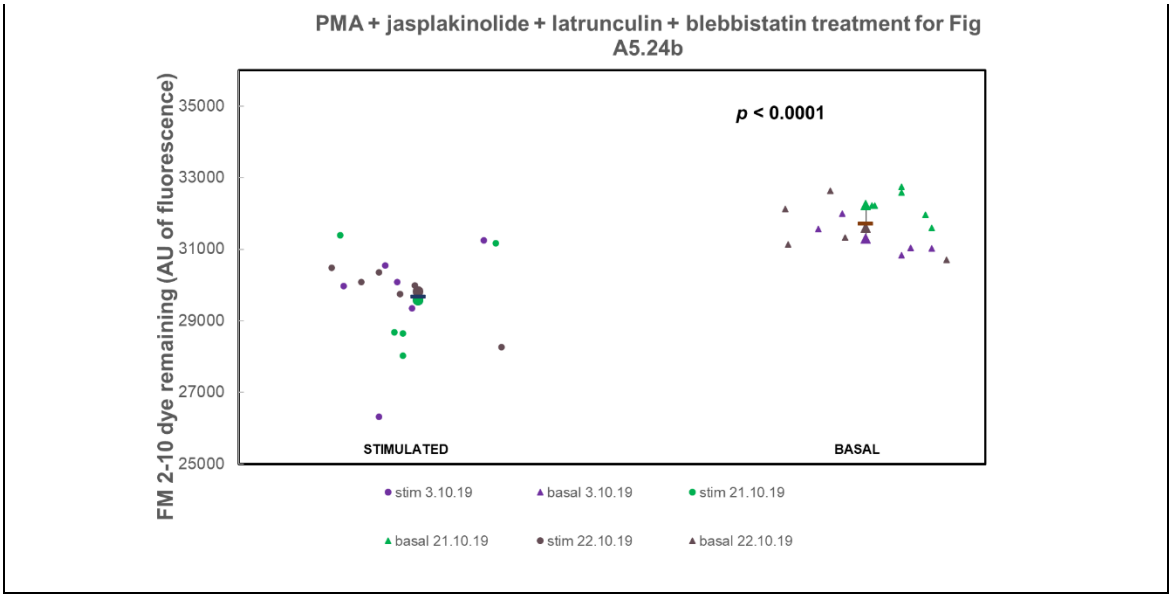
PMA + jasplakinolide + latrunculin + blebbistatin treatment for Fig A5.24b
FM 2-10 dye remaining (AU of fluorescence)
35000
33000
31000
29000
27000
25000
p < 0.0001
STIMULATED
BASAL
stim 3.10.19
basal 3.10.19
stim 21.10.19
basal 21.10.19
stim 22.10.19
basal 22.10.19

B.7 Tabulated Statistical Differences Between Conditions Calculated From the Superplot Data for Chapter 5

Latrunculin treatment inhibits the release of the RP and so there is a reduction in the amount of HK5C evoked Ca^{2+} dependent release although without correcting for the sensitivity, the reduction is not significant (Table B5.1) although this difference is significant for ION5C (Table B5.2). However, treatment with latrunculin and okadaic acid shows the significant reduction in HK5C and ION5C evoked Glu release (Table B5.1, B.2) and this is prevented by jasplakinolide treatment (Table B5.1) although this appears not significant for ION5C (Table B5.2). This is just because there is some deviation because there is variation in the sensitivity.

Latrunculin does not perturb the amount of FM dye release for HK5C (Table B.3) or ION5C (Table B5.4) but this is because it has switched the RRP to FF as shown by the fact that inclusion of okadaic acid with latrunculin fails to induce any extra FM dye release (Table B5.3 and B5.4). However, jasplakinolide prevents the action of latrunculin as shown by the significant increase in release for jasplakinolide plus latrunculin plus OA compared to other conditions (Table B5.3 and B5.4). For the experiments in which ION5C is switched to work on the NMII pathway using 40 nM PMA, latrunculin treatment with other drug treatments (apart from jasplakinolide) does cause the inhibition of release of the RP (Table B5.5) but the stats are just not significant (due to the variation because sensitivity has not been taken into account). However, when jasplakinolide is present it statistically prevents the latrunculin from blocking the RP and Glu is released from this pool (Table B5.5).

The equivalent experiments to that in Table B5.5 but for ION5C evoked FM dye release (Table B5.6) does show that in the presence of 40 nM PMA, one can switch the RRP to FF mode but that when latrunculin action is prevented when jasplakinolide plus okadaic acid or jasplakinolide plus blebbistatin are added there is an increase in FM dye release (as RP undergoes FF exocytosis and so does the RRP) although due to some large SEMs this appears not to be significant (Table B5.6), although the results in Chapter 5 are significantly different.

Condition	Mean	SEM	n	*p* relative to control	Significance
HK5C control	2305.208	220.6755	20	-	-
HK5C jasplakinolide	2285.758	351.3655	13	0.9609	not significant
HK5C jasplakinolide + latrunculin	2431.072	243.028	10	0.7272	not significant
HK5C latrunculin	1651.242	273.0169	17	0.068	should be significant
Condition	**Mean**	**SEM**	**n**	***p* relative to control**	**Significance**
HK5C control	1789.667	156.2054	11	-	-
HK5C latrunculin + OA	1109.989	32.60839	12	0.0002	significant difference
HK5C jasplakinolide + latrunculin + OA	1719.711	142.0123	9	0.7492	not significant
Condition	**Mean**	**SEM**	**n**	***p* relative to latrunculin alone**	**Significance**
HK5C latrunculin	1651.242	273.0169	17	-	-
HK5C jasplakinolide + latrunculin	2431.072	243.028	10	0.0645	should be significant
Condition	**Mean**	**SEM**	**n**	***p* relative to latrunculin + OA**	**significance**
HK5C latrunculin + OA	1109.989	32.60839	12	-	-
HK5C jasplakinolide + latrunculin + OA	1719.711	142.0123	9	0.0001	significant difference

Table B5.1: HK5C Glu release control vs drug treatments statistics using superplot data.

Condition	Mean	SEM	n	*p* relative to control	Significance
ION5C control	2237.790741	519.8976922	31	-	-
ION5C latrunculin	1401.5	1199.776207	11	0.0029	significant difference
ION5C jasplakinolide + latrunculin	2181.101488	919.0942513	27	0.7769	not significant
ION5C jasplakinolide	1888.5	886.6472899	7	0.1705	not significant
ION5C jasplakinolide + latrunculin + OA	1783.5	581.8793228	8	0.0379	significant difference
ION5C latrunculin + OA	1470.5625	558.2584584	10	0.0003	significant difference
Condition	**Mean**	**SEM**	**n**	***p* relative to latrunculin alone**	**Statistical difference**
ION5C control	0	0	31	-	-
ION5C latrunculin	1401.5	1199.776207	11	-	-
ION5C jasplakinolide + latrunculin	2181.101488	919.0942513	27	0.0368	significant difference
ION5C jasplakinolide	1888.5	886.6472899	7	-	-
ION5C jasplakinolide + latrunculin + OA	1783.5	581.8793228	8	0.4192	not significant
ION5C latrunculin + OA	1470.5625	558.2584584	10	0.8698	not significant

Table B5.2: ION5C Glu release control vs drug treatments statistics using superplot data.

Condition	Mean	SEM	n	*p* relative to control	Significance
HK5C control	-1883.5	112.3223	95	-	-
HK5C latrunculin	-1782.78	150.6906	38	0.6183	not significant
HK5C jasplakinolide	-2051.77	128.7356	30	0.4308	not significant
HK5C jasplakinolide + latrunculin	-1961.85	215.906	22	0.7598	not significant
HK5C latrunculin + OA	-1869.54	104.9216	21	0.9546	not significant
HK5C jasplakinolide + latrunculin + OA	-2564.5	306.2432	18	0.0207	significant difference
Condition	**Mean**	**SEM**	**n**	***p* relative to latrunculin + OA**	**Significance**
HK5C latrunculin + OA	-1869.54	104.9216	21	-	-
HK5C jasplakinolide + latrunculin + OA	-2564.5	306.2432	18	0.0285	significant difference

Table B5.3: HK5C FM 2-10 release control vs drug treatments statistics from superplot data.

Condition	Mean	SEM	n	*p* relative to control	Significance
ION5C control	-1793.21	138.9889	99	-	-
ION5C latrunculin	-2086.9	255.7789	44	0.2771	no significance
ION5C jasplakinolide	-1777.61	130.2158	18	0.9626	no significance
ION5C jasplakinolide + latrunculin	-1758.06	124.8777	21	0.9093	no significance
ION5C latrunculin + OA	-1783.35	66.09675	13	0.9796	no significance
ION5C jasplakinolide + latrunculin + OA	-2730.32	202.6193	18	0.0065	significant difference
Condition	**Mean**	**SEM**	**n**	***p* relative to latrunculin + OA**	**Significance**
ION5C latrunculin + OA	-1783.35	66.09675	13	-	-
ION5C jasplakinolide + latrunculin + OA	-2730.32	202.6193	18	0.0006	significant difference

Table B5.4: ION5C FM 2-10 dye release control vs drug treatments statistics using superplot data.

Condition	Mean	SEM	n	*p* relative to control	Significance
ION5C control	1380.883	230.7365	32	-	-
ION5C PMA	1371.056	150.3873	10	0.9816	not significant
ION5C PMA + latrunculin	874.5	191.4835	9	0.2672	should be significant
ION5C PMA + jasplakinolide + latrunculin	1372.417	245.6751	10	0.9846	not significant
ION5C PMA + jasplakinolide	1205.056	68.00708	8	0.7087	not significant
ION5C PMA + latrunculin + OA	708.1667	64.12603	9	0.1346	should be significant
ION5C PMA + jasplakinolide + latrunculin + OA	1342.028	104.9057	10	0.9268	not significant
ION5C PMA + latrunculin + blebbistatin	814.9674	211.8785	21	0.0952	should be significant
ION5C PMA + jasplakinolide + latrunculin + blebbistatin	1425.117	163.9781	16	0.8993	not significant
Condition	**Mean**	**SEM**	**n**	***p* relative to PMA + latrunculin + OA**	**Significance**
ION5C PMA + latrunculin + OA	708.1667	64.12603	9	-	-
ION5C PMA + jasplakinolide + latrunculin + OA	1342.028	104.9057	10	0.0001	significant difference
Condition	**Mean**	**SEM**	**n**	***p* relative to PMA + latrunculin + blebbistatin**	**Significance**
ION5C PMA + latrunculin + blebbistatin	814.9674	211.8785	21	-	-
ION5C PMA + jasplakinolide + latrunculin + blebbistatin	1425.117	163.9781	16	0.0375	significant difference

Table B5.5: ION5C Glu release control vs PMA plus other drug treatments statistics using superplot data.

Condition	Mean	SEM	n	*p* relative to control	Significance
ION5C control	-1414.98	183.6969	48	-	-
ION5C PMA	-1363.85	122.0643	20	0.8635	not significant
ION5C PMA + latrunculin	-1484	195.7664	19	0.8286	not significant
ION5C jasplakinolide	-1369.68	38.98578	18	0.8814	not significant
ION5C PMA + jasplakinolide + latrunculin	-1344.82	167.739	18	0.8261	not significant
ION5C PMA + latrunculin + OA	-1401.26	158.6195	18	0.9655	not significant
ION5C PMA + jasplakinolide + latrunculin + OA	-1923.65	538.4791	17	0.2549	should be significant
ION5C PMA + latrunculin + blebbistatin	-1398.77	402.5467	18	0.9667	not significant
ION5C PMA + jasplakinolide + latrunculin + blebbistatin	-1987.34	254.3462	23	0.0767	should be significant
Condition	**Mean**	**SEM**	**n**	***p* relative to PMA + latrunculin + OA**	**Significance**
ION5C PMA + latrunculin + OA	-1401.26	158.6195	18	-	-
ION5C PMA + jasplakinolide + latrunculin + OA	-1923.65	538.4791	17	0.3472	should be significant
Condition	**Mean**	**SEM**	**n**	***p* relative to PMA + latrunculin + blebbistatin**	**Significance**
ION5C PMA + latrunculin + blebbistatin	-1398.77	402.5467	18	-	-
ION5C PMA + jasplakinolide + latrunculin + blebbistatin	-1987.34	254.3462	23	0.2056	should be significant

Table B5.6: ION5C FM 2-10 dye release control vs PMA plus other drug treatments statistics using superplot data.